Liquid Crystalline Cellulose Derivatives for Mirrorless Lasing

---

Dissertation

zur Erlangung des Grades
"Doktor der Naturwissenschaften"

vorgelegt von
Daniel Wenzlik
geboren am 19. Dezember 1983 in Nastätten

Mainz, den 12. März 2013

JG|U

JOHANNES GUTENBERG
UNIVERSITÄT MAINZ

Die vorliegende Dissertation wurde, unter der Betreuung von   , in der Zeit von Oktober 2009 bis März 2013 am Institut für organische Chemie der Johannes Gutenberg-Universität in Mainz durchgeführt.
Diese Fassung wurde im Mai 2013 aktualisiert.

Dekan:
1. Berichterstatter:
2. Berichterstatter:

Tag der mündlichen Prüfung: 25.04.2013

D77: Dissertation Universität Mainz

Ich versichere, dass ich meine Dissertation „Liquid Crystalline Cellulose Derivatives for Mirrorless Lasing" selbständig angefertigt und ausschließlich nur die von mir zitierten Quellen verwendet habe.

Diese Dissertation wurde weder in der jetzigen noch in einer abgewandelten Form bei einer anderen Hochschule eingereicht und hat noch keinem sonstigen Prüfungszweck gedient.

Mainz, März 2013

Daniel Wenzlik

Für meine Schmetegarke

"Und bist du nicht willig, so brauch ich Geduld." (Peter Kruse)

Begriffsdefinition Polymer:

Ein Stoff, der aus Molekülen besteht, die durch eine Kette einer oder mehrerer Arten von Monomereinheiten gekennzeichnet sind, und der eine einfache Gewichtsmehrheit von Molekülen mit mindestens drei Monomereinheiten enthält, die zumindest mit einer weiteren Monomereinheit oder einem sonstigen Reaktanden eine konvalente Bindung eingegangen sind, sowie weniger als eine einfache Gewichtsmehrheit von Molekülen mit demselben Molekulargewicht, wenn diese Moleküle innerhalb eines bestimmten Molekulargewichtsbereichs liegen, wobei die Unterschiede beim Molekulargewicht im wesentlichen auf die Unterschiede in der Zahl der Monomereinheiten zurückzuführen sind; eine Monomereinheit im Sinne dieser Begriffsbestimmung ist die gebundene Form eines Monomers in einem Polymer.

(§3, Abs. 3a, ChemG)

Contents

List of Figures

1 Introduction

1.1 Liquid Crystals

1.1.1 The Discovery of Liquid Crystals

In the middle of the 19th century three different types of experiments opened the way to the discovery of liquid crystals [1], although the first observation of liquid crystalline behavior can be traced back to George-Luis LeClerc (middle of 18th century) [2]. First of all, it was found that biological specimens showed birefringent behavior when viewed under the microscope between two crossed polarizers. Birefringence was known for solid crystals, but never encountered so far for non solid samples. Second Otto Lehmann invented a microscope with a hot stage enabling him to investigate processes with magnification under a controlled atmosphere. When he added polarizers to this setup the polarizing optical microscope was born, a standard tool in todays liquid crystal laboratories. Last but not least chemists like W. Heintz and P. Planer reported about two melting points for natural fats and bluish colors when derivatives of cholesterol were cooled from the melt. All these records show liquid crystalline behavior but the scientists behind were not able to identify this new class of compounds.

The person who is given most credit for the discovery of liquid crystals is the Austrian botanist Friedrich Reinitzer. In 1888 he was analyzing cholesterol benzoate in terms of getting the molecular weight of cholesterol. He found that this substance showed two melting points upon heating [3, 4]. At the first melting point the solid was converted into a turbid liquid while at the second melting point a clear liquid appeared. Between these two points the turbid liquid additionally showed some colored reflections. Without knowing it he was the first to mention liquid crystalline behavior. Otto Lehmann considered that a substance could show crystalline order without being solid, in the same year Reinitzer reported about his observations. He was also the first to give liquid crystals their name from the German expression "Flüssige Kristalle" [5] before they were referred to soft crystals, floating crystals or crystalline fluids. He found that liquid crystals exhibit a strong

optical anisotropy and concluded that this fact is a result of a systematic ordering of anisotropic shaped molecules although the structure of cholesterol was not known at this time. He had to fight for his liquid crystal concept because many scientists like G. Tammann [6] favored the theory of mixed emulsions.
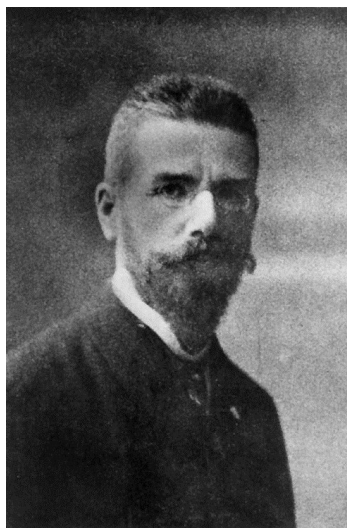
Figure 1.1: Prof. Friedrich Reinitzer in 1909 [7]

After the synthesis of the first nematic liquid crystal by L. Gattermann and A. Ritschke, Lehmann found that some liquid crystals behaved differently from others and that a liquid crystal can be aligned if in contact with a solid surface. This finding is most important for today's LC-technology. Daniel Vorländer concluded from Lehmann's results and after synthesizing hundreds of liquid crystalline compounds that there is more than just one liquid crystalline phase and that an anisotropic shape of the molecules is mandatory [8]. The polymorphism of liquid crystalline compounds - together with a classification and the first use of the words nematic, smectic and cholesteric - were published by Georges Friedel in 1922 [9]. Here he explained the idea of molecular ordering and showed that the lines visible under the polarizing optical microscope were defect lines representing drastic changes of the ordering vector, called director. Furthermore he understood that liquid crystals could be oriented using electric or magnetic fields, the second important issue for today's LC-technology.

From the theoretical point of view L. Onsager [10], W. Maier and A. Saupe [11, 12], P.J. Flory [13] and P.G. de Gennes [14] were the most influencing scientists. Many liquid crystalline materials consist of elongated or otherwise anisotropically shaped compounds. Such molecules tend to align into the same direction for entropic as

well as energetic reasons. If aligned, they can move more freely in a densely packed solution or melt. Onsager showed that hard rods tend to be parallel if their volume fraction is greater than 4.5 times their breadth-to-length ratio, while Flory found that a length to diameter ratio greater than 4 is necessary. In Onsagers hard rod model the excluded volume of two approaching idealized cylinders is calculated and he found that if rods are aligned parallel, the excluded volume decreases. This lowers the orientational entropy but increases the positional entropy. Above a critical concentration a solution of these hard rods will undergo a phase transition from the isotropic to the nematic phase. The concept of this model is very helpful but the assumptions made therein limit its applicability to real systems. In the statistical approach of Maier and Saupe, on the other hand, it was shown that van der Waals forces, arising from anisotropic molecular polarizability, give rise to parallel alignment between two adjacent LC molecules. The anisotropic attraction stabilizes the arrangement of neighboring molecules. This theory predicts the thermotropic nematic to isotropic phase transition. A more modern approach is the elastic continuum theory [15] where the LC is considered as a continuum and molecular details are ignored. Here distortions of a presumed oriented sample are ascribed by the Frank free energy density. Three types of distortions, twist, splay and bend, can be identified, which incur with energy penalty. The response of the system is then decomposed into terms based on elastic constants. This theory is primarily used for modeling liquid crystal devices.

During the second world war the interest in liquid crystal research decreased because there were no real applications and scientist thought almost all questions about liquid crystals had been solved [1]. In 1957 Glenn H. Brown reviewed the results obtained so far [16] and in 1965 he founded the Liquid Crystal Institute at Kent State University, the first research center focused on basic and applied research on liquid crystals [17]. The interest was regained during the 1960s because of the invention of the major application of liquid crystals: The liquid crystal display. The first LCD-prototype presented in 1966 and the development of the twisted nematic cell as well as the switching of colors with an electric field in 1968 were the starting points for a new era of liquid crystal science [2, 18]. Until today thousands of scientists are working on that field, numerous conferences covering all aspects of the topic were held and millions of items based on liquid crystal technology are sold every year.

1.1.2 Classification of Liquid Crystals

As liquid crystalline phases [19] combine properties of the liquid as well as the solid (crystalline) state of matter, they are also called mesophases, from the Greek expression for "in between". In the same way molecules forming liquid crystals are referred to as mesogens. The main difference to non liquid crystalline substances is the more or less rigid but in particular anisotropic shape of the mesogens. Liquid crystalline phases are known from rodlike (calamitic), lathlike (sanidic) [20] or disklike (discotic) [21] shaped molecules. Furthermore exotic designs like banana-shaped mesogens [22], pyramids [23] and shuttlecocks [24] have shown to be capable of self organization. Besides a rigid interior, mesogens need to possess some flexible compartments at their proximity to ensure a sufficient movability. Rigid parts are usually consisting of aromatic rings connected via bonds showing full or partial double bond character. In addition to low molecular weight compounds there are also polymeric compounds exhibit liquid crystalline behavior (see section 1.1.4)

A second classification is used to distinguish the so-called thermotropic and lyotropic liquid crystals. In thermotropic liquid crystals, the shape of molecules dictates the orientational order and thermal motion gives the mobility. Lyotropic liquid crystals, which appear in nature and in living organisms, acquire mobility by addition of a solvent, and their liquid crystalline properties are governed by the relative concentration of the solute. However, the distinction between the thermotropic and lyotropic liquid crystals is not well defined and there are materials which exhibit both thermotropic and lyotropic liquid crystalline properties. They are called amphotropic. Nowadays, light is known to be an additional stimulus to introduce liquid crystalline behavior [25].

The most simple liquid crystalline phase is the nematic phase, where rodlike mesogens point in average to the same direction (see figure 1.2) . The centers of mass are distributed randomly and they are free to move, like in a fluid, but their average orientation will remain the same, similar to a crystal. Thus the material is anisotropic. The order parameter S (see equation (1.1)) quantifies the variation of the mesogen's orientation from the average vector $\vec{n}$ (director). Physically, $\vec{n}$ and $\overrightarrow{-n}$ are equivalent.

$$S \;=\; \frac{1}{2}\langle 3cos^2\theta - 1\rangle_\theta \tag{1.1}$$

Here θ is the angle between the mesogens long axis and the director, $\langle\rangle$ denotes the statistical average. In a perfect crystal S is equal to 1, while in an isotropic liquid it is 0. If all molecules would be aligned perpendicular to the director, the value for S is $-\frac{1}{2}$. The typical range of S is between 0.3 and 0.7 for liquid crystals. The second major class of rodlike mesogens is the smectic phase. In addition to a preferred orientation the mesogens are well placed in a layered structure, but have no fixed position within the layer. There are several smectic phases attributed with letters in accordance to their discovery. For example in a smectic A phase the mesogens long axes are aligned parallel to the layer normal while in smectic C they are tilted at a certain angle. Hence the order parameter S is higher for these phases then for nematics. Another type of liquid crystalline phases with two-dimensional order is the columnar phase, formed by disk-shaped molecules. Here the center of mass is along the centerline of one column. The columns are organized in a hexagonal or rectangular geometry perpendicular to the column.
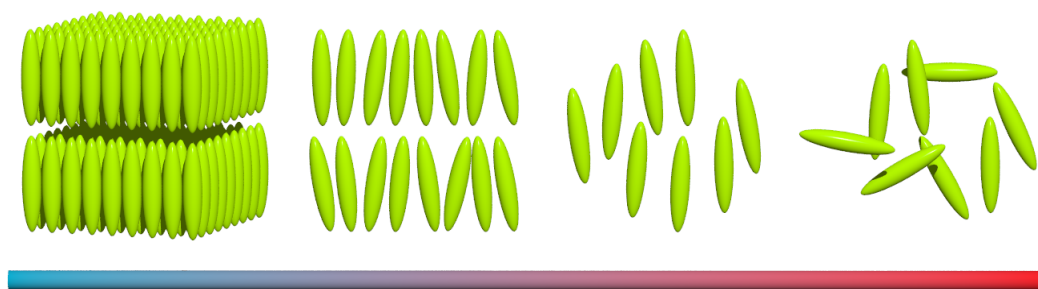
Figure 1.2: From left to the right (temperature increases, S decreases): Crystal, smectic LC, nematic LC, isotropic liquid

Going back to rodlike species there is the chiral nematic phase where the mesogens tend to align in nematic layers. These layers rotate along an axis normal to the layer. They are called cholesteric liquid crystals because many cholesterol derivatives show this phase. A more detailed description of the cholesteric phase is provided in section 1.1.3. Often natural polymers form this type of liquid crystalline phase due to their intrinsic chirality (see Section 1.1.4). The most prominent property of liquid crystalline substances is birefringence. For a rodlike molecule two different refractive indices can be defined: the extraordinary index n_e along the long molecule axis and the ordinary n_o along the short axis. This refractive index difference causes that light traveling through the LC, at different directions relative to the director, has different propagation velocities. The polarization direction of the incident light is changed and the combination with the phase shift is the cause

for textures and beautiful colors of LC samples in the polarizing optical microscope. Areas which are oriented parallel to one of the polarizers appear black while all others show colors in dependence to film thickness, temperature and LC phase. To estimate either film thickness or birefringence the Michel-Levy birefringence chart (figure 1.3) is a useful tool.
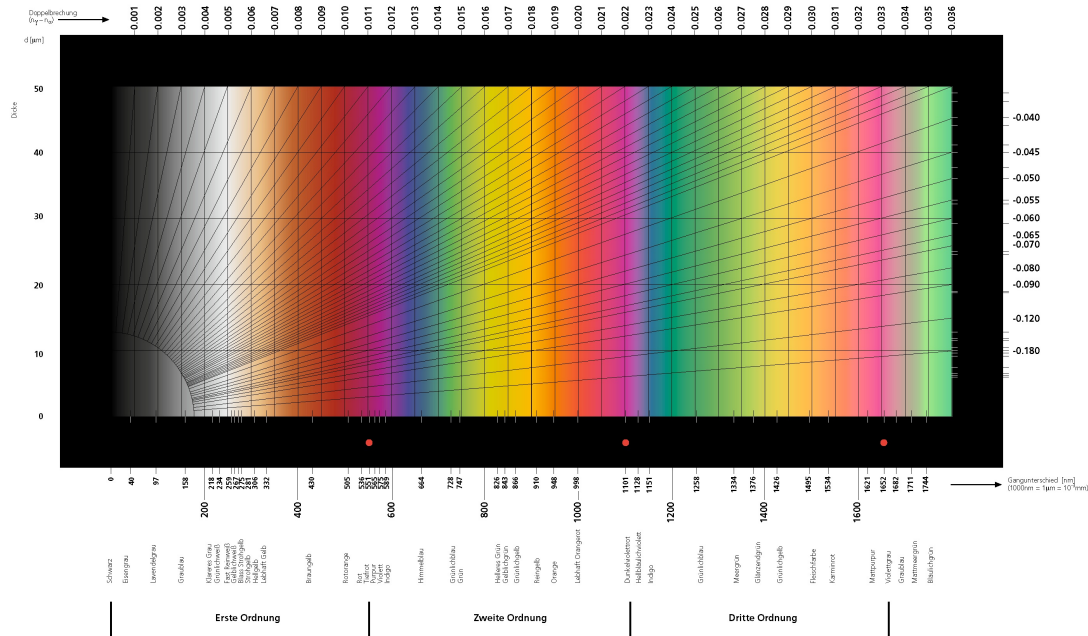
Figure 1.3: The Michel Levy color chart [26] for determination of film thickness or birefringence, if the other value is known.

1.1.3 Cholesteric Liquid Crystals

The presence of chiral molecules has serious effects on the orientation of liquid crystals [27]. A chiral dopant in an achiral nematic LC (NLC) or chiral rodlike mesogens yield chiral nematic liquid crystals. Due to the chiralty a helical twist is introduced to the director field. Hence chiral nematics consist of nematic layers, but the director rotates along an axis normal to the layers. Chiral nematic phases are formed by cholesterol derivatives, due to their intrinsic chirality without dopants. Thus chiral nematic phases are referred to as cholesteric liquid crystals (CLC). An important value for characterizing this state is the pitch p. It is the distance needed for one 360° rotation of the director and covers the range from 200 nm to several μm (see Figure 1.4).

Positive values for p are assigned to right handed twist sense, negative for left
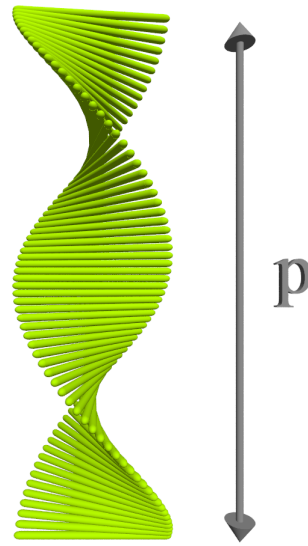
Figure 1.4: The helical superstructure of calamitc mesogens in a cholesteric liquid crystal (Pitch p)

handed twist. A right handed twist sense is present if, viewing along the helical axis, the molecules rotate clockwise during going away from the viewers point. If the CLC is a mixture of a dopant and an achiral LC the pitch is defined as

$$p \;=\; \frac{1}{(HTP*c)} \tag{1.2}$$

where c is the weight concentration of the dopant and HTP is its helical twisting power. The sign and value of HTP depends on the detailed molecular structure of the chiral dopant, the interaction with the host LC and the temperature, but to date no universal relationship has been found [27]. The pitch and therefore the resulting optical properties can be varied by using external stimuli like temperature change, mesogen and dopant concentration, sensitivity to special additives [28], light [29] and electric fields [30], just to name a few examples.

For CLC between two solid substrates there are different textures, namely the planar, the homeotropic and focal conic textures. In principle a texture [31] is the image of a LC sample one gets through the polarizing optical microscope. Numerous textures have been already assigned to the corresponding LC phases, which can be used for a preliminary classification of unknown phases. But just a texture is usually insufficient to distinguish between different phases, so X-Ray experiments are today's standard for LC characterization.

In the planar state (see figure 1.5) the long axes of the mesogens are aligned parallel to a solid surface. Consequently a CLC in the planar state has its director always parallel to the surface, while the helical axes are perpendicular to it. To introduce planar orientation several methods like rubbed alignment layers [32] or molten PTFE layers [33] have been developed. The glass-made cells are filled with the LC material by capillary forces, because flow shear supports the alignment along the flow direction parallel to the substrate. It is sometimes sufficient just to rub the bare glass slides with a cellulose sheet. As most of the low molecular weight CLC do need such alignment layers, some polymeric LC are capable to orient parallel to a bare flat surface. As the planar state shows the most interesting and useful optical properties there have been lots of attempts for improving the planar alignment to yield an idealized situation [34, 35]. It is meant to reduce defects in the samples and to ensure all helical axes are perpendicular to the substrate. One of its unique optical properties (see Section 1.2.1) is the selective reflection of light. The texture resulting from this orientation is called oiley streak texture. It shows uniformly colored areas which are separated by bright lines in between. The lines correspond to bundles of defect lines, so called Grandjean-lines, where the helical axes are distorted, while the uniform parts are in the planar state. This state is not birefringent and only uniformly colored if the pitch is in equal size to the wavelengths of visible light. Otherwise the picture in POM appears black, if defects are neglected.

The second orientation of CLC is the homeotropic state (see figure 1.6). The helical axes are now parallel to the substrate. If the pitch is large enough a lamellar pattern can be observed in the POM. This pattern is called fingerprint texture. The dark lines represent nematic layers where the mesogens are perpendicular or close to perpendicular to the glass substrate. Because this happens twice per pitch the distance between two lines equals half of the pitch [36]. This orientation can be obtained by applying an electric field to the sample [37]. In addition to the fingerprint texture there are different focal conic textures. There are different origins described in literature. Nawa [37] describes it as a homeotropic aligned CLC where the helical axes are randomly oriented inside the plane of the LC film. A second group showed a focal conic state as a multidomain-like fingerprint [38]. Yet another description is that cholesteric planes are arranged in the form of a double spiral, ending in the center of the spiral [39]. And last but not least it is presented as a not oriented destroyed texture [40]. A special case of a focal conic defect in which the line discontinuities form a pair of confocal parabolae has been observed in cholesteric as well as in smectic liquid crystals. The polygonal texture obtained

by dilation of smectic A and cholesteric planar texture is shown to be an array of parabolic focal conic defects [41]. Nevertheless this state is more interesting to investigate pattern formation and LC textures.
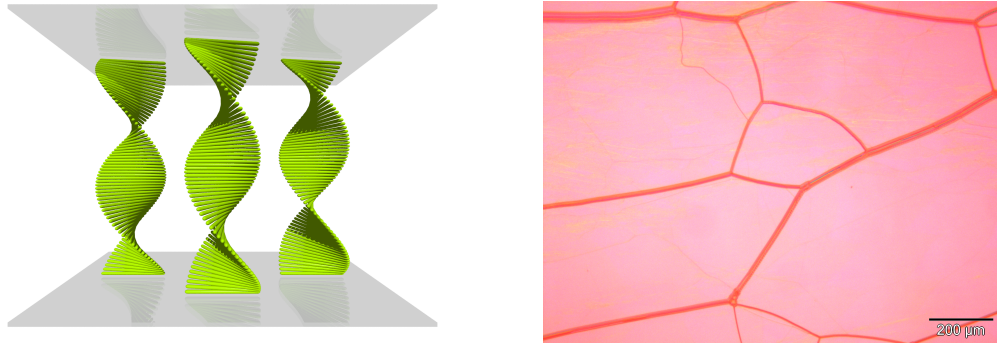
Figure 1.5: Planar state of a CLC (schematic and texture).
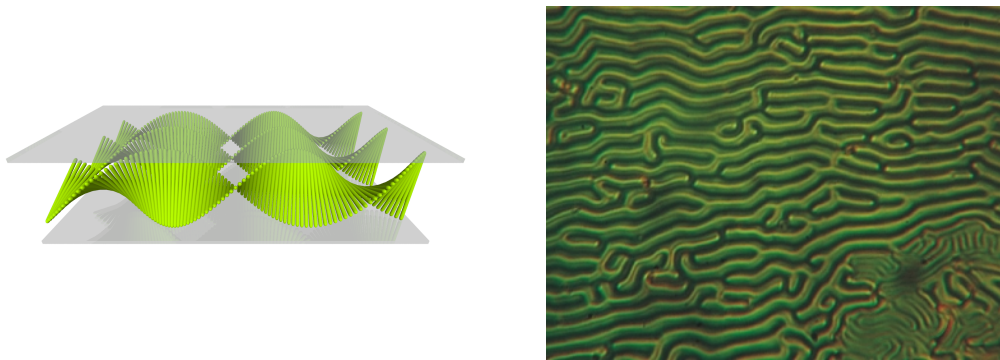
Figure 1.6: Homeotropic state of CLC (schematic and texture[42]).
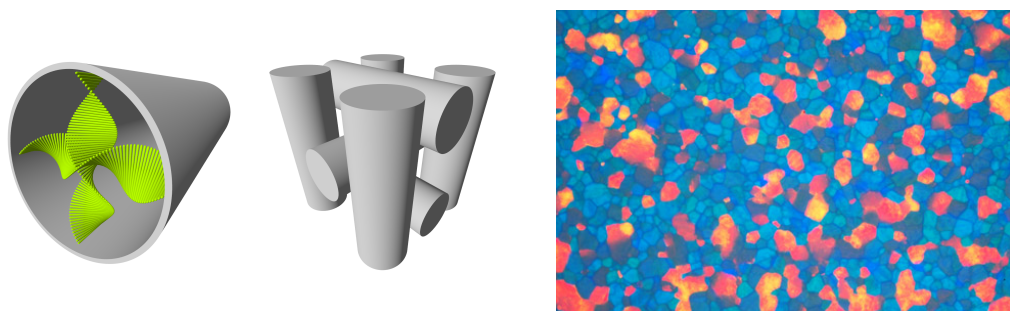
Figure 1.7: Blue Phase II (schematic of double twist cylinder and their arrangement and texture [43]).

Another type of LC phases, mostly observed in cholesteric materials, are the so-called blue phases (see figure 1.7) labeled BP-I - BP-III and they usually appear in a very small temperature range between the cholesteric and the isotropic liquid state. They occur in this order with increasing temperature and are prepared by cooling very slowly from the isotropic liquid and a platelet texture is visible in the

POM. Blue phases are very different from all other LC phases because they consist of a fluid lattice stabilized by lattice defects [44]. Their structure is based on a delicate balance between the intermolecular interaction and the topological requirement, resulting in a frustrated system. Here cylinders are formed of double twisted cholesteric arranged mesogens. These cylinders are stacked in a three dimensional lattice with a body centered structure for BP-I and a cubic symmetry for BP-II. The lattice period is similar to the wavelength of light, so that these phases exhibit reflectance properties like the planar state of cholesterics but in 3 dimensions. BP-III is seemingly amorphous with a cubic local structure. While the very narrow temperature window, in which blue phases exist, limit their application, many efforts have been conducted to stabilize them over a broader temperature range, using polymerization [44] and refill techniques [45].
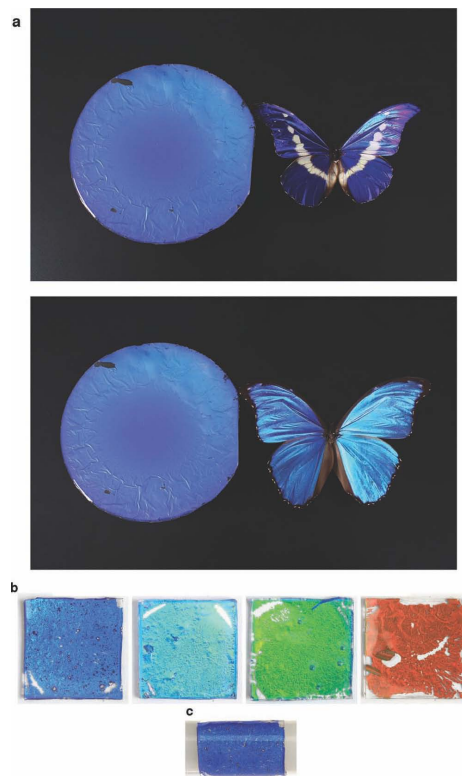
Figure 1.8: Opalescent colors of butterflies are often originated from photonic structures, which can be reproduced artifically [46].

Cholesteric liquid crystals have various applications because of their optical properties. They can be used in temperature and UV sensors, selective mirrors, for reflective displays, image converters and as feedback cavities for mirrorless lasing

devices [40] (see section 1.3.2). Furthermore there are various paints made with either cholesteric or other photonic structures (see section 1.2) to create coatings that change their color with respect to the viewing angle. Additionally nature uses photonic structures which can be mostly seen at insects like beetles with beautiful iridescent colors.

1.1.4 Polymer Liquid Crystals

Besides low molecular weight LC there are lots of polymer substances which exhibit liquid crystalline behavior [47]. In 1923 Daniel Vorl"ander [48], who played a major role in the discovery and synthesis of liquid crystalline materials, already synthesized oligomers with 1 to 3 linked mesogens. He synthesized PBA and reported this polymer as a birefringent powder which would not melt but decompose upon heating. This fact limited his efforts to get stable polymers which show LC properties in the melt. It took several years until the problem with decomposition before melting in LCP was solved by using random copolymers. As one of the first lyotropic LCP PBLG was synthesized in 1950 [49]. A few years later DuPont commercialized the first LCP, an aromatic amide fiber known as Kevlar. This polymer was spun from anisotropic solutions and therefrom it had outstanding tensile properties. Here it was known that the LC state in the solution was the cause for the resulting qualities. On the other hand product development proceeded without knowing that some interesting properties were the result of liquid crystallinity. Extremely high melting points of polymers consisting of rigid functionalities gave rise to develop different polymer architectures to overcome this problem. Today there are many different kinds of polymers with thermotropic LC qualities. They are classified as main-chain LCP where mesogenic groups are part of the polymer backbone. The mesogenic compartments can have various shapes like rods, discs or planks. To reduce the transition temperature from the crystalline to liquid crystal state, it was necessary to give the mesogens some more freedom of movement, as they were already very restricted while being part of a polymer. This could be achieved by increasing the spacer length between the mesogens, copolymerization of different mesogenic monomers or via attachment of space filling chains to them. Another approach was to link the rigid group to a polymer backbone as side chains (side-chain LCP). There are two different orientations how a mesogen can be linked to the polymer: side-on or end-on. It is also possible to combine both types of LCP to obtain a main-chain LCP with attached mesogenic side chains [50]. All these different architectures decrease the transition temperature to the LC state to obtain

stable liquid crystalline phases before the LCP decomposes.

Figure 1.9: Main-chain LCP with linear (left) and lateral architecture.
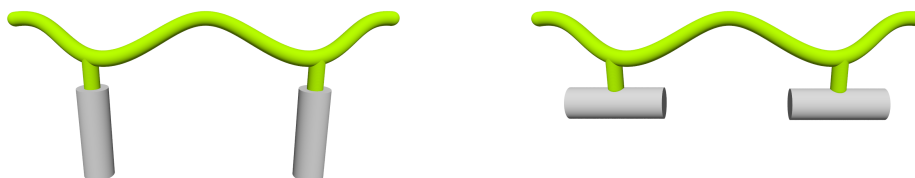
Figure 1.10: Side-chain LCP with end-on (left) and side-on architecture.

Lyotropic LC can be obtained by adding a low molecular weight solvent to LCP. Here the polymers do not need to be heated to very high temperatures and therefore there is no risk of polymer degradation. Among lyotropics another class of LCP are rigid-rod polymers, where the polymer backbone is in a stretched, more or less rigid, conformation. This class is mainly known from natural occurring polymers like cellulose [51], chitosan [52] or DNA [53]. Their phase behavior is mainly dependent on the concentration of the solvent but temperature plays an important role, too. Liquid crystallinity is only apparent in a certain concentration range above a critical value. At lower concentrations, solutions of LCP are isotropic, while phase separation appears above the LC range. The lower critical concentration increases with increasing flexibility of the chain due to a decreasing persistence length. Rigid-rod polymers do not possess small rigid compartments but the whole polymer chain is considered a rigid or semirigid rod. The asymmetry of the molecular shape is the most crucial prerequisite to form LC phases. Furthermore the free rotation of chain units around single bonds has to be gradually restricted [54]. A restriction of free rotation can be obtained via the introduction of cyclic units into the backbone (glucopyranosic units in cellulose and its derivatives), the formation of intramolecular hydrogen bonds (polypeptides or residues in

cellulose derivatives), a quasi-conjugation and coplanarity of some backbone bonds (amide bonds in polyamides) or the formation of ladder type polymers. The asymmetry is represented by the persistence length, which can be seen as the distance where a unit's orientation is not influenced by the previous unit anymore. A long persistence length leads to a high rigidity. One example for a very rigid polymer is PBLG, which is in principle referred to the class of flexible chain polymers. In fact the polymer forms the α-helical conformation and combines to bundles with other polymers due to hydrogen bonds. Especially for the polymers mentioned previously the persistence lengths are far shorter than the total length of the polymer [13]. Typical numbers for persistence length are between 5 and 40 nm, but the measured value is strongly dependent on the determination method used. Possessing a certain flexibility these polymers are called semirigid rods, but their shape is far more elongated than for random coil polymers. Derivatives of cellulose are one representative of this type of LCP and will be discussed more in detail in section 1.1.5. Polymers where free rotation around valence bonds is possible acquire a random arrangement at any concentration and thus their solutions will always be isotropic. Their persistence lengths are usually below 5 nm.

Alongside various other variants of this theme a new twist to polymer liquid crystals is provided by liquid crystal elastomers. Through the addition of a small amounts of crosslinkable monomers, the polymer backbones form crosslinked networks, which allow to control the LC phase behavior through external mechanical fields. On the other hand mechanic action can be created through temperature change like in LCE actuators [55]. Inorganic nanorods can be considered as the inorganic counterparts to LCP. They are far more rigid then organic polymers and hence capable to form anisotropic solutions. To prevent aggregation and enhance solubility, nanorods have been modified with polymers and the resulting solutions show nematic as well as smectic LC phases [56, 57].

1.1.5 Derivatives of Cellulose

Cellulose [58] is the most abundant polymer on this planet. More than 10^{12} tons are synthesized by nature each year. It is the unbranched polymeric version of β-1,4-glucopyranose, where glucopyranose is the ring form of D-glucose. In aqueous solution glucose exists in three different forms (see figure 1.11): the open form, α- and β-glucopyranose. The word pyranose says that 5 of the 6 carbon atoms form with the oxygen at C5 a sixmembered ring, while C6 is not included in the ring. In cellulose β-1,4-glucopyranose units are linked via glycosidic ether bonds, which

connect C1 of one unit with C4 of the following unit.
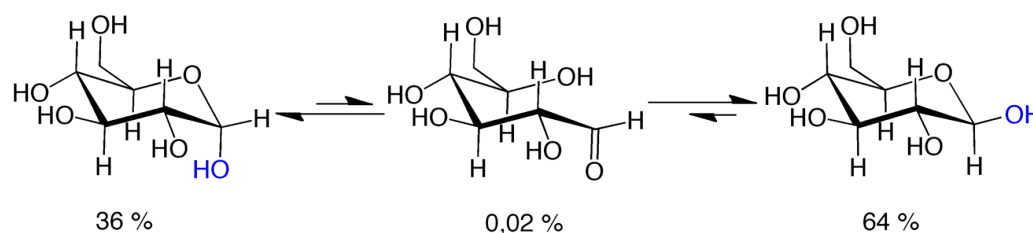
Figure 1.11: α (left), β (right) and open (middle) form of Glucopyranose in aqueous solution and their equilibrium percentage.

The only difference between α- and β-glucopyranose is the position of the hydroxyl group at C1. In α position it is axial (perpendicular to the ring plane) while in the β case it is equatorial or parallel to the plane of the pyranose ring. This feature has tremendous effects on the biological appearance (see figure 1.12) of the resulting polymer and on the synthesis of liquid crystalline derivatives. The polymer of α-1,4-glucopyranose is called amylose and is a major ingredient of natural starch. It is soluble in water and forms a helical structure due to intramolecular hydrogen bonds and the α-position of the hydroxyl group at C1. It is part of all starch containing foods and can be metabolized by almost all living beings. On the other hand poly (β-1,4-glucopyranose) or cellulose is not soluble in water and intramolecular hydrogen bonds force the polymer backbone in a more stretched state. The huge number of free hydroxyl groups along the backbone cause multiple intermolecular hydrogen bonds and parallel cellulose molecules form fibrils. This leads to very strong compartments. Hence cellulose plays an important role in wood containing plants where its fibrils are integrated in the plant cell wall and are responsible for its tensile strength. Therefore trees for example can grow up to 130 meters in height and do not dissolve in rain. Although there are many animals eating plants a special enzyme is necessary to metabolize cellulose. For commercial use cellulose is extracted from wood using hydrolitic processes under harsh conditions. These undefined methods lead to a high polydispersity of the starting materials for the synthesis of cellulose derivatives. The most famous commercial products containing cellulose are paper and cotton wool.

The special conformation of cellulose is an advantage as well as a disadvantage for the preparation of liquid crystalline derivatives. The advantage comes from the already stretched shape of the backbone which is a good starting point for the synthesis of derivatives with high persistence lengths. But the high number of hydrogen bonds restrict the number of possible solvents for synthesis and leads to a
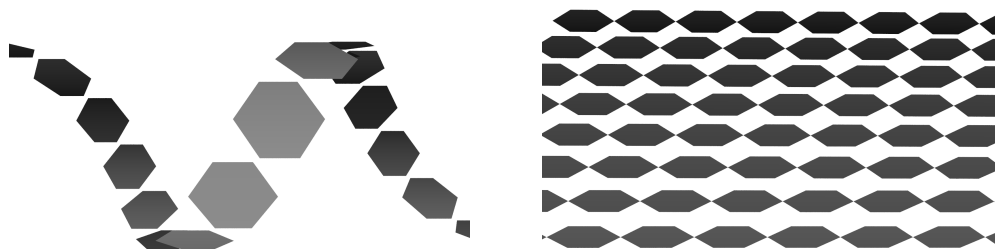
Figure 1.12: Structure of amylose (left) and cellulose.

high crystallinity of cellulose. Here reactants only have very restricted access to the hydroxyl groups. The aim of the derivatization of cellulose is to break hydrogen bonds between different cellulose strands and to introduce new ones, within one chain, to enforce the stretched conformation and a high persistence length. To circumvent the prior mentioned disadvantages, methods have been developed with solvents capable of dissolving natural cellulose [59] or with reactants which swell and activate the cellulose prior to derivatization reducing its crystallinity [60, 61]. Besides these methods there are a number of heterogeneous reactions where cellulose reacts without dissolving the starting material [62]. During the reaction the starting material is then converted into the soluble derivative.

Typical derivatives of cellulose are: Cellulose-ethers, -esters of organic and inorganic acids, -carbamates and silyl celluloses. In this thesis we will focus on cellulose tricarbamates (CTC) because of their high solubility in various organic solvents. Cellulose tricarbamates were first synthesized in 1920 [63] via the reaction of cellulose with isocyanates. As it can be seen in figure 1.13 this reaction converts the free hydroxyl groups (3 per glucopyranose unit) into esters of carbamoic acid.

This derivatization breaks intermolecular hydrogen bonds, because all hydroxy groups are converted. The introduced urethane functionalities cause new hydrogen bonds between the carbonyl group of one glucose unit and the imide group of the neighboring unit. Thus the rotation around the glycosidic bonds is further hindered, in addition to the hindrance because of the cyclic units, which leads to a greater rigidity of the polymer backbone. Here the degree of substitution (DS) plays an important role. The closer the DS to 3 (100% for 3 groups per glucose unit) the lower is the possibility of a random orientation of parts of the polymer. If these materials are dissolved in organic solvents they form anisotropic solutions above a critical concentration [13]. Below this threshold the solutions are transparent and do not show any birefringence. In addition to these lyotropic LC, several
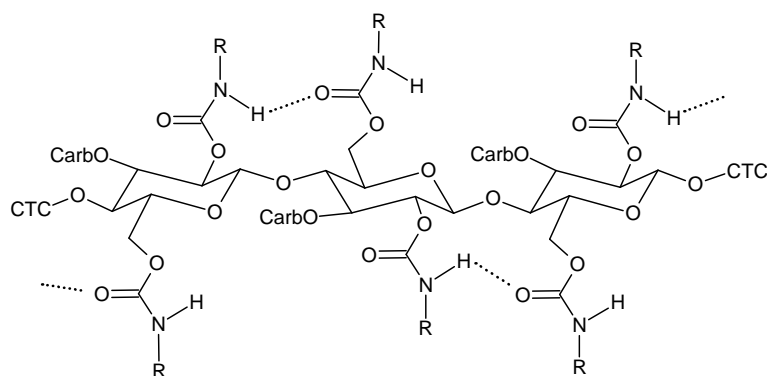
Figure 1.13: General chemical structure of cellulose tricarbamates (introduced hydrogen bonds are represented by the dotted lines).

cellulose derivatives form an LC phase in the melt or show amphotropic behavior. Nevertheless the most investigated class of cellulose derivatives are lyotropic ones.
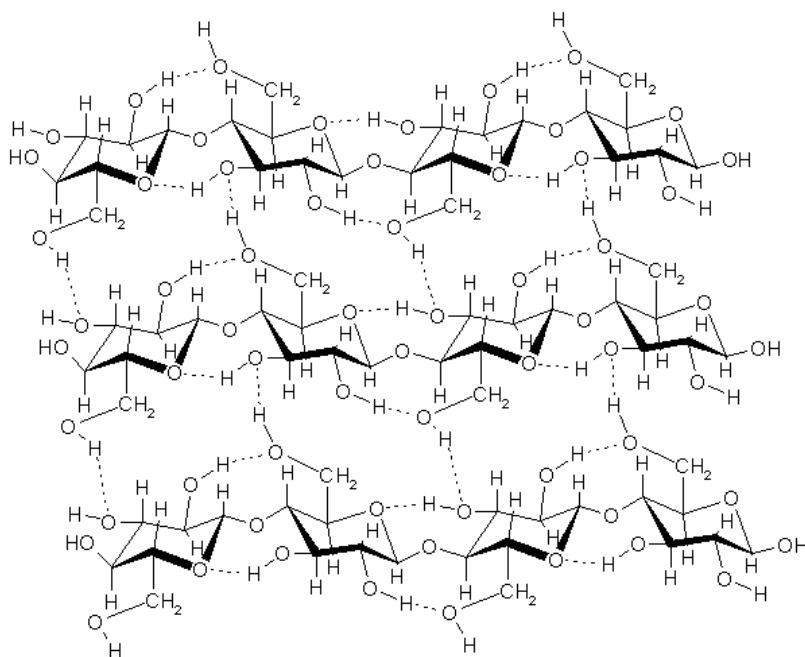
Figure 1.14: Inter- and intramolecular hydrogen bonds of natural cellulose causing its stability and occurence [64] (see figure 1.12).

Cellulose derivatives are soluble in a large variety of organic solvents that are capable to maintain solutions at very high concentrations. It is well known that solvents containing carbonyl functions like ester and keto groups or with ether-

functionalities are well suited for this purpose [65]. On the other hand very polar solvents like water are used as precipitation solvents during the synthesis. Solvents that lack of interaction with these polymers, because of e.g. steric hindrance, do not show anisotropy in their solutions [66]. These close polymer-solvent interactions are very important for the formation of a LC phase and will play a major role during the improvement of the optical properties of the resulting LC films. Acrylates and methacrylates are very valuable solvents for CTC. They show a necessary carbonyl functionality and they are polymerizable via radical polymerization. If these solvents are used, films of CTC solutions can be fixed via polymerization [29].

Due to the rigidity of the polymer backbone derivatives of cellulose exhibit a rod-like shape with high persistence lengths in the range from 5 to 10 nm [67] and up to 100 nm [68] while PBLG shows persistence lengths up to 150 nm. In highly concentrated solutions or melts the isolated cellulose strands are getting very close and form anisotropic liquids. Because of the chirality of glucose, cellulose is chiral as well, hence LC phases of these materials are chiral, too. Like many other chiral polymers [69] cholesteric LC are formed originated from the asymmetry of interactions between chiral macromolecules [70]. Thus the short range order can be considered as nematic whereas the long range order is helically twisted. The optical properties are very similar to those of low molecular LC (see section 1.2.1). If the pitch is in the range of visible light anisotropic solutions show iridescent colors and very high optical rotation. But, because of their high molecular weight and coincident high viscosity, as well as others factors, the optical quality of CTC solution films is not comparable to low molecular weight CLC [71]. The pitch is in a strong dependence of the solvent used and can be influenced by temperature change, mesogen concentration and additives. In the cellulose derivative case, the pitch can be influenced by the degree of substitution and the molecular weight [72, 73]. The polymer molecular weight or rather the aspect ratio can be varied using acidic treatment, which cleaves some of the glycosidic bonds without further degradation. This treatment reduces the polydispersity of the sample because the probability for a long chain to be cleaved is much higher than for an already short chain.

During the last 20 years it has been shown that cellulose does not need to be derivatized to obtain liquid crystals with cholesteric order [74]. If cellulose, from filter paper for example, is treated with strong acids the amorphous parts are dissolved, while small rodlike crystals of pure cellulose remain. Because the chirality is caused by the backbone of cellulose and electrostatic repulsion keeps the crystals in solu-

tion, CLC form above a critical concentration. Besides liquid crystal science there is a huge production on cellulose and derivatives thereof. They are used in explosives, cosmetics providing shiny hair, paints, glues and concrete, usually for adjusting its viscosity, and in the paper industry.

1.2 Photonic Crystals

The velocity of light c within a transparent medium is lower than the velocity in vacuum c_{vac}. The refractive index n of a material defines the ratio between the velocity of light in vacuum and in the medium.

$$n \;=\; \frac{c_{vac}}{c} \tag{1.3}$$

Hence all transparent materials have a refractive index higher then 1. If a light beam travels through a medium and reaches the interface with another medium, for example between air and glass, a part of the beam is reflected due to the refractive index difference between the two media [75]. The other part of the beam is refracted at the surface in dependence of the refractive index contrast. A photonic crystal [76] is a periodic stack of layers with different refractive indices. One distinguishes between one-, two- and three-dimensional PC if its periodicity appears along one, two or all three axes respectively.
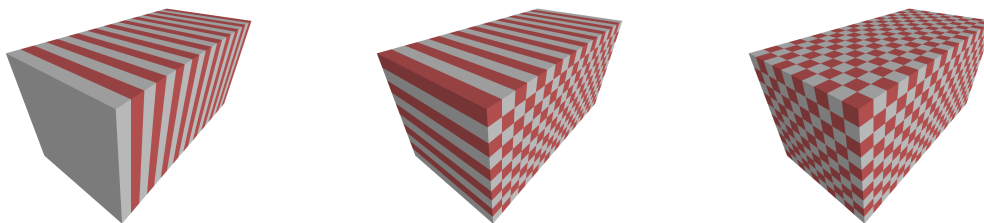
Figure 1.15: 1D (left), 2D (middle) and 3D photonic crystal.

Such a periodic medium exhibits a so-called photonic bandgap (PBG), in analogy to an electronic bandgap in semiconductors. These are frequencies of radiation which are not allowed to pass through the material, due to multiple reflections. Visible light will be reflected, if the periodicity is of the same size as wavelengths of visible light. These structures are used to influence the spectrum or the path of light in optoelectronic devices. If light is emitted from the inside and the PBG

of the PC overlaps with this emission, a photon localization is possible, the basic principle of distributed feedback lasers (see section 1.3.2). Methods creating periodic structures date back to the 1980s when Yablonovitch [77] aimed to influence the radiative properties of materials and John [78] to introduce random refractive index modulations to achieve photon localization. Defects in the lattice create localized photonic states inside the photonic bandgap. Liquid crystal lasers based on defect modes are using this principle. The nature of the defect has a great influence on the resulting photonic modes. A point defect can act as a microcavity, a line defect as a waveguide and a planar defect as a perfect mirror. As the electronic bandgap in semiconductors is a natural phenomenon PC have to be fabricated artificially. Although there are many examples in nature, where beautiful colored animals, mostly insects [46], use photonic crystals for their appearance (see figure 1.8), the creation of a photonic crystal requires state of the art technology. Besides different lithographic methods, artificial opals [79] are one way to achieve materials with a PBG. The spherical nature of the used colloids in a densely packed cubic lattice yield a three dimensional PC.

One simple and easy controllable way to prepare PC is the use of liquid crystals. But only chiral LC like cholesterics, smectic C* and blue phases show a photonic bandgap. Because of the refractive index anisotropy of the mesogens and their arrangement in chiral liquid crystal films, a periodic refractive index modulation is present at certain axes. The chiral LC has to be in an ordered, perfectly aligned and defect free state to provide a high quality of the photonic structure. The ease of LC is that they self assemble once the circumstances are right, but they will always be accompanied with defects. So the requirements on the preparation methods are very high. One example for photonic bandgaps in liquid crystals are CLC. In the planar state they exhibit a PBG along the helical axes normal to the film surface (see section 1.2.1).

1.2.1 Optical Properties of Cholesteric Liquid Crystals

As described in section 1.1.3 a CLC consist of rodlike molecules arranged in nematic layers rotating along one axis parallel to the layer normal. If such a sample is prepared on one rubbed substrate, the mesogens in contact with the substrate orient along the rubbing direction while those at the free surface are free in their orientation. Between two rubbed substrates the mesogens at both surfaces do orient along the rubbing direction which may cause slight pitch variations [14]. To show the optical properties we will consider an ideal defect free CLC in the planar state. This

arrangement is equal to a one dimensional photonic crystal because the modulation of the refractive index is only apparent along the helical axes. This causes a Bragg reflection with its maximum at λ_0 defined by the following equation

$$\lambda_0 \;=\; n * p \tag{1.4}$$

with the pitch p and the average refractive index n. Experimentally, one does observe only the first order Bragg reflection because higher orders are forbidden for normal incidence. Due to the helical arrangement of the mesogens the reflected light is circular polarized. This phenomenon is known as circular dichroism. As the pitch is in the range of several hundred nanometers the Bragg conditions are realized for visible light. CLC films reflect, under this condition, selectively certain frequencies of light, creating their colorful appearance. The full width at half maximum of this reflectance band $\Delta\lambda$ is a function of the refractive index anisotropy Δn.

$$\Delta\lambda \;=\; \Delta n * p \tag{1.5}$$

Highly anisotropic materials like cholesterol derivatives create very broad bands while derivatives of cellulose with a very low anisotropy create narrow bandwidths. But the higher the refractive index anisotropy the stronger is the light scattering outside of the bandgap. With increasing Δn the films appear slightly turbid. The position of the maximum the selective reflection (SR) shifts to shorter wavelengths with decreasing angle θ of the incident light relative to the substrate [80].

$$\lambda_0(\theta) \;=\; n * p * sin(\theta) \tag{1.6}$$

This equation requires that the angle of incident light and the viewing angle are the same with respect to the film normal. If the viewing direction is perpendicular to the substrate equation 1.6 converts into equation 1.4. Due to the circular dichroism incident linear polarized light is split at the surface of a CLC film into right and left handed circular polarized light. Circular polarization can be defined by handedness and helicity. Handedness is associated with space alone while helicity is associated with space and time. Helicity is associated with the sign of angular momentum

projected onto the propagation direction. Light has both handedness and helicity; the cholesteric structure only handedness. The handedness of a helix is still the same, regardless the viewing direction, while a time evolving light beam changes its rotation when the viewing direction is changed. Because there are two possible definitions of the rotation sense of light, the modern quantum physics one and the classical optical one, there are disaccording reports in literature which kind of handedness reflects which type of circular polarized light. Generally it can be said that the part of light with the same twist sense as the helix is transmitted through the material, while the part with the opposite twist sense is reflected [40]. Incident light at frequencies outside of the selective reflection band can pass through the material without any hindrance. As the reflectance is 100% for circular polarized light, it is 50% if the incident light is linear polarized or unpolarized. This can be shown in UV-VIS spectra.
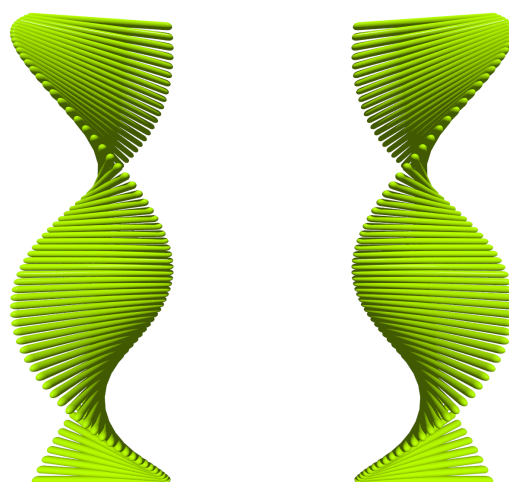
Figure 1.16: Left (left) and right handed helix of rodlike mesogens

In transmittance as well as reflectance spectra a peak of 50% can be observed. Doing optical rotation dispersion (ORD) or circular dichroism (CD) measurements, working with circular polarized light, one can see that CLC exhibit extreme values of optical rotation (several $10000°$ per mm). This value decreases rapidly if the CLC is transferred to the isotropic phase, which is a proof that these values of rotation are caused by the helical structure and not by the chirality of the mesogens. The position of SR depends on several internal and external factors like temperature, shear, cell thickness, mesogen concentration (for lyotropics), other ingredients like additives, dopants or initiators, substrate treatment, light curing and electric or magnetic fields. To overcome the limits of only 50% reflectance or to prepare sam-

ples with a reflection band across the whole visible spectrum, various methods have been developed [81].
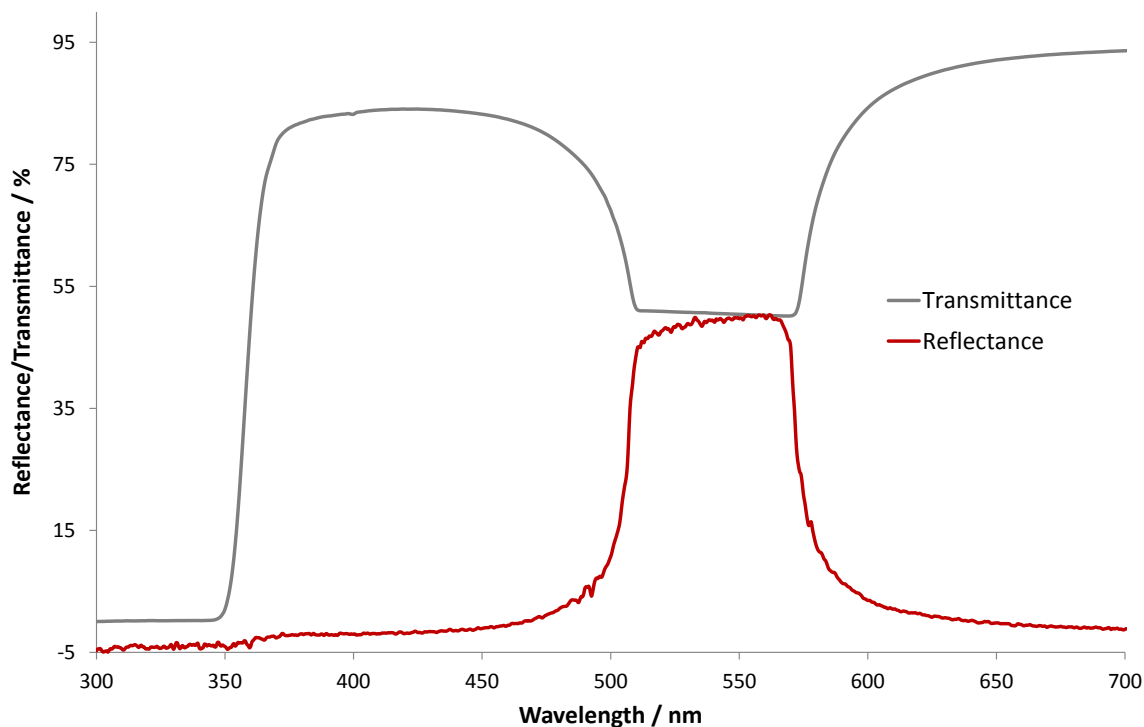
Figure 1.17: Typical UV-VIS spectra (transmittance = grey, reflectance = red) of a low molecular weight CLC (Merck MDA-00-3907) in the planar state. Both spectra were measured perpendicular to the substrate.

1.3 Laser

The acronym LASER [82] stands for light amplification of stimulated emission of radiation and describes a light source with very special characteristics. It uses two processes: the stimulated emission of light and a feedback provided by an optical, mode-selecting cavity. It consists of three mandatory components: A gain material capable of absorbing light or current energy and of emitting radiation with a high efficiency. Second a pump source that excites the gain material and last but not least a feedback structure, two parallel mirrors in the simplest case, which surrounds the gain material to increase the effective optical path length through multiple recirculation. The resulting emission is completely different from standard light sources like a light bulb [83]. It shows a high degree of directionality, coherence as well

as parallel alignment and covers only a very small range of optical frequencies, so-called monochromatic emission, while a light bulb emits abroad of frequencies to all directions. Lasing emission is possible from X-Ray wavelengths to microwave radiation. Due to the very narrow emission shape the energy density can be extremely high, so it is no challenge for some laser devices to burn wholes into stone. A laser can be run either in continuous or pulsed mode where pulses as short as a few attoseconds are already realized [84], a time span much shorter than electric pulses. Today lasers are part of countless technical, medical and analytic applications and ensure a smooth running of our daily lives. Lasers with output powers between 1 μW to 1 TW and sizes in the range of 1 mm for semiconductor lasers to 100 m for fusion lasers are available.

The development towards lasers started with Einstein's considerations about stimulated emission in quantum theory [85]. If a chromophore absorbs energy of a distinct, amount one of its electrons is taken from the ground state to the excited state. This amount of energy is emitted as radiation if the electron goes back to its ground state. The absorption of energy exceeds the emission from the excited molecules and due to thermal movement a lot of the incoming energy is converted into heat. This process is called spontaneous emission. Using increased pumping energy it is possible to achieve a population inversion, where more molecules are in the excited state than in the ground state. Now incoming light stimulates the decay of excited electrons to the ground state. During this decay light is emitted with the same phase, wavelength and direction of the incoming light and amplification of emitted light intensity is the result. Rudolf Ladenburg was 1928 the first to experimentally verify this process [86]. Almost 30 years later the microwave version of a laser, the MASER, was presented based on ammonia molecules [87]. From the microwave emission, based on molecule oscillations, to the emission of visible light it took only six years, when Theodore Maiman [88] used a stick of ruby with two parallel polished surfaces at each end. They represent the optical cavity reflecting the stimulated emitted light back into the gain material. The final laser emission leaves the cavity if one of the mirrors has a reflectivity slightly below 100%. Because of the planar surfaces light is reflected from mirror to mirror through the gain material. Every photon reflected by one of these mirrors is causing a stimulated emission that creates several additional photons traveling on the same path - amplification occurs. But for a continuous operation the population inversion must be preserved. There is a certain threshold energy which has to be put in until laser action occurs and can be maintained.

Until today a big variety of different laser media and structures has been developed. There are solid state and gas lasers using ions or gas as gain materials, systems based on organic or inorganic dyes and semiconductors. Besides the standard Fabry-Perot cavity, build from two parallel mirrors, structures with fibers, waveguides and distributed feedback in photonic crystals (see section 1.3.2), gases and semiconductors are realized. In actual research projects it is the aim to reduce threshold energies, to maximize slope efficiencies (the ratio between input and output energy), to obtain wide wavelength tunability, the miniaturization of lasing setups (see section 1.3.1), low cost production and most important systems pumped via electric energy instead of light.

1.3.1 Microcavity Laser

Thinking about applications of lasers and today's trends in technology there is a conflict visible. Electronic devices are getting smaller and smaller while lasers are, due to their resonators and other optical elements, too big if constructed in the traditional way. Fabry-Perot resonators and their folded or ring versions are complex, expensive and difficult to assemble. The properties of these mirrors require the use of the most optical transparent elements to yield a high reflectivity and low losses. In the competition of engineering towards very small lasers many different architectures were created. External cavities have been decreased in size or replaced by other structures. The most common type of miniature laser is the laser diode utilized in all types of disk drives. It is similar to a LED where light is generated through the injection of electrons and holes into a p- and n-doped semiconductor heterojunction. The combination of electrons and holes releases energy as radiation. The inner surfaces of the diode housing are metallized creating a resonator and a standing wave between them, resulting in laser emission. For high power output laser diodes many of these cells with heterojunctions are combined to bars achieving demands up to 70 W [82].
While many diode lasers work as multimode lasers, distributed feedback (DFB) and distributed Bragg reflector laser (DBR) laser show a mode selection because of their periodic structure. The mode selectivity is generated by the optical properties of the periodic structures (see section 1.2) because only the modes which fulfill the Bragg-conditions are reflected with significant lower losses than all other modes.

$$n\lambda = 2d\sin(\theta) \tag{1.7}$$

Here λ is the wavelength, d the distance between two parallel planes in the periodic structure, θ is the incident angle and n is the order of diffraction. Hence the feedback does not take place at the surface but is distributed throughout the periodic structure. Distributed feedback and distributed Bragg reflector laser use periodic structures as the cavity. DFB structures are PC which are doped with chromophores, while DBR lasers have a miniature Fabry-Perot cavity where the mirrors are replaced by periodic gratings [89]. A special geometry of DBR lasers are V(E)CSEL where the active layers and the Bragg or external cavity are a stack of films and the emission takes place normal to the surface. They have been realized with pure organic mixtures of polymers and dyes as well as with III-V semiconductors until electrically driven DFB lasers. One type of DFB laser is based on chiral liquid crystals (see section 1.3.2). Their anisotropic behavior and the resulting photonic structures doped with dyes are suitable candidates for tunable DFB lasers. Putting a dye doped CLC in a confined geometry the one-dimensional bandgap can be extended to three dimensions. CLC spheres, with radial distribution of the helical axes, have been shown to lase in three dimensions [90].

Despite Fabry-Perot cavities and structures like DBR and DFB there is a rapidly growing field of monolithic resonators in which the closed trajectories of light are supported by any variety of total internal reflection in curved and polygonal transparent dielectric structures [91]. The circular modes in such resonators can be understood as closed circular beams supported by those internal reflections from the boundaries of the resonators which show a very high refractive index contrast. The Q-factor which describes the quality of a cavity is defined by equation 1.8.

$$Q \approx \frac{\lambda}{\Delta\lambda} \tag{1.8}$$

$$\tau = \frac{Q}{2\pi v_c} \tag{1.9}$$

with the emission wavelength λ and the width of the mode $\Delta\lambda$. It can be very high for whispering gallery resonators (WGR). Q is also proportional to the photon dwell time τ (see equation 1.9). Hence this basic factor is related to the lifetime of light energy in the resonator mode. The higher Q, the longer is τ and the lower is the threshold and a very narrow emission represents a very high quality of the cavity. WGR can be of extremely small size which gives excellent mechanical stability. Because of their easy tunable properties they are well suited for integration into

optical networks. The name for this kind of resonator dates back to the beginning of the 20th century, when Lord Rayleigh studied the propagation of sound waves on a curved gallery surface [92]. The simplest geometry can be either a disk, a ring [93] (see figure 1.18), a sphere or a cylinder. If the reflection boundary has a high contrast and the curvature exceeds several wavelengths, radiative losses become very small and Q is only limited by material attenuation and imperfections like surface roughness. Therefore very precise preparation methods like electron beam etching and lithography come to use to produce these small cavities.
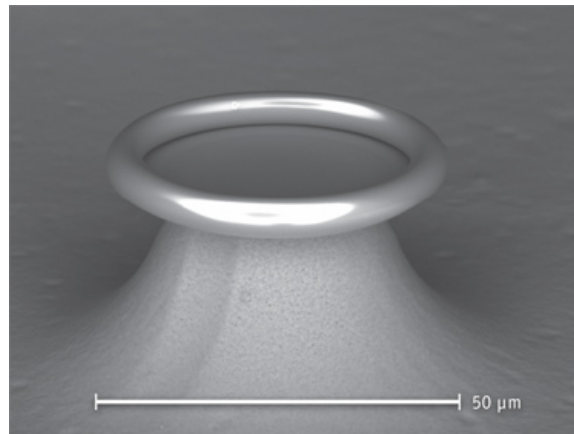
Figure 1.18: A ring shaped whispering gallery resonator [94].

1.3.2 Liquid Crystal Laser

Liquid Crystal Laser [95, 96] are very small dye lasers where an organic dye provides the gain and a chiral liquid crystal, like CLC or SmC*, provides the feedback. This kind of laser is called mirrorless laser because the feedback, necessary for amplification, is not provided by external mirrors but by the distributed feedback throughout the periodic structure of the LC host material. This generates a mode selection because only a few modes are promoted. One of the major advantages all dye lasers show is the frequency tunability and the very narrow linewidth of the emitted light. Nevertheless the tunability is limited to the dyes emission bandwidth of usually 30-60 nm. But the use of dye mixtures, pitch gradients or different configurations of the same materials enables tunability over the whole visible range of light. The frequency tunability is possible because the Bragg conditions can be influenced by various external stimuli (see section 1.2.1). LCL are pumped by pulsed non-tunable solid-state lasers although, after first attempts by Coles et al [97], continuous pump conditions have been successfully established recently [98] for the

first time. There is a wide range of applications for these lasers, naming just a few: non-linear optics, communication, spectroscopy and medical applications.

The history of DFB lasers started in 1971 [99] where Rhodamine 6G was incorporated into a periodic stack of gelatin films. The resulting Bragg scattering on the periodic structure provided the feedback necessary for lasing whereas the dye acted as a gain medium. Additionally the periodic structure restricted the oscillation to a narrow spectral range. Fundamental results have been obtained for the modulation of the refractive index according to theoretic explanations. The frequency difference between the lasing band and the Bragg frequency is determined by

$$\omega - \omega_{\text{Br}} \approx \frac{\pi c}{2nd} \tag{1.10}$$

where c is velocity of light in vacuum. It is only determined by the average refractive index n, the total thickness of the stack d and independent from Δn. The threshold gain α_{th}

$$\alpha_{\text{th}} \approx \frac{\lambda^2}{\Delta n^2 d^3} \tag{1.11}$$

dramatically decreases with increasing stack thickness d and increasing optical anisotropy Δn. This fact plays an important role when low Δn materials like derivatives of cellulose will be used as feedback material (see section 1.3.3). For the modulation of the gain material the lasing frequency coincides with Bragg frequency ω_{Br} and the lasing threshold is solely determined by the stack thickness. Further theoretical considerations have been made by deVries [80] and Kats, while the latter one solved the Maxwell equations for this case, which remain unchanged until today.

In 1973 it was realized that the periodic structure of a CLC, due to the strong refractive index modulation, is a suitable candidate for DFB lasers. In a patent [100] cholesterol derivatives where doped with an organic dye while the dyes emission and the PBG of the CLC were overlapped, but no experimental results were shown. It took almost seven more years until the first experimental proof of lasing with a dye doped CLC was published [101]. A very narrow PBG from cholesterol derivative mixtures with very low optical anisotropy generates very narrow laser lines, tunable over 40 nm utilizing temperature variation. The authors mentioned that the emission occurred at the center of the cholesteric reflectance band. Because this

band is so narrow, the generated emission lines from the bandedges merge forming single or multi mode signals. Later experiments with high optical anisotropy LCs showed clearly distinguishable lines emitted at the band edges of the cholesteric bandgap. Because of the high optical anisotropy the bandwidth is much bigger than for the cholesterol derivative mixtures [102].
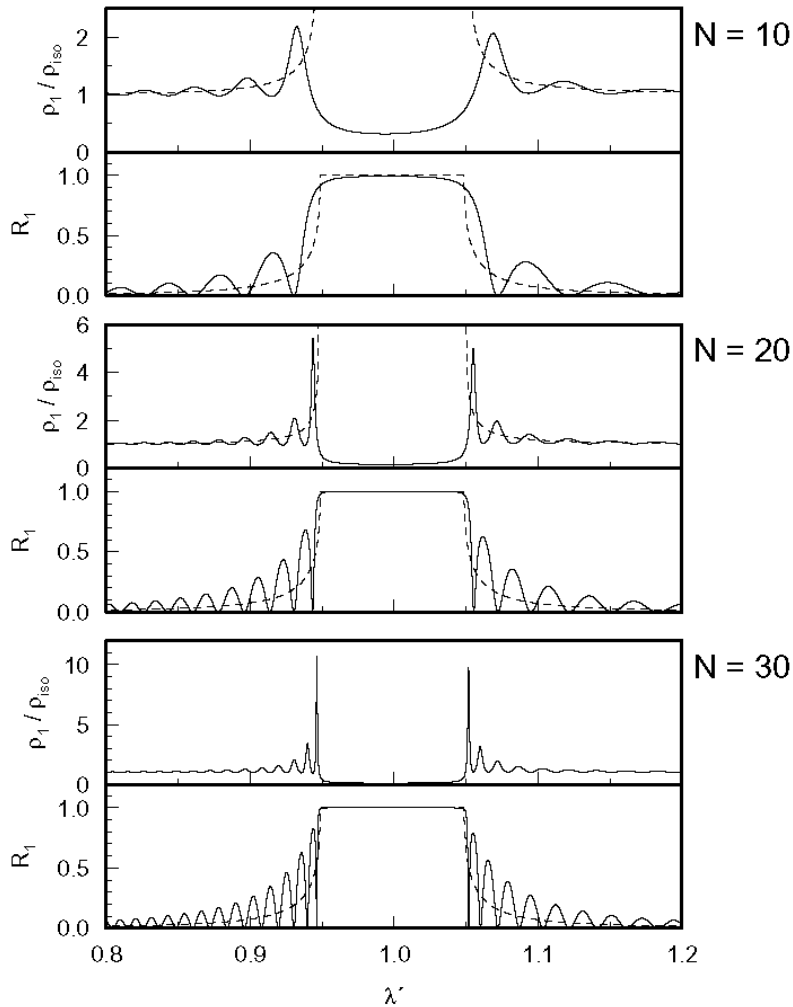
Figure 1.19: Relative DOS $\frac{\rho 1}{\rho iso}$ and reflectivity R1. Solid curves calculated for the film thicknesses N indicated on the right; dashed curves calculated for infinite thickness (i.e., neglecting multiple reflections) [103].

The key concept of DFB laser is the density of optical modes or density of states [95] (DOS) known from the physics of solid state lasers (see figure 1.19). DFB laser provide resonance through their periodic structure and possess high degrees of spectral selectivity. Light propagation only occurs for allowed (or cavity) modes whose number is proportional to the density of states. The number of states ρ is

given by

$$\rho(\omega) \quad = \quad \frac{dk}{d\omega} \tag{1.12}$$

where k is the wavenumber and ω is the frequency [104]. According to Fermi's golden rule the probability of photon emission is proportional to the DOS [105]. Inside the PBG of a CLC the DOS is suppressed but enhanced at the bandedges. When calculating the density of states it reaches its maxima at the bandedges of the cholesteric stopband [103]. Here the photon velocity decreases to zero while the photon dwell time increases to infinity because of multiple reflections from the periodical structure. The effective light path along the helical axis is elongated in the amplifying medium and the threshold becomes lowest at that frequencies corresponding to the longest dwell times. This is observed for wide bandgap CLC materials. For low Δn materials the emission wavelength with the lowest threshold appears at various positions throughout the bandgap because the bandedge is not as sharp as for high Δn materials. Additionally the two bandedges are very close together so their thresholds are very similar. The bandwidth $\Delta\lambda$ of a CLC is determined by the optical anisotropy Δn and the pitch of the CLC (Equation 1.5). The stimulated emission of the gain material in a DFB laser at that frequencies where the DOS reaches its maxima can be considered as a standing wave. For one of the standing waves (in-phase) the polarization direction is always parallel to the director and feels the extraordinary refractive index of the LC and has a lower energy which corresponds to the low energy bandedge. Therefore the threshold for the low energy bandedge is lower than at the other bandedge, where the polarization direction is perpendicular to the director (out-of-phase standing wave). Lasing may be found first at the low energy bandedge, but at sufficient high pumping power at both edges [106].

Over one decade later, with advanced characterization technology, the mechanism of bandedge lasing was understood in terms of the photonic bandedge effect. The interpretation of the bandedge lasing was made by comparison of the density of modes spectra, which were found experimentally as a ratio of emission intensities of the left and right handed circular polarized modes. The emitted laser light from CLC is circularly polarized with respect to the twist sense of the host CLC. The emission frequencies can be tuned by various external stimuli (see section 1.1.3) which are shifting the PBG of the CLC to the blue or to the red. If the threshold is reached the emission from the dye doped CLC changes from incoherent fluorescence to co-
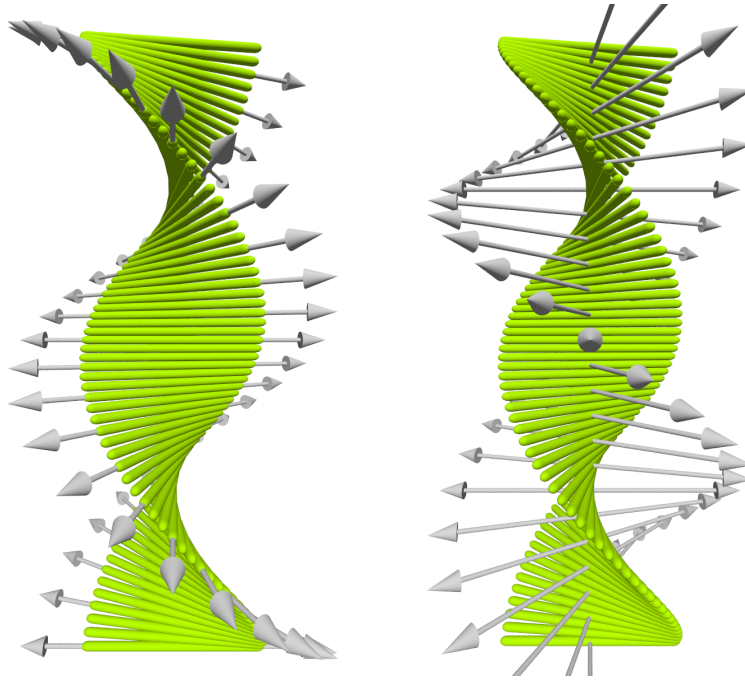
Figure 1.20: In-phase (left) and out-of-phase standing wave in a liquid crystal laser. The polarization direction of the gain material emission is indicated by the grey arrows.

herent laser emission with long coherence time and length. Even lasing without any additional dye was observed from a fluorescent CLC [107]. The same group showed one year later that lasing is also possible from the cholesteric blue phase II [108], which represents lasing in three dimensions due to the unique optical properties of blue phases. Another attempt of 3D lasing has been made by preparing cholesteric droplets with radial helical axes. The bandgap of a 1D photonic crystal is now applied to a spherical geometry as well as the resulting lasing emission [90]. The concept of a defect mode is borrowed from solid state lasers, too [95]. Photon localization at a defect in the photonic structure can also lead to mirrorless lasing devices operating at lowest thresholds. A defect in the photonic structure creates fine bands of allowed transmissions inside the PBG, if it exceeds a critical thickness (see section 1.2). A defect is created by an isotropic or an anisotropic layer between adjacent CLC layers where the position within the PBG is related to the refractive index of the defect layer [109]. Furthermore several other techniques have been developed to introduce defect modes into the PBG of CLC: Phase shifts [110], particle stabilized defects [111], deformation of the CLC helix [112], which leads to a tunable defect mode position and local polymerization [113]. The threshold of defect mode lasers are the lowest among all CLC lasers and are as low as a few nJ

per pulse [114].

Besides those two possibilities for a defined feedback mechanism, random lasing is an additional way of mirrorless lasing. A dye is dispersed in a media with scattering particles like titanium dioxide or in a CLC with a high number of domains. Another way to generate random feedback is to use droplets of CLC at very small size [115]. The feedback is generated by reflections at boundaries between the isotropic media and the scattering particles or at the domain boundaries in the CLC. Because of the random organization of the feedback material the amount of possible losses is higher than in a ordered sample with a monodomain cholesteric structure. These losses, due to light that escapes from the sample without being scattered back to the inside, can be reduced by increasing the number of possible scatters, increasing layer thickness or dye concentration. A higher dye concentration provides more gain and stronger scattering increases the time the light is trapped in the sample. The aim is to trap the emitted light as long as possible inside the sample until lasing action occurs [116]. The aggregation of scattering particles in these materials is usually prevented by solidification of the sample through polymerization or the usage of high viscosity materials [117]. If a random material is infiltrated with a liquid crystal, different layers of mesogens can act as scattering boundaries because of different refractive indices. Here the amount of scattering becomes temperature dependent as the LC goes through different states with changing temperatures.

The emission characteristics of random lasers are somehow in between a common laser and a light bulb. There is no defined emission direction because of the randomness of the sample. This causes a much broader emission linewidth but, nevertheless, the color spectrum is well defined. Additionally the threshold is higher than for well ordered structures [115]. But their preparation process is more easily because only a homogeneous sample has to be prepared regardless its alignment.

All of the previous mentioned LC lasers have something in common. They are of microscopic size, show tunable emission properties and are cheap and easy to prepare (if you know how) because of the LC self assembly. But they suffer from the same problems most of all dye lasers have. The dye is bleaching very fast upon optical excitation and with increasing threshold. During the pumping a lot of heat is generated, affecting the CLCs properties, if they are not fixed. In addition there is only one setup allowing continuous wave emission [98]so far.

1.3.3 Lasing in Liquid Crystalline Polymers

Polymerization is a useful tools to fix alignment in organic samples. As liquid crystals are fluids their alignment can be easily influenced, but after the alignment a permanent fixation is advisable. Especially during the pumping of the sample a lot of heat is generated, disturbing or changing the LC's properties. Polymerization can be accomplished if the LC itself is polymerizable [112] or the solvent in lyotropics contains acrylics for example. The resulting films can be prepared as free standing ones and, depending on the use of crosslinker, be rigid or flexible. Bending these films can be used for focusing or widening the emitted beam. One special type is the group of liquid crystalline elastomers made with cholesteric order and allowing tunability through mechanic stretching [118].

Besides the polymerization of low molecular weight LC, the usage of liquid crystalline polymers have attracted interest. Though, in comparison to low molecular weight LCs, the number of publications of LCP is still very limited. The cause is the optical quality of the resulting films from LCP. Due to their molecular weight, melting occurs only at elevated temperatures and solutions above the critical concentration show very high viscosities. The combination of huge molecule size and high viscosity makes alignment to well oriented monodomain samples very difficult. Additionally the refractive index anisotropy is very small for many LCP originated from natural polymers like cellulose [119]. Hence the index contrast between the layers in polymer CLC is very weak, decreasing internal reflections and the quality of the cavity. Lasing at the band edges in planar CLC requires a very high quality alignment and a monodomain film. There threshold is very low and the slope efficiency increases. But multidomain samples can have advantages, if defect mode or random lasing is desirable. In this case the domain boarders represent defects creating additional modes inside the PBG or act as random scattering objects needed for random lasing [119].

So far different polymers have been utilized to create cavities for mirrorless lasing samples. There are synthetic polymers like PBLG [119], polyisocyanates [120], aromatic polyester [121] and polysiloxanes [122] or derivatives of natural occurring polymers like cellulose [117]. Samples prepared from these materials have the same previously mentioned limits in common. If lasing is possible at the band edge the thresholds are very high or only defect mode or random lasing can be observed. Samples of the latter mode need to have an increased thickness to provide a sufficient feedback because of the low scattering intensity at the domain boundaries. Different preparation methods like spincoating [121] have been applied to enhance

the optical quality. In total only these few papers report about band edge lasing in polymeric samples and those show very broad or multimode emissions. Properties like diffraction rings and very narrow spectral width of the emission, as usual for lasing experiments with low molecular weight CLC, have not been shown due to the imperfection of the alignment.

Polymers, especially those derived from natural sources, are very desirable for cavity preparation because of the use of renewable resources and easy synthesis. Their low refractive index anisotropy offers one big advantage. If the CLC is close to perfect orientation the scattering of light outside of the PBG is very low. In result the films are very transparent and the liquid crystal does not absorb any of the pump light. Architectures with multiple stacks of different films are realizable because the films do not absorb the emission of their neighboring films. As a consequence of the low refractive index anisotropy the bandwidth of the PBG is much lower than for low molecular weight CLC which can be tuned in very small steps. So it is possible to achieve many samples with different emission wavelengths from the same LC dye mixture.

1.4 Nanoparticles

The word nano is repeatedly used in today's science articles as well as in TV advertisements. Nanoscience is one of the most rapidly growing fields in science, due to remarkably interesting properties of nanoparticles, which differ completely from their macroscopic counterparts made of the same material. During the last 20 years the optical, electric, magnetic and other properties, various synthesis and stabilization methods and nanoparticle architectures have been developed [123].

In principle particles in the range of 1-10 nm are considered nanoparticles, although particles up to 200 nm are often called nanoparticles in the literature. They are mainly made of metals or metal oxides. Their synthesis is done by reduction of metal salt solutions with reducing agents or radiation, electrochemical dissolution or matrix assisted growth of metals where other molecules are present, which actively attach to the growing particles surface. These, mostly organic, surfactants have a great influence on both, shape and size of the synthesized particles. Furthermore all reaction conditions like solvent, concentrations, temperature and reducing agents affect the synthesis' product. Surfactants cover two different aspects during the synthesis of nanoparticles. First of all they prevent growing nanoparticles from agglomeration and secondly they preferably interact with certain surfaces of the

nanocrystals which enables one to synthesize different shapes of particles by choosing the right surfactant. Surfactants consist of an anchor group for the nanoparticles surface and a tail which provides sufficient solubility in the reaction medium. The bond between surfactants and NP needs to show a certain degree of fragility, because the growing process involves attaching and detaching processes to allow the NP to grow. Until today many different shapes like spheres, rods, wires, tri- and tetrapods, disks and cubes are realized [124]. They contain either only one or several different materials. Hybrid particles like a spherical dot with a rodlike shell [125] are synthesized via seed mediated growth.

Figure 1.21: Fluorescent semiconductor nanoparticles in solution. The emission wavelength is dependent on the particle size (increases from left to right) [126].

Consisting of a few to a few hundred thousand atoms NPs show properties between a solid state material and single atoms [127]. Because of their very small size the effective surface area is extremely large leading to a very high reactivity in chemical reactions. The amount of atoms at the surface increases if the size of the particle decreases. Atoms at the surface with a reduced number of neighboring atoms show a greater reactivity as those inside the particle. The combination of a high percentage of unsaturated atoms and high surface area enables NP to be very reactive catalysts. A second effect comes from the low number of atoms per particle. Here the amount of electrons is significantly lower than in the bulk material and hence their average distance to each other is much bigger. Hence there are discrete energy levels instead of a quasi continuous level throughout a macroscopic particle. While the level in big particles is fixed by the materials properties, the discrete levels change with the size of the NP. This is the reason why semiconductor nanoparticles show fluorescence with a size dependent emission wavelength (see figure 1.21). The energy distance between the valence and conduction bands varies with size, causing different colors when illuminated with UV-light. This ef-

fect is known as the quantum-size effect [128] because the particle boundaries act as geometrical constraints and electrons feel the presence of boundaries and adjust their energy levels. This tunability makes NP interesting candidates for the replacement of organic dyes, because NP are very resistant towards light and show very high quantum yields. Applications like LED [129], LC-Displays [130], hybrid solar cells [131] and lasers [128] are already realized.

1.4.1 Composites with nanoparticles

In addition to the remarkable characteristics of nanoparticles it is of emerging interest to create composites of these in organic matrices [132]. They combine qualities of hard inorganic NP like emission of light and those of the soft organic part, which is very flexible, easily synthesized and can be tuned with tools of organic chemistry. Although NP can be stabilized via electrostatic charges in aqueous solutions, their electronic properties are lost. Therefore the incorporation of NP into organic matrices can be used to maintain all the typical nano properties. Most prominent are composites of LC and NP, because LC offer a high degree of order and fluidity at the same time. The available anisotropic shapes of NP are in a good agreement with the shapes of mesogens. But guest and host material do not simply mix to give a homogeneous composite. The inorganic part always tends to minimize the shared surface with the organic host and forms aggregates, which do not provide typical nanoparticle qualities. The nanoparticle's surfaces need to be capped with suitable surfactants, preventing agglomeration. Often surfactants from synthesis are not bound as strong as required to prepare composites, so they need to be exchanged. On one hand low molecular weight surfactants can be used, having anchor groups that strongly attach to the surface and therefore replace the surfactants from synthesis and ensure a permanent surface modification. On the other hand polymers have proven to be useful tools to create surfactants with tailored properties. For example block-copolymers contain an anchor block with several possible attachment points creating a much stronger bond to the surface (chelate effect). The second block of the polymer can be synthesized according to the needs of the host material by various controlled techniques (see section 1.5). Due to their size, polymer surfactants create reliable distances between single particles necessary to prevent aggregation. This so called hairy-rod concept [133] can be extended towards polymer functionalized nanorods which self assemble into liquid crystalline phases without any additional organic matrix [57].
Nanoparticles in liquid crystals [134] create an immense interest in academia as

well as in the industry. They are used to combine the particle's properties and the tunability of liquid crystals. Furthermore NP are utilized to study defects in LC [135] or to stabilize liquid crystalline states [136]. Surfactants with mesogenic groups create a stronger link between the NP and the LC host for greater miscibility. Due to the self assembly of LC it is possible to align anisotropic NP in the same way the liquid crystalline template does [137]. There are lots of applications for inorganic-organic composites but their delicate synthesis and the used metals often create high costs, hindering an economical use where lots of material is needed. Technologies with nanocomposites, like dentistry or coatings, where only small amounts are applied, are already available. Often the inorganic part is needed to enhance the stability of the pure organic material. For example do composite coatings avoid scratches on plastics. Especially for glasses this is useful solution, given that NP do not scatter visible light due to their small size.

1.5 Reversible Addition Fragmentation Chain Transfer Polymerization

The controlled synthesis of well defined polymers regarding chain and block lengths, architecture, functionalities and polydispersity is a great challenge. Polymerization methods offering a high degree of control are often very sensitive towards impurities and require extremely pure reactants, reaction conditions and sometimes very long reaction times. On the other hand free radical polymerization is very easy to use under mild conditions and many monomers are usable. But due to the lack of control and the high reactivity of the reactants, well defined architectures are not available in a free radical approach. Lots of side reactions like transfer and termination of the reactive chain end form undesired products. Hence several methods which combine control and the advantages from free radical polymerization have been developed.

The anionic polymerization is the only example of a truly living polymerization. There are no side reactions that terminate the reactive chain end, hence the addition of monomer always results in growing polymers. The total number of growing chains at the same time is close to constant and all chains grow to a similar length. This is shown in polydispersity indices very close to 1 and a good control over the molecular weight. The molecular weight can be determined only by the concentrations of initiator and monomer, but ultra pure reactants and solvents under inert gas atmosphere are required.

a)

Initiator (I) $\longrightarrow$ I• $\xrightarrow{\text{Monomer (M)}}$ P_n•

b)

c)

R• $\xrightarrow{\text{M}}$ P_z•

d)

e)

Initiator + Monomer +

Figure 1.22: Detailed mechanism of the RAFT polymerization
(for explanation see text).

Methods like NMP, ATRP and RAFT are called "quasi living" because they gain
control over the chain growing process via special reactants which suppress side
reactions. This can be done if the reactive chain end is converted into an inactive,
so-called dormant, species but can be revived reversibly. There is an equilibrium be-
tween the actively growing and the dormant state. In comparison to the initiation

rate the growth rate is low, ensuring a close to equal growth to all chains, obtaining a product with a low polydispersity. During the RAFT reaction [138] a chain transfer agent is added which converts active chain ends into dormant species but releases it reversibly for chain growth after a fragmentation reaction. Sulfur containing molecules like dithio esters and dithio carbamates are often used as CTA. The detailed mechanism is shown in figure 1.22. The polymerization is started with classical radical initiators a) creating chains with a radical at the end. These growing chains react with the CTA to the dormant species and the residue R b). The residue contains a radical capable of adding monomers c). If now a growing polymer chain reacts with a sleeping species the previously bound polymer chain is set free to grow further. This addition fragmentation mechanism d) is very quick, which provides equal possibility for all chains to grow. It runs until all monomer is consumed or the reaction is stopped e). At the end of the reaction all polymers contain the CTA as an endgroup. As long as this group is not deactivated or cleaved from the polymer chain, it is capable of adding monomers. Block-copolymers synthesis is possible with this reaction. After the first cycle the polymers with CTA endgroups are purified and a second polymerization with another monomer and fresh initiator can be run. The residues R and Z at the CTA need to be adjusted according to the monomer used. With choosing a special fragment for Z a selective endgroup modification is realizable. To prevent side reactions the CTA endgroup should be cleaved at the end of the final reaction polymerization. In conclusion this method provides good control over molecular weight, polydispersity, architecture and block length under mild and easy conditions.

In combination with the RAFT method the use of reactive ester polymers is advantageous to synthesize polymer surfactants with defined architectures and anchor groups. Although RAFT polymerization is very tolerant towards functionalities many monomers cannot be polymerized directly. In this case reactive ester monomers can be used to polymerize a polymer block convertible via polymer analogous reaction afterwards [139]. Monomers with reactive ester sidegroups are easy to polymerize and react with nucleophiles like amines. The synthesis of a polymer surfactant, to disperse nanoparticles in an organic host material, is done by the following steps. A first block of a monomer, very similar to the structure of the organic host, is polymerized via RAFT. After purification a second block made of reactive ester monomers is added via RAFT, too. The CTA endgroups are cleaved and the reactive ester is reacted with amines containing the anchor groups for the particle's surface. The functionalized nanoparticles then show increased solubility

in the organic host and aggregation in minimized. Using this technique a whole library of different anchorgroups can be attached to the same polymer, to disperse different inorganic nanoparticles in the same organic host.

1.6 Microfluidics

Microfluidics [140] is a microfabrication technique to synthesize microsized polymer particles. In contrast to traditional techniques like heterogeneous polymerization or precipitation processes, particles made from microfluidics show a very narrow size distribution and a continuous production is possible. Particles generated via microfluidics can be polymerized downstream. The fluids are processed in small channels with diameters in micrometer regime.
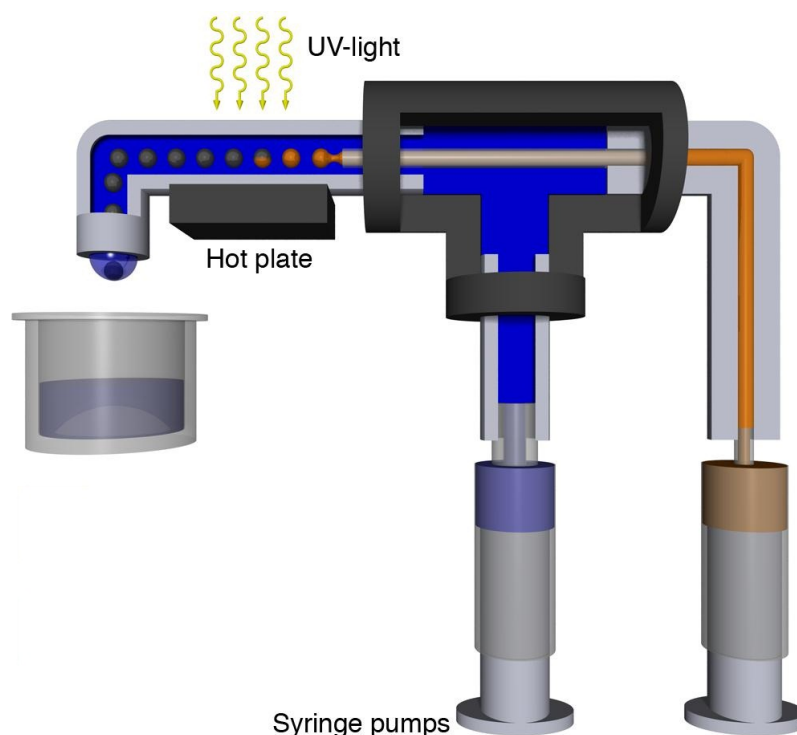
Figure 1.23: Schematic of a co-flowing injection microfluidic device (blue = carrier fluid, orange = monomer) [141]

Two different ways are common to create micrometer sized channels: Lithography [142] or micro milling [143] produce channels in planar substrates at very high resolutions and complex geometries but only of rectangular shape. The second way is the use of very thin capillaries connected via standard methods. Geometries are more simple but capillaries are commercially available in very different shapes,

allowing the preparation of non-spherical particles. The most common method is to emulsify a liquid monomer in an immiscible carrier fluid and polymerization yields solid droplets. The easiest technique to emulsify two immiscible fluids is co-flowing injection [144] (see figure 1.23).

In this setup the material, from which the particles are made, is injected through a thin needle into a surrounding microtube channel with the carrier fluid going through. If the flow rates of both liquids are tuned properly the carrier fluid rips of small droplets from the tip of the needle in dripping mode. In jetting mode a jet of monomer leaves the needle collapsing into droplets further downstream. Under different flow conditions it is possible to prepare fibers [145] instead of particles. Particle size and shape are adjustable by different parameters like flow conditions, capillary dimensions and flow profile. The parabolic flow profile causes shearing motion that introduce alignment forces at the particles surface. As liquid crystals can be oriented with shear, droplets of liquid crystalline materials show interesting alignments. Additionally the particles shape is often in conflict with the liquid crystals preferred alignment. Particles made of liquid crystals, especially cholesteric liquid crystals, show very special optical properties and defect structures. Different director orientations originate different optical qualities [146], some are useful for lasing applications [90].

2 Scope

The scope of this work was the preparation of liquid crystal/chromophore composites capable of mirrorless lasing. The liquid crystalline host was to be made of derivatives of cellulose dissolved in a polymerizable monomer solution. The gain material were organic dyes, used in known systems, or inorganic nanorods.

Following from the preparation of such composites, two main issues have to be accomplished. The optical quality of the liquid crystalline host came in first place. The properties were tuned to the same level which low molecular weight liquid crystals exhibit. In addition the tunability of the host was to be studied to match the optical properties with those of the gain material. As a natural resource, cellulose is available in large scales and can be converted very easily into liquid crystalline derivatives. Films of those did not need alignment layers and were polymerizable. They self assembled towards photonic structures providing resonance for light waves. Cellulose was the material of choice because the rodlike shape of the resulting mesogens and their size is very similar to those of inorganic nanorods. Inorganic nanorods are proven to be very stable towards light and chemicals and were supposed to be a good replacement for organic dyes. Additionally their optical properties are tunable and, in combination with the tunability of the liquid crystalline host, a wide range of different composites were able to be prepared from the same materials. A replacement of organic dye is advisable, because of their quick bleaching during the pumping of lasing films. It was speculated that molecular object, similar in their geometrical shape, mix to homogeneous composites better than rodlike shaped mesogens with spherical nanoparticles. As phase separation between host and guest materials was the second issue to solve, the synthesis of defined blockcopolymers as surfactants was necessary. Alongside the shape match between guest and host material, the surface modification of the guest particles with polymers was expected to ensure a molecular dispersion of nanorods as a steady state. Polymerization of the composite afterwards was meant to permanently fix the alignment of the liquid crystal as well as the distribution of the guest material. The lasing behavior of composites with nanorods or organic dyes was to be investigated and a comparison with already existing systems to be done.

In a second project the technique of microfluidics was to be used to prepare microparticles of the above mentioned liquid crystalline mixture. This technique, applied to liquid crystalline elastomers, was to be extended to lyotropic liquid crystalline polymers. The processing of highly viscous liquid crystals was to be realized and the influence of the flow shear to the liquid crystal alignment and the optical properties of the resulting microparticles was examined.

3 Results and Discussion

3.1 Overview

As mentioned in the scope of this thesis (see section 2) it was the aim to prepare composite films made of a cellulosic liquid crystal and organic or inorganic chromophores. In densely packed systems packing constraints dominate the miscibility of both compartments. Rodlike inorganic nanoparticles do have the same shape as calamitic mesogens and CTC are of similar length than the nanorods. In addition to the camouflage of the NP with tailored surfactants, to induce a chemical match, we suppose a good miscibility both molecules due to similar shape. Upon optical excitation these films are supposed to act as mirrorless lasing devices, where the liquid crystal provides the feedback and the chromophore the gain. As composites consist of several ingredients the results of this thesis will be split into five main parts, covering all aspects on the way to lasing films and the preparation of cholesteric microparticles. Starting with the feedback material it will be shown how the optical properties of cellulosic liquid crystals can be improved until a sufficient feedback is provided. In the second part the synthesis of defined polymers and their employment as surfactants for inorganic nanorods as well as composite preparation is described. Parts three and four cover the preparation of organic dye - CLC composites and their behavior under optical excitation. The last section is about the attempts to prepare cholesteric microparticles from the same liquid crystal utilized for mirrorless lasing films. Every part will start with an introduction to show the state of the art in literature and what was the starting point for this thesis. The requirements, as well as a comparison to already existing work, will be drawn. At the end of each part a short conclusion summarizes the main achievements and gives an outlook to possible future experiments.

3.2 Feedback Structures Made of Cellulose Derivatives

3.2.1 Introduction

A cholesteric liquid crystal, made of derivatives of cellulose dissolved in acrylic monomers, is the material of choice to prepare films with a photonic structure, causing a feedback mechanism. CTC match the size of the preferred inorganic guest molecules and an acrylic solvent provides the possibility to polymerize to the sample. A very high quality of the cavity is mandatory to achieve lasing action at sufficient low thresholds. The use of a LCP [120, 119, 121, 117, 122] and polymerized liquid crystals [112, 147] was documented already in literature. About LCP cavities it was reported that their optical quality limit their application as feedback materials. A low refractive index anisotropy and bad alignment properties do not match the requirements for a cavity of mirrorless lasing devices. A photonic structure with close to ideal alignment in the planar state is needed. This includes a well defined PBG perpendicular to the substrates and a monodomain film or very well aligned domains with a low number of defects in between. Furthermore the material needs to be tunable to fit to the emission of the gain material and be polymerizable to fix the alignment permanently. Finally the liquid crystal should be miscible with inorganic and organic gain materials.
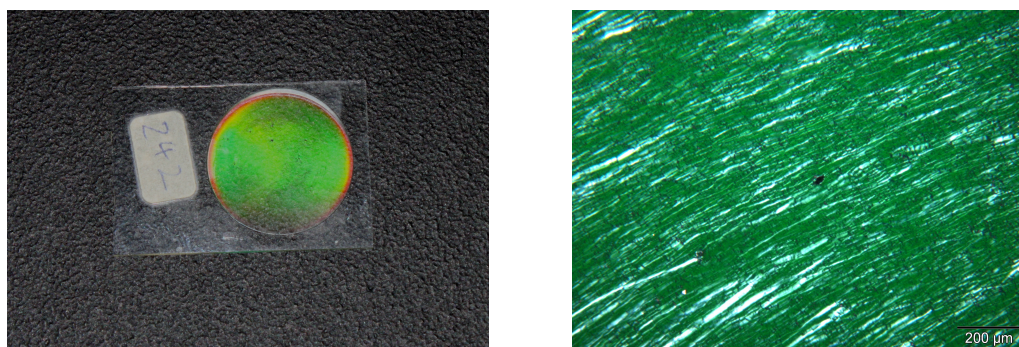
Figure 3.1: Photograph (left) and POM image of starting CLC films made of CTC (45% w/w) with m-trifluoro methyl phenyl residues dissolved in DEGDMA.

Cholesteric films of cellulose derivatives have already been prepared by Müller et al [29]. This was the starting material for this thesis (see figure 3.2) A solution of 45% w/w of CTC (DP $\approx$ 230, based on Avicell PH101 cellulose) with m-trifluoro methyl phenyl residues in DEGDMA and Lucirin TPO as UV-initiator. The mixture was left to stand for several days forming a homogeneous solution. The highly

viscous material, prepared between two flat glass slides, exhibits cholesteric order, visible by the selective reflection of light. But taking a closer look at the films, the alignment was truly bad in comparison to low molecular weight LC. It can be seen in figure 3.1 that the film appears greenish. On the other hand the POM image on the right indicates a lot of defects (bright lines) oriented in the same direction of the material flow during film preparation. To verify the alignment's and therefore the optical quality, reflectance and transmittance measurements have been conducted (see figure 3.3). The grey graph shows the film's transmittance perpendicular to the substrate. The transmittance value does not exceed 90% because of light scattering at domain boundaries. Since the used CTC do not absorb light at wavelengths between 300 and 700 nm, this turbidity has to arise from the multidomain structure of differently oriented domains in the sample.
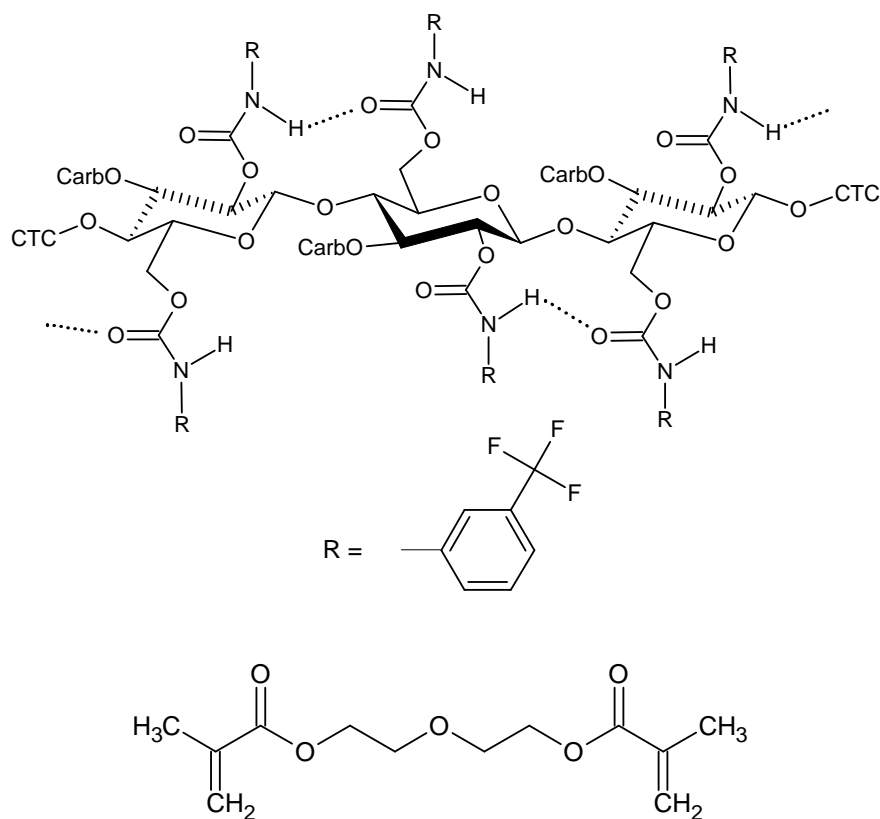
Figure 3.2: Chemical structures of the starting CLC ingredients: 3-(trifluoromethyl) phenyl urethane of cellulose (top) and diethylene glycol dimethacrylate (DEGDMA).

Outside of the bandgap the films should be as transparent as possible ensuring no absorbance or scattering of the pump light. This is of dire need since all the pump light is supposed to be absorbed by the gain material throughout the whole film. In
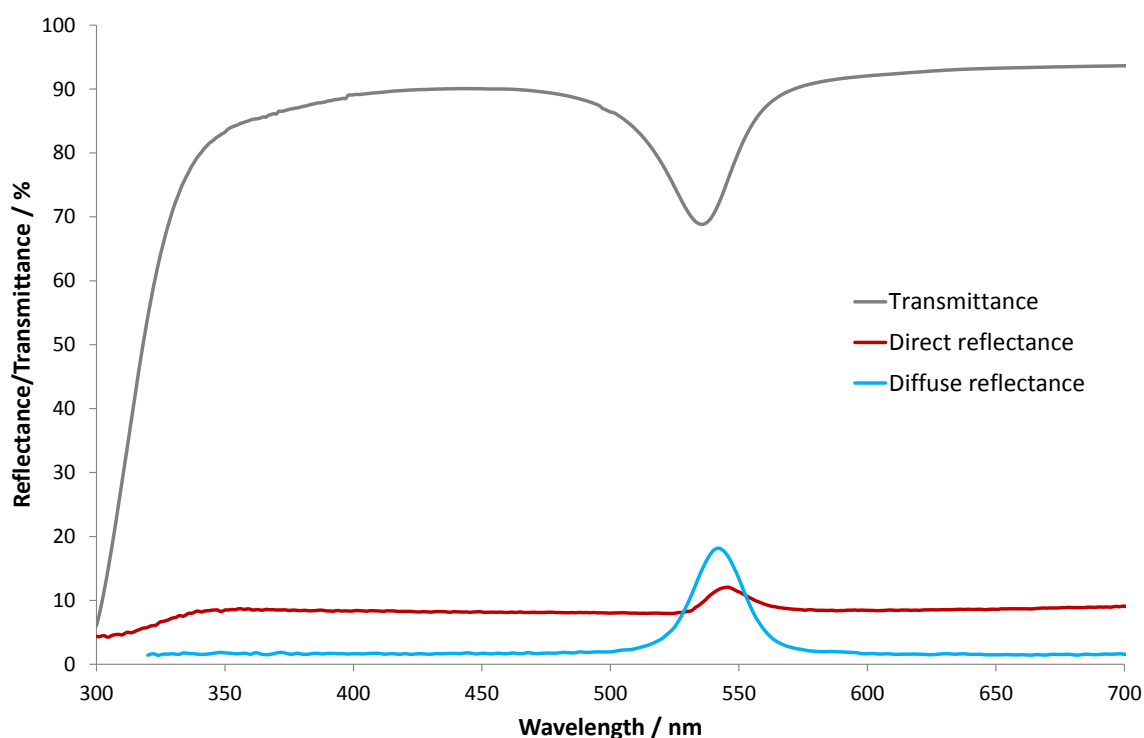
Figure 3.3: UV-VIS spectra of starting CLC films made of CTC (45% w/w) dissolved in DEGDMA.

theory 50% of the incident light should be reflected, which creates a peak of 50% in both spectra, transmittance and reflectance. Here a peak in transmittance is present with a maximum at 540 nm but its intensity is only $\approx$ 20%. The presence of this peak confirms the cholesteric nature of the material, though as the peak's intensity is low a bad alignment can be presumed. A second evidence for bad alignment is the width of the PBG. As CTC are known to show a very low refractive index anisotropy, a well aligned sample would exhibit a very narrow PBG with a FWHM $\approx$ 20 nm. Here the width is much bigger for this low intense peak. Additional bandwidth is created through a pitch distribution because of defects or variations of the angles of the helical axes towards the substrate. The red graph shows the amount of reflected light perpendicular to the film surface. This peak should have an intensity of 50%, too, or at least the same as the one in transmittance. In fact it is much lower. The total amount of light which is not allowed to pass through the film is indicated by the peak intensity in transmittance spectra. But the direction of the reflected light can be estimated by reflectance measurements. Only a small percentage is reflected perpendicular to the film, shown by the intensity of the direct reflectance peak. The rest is reflected at various angles indicated by the blue graph. Here

all the light, which is reflected not perpendicular to the film, is measured by an integration sphere, also known as an Ulbricht-sphere. The sum of both intensities, from the blue and the red graph, is equal to the grey one. In a well aligned sample (see figure 1.17 for comparison) the whole amount of reflected light is reflected perpendicular to the film.
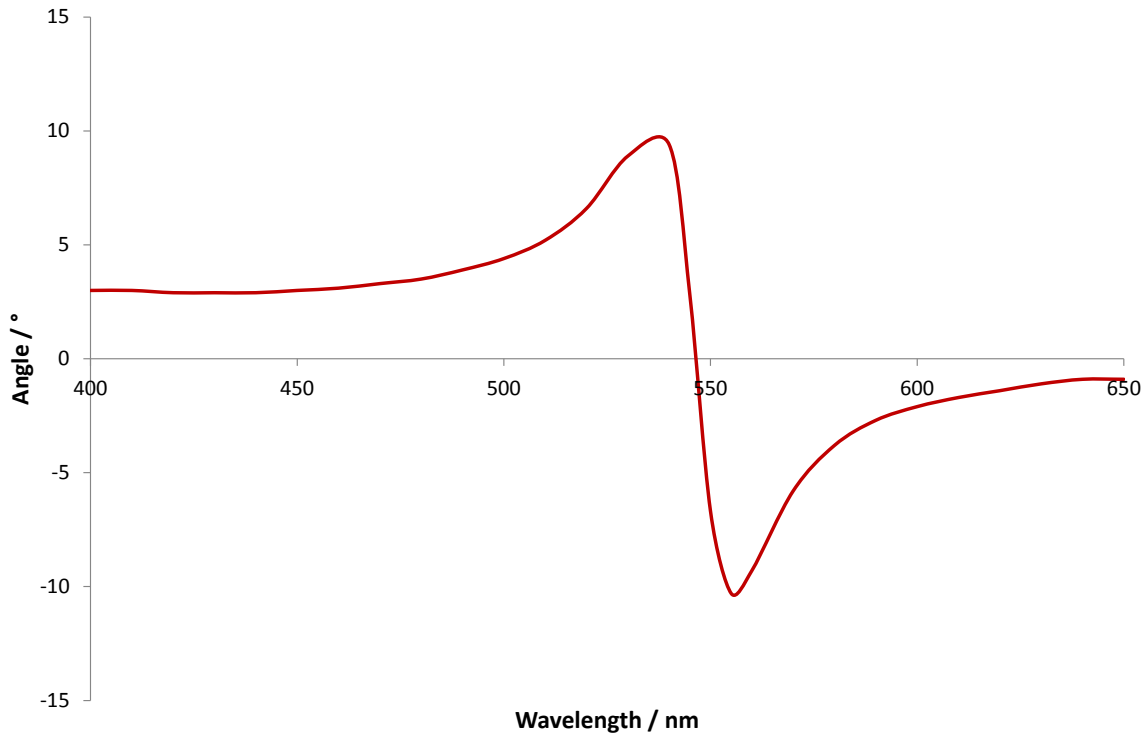
Figure 3.4: ORD spectrum of starting CLC films made of CTC in DEGDMA.

Another method to verify and somehow quantify the cholesteric order is optical rotation dispersion (ORD) [148]. Here the rotation of the polarization plane of linear polarized light is measured. Linear polarized light (LPL) can be split to left (LCPL) and right handed circular polarized light (RCPL) of equal amounts. In chiral media LCPL and RCPL do have different refractive indices and hence travel through the medium at different velocities. After passing through a chiral sample, which does not absorb in this wavelength range, both are recombined to LPL but its polarization plane has rotated. If the sample absorbs or reflects one of the circular polarized parts (in the CLC case along the helical axes), the passed through light is elliptically polarized. This is because the combination of different amounts of RCPL and LCPL produces a vector rotating within an elliptical shape perpendicular to the propagation direction. In an extreme case one of the circular polarized components is completely absorbed or reflected (at the center of the PBG in cholesterics) and

the incident LPL is converted into circular polarized light. This so-called Cotton effect, based on the circular dichroism or the difference of absorption coefficients for RCPL and LCPL, causes an S-shaped curve in ORD spectra. The twist sense of the sample can be determined according to the shape of the curve. Starting at short wavelengths, in cholesteric samples, the angle of rotation changes with increasing wavelengths and approaches a maximum close to the center of the PBG. Up to this point the transmitted light is elliptically polarized because of an increasing amount of reflectance for one of the incident circular polarized components. At the center of the PBG the curve crosses the zero line because the incident light is converted into circular polarized light. This is due to the total reflection of one of the circular polarized components and hence no rotation of the polarization plane can be determined. Following right after the center of the PBG the curve reaches a minimum before approaching an asymptote below the zero line. As stated in the introduction to this thesis, cholesterics exhibit extreme values of optical rotation. In figure 3.4 the ORD spectra corresponding to the UV-VIS spectra in figure 3.3 is shown. The angles are below $15°$ and the line between the two maxima is not very sharp, indicating a low circular dichroism and hence a bad alignment. The S-shape of this curve is called a negative Cotton effect showing a right handed helical twist sense in the cholesteric medium.

A thesis done in Marburg, dealing with chromophores in CLC made of cellulose esters came to the conclusion, that these materials are not capable of forming well aligned samples [149]. With the previous mentioned aspects, in addition to those in literature about the reflectance properties of cholesteric LCP, there is a significant need of improved alignment. Many papers, reporting about optical properties of cholesterics, show only transmittance spectra and conclude that the shape of the corresponding reflectance curve is similar. But, as shown previously, both curves may differ significantly: An evidence for bad alignment of the liquid crystal. In the following sections the way towards cholesteric films, made of derivatives of cellulose, with optical properties similar to those of low molecular weight LC, as well as theoretical predictions is described. The resulting films will be capable of providing sufficient feedback for defined bandedge lasing devices.

3.2.2 Solvents for Lyotropic CTC

This section will focus on the low molecular weight solvent, allowing the CTC to exhibit a liquid crystalline state. Solvents interacting strongly with the solute are capable to dissolve big amounts of it and maintain solutions without phase separation at high concentrations. Solvents containing carbonyl functionalities, like ester and keto groups, or with ether-groups are well suited for this purpose [65]. In contrast liquids with very high polarity are used as precipitation medium. For example CTC dissolve very well in acetone but precipitate in water. It must be pointed out that the volatility of acetone limits its, as well as many other suited and highly volatile organics, use regarding to film preparation. As the resulting films should be polymerizable, the solvents of choice are acrylates or methacrylates. (Meth)acrylates are the esters of (meth)acrylic acid and provide a wide range of residues, causing different polarities, vapor pressures and viscosities. Monofuntional and multifunctional (meth)acrylates are commercially available, where multifunctional ones yield crosslinked polymer networks if polymerized. The samples of Müller et al were prepared with DEGDMA as a solvent. This is a dimethacrylate linked by two glycol units in the middle. It shows a very low vapor pressure, suiting it well for film preparation. However, the liquid itself shows a very high viscosity and so does the resulting liquid crystal compound, as very high concentrations are needed for anisotropic solutions. The two functionalities and the large size of that molecule is responsible for the high viscosity of the liquid crystal, which creates two main disadvantages. First of all the time needed to prepare a highly concentrated solution is very long. As often reported in literature [150, 151] dissolution times range from a few days to several weeks and even mechanical stirring does not speed up the process very much. Second, the mesogens are very restricted in their movability during the preparation of films. The film preparation applies biaxial shear to the LC and due to the very high aspect ratios of CTC they tend to orient parallel to the shear direction. This supports a planar alignment, but only if the mesogens can follow the shear flow, which is not the case at very high viscosities. Therefore, the first issue was to replace the DEGDMA by another (meth)acrylate to obtain a LC with lower viscosity. The (meth)acrylate should provide a sufficient low vapor pressure, a low viscosity as an isotropic liquid, a small but not too small residue, a good solubility for the UV-initiator and it should be non-degradable to CTC.

Very small molecules like methyl (meth)acrylate do have a very low viscosity and yield low viscous liquid crystalline solutions but are, like acetone, too volatile for film preparation.
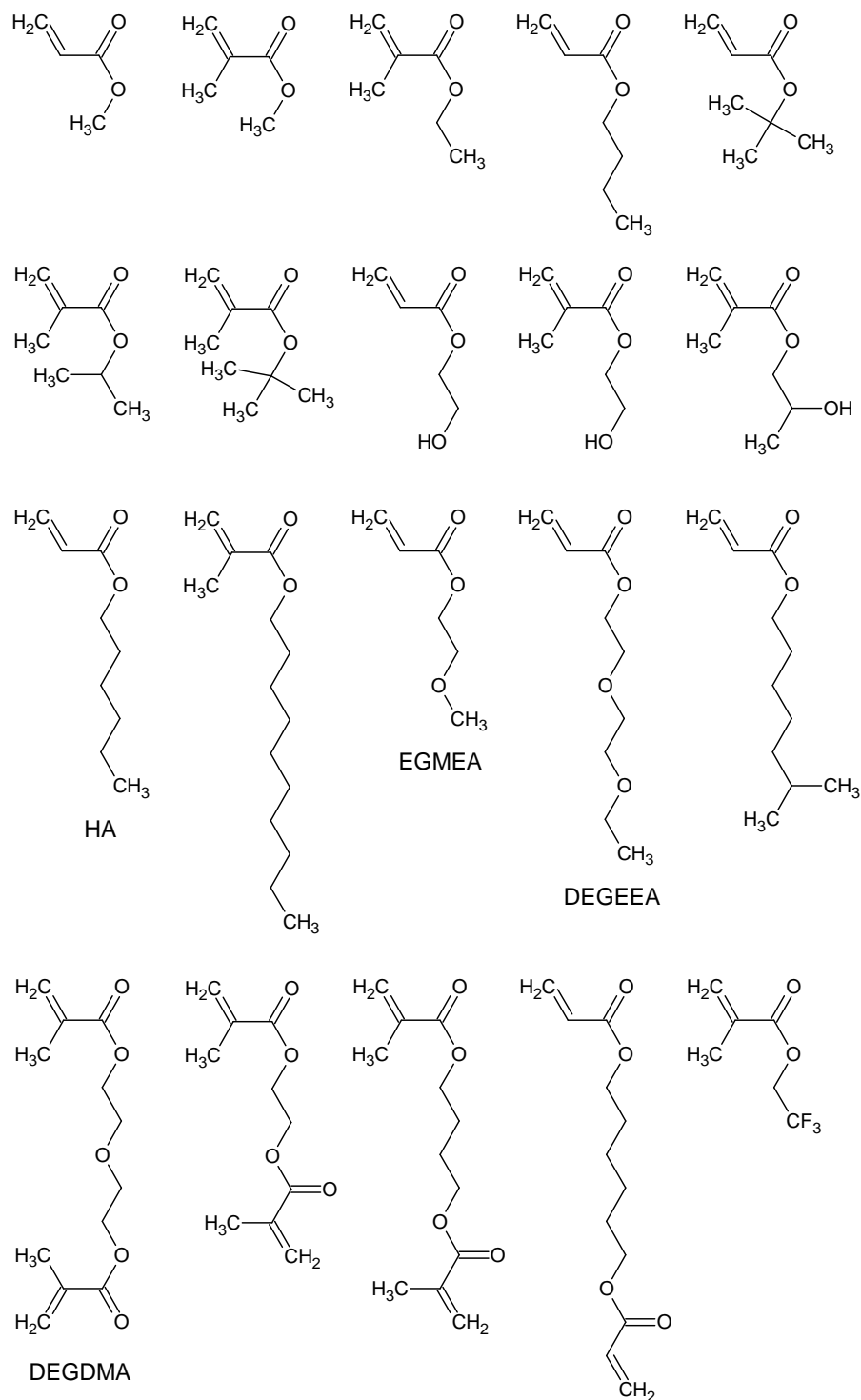
Figure 3.5: A selection of tested (meth)acrylates as solvents for CTC. Commonly used acrylics in this thesis are named with their abbreviations.

If the residue contains about 10 carbon atoms as in decyl acrylate, the vapor pressure is sufficiently high but the viscosity of the LC is even higher than for DEGDMA.
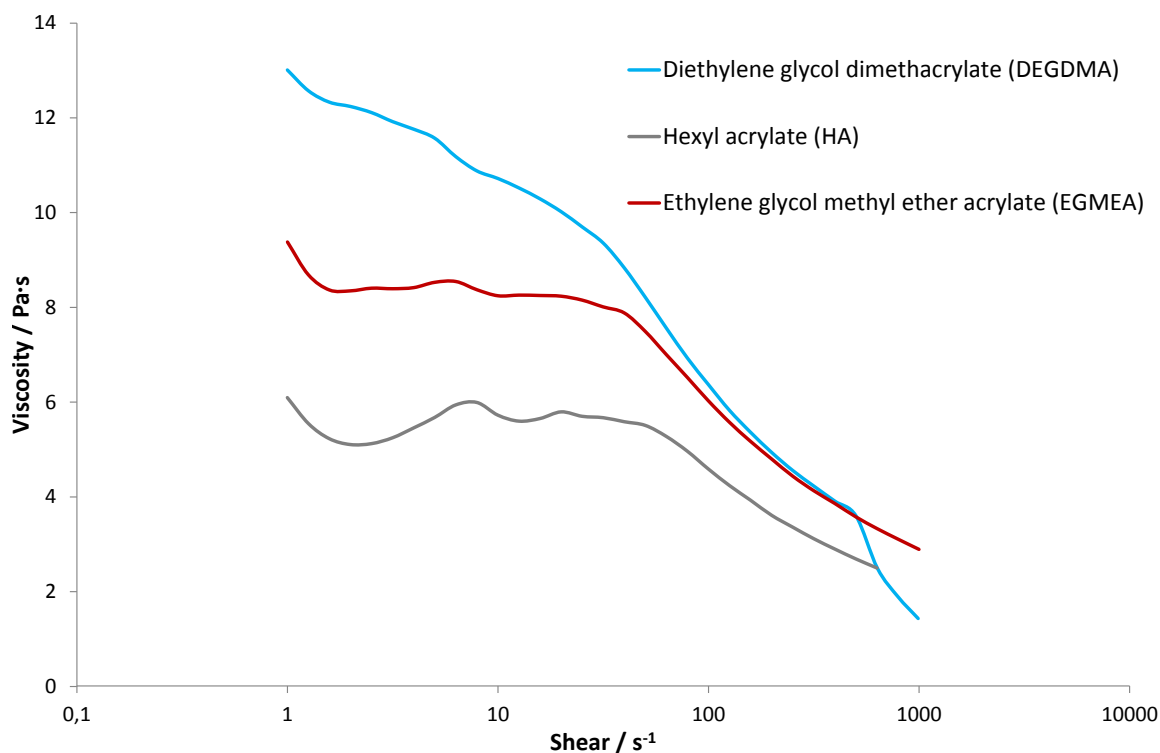
Figure 3.6: The viscosity of CTC with *m*-trifluoro methyl phenyl residues in different solvents at the same concentration in dependence to the applied shear.

Medium sized residues between four to six atoms, like HA and EGMEA, have shown to be a good compromise. As it can be seen in figure 3.6 choosing a different solvent can decrease the viscosity of the LC by almost 50%. In this figure the viscosity was measured in dependence to the applied shear. The shape of these curves is typical for LCP [47]. At very low shear the viscosity is very high and decreases when the shear rate is increased until it reaches a plateau. This behavior can be explained with the introduced order to the anisotropic molecules. In the first place, when the liquid crystal is placed in the apparatus, the mesogens have a more randomized orientation to the shear direction. The LC orientation exists only locally. When starting the measurement the molecules align with the shear until a steady state is reached and the viscosity becomes barely depending on the shear rate. Following the plateau the viscosity increases slightly. Here the orientation movement of the mesogens is slower than the applied shear, introducing distortions to the LC alignment. With further increasing shear the viscosity drops down and the liquid crystal liquefies. This plateau is visible for HA and EGMEA but not for DEGDMA, which shows that the mesogen's movability is too low, even at low shear rates. The highly viscous LC does not align with shear. During film preparation between two glass

slides low shear is applied by pressing the two glass slides together. This shear is comparable to the plateau range in figure 3.6. For HA and EGMEA this preparation method provides help with the alignment of the LC. If the mesogens do not align with the shear, they need a lot of time to align during the tempering of the film after preparation.

With regard to the application as a feedback structure, the selective reflection of the liquid crystal should be close to the emission wavelength of the gain material. During the search for a suitable solvent over 50 different polymerizable and non-polymerizable liquids were tested. Keeping all factors like temperature and concentration fixed, the different liquid crystalline mixtures showed selective reflections, distributed over the whole spectrum between UV and IR wavelengths. There was no clear trend going with polarity of the solvents, so that there was no possibility to predict the selective reflection of a new CLC. Although HA provides a lower viscosity at low shear rates the solvent of choice was EGMEA. Due to the slightly shorter chain and the oxygen at the end of the chain it very well matches the polarity of the used CTC. With this solvent dissolution times of about 3 hours were realized applying mechanical stirring. The shortest dissolution time of about only 15 minutes was achieved with vinyl acetate. The liquid crystal showed an extremely reduced viscosity but the peaks in transmittance spectra were very low.

The difference between two very similar solvents, EGMEA and DEGEEA, is shown in figure 3.7. They differ at the residue by one ethylene glycol unit. The liquid crystal with EGMEA has a lower viscosity and the following 100 minutes after film preparation are shown in steps of 10 minutes. The reflection band develops from the starting point at 0 minutes (red curve) to the end point at 100 minutes (dark grey curve). Outside of the PBG the film is almost transparent as the transmittance is about 97%. The PBG, centered at 700 nm, reaches an intensity of 40% and has a smaller FWHM than the one in figure 3.3. With time proceeding the band sharpens and becomes more intense. This shows that the simple change of solvent and a liquid crystal with a lower viscosity allows the mesogens to move more freely. Hence the quality of alignment is increased. In comparison to EGMEA, the same LC with DEGEEA is shown in figure 3.7. The larger residue of DEGEEA causes a higher viscosity. Accordingly the bandgap is much broader and weaker. During the same period of time there is no significant change of the bangap's shape.
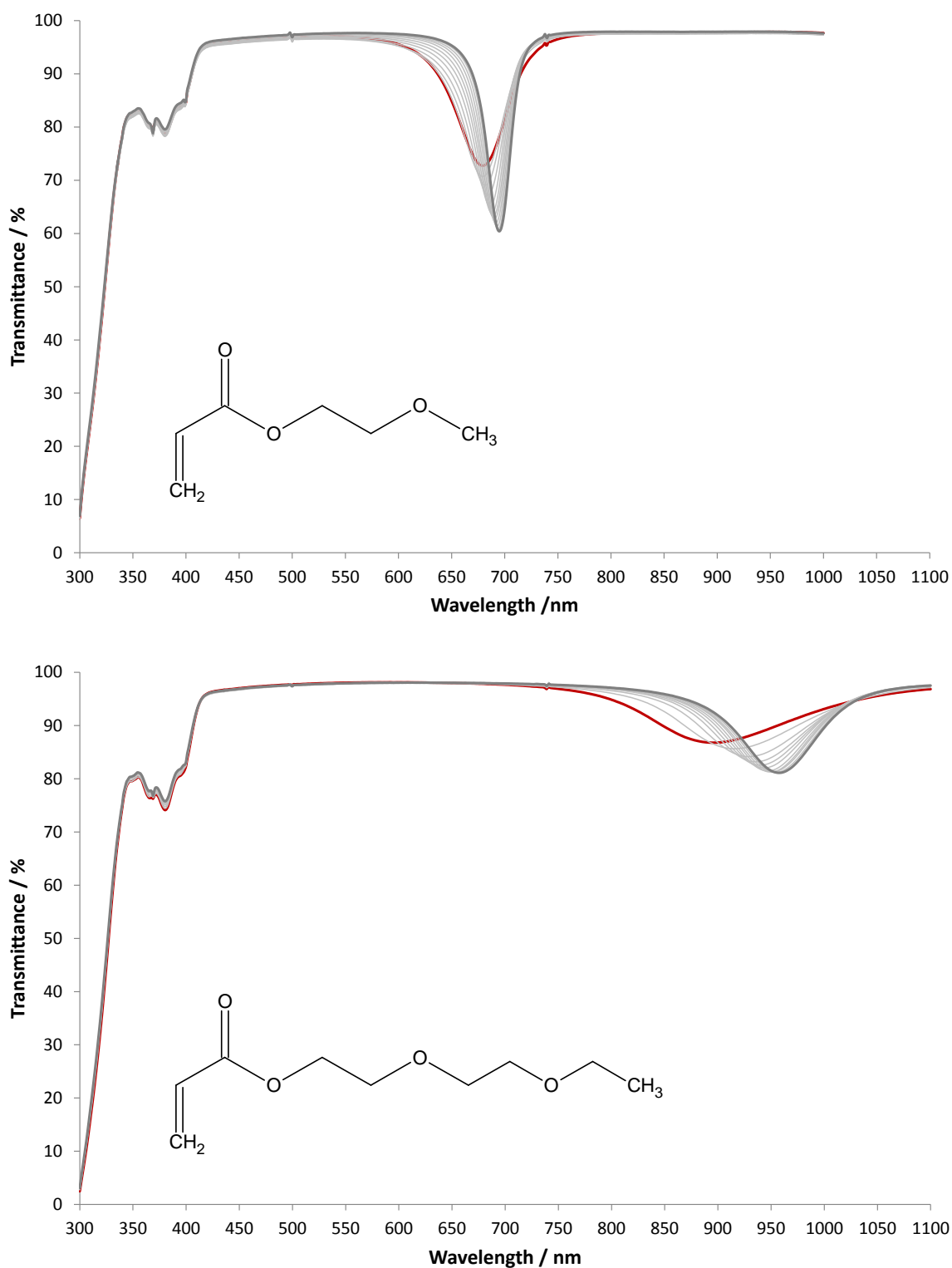
Figure 3.7: Time resolved UV-VIS spectra of CTC in EGMEA (top) and DEGEEA. Starting points are the red lines (0 min) and end points are the dark grey lines (100 min), 10 minute steps in between (light grey). Chemical structures of the solvents as insets. UV-initiator absorbance at 380 nm.

Furthermore the center of SR is red shifted to be centered at 960 nm. The bigger residue causes a larger distance between the mesogens and hence a larger pitch. Crosslinked films can be made of EGMEA - DEGDMA mixtures, where the percentage of DEGDMA is in the range of 10-20% w/w. Another way, to obtain lower viscosities, is to dilute the LC with a non polymerizable liquid, like acetone. During the film preparation the material is not in the liquid crystalline state and hence the viscosity is lower. However, the alignment is not very effective because in diluted liquid crystals the mesogen's distance is to large, so there are no interactions between them. This means, that after the shear is applied, they are free to rotate without any hindrance due to thermal motion. Additionally acetone is very volatile but does not evaporate if the liquid crystal is prepared between two glass slides. This evaporation is necessary to increase the mesogens concentration in the final film to the liquid crystal concentration range. On the other hand this dilution technique will be applied during the preparation of micrometer sized particles (see section 3.6).

3.2.3 Derivatization of Cellulose

In this section all aspects about the mesogenic derivatives of cellulose will be covered. The used derivatives of cellulose are tricarbamates. Cellulose is reacted with an excess of isocyanates carrying the desired sidegroup. The hydroxyl groups, three per glucose unit, react with the carbonyl functionality of the isocyanates to give an urethane or carbamate group. If all three hydroxyl groups are converted the material is called cellulose tricarbamate. It strongly depends on the reaction conditions (heterogeneous or homogeneous) if all hydroxyl groups have reacted and the DS is equal to three or 100%. The derivatization has two purposes: Hydrogen bonds between cellulose chains are cleaved and isolated polymer chains are achieved. The second purpose is the introduction of intramolecular hydrogen bonds between neighboring urethane residues (dotted lines in figure 3.8). The ring shaped units in cellulose backbones as well as the restricted rotation around the glycosidic bonds give the CTC an elongated shape instead of random coil formation. Additionally the introduced hydrogen bonds further restrict the rotation of single units within the polymer chain. But this polymer is not as rigid as inorganic nanorods and hence it is considered as a semirigid rod. At a DS below 100% there are unsubstituted hydroxyl groups left. At these points the rotation is restricted but not impossible and the polymer chain is more flexible than in the fully substituted more rigid parts. The idealized rodlike shape is not apparent anymore. It is rather like several rodlike

parts connected via flexible spacers. Looking at the alignment of rod shaped objects it is best if all molecules exhibit a rod shape without any kinks. Here the alignment to helical superstructures is not disturbed creating a well aligned liquid crystal with optimized optical properties. It is mandatory to achieve the highest possible DS during the derivatization. Additionally every unsubstituted hydroxyl group is a possible hydrogen bond attachment point. In solutions of very high concentration the single polymers come very close. During the applied shear the polymers move relative to the adjacent molecules. In case of free hydroxyl groups, there are hydrogen bonds linking two polymers together, preventing a relative movement. As already shown, from aspects of the liquid crystal's viscosity, a solution with freely movable polymer chains yield a much better alignment and optical properties.
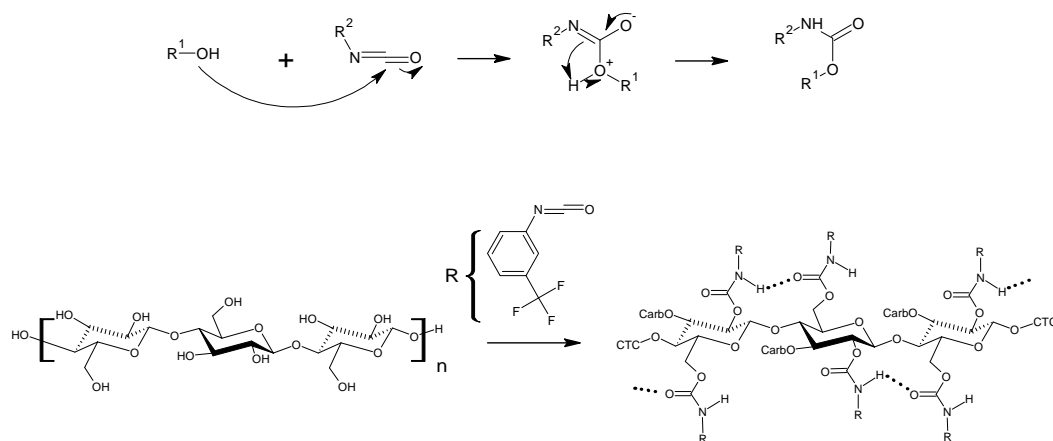
Figure 3.8: Mechanism of the CTC synthesis starting with cellulose. Top: General mechanism of the reaction between a hydroxyl functionality and isocyanates. Bottom: Cellulose is converted with *m*-trifluoromethyl phenyl isocyanate towards the corresponding CTC.

The reaction with isocyanates is done under heterogeneous conditions where the starting material is dispersed in the reaction solvent and during the reaction a conversion to the soluble derivative takes place. There are alternatives for this type of reaction, where cellulose itself is dissolved in very polar solvents. Homogeneous reactions do have the advantage that reactants can access and convert the hydroxyl groups more easily since the polymer is properly dissolved. But the reaction conditions and the used chemicals require a lot of synthetic effort. On the other hand heterogeneous reactions are more easily to conduct, but the reaction with isocyanates only takes place at the surface of the dispersed cellulose crystallites. Cellulose is highly crystalline due to polymer chains connected via thousands

of hydrogen bonds and a defined fibril architecture. In a dispersion the hydroxyl groups inside the crystallites are not accessible to the reactants. During the reaction, the crystallites are converted layer by layer and after conversion the polymer chains go into solution. Depending on the starting cellulose there are ways, like ammonia treatment, to reduce its crystallinity and enhance its reactivity towards isocyanates [60]. As a matter of fact isocyanates are very sensitive towards humidity, with the consequence of side reactions instead of hydroxyl group conversion, as long as water is present. Therefore well dried starting material, dry solvents and inert gas atmosphere are necessary for reaction. As cellulose is very hygroscopic a complete removal of water cannot be obtained during drying. In result, even with an excess of isocyanates, the DS is not close 100%. For purification the product is precipitated and redissolved several times to remove byproducts from the reaction between water and isocyanates. It often happens that the product gelatinizes when redissolved, due to lots of unreacted hydroxyl groups building a network of hydrogen bonds.

The solution to this problem, without changing to other reaction conditions, is to redo the same reaction two times. The second cycle benefits from the first reaction, since the cellulose is now sufficiently functionalized to give a homogeneous reaction solution providing easy accessibility to the residual free hydroxyl groups. After three cycles the highest possible DS, close to 100% is reached. The discussion of optical properties of films with these CTC is shown in the section 3.2.5 because fluorinated additives mediate remaining hydrogen bonds in the liquid crystalline mixture. Hydrogen bonds with other polymer chains form aggregates in dilute solution, too. Light scattering experiments on CTC were conducted after one and three reaction cycles to determine the particles' hydrodynamic radii (see figure 3.9) and the $\frac{dn}{dc}$ was measured to be 0.138. The reduced capability of forming hydrogen bonds with increasing DS should result in decreasing particle size. The high polydispersity of the samples leads to unexpected absolute values of radii and molar weight but in comparison the particle's size decreases with increasing number of reaction cycles. Additional a higher DS reduces dissolution times in the acrylic solvents. While CTC, only reacted once with isocyanates, take 3 hours to dissolve, only one hour is needed in the same solvent and concentration after three reaction cycles. Polymer-polymer interactions in solid CTC get weaker with a decreased number of intermolecular hydrogen bonds.

However, the determination of the DS is rather difficult. The solution behavior gives a first idea about this value. Gelatinizing of the CTC in a good solvent is a

clear hint of a DS significantly below 3.
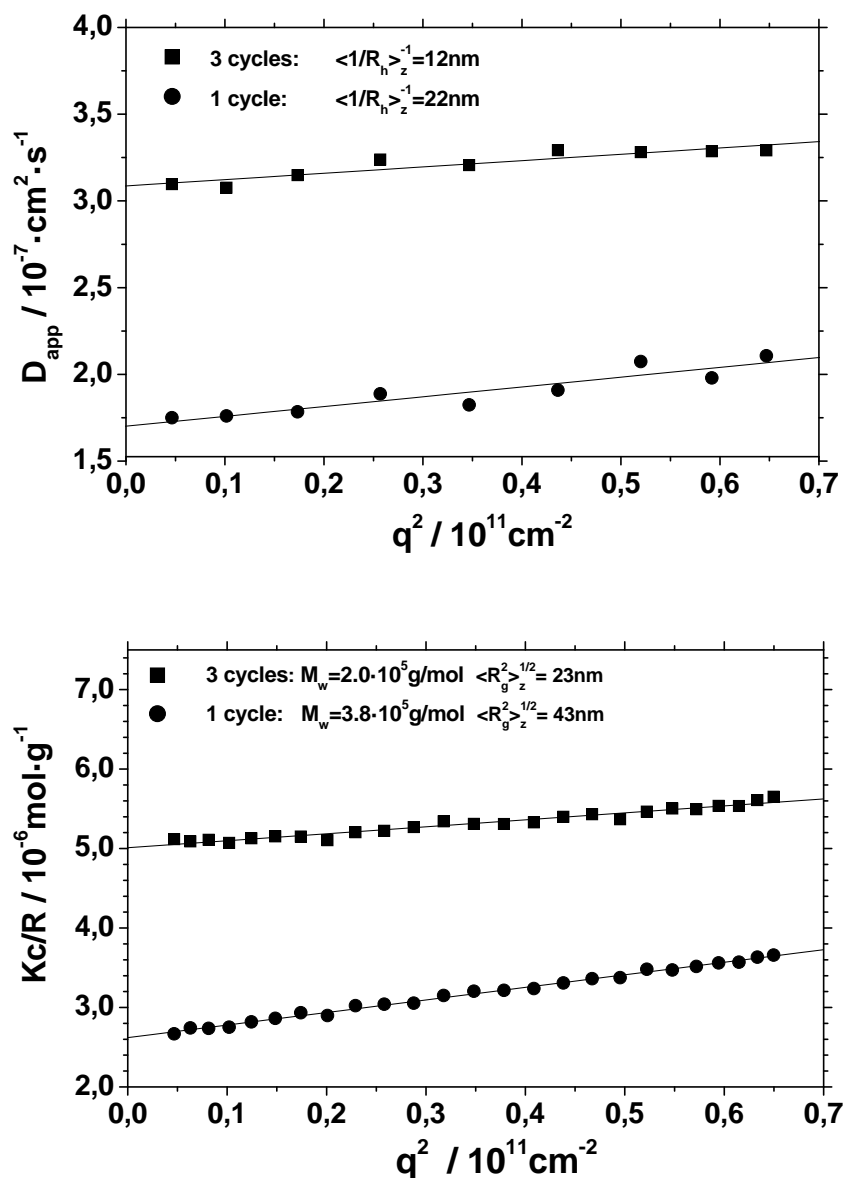
Figure 3.9: Dynamic (top) and static light scattering results from CTC after one (circles) and three reaction cycles (squares) in diluted methanol solution.

The use of infrared spectra is very common for determination of chemical substitution. In figure 3.10 the IR spectra of the starting cellulose Avicell PH101, CTC after one and three reaction cycles are shown. The peak at 3300 $\frac{1}{cm}$ represents the valence vibration of hydroxyl groups of cellulose and hydrogen bonds derived therefrom. It gets significantly smaller, but does not vanish completely, even not after three reaction cycles, because the DS is still slightly below 3. With this mea-

surements it can be shown that some non-substituted hydroxyl groups or some water always remain but it is not possible to quantify the DS, as the grey and the red curve are very similar.
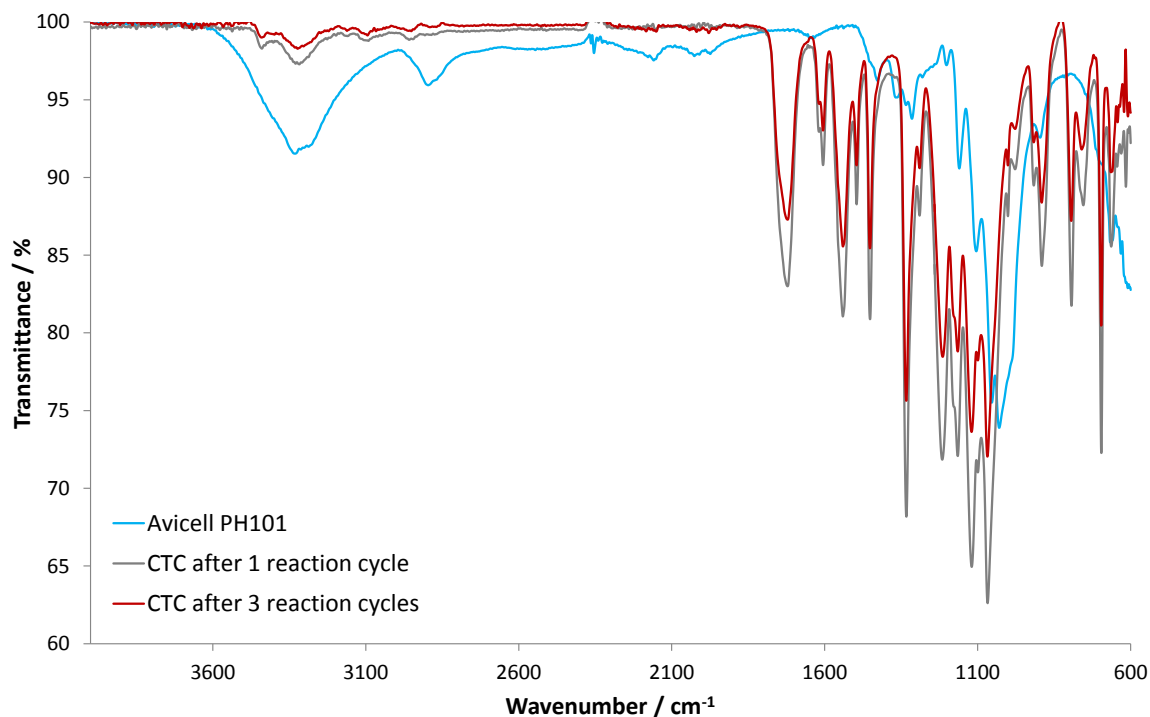
Figure 3.10: IR spectra (powder) of cellulose (Avicell PH101) and CTC with *m*-trifluoro methyl phenyl residues after one and three reaction cycles.

A quantification of the DS can roughly been done with elementary analysis. During the carbanilation reaction nitrogen is introduced to the cellulose polymer. Its weight percentage depends on the average number of substitutes per glucose unit. The following values were calculated for CTC made with *m*-trifluoromethyl phenyl isocyanate:

DS	Carbon % w/w	Hydrogen % w/w	Nitrogen % w/w
3	49.8	3.07	5.81
2	49.26	3.38	5.22
1	48.14	4.04	4.01
0	44.44	6.22	0

Considering a measurement uncertainty of 10% it can be determined if the DS is one or three, but a DS of 2.8 can not be distinguished from a DS of 2.9. Usually

these CTC samples showed a nitrogen content of 5.8% w/w after the first reaction cycle. Small changes of the DS during the following two reaction cycles do not create different readings in elementary analysis. However, after three conversion reactions, all done with an excess of isocyanates, a quick dissolution of the CTC without gelatinizing and the results from light scattering experiments the DS can be considered to be very close to 3.

Another important factor, besides the DS, is the molecular structure of the isocyanates. Aromatic sidechains are well known while aliphatic residues are more difficult to introduce because of their lower reactivity towards the hydroxyl groups. In figure 3.11 six different CTC sidechains with similar structure are shown, synthesized via the use of different isocyanates The sidechain in the top row on the left was already known to create CTC with very good solubility and film forming characteristics. Trifluoro methyl groups are responsible for good interactions with solvent molecules. Their position at the aromatic ring and substitution was changed. In addition derivatives with a methoxy group at the benzene core were synthesized. All five variations gave CTC with lower solubility in the solvent chosen to be the best for the first residue. The variation of the position at the ring causes the trifluoro methyl group to be hidden from solvent molecules (see figure 3.8 for structural details of CTC), decreasing solvent-polymer interactions necessary for a good solubility. The methoxy group is less polar than trifluoromethyl groups. As the polarity of EGMEA was tailored to CF_3 containing residues, their solubility was lower in this solvent, too. All variants are either not able to form highly concentrated solutions or a matching solvent is needed. There is no potential for improvement in changing the residues at the CTC to achieve a better optical quality with the set solvent.

In addition to the DS and the chemical constitution of the sidechains, the total polymer length has a significant influence on the CLC properties. Derived from Avicell, CTC with a high molecular weight of about 200.000 $\frac{g}{mol}$ and a polydispersity of 2.5 - 4 are obtained. The molecular weight corresponds to an average chain length up to 140 nm, taking into account that one glucose unit is 0.5 nm long [152, 153] and a totally stretched conformation. The CTC were characterized via GPC measurements, utilizing polystyrene standards in THF. After one reaction cycle there is a shoulder visible (see figure 3.12), representing incomplete substituted polymer chains with a lower molar mass. After three cycles this shoulder has vanished, resulting in a decrease of PDI from four to three and an increase of M_w from 190,000 to 225,000 $\frac{g}{mol}$ due to a reduced weight fraction with lower molar mass. This fact is another proof that three conversion reactions yield nearly fully substituted CTC.
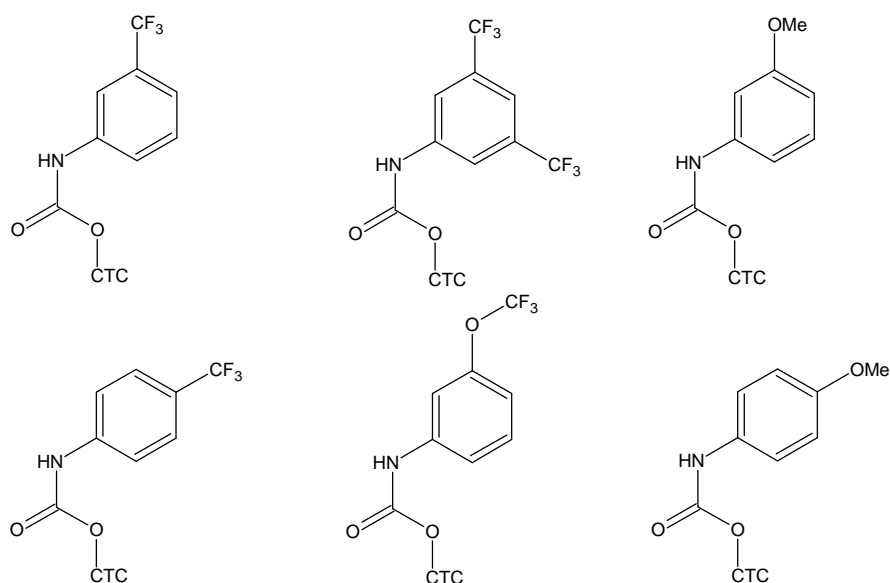
Figure 3.11: A selection of sidechains with an aromatic core applied to cellulose.

Byproducts from the reaction of isocyanates with water (see figure 3.13) can be seen in the elugram in the area between 100 to 500 $\frac{g}{mol}$, if the purification was not done properly. It was found that a certain precipitation medium of methanol/water 70%/30% v/v is suitable to remove these byproducts [154].

The glycosidic bonds between the glucose units are labile to acidic treatment. With a time controlled degradation of the material, different chain lengths are available [155]. The following table gives an orientation about the degradation time needed for a specified molar mass or polymer length.

Degradation time minutes	Molar mass M_W $\frac{g}{mol}$	PDI	Polymer length nm
0	208,000	4.4	140
60	120,000	3.3	90
120	85,000	2.9	60
240	52,000	2.5	40

The degradation process has different advantages: The reduced average chain length causes a reduced CLC viscosity (see figure 3.14) and the nature of the cleavage reaction decreases the polydispersity of the sample [155]. Hence dissolution times of the shortened CTC are shorter than of the initial ones. The effect on viscosity reduction is much larger from decreasing polymer length than from exchanging the solvent (see figure 3.6). Going from long the short chain lengths the curves are
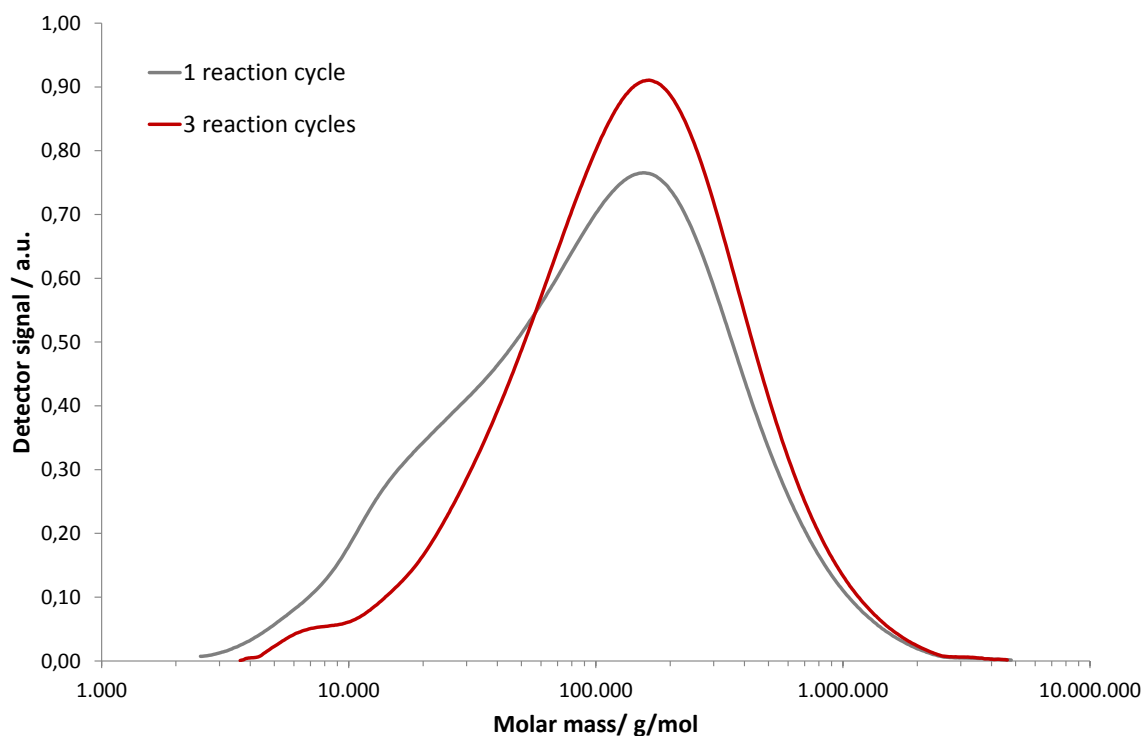
Figure 3.12: GPC molar mass distribution of CTC with *m*-trifluoro methyl phenyl residues after one (grey) and three (red) reaction cycles based on Avicell PH101. Values of molar mass are in poly(styrene) equivalents.

getting more independent from the applied shear rate. As explained previously this is caused by how fast the mesogens are able to follow the shear flow. Short, more movable chains have a higher degree of order before the measurement and follow the shear flow without hindrance. A very flat curve (as shown for the shortest mesogens) represents a well ordered sample where no or very low shear is needed to induce alignment. For the longest mesogens, there is no plateau visible, suggesting that even the lowest shear rates are too fast for the polymer chain to follow. But not only the viscosity is affected by the chain length variation. It was shown [155] that the SR maximum shifts to shorter wavelengths with decreasing chain length. Besides the viscosity reducing effect, short mesogens have more freedom to rotate around the short axes of the molecule, due to a decreased aspect ratio. Hence the alignment is not very stable which is of importance during polymerization of the films (see section 3.2.6).

The position of the SR maximum is influenced by a large number of factors. One most important is the concentration of CTC in the solution. Liquid crystallinity is observed for a concentration range, starting above a critical value. For CTC in
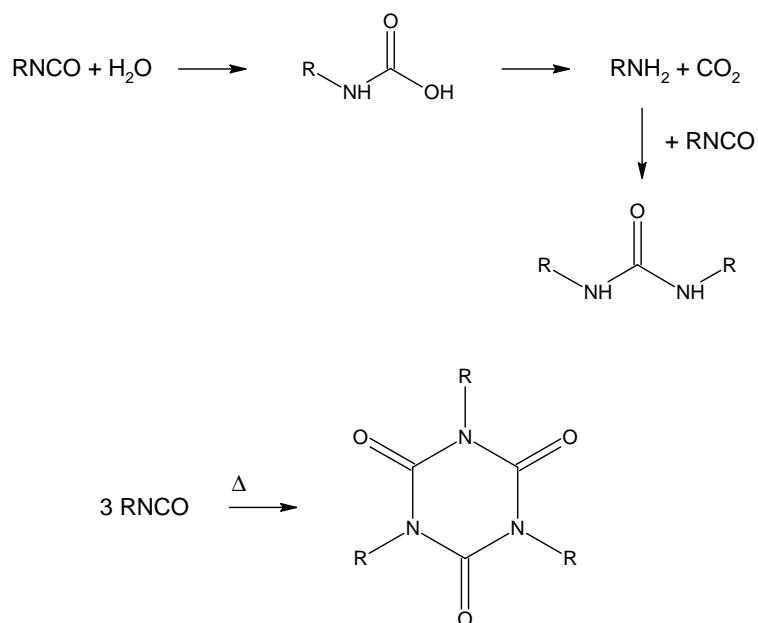
Figure 3.13: Sidereactions of isocyanates with water during the carbanilation reaction.
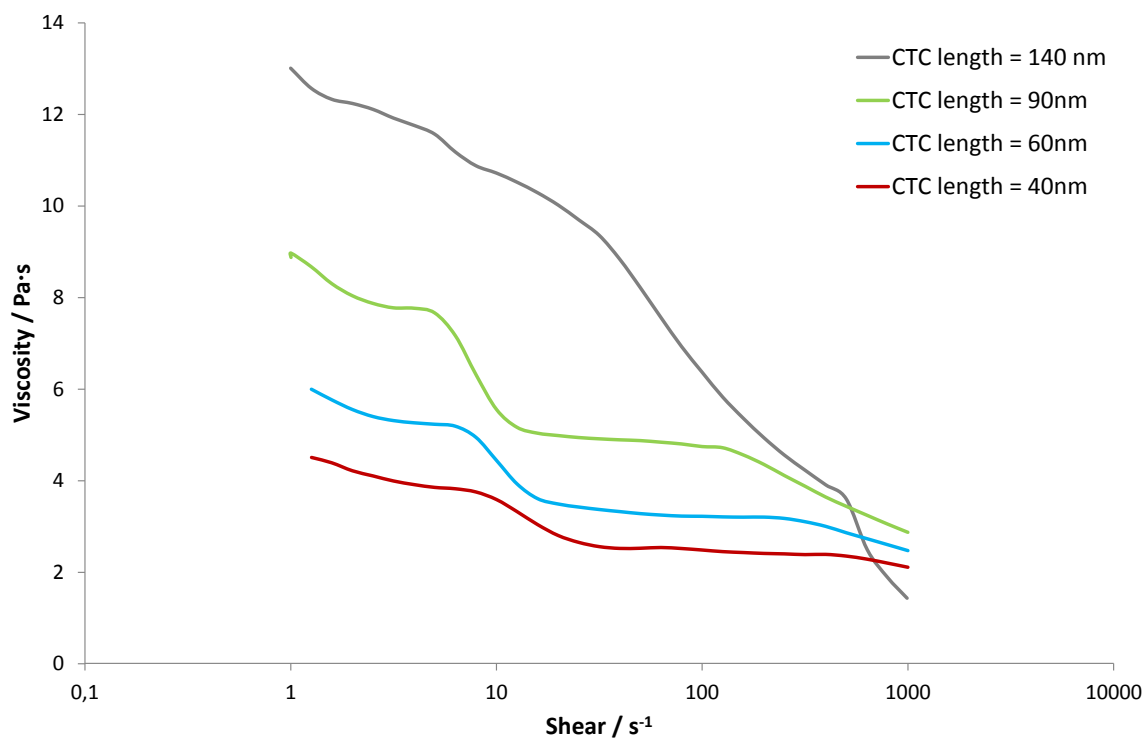
Figure 3.14: Viscosity of solutions with different CTC chain lengths at 45% w/w in EGMEA/DEGDMA 80%/20% w/w in dependence to the applied shear.

EGMEA this critical value is 35% w/w and the range ends at 46% w/w. Looking at figure 3.15 one can see that for the lowest shown concentration the SR is very weak and centered at 920 nm. Higher concentrated solutions show increased SR intensity and a blue shift. As the concentration increases, the pitch decreases. A more densely packed solution enhances the optical properties of the planar state. To achieve the most intense SR, the concentration needs to be close to the upper concentration limit where the highest number of intermolecular alignment forces is present. However this value is not to be exceeded because phase separation occurs above. The films are getting turbid and the SR intensity drops down dramatically. This already happens at 1% w/w above the upper concentration limit.
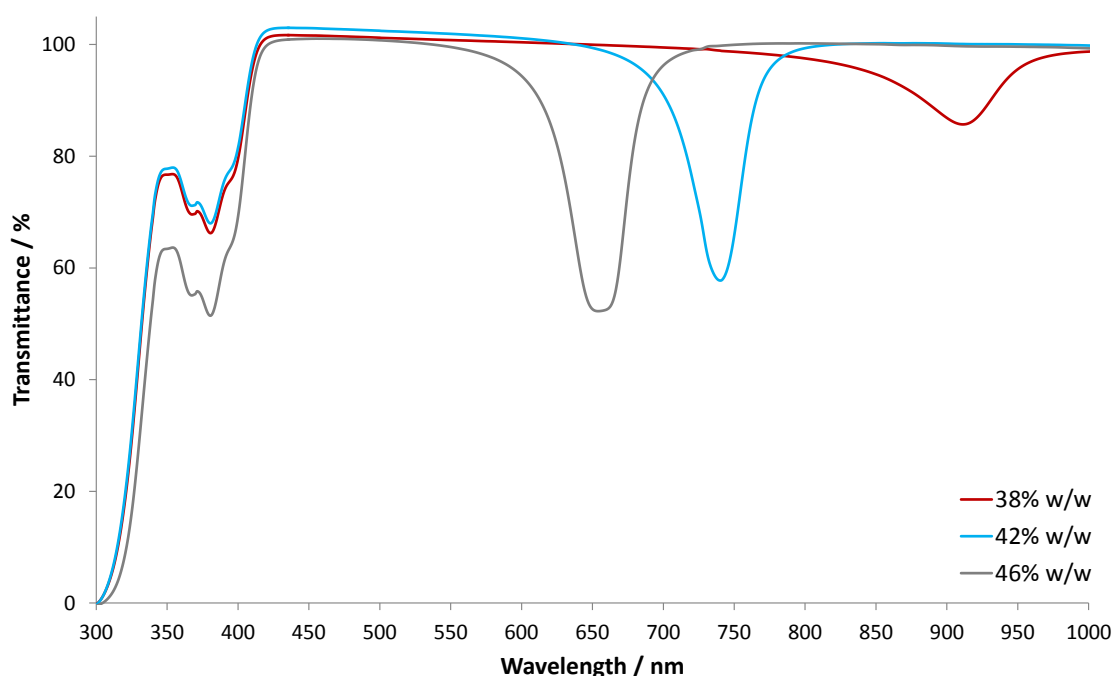
Figure 3.15: Transmittance spectra showing the dependence of mesogen concentration to SR maximum position and intensity. CTC length is 140 nm ($M_w = 208.000\ \frac{g}{mol}$), UV-initiator absorbance between 320 - 380 nm.

3.2.4 Alignment Methods

Liquid crystals align through self assembly into ordered structures. Films of liquid crystalline materials are usually prepared on flat substrates. According to the boundary conditions the orientation of those mesogens close to the substrate is

affected by the surface itself. Planar boundary conditions induce a parallel orientation to the surface while homeotropic conditions induce a perpendicular orientation. For this purpose alignment layers are applied on the substrates, controlling the tilt angle between the mesogen's long axes and the substrate. Most prominent among alignment layers are polyimides [156]. A precursor solution is cast onto the substrate via spincoating or doctor blading. After solvent evaporation at ambient temperatures, the films need to be baked at high temperatures. The precursor polymers are now fully imidized and insoluble in any solvent. At the end the films are rubbed unidirectionally with a velvet cloth. Here very small scratches and polymer orientation is introduced to the polyimide film. Mesogens tend to align along the rubbing direction and, according to the polyimide used, with a certain angle to the substrate. To enhance the alignment effect, cells of two face to face substrates are made with a thin spacers in between. The liquid crystal is filled into the cell by capillary forces and the shear flow helps to orient the molecules. In case of CLC the planar state with an idealized alignment is desirable. Mesogens at the substrate-LC interface should be oriented parallel to the substrate without any tilt angle. Mesogens far from the interface will be affected by the orientation of their adjacent molecules and hence alignment layers do induce a well suited alignment of the whole LC sample. With this method it is possible to introduce different geometries to liquid crystals. If two coated substrates are combined face to face with their rubbing directions perpendicular to each other a twist can be introduced. For example in a twisted nematic cells, because the mesogens close to the substrate tend to align parallel to the rubbing direction.
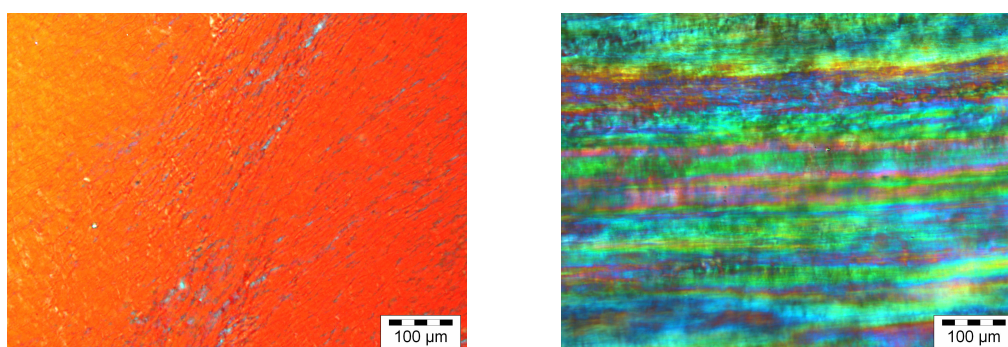
Figure 3.16: POM images of cellulosic CLC samples prepared by standard method (left) and with the use of capillary forces.

Methods applicable very easily to low molecular weight LC, are difficult to apply for highly concentrated solutions of CTC. One issue to fix is the polarity of the CLC

and the alignment layer. Polyimide or PTFE layers are very hydrophobic, while the CLC made of CTC and EGMEA prefers a more polar surface. The used alignment layers need to be etched with oxygen plasma to make their surfaces more hydrophilic. Otherwise the liquid crystal minimizes its interface with the alignment layers, resulting in insufficient boundary conditions for a planar state. However the plasma treatment has to be applied carefully, in order not to remove the rubbing introduced structures. Additionally the viscosity of lyotropic LCP solutions limit the use of cells with alignment layers, considering that sufficient high capillary forces are only present in very thin cells. This causes a lack of SR intensity because a minimum sample thickness is required for an intense SR. As already discussed in the previous section, it is difficult for long semirigid polymer chains to follow a flow profile. The result is shown in figure 3.16. The left POM image shows a sample that was prepared by the standard method via pressing two substrates together. On the other image, capillary forces were used to fill a cell with the CLC. As the left images shows a homogeneous color (pitch) and only a few defect lines, the liquid crystal on the right is completely distorted. For sufficient thick samples the forces only provide flow for a very small film area until the material stops flowing into the cell. The only way to use alignment layers with highly viscous LC is to put the LC onto one substrate, placing the second on top and applying some pressure to form a film.

On the contrary to low molecular weight LC, films of CTC prepared with alignment layers on the substrates do not show any enhanced optical qualities. The shear motion applied during the film preparation is sufficient to force the polymers close to the substrates into a parallel orientation. Their huge aspect ratio does not allow a different orientation to the substrate. It seems that rubbed polyimide surfaces do not have any promoting influence to the LC's alignment. On the other hand rubbing bare glass substrates with cellulose sheets is known to orient LC as well. Very thin scratches on the glass are the result of the rubbing. Preparation of CTC samples on rubbed glass slides, which were treated with oxygen plasma beforehand, show much better reflectance properties than films on bare glass. The plasma treatment removes any organic residues from the glass, polishes the surface and increases hydrophilicity. During the rubbing with cellulose sheets the glass surface is getting slightly less hydrophilic, as contact angle measurements indicate. Although a high aspect ratio is meant to be sufficient for a planar alignment, rubbing does have, at least on bare glass, an orienting effect. Here the rubbing structures must be very small. If an abrasive paper is used to rub glass slides, the rubbing structures are

too large and their influence is addressed to whole domains instead of polymer chains. How substrate treatment affects the reflectance properties is shown in figure 3.17. All curves in this figure include the usage of additives discussed in section 3.2.5. The film on bare glass (red curve) shows a reflectance intensity of 30%, while rubbing with cellulose sheet or oxygen plasma treatment only increase this value about 5%. But the combination of both, shown in the green curve, yield almost above 40% reflectance perpendicular to the film. A detailed way how to prepare films from lyotropic CLC made of CTC is described in section 4.3.
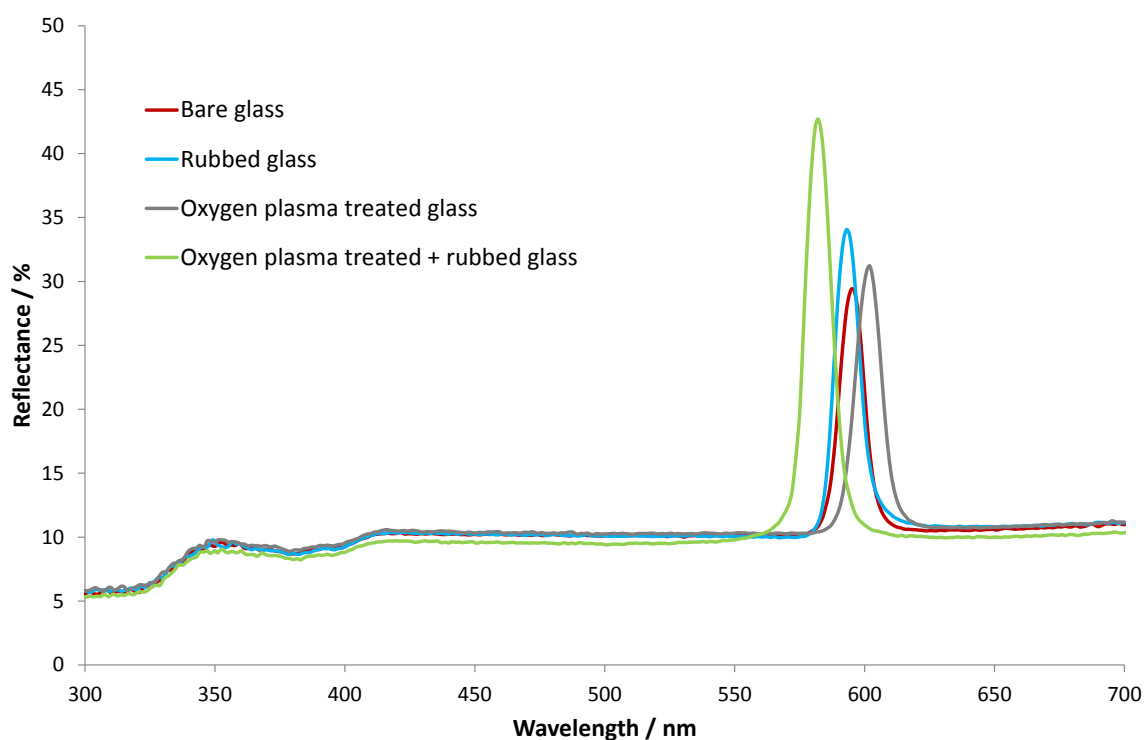
Figure 3.17: Reflectance spectra showing the effect of substrate treatment to the intensity of the SR perpendicular to the film. The CLC is a 46% w/w solution of 140 nm CTC in EGMEA/DEGDMA 80%/20% w/w, with small amounts of TFAA.

In some cases for low molecular weight LC, the application of alignment layers is not sufficient to achieve a perfectly aligned LC. Temperature variations in a cycled manner are utilized to support an improved alignment [34].

The multidomain liquid crystal is placed in a cell and heated very close to the liquid crystalline - isotropic liquid transition temperature. The liquid crystalline order is still maintained but the thermal movement is similar to that in an isotropic liquid. If the sample is now cooled down with a low cooling rate, the mesogens at the interface start to align along the rubbing structures. Mesogens inside the sample
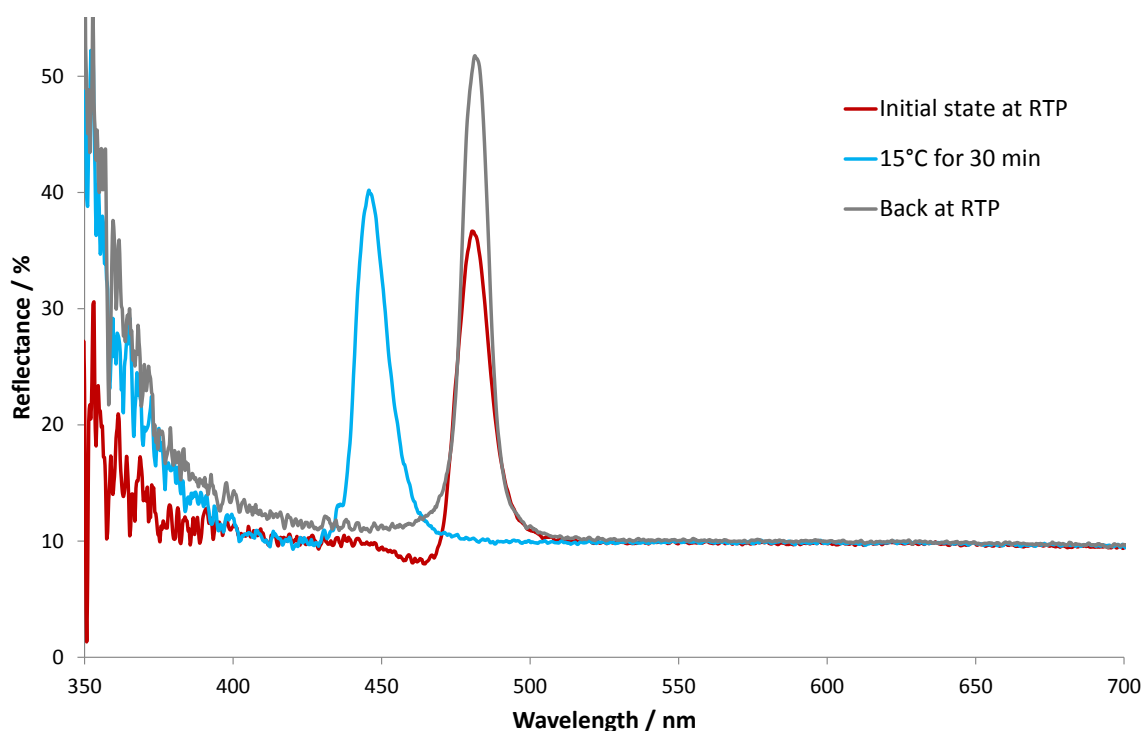
Figure 3.18: Reflectance spectra of 140 nm CTC in EGMEA/DEGDMA 80%/20% w/w film starting at room temperature (RTP), cooling to 15°C for 30 minutes and slowly heating back to RTP.

do have the chance to move more freely until they are integrated very well into the cholesteric structure. With decreasing temperature their moving is slowed down. Repeating this heating and cooling cycle several times yield a well aligned LC sample. Unfortunately this way is not applicable to LCP, because after heating close to the transition temperature the polymer chains do not align with the rubbing direction without any shear applied. Furthermore the cholesteric structure is very labile to such huge temperature changes. When the sample is cooled the polymers do not have enough time and movability to integrate very well into the cholesteric order. Additionally CTC lose some of their rigidity with increased temperatures [157]. Nevertheless some thermal stress can help to increase reflectance perpendicular to the film, if temperature changes are applied very slowly. The red curve in figure 3.18 shows a reflectance spectrum of a CTC sample at RTP. The sample is cooled to 15°C with $1\frac{°C}{min}$ and left at this temperature for 30 minutes (blue curve). Twenty minutes after heating back to RTP with the same rate the sample shows an improved reflectance. The cooling causes a denser packing of polymer chains, forcing them to relatively align to their neighboring chains. Back at RTP the stress

is released but the improved orientation still remains (grey curve).
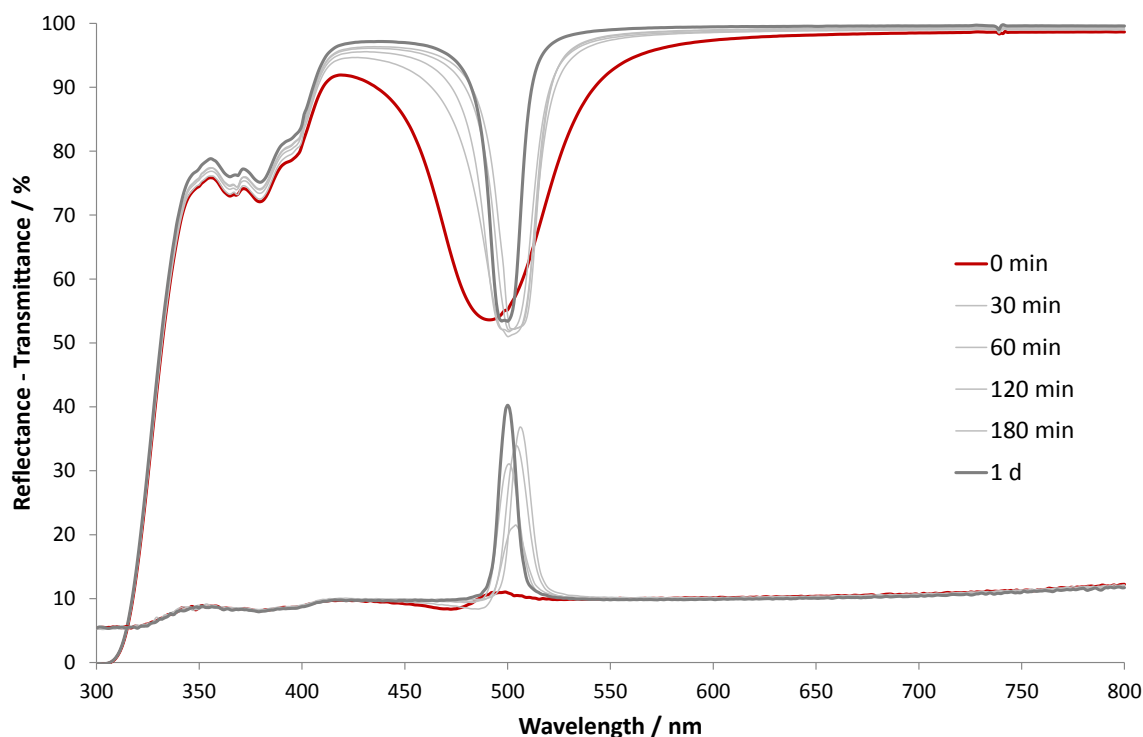
Figure 3.19: Time resolved transmittance and reflectance spectra show the evolution of the SR band.

One aspect which low and high molecular weight LC have in common is the amount of time needed to equilibrate. Figure 3.19 shows time resolved transmittance and reflectance spectra of a CTC in EGMEA film. The red curves belong to the initial state of the sample directly after preparation. The peak in transmittance is already at 50% intensity but very broad. This is due to the multidomain structure and the initial bad alignment of the liquid crystal. The peak intensity shows that the cholesteric superstructure is present from the beginning but the peak in reflectance is hardly present at the same time. The helical axes are not perpendicular to the substrate yet and hence the reflectance in the same direction is low. The thin grey curves represent the next three hours, where the transmittance peaks become significantly narrower and remain at the same intensity. The narrowing in transmittance curves and the gaining of intensity in reflectance spectra are due to the ongoing alignment of the CLC. After one day the maximum of reflectance is reached. Waiting for longer times does not yield higher values of reflectance perpendicular to the film. As reported in literature dissolution as well as equilibration times range from several days up to weeks for derivatives of cellulose [150, 151].

For the optimized samples studied here both processes happen in a shorter time.

3.2.5 Additives

In this section the influence of low molecular weight liquid crystals as partial solvent substitutes and of fluorinated additives will be covered. A commonly used NLC is 4-pentyl-4'-cyanobiphenyl (5CB). It is liquid crystalline at RTP with a clearing point at 35°C. This liquid crystal was chosen because its miscibility with HA and EGMEA. 5CB was used to substitute parts of the solvents. As the liquid crystal has a higher viscosity than the acrylic solvents the viscosity of the doped CLC was higher than of the undoped. The upper limit of substitution is 20% w/w but due to interactions between the cyano group of 5CB and the carbonyl functionalities of the cellulose derivatives there are some interesting results regarding the temperature stability
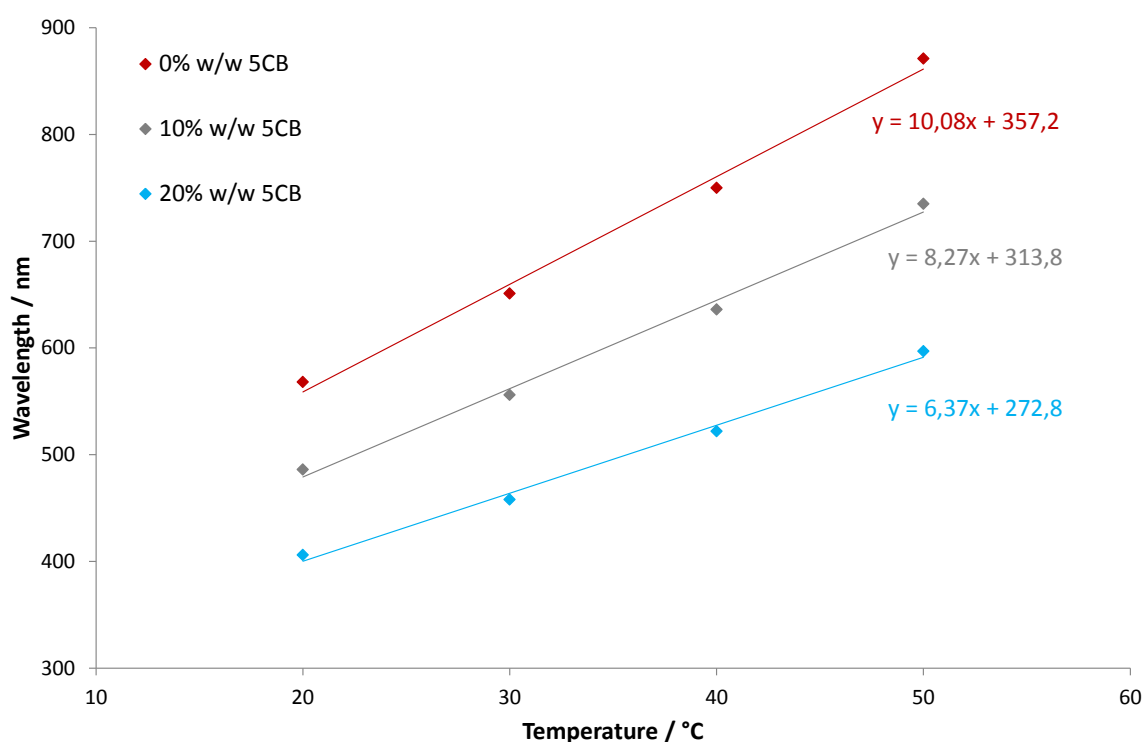
Figure 3.20: SR maxima of CLC doped with different amounts of 5CB at different temperatures.

of the resulting CLC. Figure 3.20 shows CLC with different amounts of 5CB in the temperature range between 20 and 50 °C. The red line represents the CLC without any dopant. The SR is centered at 570 nm and shifts to the red if the sample is heated. There are two differences if the CLC is doped with variable amounts of 5CB.

First the SR is shifted to shorter wavelengths with increasing amount of 5CB. Second a shift of SR upon heating towards longer wavelengths is getting smaller with increasing amount of 5CB. To clarify this fact the regression equations are shown in the figure as the gradient indicates the intensity of the wavelength shifting. We assume that the reason for this behavior is due to a close interaction between the cyano group of 5CB and carbonyl moieties of the cellulose derivatives. As 5CB is liquid crystalline at RTP and the mesogens can be considered rodlike, they may fit perfectly into the cholesteric structure. So far it is not known why this causes a blue shift of the SR at the same temperature. Depending on how 5CB molecules orient relative to the CTC it can be understood why this mixture shows a better stability towards temperature change. During heating it is necessary to overcome the order of 5CB molecules in addition to the pitch variation. Here more energy is needed and hence the shift towards the red is smaller for higher amounts of 5CB. But as the viscosity increases with increasing amount of 5CB there is no improvement of the optical quality noticeable.

Trifluoro acetic acid (TFAA)   Trifluoro ethanol (TFE)   Hexafluoro isopropanol (HFIP)
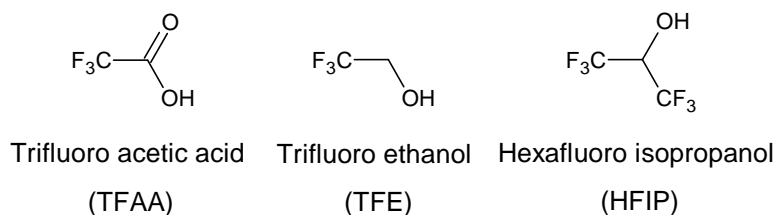
Figure 3.21: Chemical structures of fluorinated additives.

A great potential for optimized optical properties is provided by the molecules shown in figure 3.21. Trifluoroacetic acid (TFAA) is a well known solvent especially for derivatives of cellulose [158]. Very acidic solvents were shown to be capable of dissolving of high amounts of cellulose polymers depending on their acidity [66]. It was investigated at which threshold concentration an anisotropic solution formed. Solvents showing strong interactions with the polymers showed the smallest threshold concentration. With decreasing acidity this value increased due to weaker polymer-solvent interactions. Because of three fluorine atoms TFAA has a low pK_s value and thus is highly acidic. It dissolves derivatives of cellulose starting to give an anisotropic solution from 30% w/w. Pure TFAA yields low viscosity CLC due to a lower threshold concentration[159]. It influences the hydrogen bonds of cellulose derivatives [160] showing a certain selectivity. TFAA cleaves intermolecular hydrogen bonds but leaves intramolecular ones unchanged. If films

of cellulose acetate were treated with the vapor of TFAA, their tensile strength can be improved due to an improved alignment. As discussed in section 3.2.3 hydrogen bonds play an important role during the formation of well oriented cholesteric phases. Intermolecular hydrogen bonds connect different cellulose polymers restricting their movability in an already highly viscous solution. On the other hand intramolecular hydrogen bonds are necessary to maintain the extended shape of these polymers, so TFAA can support both hydrogen bond effects.
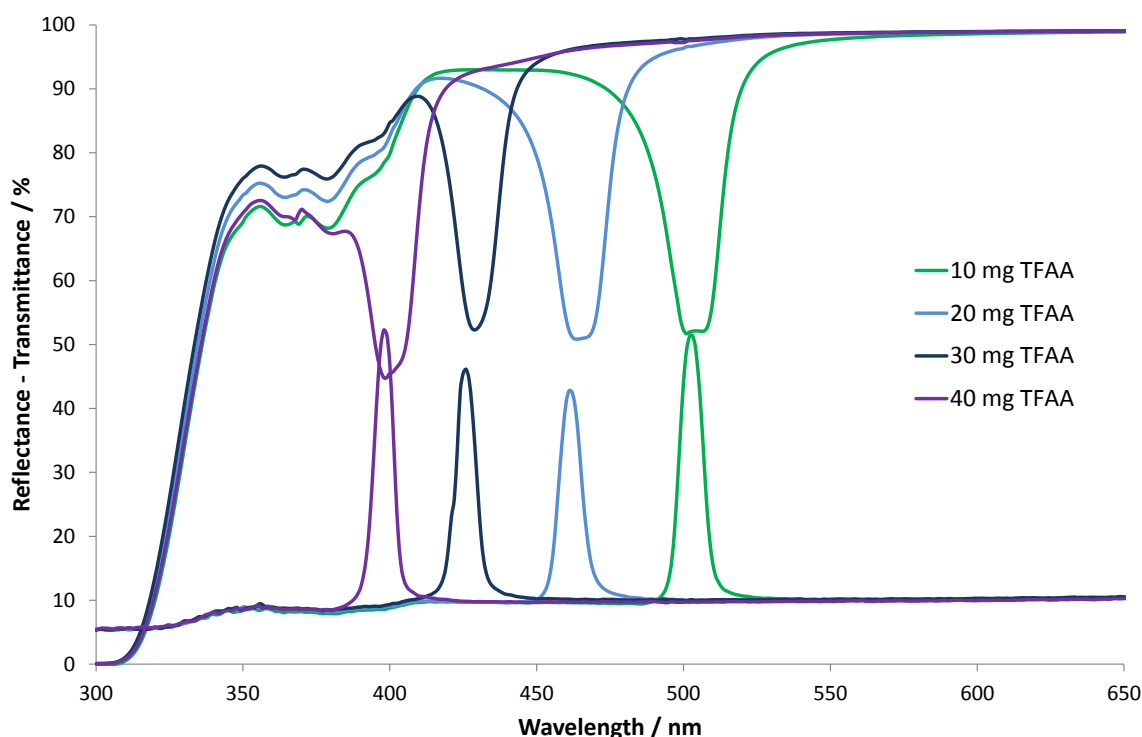
Figure 3.22: Transmittance and reflectance spectra for different amounts of TFAA (per 0.5 g CLC) in CTC (46% w/w) dissolved in EGMEA/DEGDMA (80%/20% w/w).

In CTC there are always a few unsubstituted hydroxyl groups left, forming intermolecular hydrogen bonds. The fluorine atoms in TFAA cause an increased reactivity of the carbonyl functionality. Thus is was shown that TFAA reacts with unsubstituted hydroxyl groups, cleaving intermolecular hydrogen bonds [161]. TFE was also shown to have a low threshold concentration, but the lack of a carbonyl group does not allow to apply the above explanation [66]. The fluorine atoms have a very high electronegativity, making the hydroxyl group a good acceptor for hydrogen bonds. Hence unsubstituted hydroxyl groups will chose TFE or HFIP molecules to form hydrogen bonds with, instead of linking cellulose strands.

In this work the aim was the preparation of polymerizable cholesteric films made of derivatives of cellulose. The described possibility to control hydrogen bonds in the liquid crystalline mixture has to be combined with the polymerizability of acrylates. Therefore the fluorinated substances TFAA, TFE and HFIP were used only as additives in small amounts to the already described mixture. Figure 3.22 and 3.23 show the effect to the SR if the CLC is doped with different amounts of TFAA and TFE, respectively. All samples show a reflectance above 40% perpendicular to the film surface. The amount and the nature of the additive has a great impact on the position of the SR. With increasing amounts the SR is shifted towards shorter wavelengths. This effect is strongest for TFAA followed by HFIP and TFE. So far it is not understood by us how these additives affect the pitch. They are structurally very similar but the effect of shifting the SR is different.
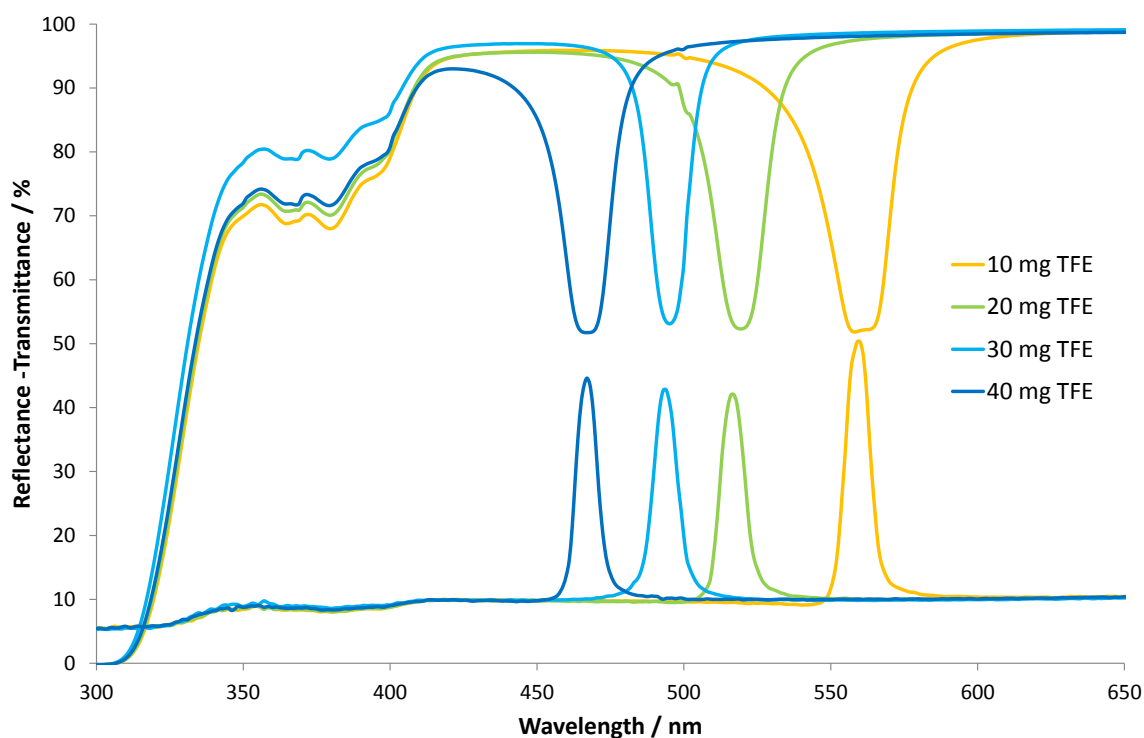
Figure 3.23: Transmittance and reflectance spectra for different amounts of TFE (per 0.5 g CLC) in CTC (46% w/w) dissolved in EGMEA/DEGDMA (80%/20% w/w).

On the other hand the effect of shifting the SR is in reverse order in the case of vinyl butyrate as solvent. Here the SR is shifted to the red and the intensity of the reflectance band is decreased with increasing amount of TFAA. Nevertheless dissolution times are also reduced with increasing amount of additive. Another

attribute is the change of the upper limit of the liquid crystalline concentration range. With the usage of additives this limit is about 1 - 2% w/w higher than for undoped solutions. The amount of isotropic liquids in the CLC mixture is slightly larger due to the volume of additive, but it is too small to explain this fact. It is more reasonable to consider the denser packing of cellulose polymers as a direct effect of adding the fluorinated compounds. Furthermore this explains the shift of pitch and SR as well. Interestingly the effect of enhancing optical properties is reserved, as far as we know, to fluorinated compounds. It does not work with acetic acid or other solvents known to break hydrogen bonds, e.g. dimethyl sulfoxide or dimethyl formamide. An improvement was not visible neither as pure solvents for the CTC nor in small portions as additives. This fact serves as an argument for the theory that fluorinated compounds act as preferred hydrogen bond partner due to the electronegativity effect.
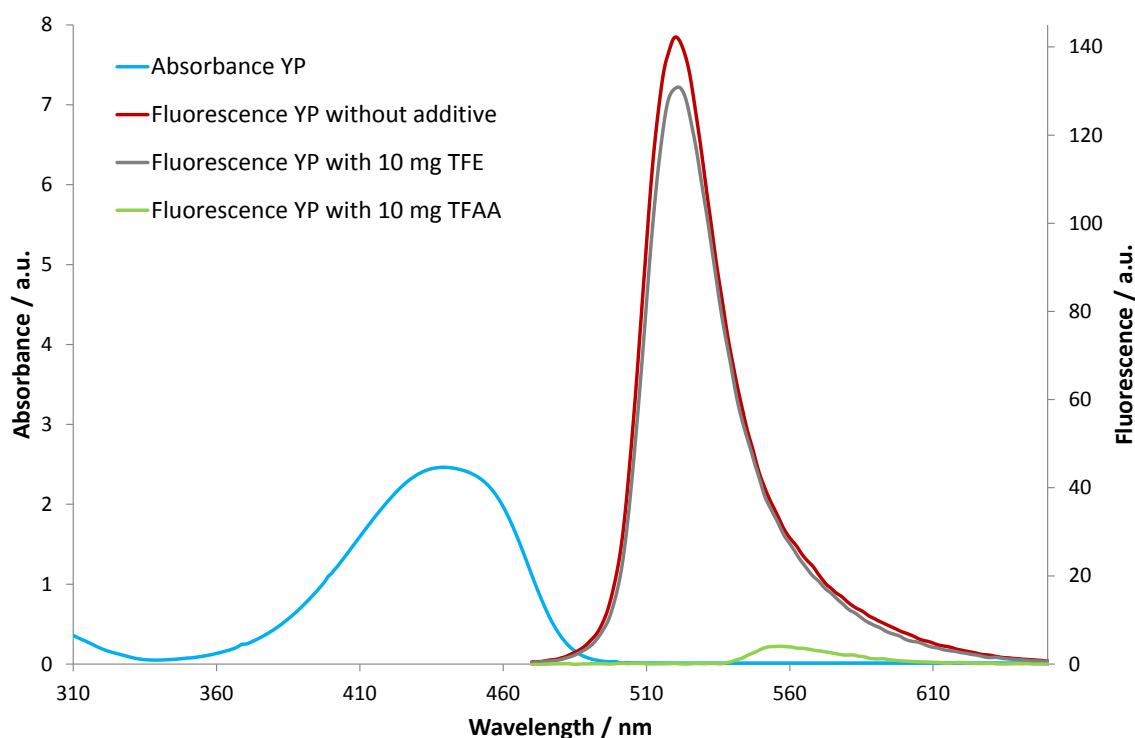
Figure 3.24: Fluorescence spectra of solutions of YP in EGMEA with TFAA and TFE. The blue curve shows the absorbance of the dye. All fluorescence curves were measured with 440 nm excitation.

With regard to the use of the CLC material as a host for organic dyes, the additives have been tested for side reactions. Many organic dyes change their emission properties at different pH-values. TFAA is very acidic and hence protonates organic

dye molecules. Furthermore does the amount of additive control the position of the SR, which is supposed to overlap with the emission of the gain material. Figure 3.24 shows fluorescence spectra of the dye Yellow Potomac (YP) in EGMEA solution with TFAA and TFE as additives. This dye provides a medium solubility in EGMEA but is very cheap, non toxic and shows a high quantum yield. As the absorbance spectrum indicates, 440 nm is the favored excitation wavelength, which was used to measure the fluorescence spectra. The red curve shows the fluorescence without any additives. With TFE shape and intensity of this peak is maintained. Instead, TFAA completely degrades the fluorescence (green curve) through protonation of the dye. The structure of YP is undisclosed by the manufacturer, so the previous statement is considered an assumption. Besides this fact, TFAA, even in small amounts, does shift the SR far to the blue and far away from the emission of YP. Hence TFE is the additive of choice. With little amounts the optical quality can be maintained at a high level and the position of the SR is tunable to the exact position needed.

3.2.6 Polymerization of Cellulosic CLC Films

After many improvements regarding the optical properties of a well aligned planar state of CTC films, a permanent fixation is desirable. In the liquid crystalline state the films are very sensitive to temperature changes or mechanical influences. For polymerization acrylates are used as solvents with a dissolved UV-initiator. The initiator Lucirin TPO is highly soluble in EGMEA and other acrylic solvents. Initiation of polymerization via UV treatment is preferred because temperature initiation affects the LC. The films were exposed to UV light of high intensity ensuring a quick and complete polymerization. The initiator decomposition upon UV illumination is shown in figure 3.25. How the power of the UV lamp and the initiator concentration affect the optical properties of the final film has already been investigated [155].
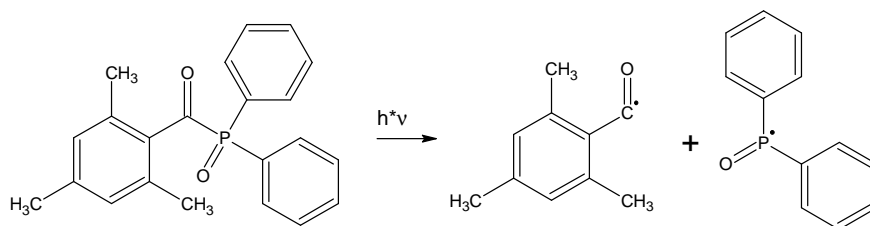
Figure 3.25: Lucirin decomposition upon UV illumination.

All previously shown improvements and measured spectra were shown for non polymerized films. It is now crucial to maintain the alignment and hence the SR from the fluid to the polymerized state. During polymerization the SR is shifted towards shorter wavelengths because of a volume shrinkage of the whole sample. In the fluid liquid crystal the monomers have van der Waals distance to each other, while in the polymerized state their distance shrinks to the length of atomic bonds. This leads to a macroscopic shrinkage, contracting the pitch of the CLC as well.
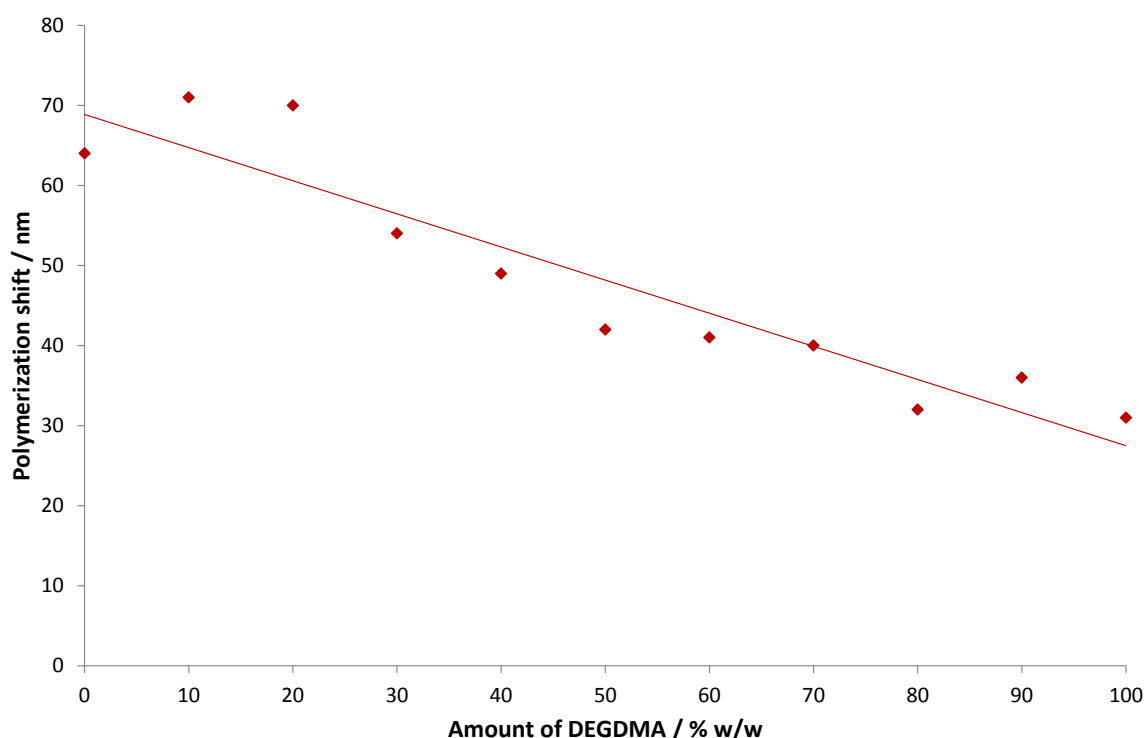
Figure 3.26: Absolute shift of SR during polymerization in dependence to the percentage of DEGDMA in the monomer mixture with EGMEA.

The polymerization itself takes place within a few seconds and during this time there is a lot a movement in the system. The alignment may be distorted and the reflectance band reduced. The shift is usually between 30 and 40 nm, while several factors have an effect on how much the reflectance is decreased. For higher mesogen concentrations the shift becomes smaller. As the best reflectance results are obtained at maximum concentration inside the liquid crystalline range the concerned shift is small. Fluorinated additives decrease the shift as well and maintain the reflectance intensity in most cases. For the polymerization process a low movability is advantageous for the mesogens to stay in the same place and maintain the alignment. Hence the choice of a solvent mixture, providing a sufficient movability

during the alignment but a decreased flexibility during polymerization, is crucial. Mixtures of EGMEA and DEGDMA have proven good abilities. As a crosslinking monomer, DEGDMA creates a dense polymer network in a very short time, not allowing the mesogens to move. Figure 3.26 shows the shift of SR during polymerization in dependence of the percentage of crosslinking DEGMDA in the solvent mixture with a monofunctional acrylate. With increasing amount of DEGDMA the viscosity of the CLC increases but the shift during polymerization is reduced. At the end of the film preparation procedure it is not sufficient just to have lowest viscosity possible but a tailored one.
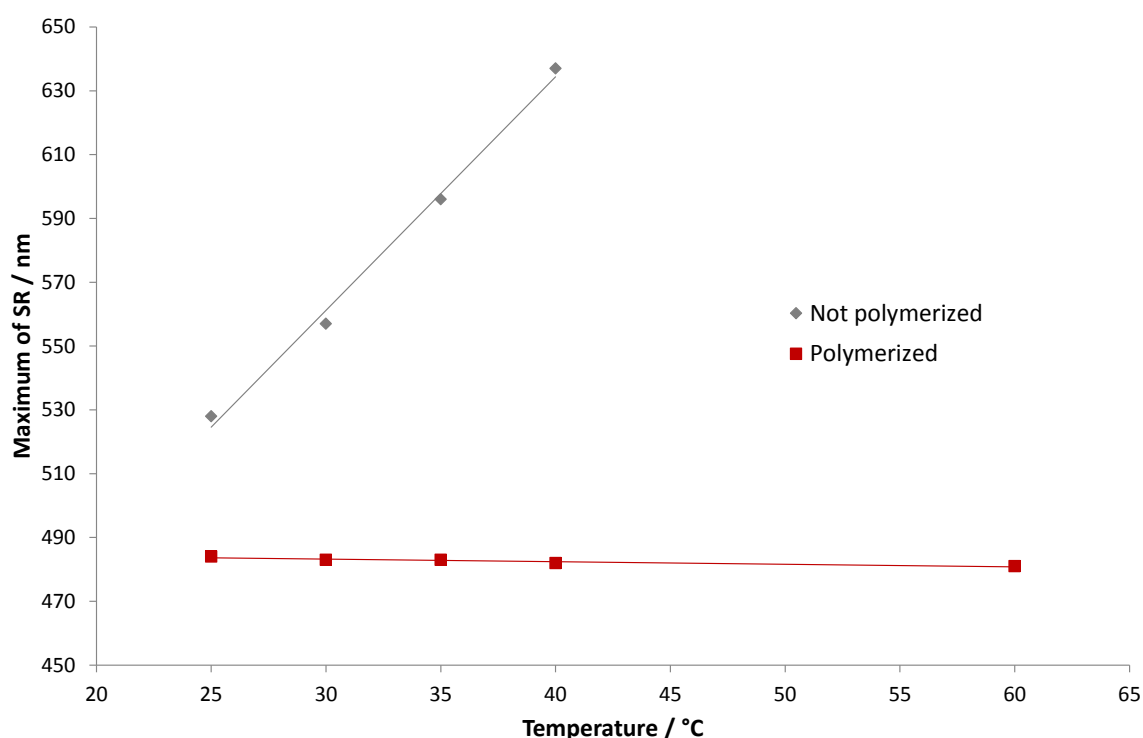
Figure 3.27: Shift of the SR in a CLC sample prior and after polymerization according to temperature change.

Figure 3.27 indicates the necessity of polymerization after the alignment of the CLC. A temperature change of 10 °C causes a SR shift of almost 60 nm to the red. This is far outside of the typical emission band of an organic dye, if the SR was in its middle beforehand. Since the samples are pumped optically using a focused laser beam, the energy density is very high and a large amount of heat, i.e. movement is introduced into the sample [162]. Not neglectable is the heat coming from the excitation of dye molecules. Locally holes were burned into the film, although polymerized films are resistant until 200 °C [155]. Polymerization yields free standing

solid films, resistant to temperature changes. Every spot can be excited for a much longer time until degradation happens. Furthermore the polymerization will play an important role during the preparation of composites (see sections 3.3 and 3.4). Somehow polymerized films are not as fixed as they may appear. Depending on the amount of crosslinking monomer in the solvent mixture the films are between flexible like a sheet of paper and very brittle. Polymeric mesogens are not expected to move in a polymerized crosslinked film, while their movability is already restricted in the liquid crystalline state. But measurements of reflectance spectra of polymerized films 30 days after their polymerization have shown that the reflectance peak gained intensity (see figure 3.28). A movement of mesogens towards a slightly better oriented structure may cause this rather small but interesting fact.
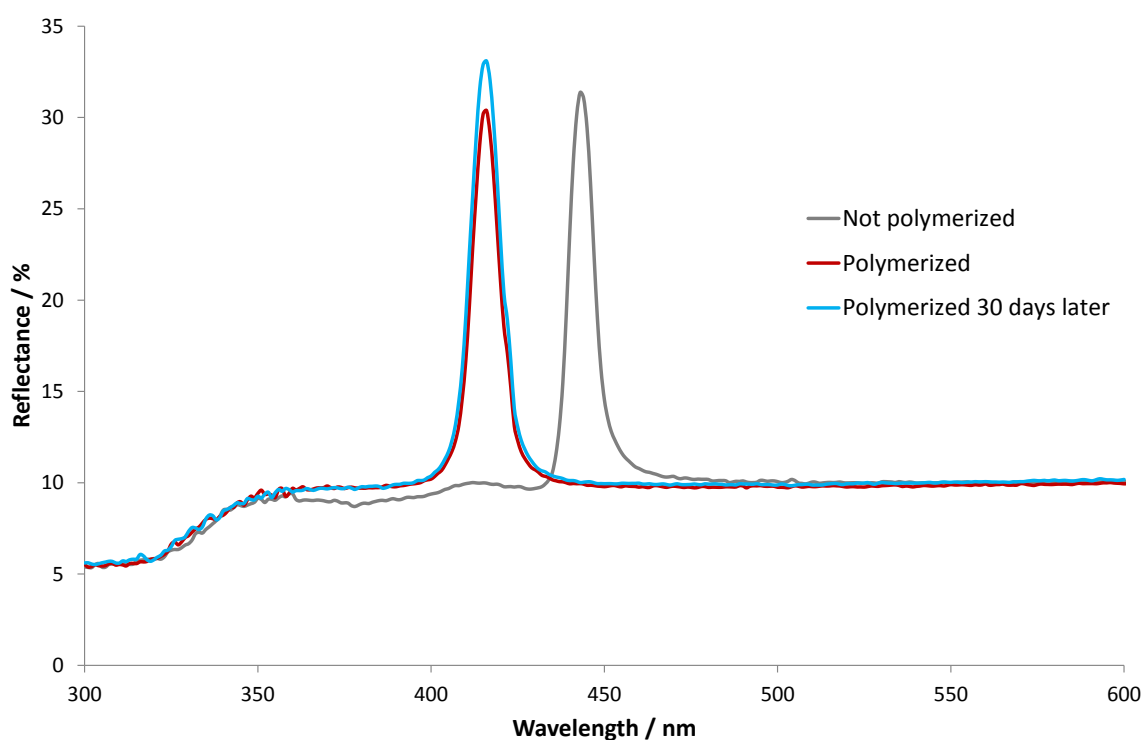
Figure 3.28: Reflectance spectra of the same film prior, after and 30 days after polymerization.

3.2.7 Conclusion

The cellulosic CLC was tuned from the introductory starting material to the state shown in figure 3.29. Peaks appearing in transmittance spectra are very narrow, usually the FWHM is below 25 nm. This value is consistent with the low refrac-

tive index anisotropy of cellulose derivatives and shows that the film is in a well ordered state; in comparison to the starting material (see figure 3.3) where the SR band was very broad and of lower intensity. The transmittance outside of the bandgap is above 90% indicating very low light scattering at domain boundaries and hence a reduced number of domains. In the optimized CLC samples, the reflectance peak perpendicular to the sample has the same shape and intensity as the one in transmittance, but the FWHM is somewhat more narrow. During the polymerization both peaks are shifted towards shorter wavelength but their intensities remain. Both peaks are getting a little broader because of the volume shrinkage effect. As expected, the absorption band of the UV initiator (grey curve, between 320 and 380 nm) vanishes during polymerization.
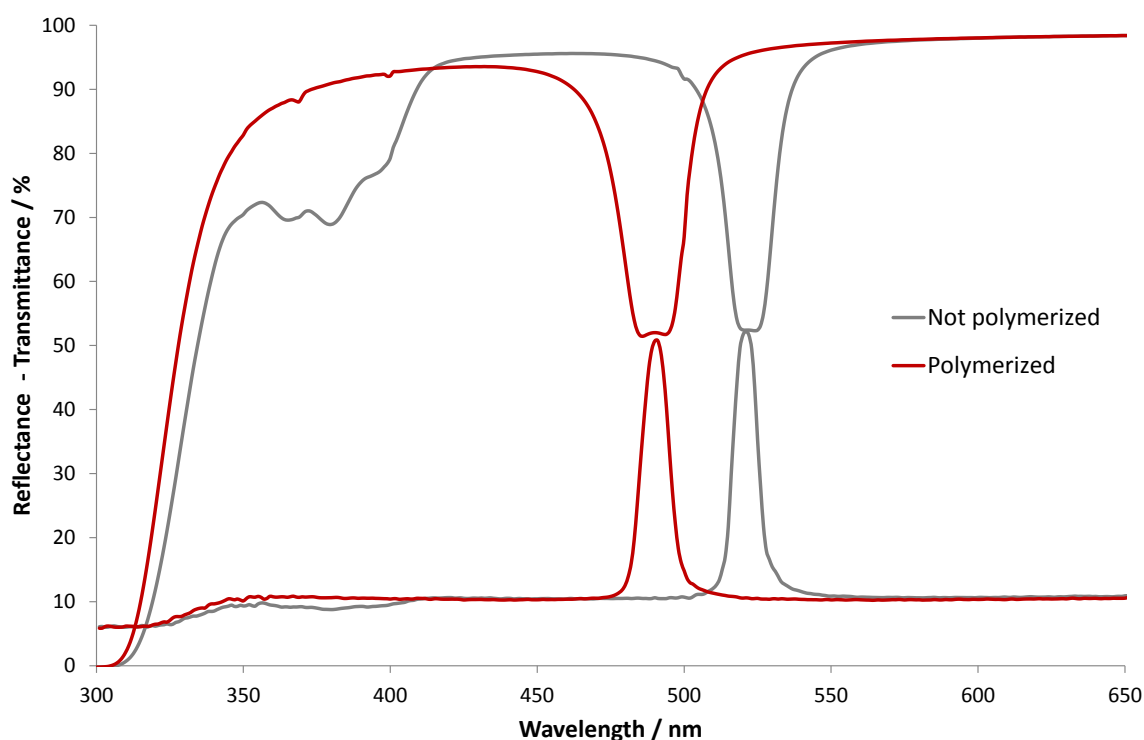
Figure 3.29: Reflectance and transmittance spectra of an improved 25μm thick CLC sample made of 140 nm CTC (46% w/w) dissolved in EGMEA/DEGDMA 80%/20% w/w, using TFE as an additive.

Although transmittance and reflectance peaks are shaped as predicted in theory, the order and alignment of the polymeric CLC is not as close to ideal as in a low molecular weight CLC. Measurements of the diffuse reflectance for the polymeric films (see figure 3.31) and, in comparison, for a low molecular weight CLC (figure 3.30) show significant differences. For the low molecular weight CLC the diffuse
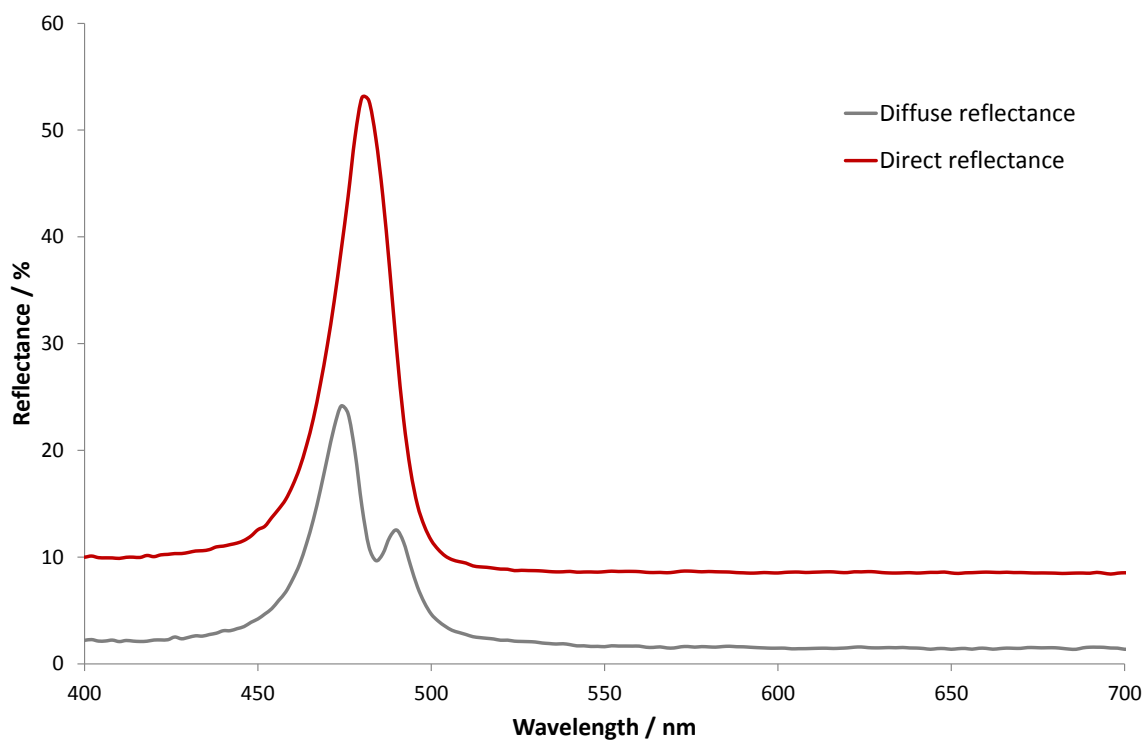
Figure 3.30: Diffuse and direct reflectance of a polymerized CLC film made of 140 nm CTC (46% w/w) dissolved in EGMEA/DEGDMA 80%/20% w/w.
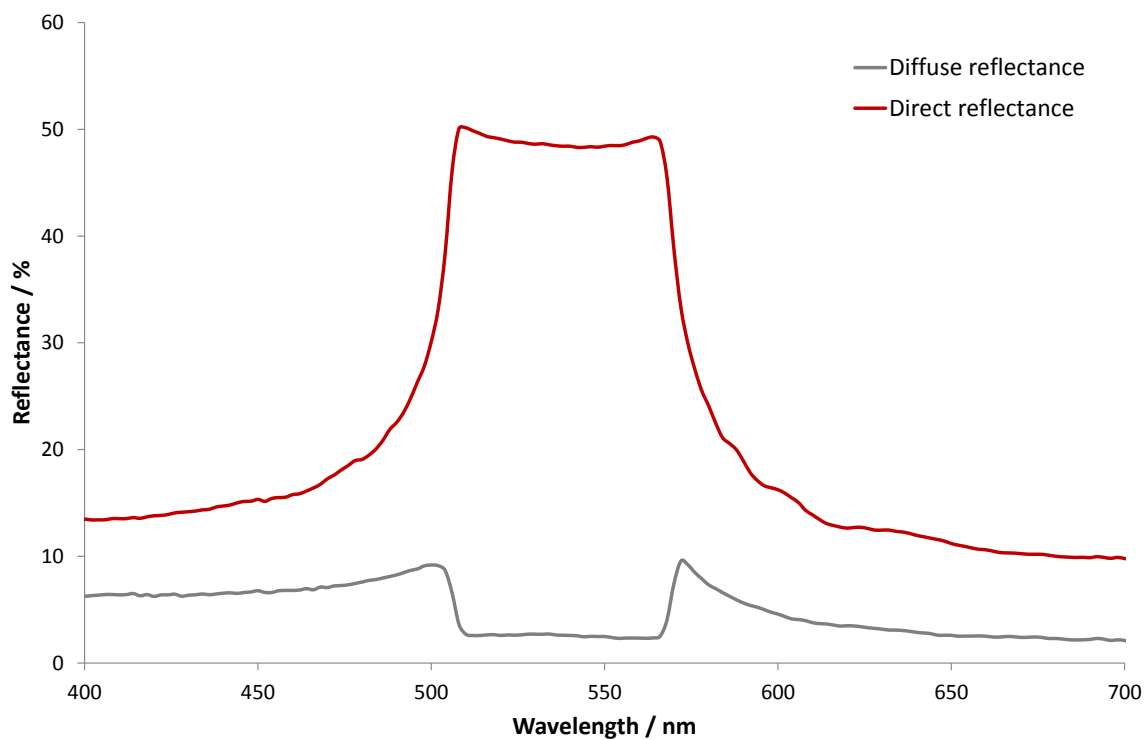
Figure 3.31: Diffuse and direct reflectance of a low molecular weight CLC (Merck MDA-00-3907).

reflectance inside the PBG is equal to zero, meaning that all reflected light is reflected perpendicular to the substrate and parallel to the helical axes. For the improved polymeric CLC the situation is much closer to the idealized state than shown in figure 3.3, but there is still diffuse reflected light detectable. At the center of the PBG its intensity is lowest similar to the low molecular weight CLC, but much higher at the bandedges. As diffuse reflected light is not recorded in reflectance measurements perpendicular to the film, its intensity does not contribute to the peak width. This causes broader peaks in transmittance spectra where all the reflected light, regardless its direction influences the peak width.
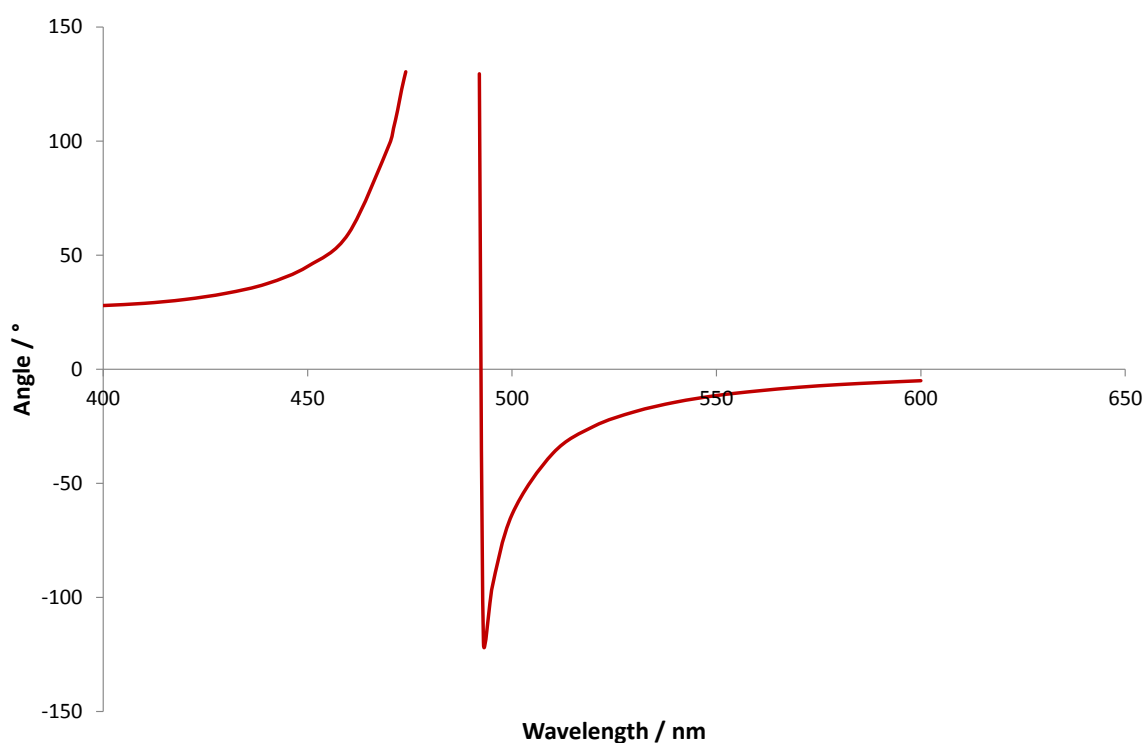
Figure 3.32: ORD spectra of an improved CLC sample made 140 nm lyotropic CTC (46% w/w) dissolved in EGMEA/DEGDMA 80%/20% w/w.

Another proof of an improved alignment are ORD measurements. In the planar state, CLC exhibit extreme value of optical rotation (see section 1.2.1) caused by the helical superstructure. The starting material showed, due to misalignment, only very low values of optical rotation (figure 3.4). During the ORD characterization of the improved cellulosic films, the limit of our ORD setup, regarding to rotation angles, was exceeded (figure 3.32). The estimated limit is in the range several hundred degrees. Between the two maxima the curve changes sign very sharply. This fact and the absolute values of rotation indicate a very well ordered sample.

The cotton effect is still negative representing a right handed twist sense of the cholesteric helix.

If the photographs of the starting and the improved material are compared, no obvious differences are visible. All films reflect a defined parts of visible light, causing their colored appearance. In figure 3.33 different values for the cholesteric pitch result in different colored films. The reflectance seems to be intensive to the naked eye for both materials, before and after improvement. However POM images suggest a difference, where lots of defects are visible for the starting material and no defects remain after improvement. Although the films appear very similar, only optical characterization can show the distinction of optical qualities, regarding to the use as a feedback material. So far, to the best of our knowledge, these optical characteristics have not been reported for a CLC made of derivatives of cellulose. Only a few papers report about the absolute value of direct reflectance [163] and papers mentioned in section 1.3.3 claim about the bad feedback qualities of cholesteric films based on lyotropic polymers. With the improved materials the basis for a sufficient feedback in mirrorless lasing devices is given. The optical properties can be tuned via the amount of additive or temperature change to fit perfectly to the emission properties of the gain material. Permanent fixation via polymerization is easily done to yield solid and free standing films. The optical performance is close to theoretical predictions and close to the behavior of low molecular weight CLC. Nevertheless, a mirrorless lasing sample with a low threshold requires a high cavity quality which is related to the alignment of the CLC. Residues applied to cellulose that increase the birefringence, automated rubbing and repeated alignment methods [164, 165] and further viscosity reduction may open the way to CLC film with even more advanced optical properties.
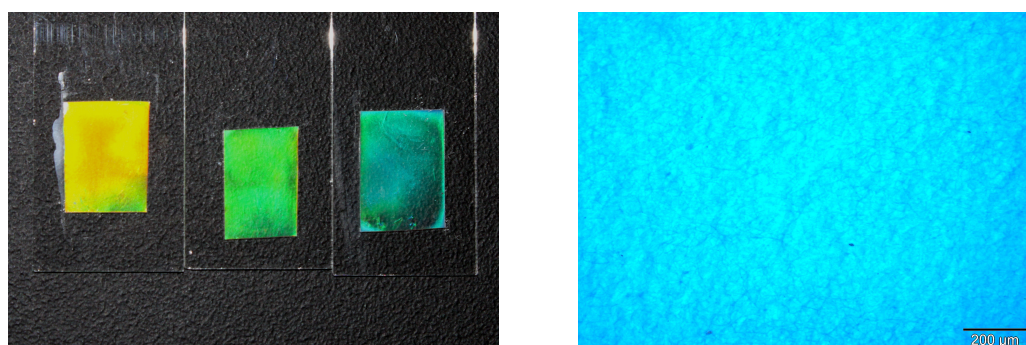
Figure 3.33: Photograph (left) and POM image of improved CLC films made of CTC (46% w/w) dissolved in EGMEA/DEGDMA 80%/20% w/w doped with TFE.

3.3 Composites of Cellulosic CLC with Inorganic Nanoparticles

3.3.1 Introduction

The preparation of mirrorless lasing films includes two components: The cavity providing feedback and a chromophore providing gain. In most of the setups both compartments are organic materials. But organic dyes do have the disadvantage of degradation reactions, if the film is optically pumped with high intensity. On the other hand they are commercially available in large quantities, can be tailored with tools of organic chemistry and are easily introduced into organic host materials. The degradation of the gain material limits the usability of the sample when the pumped spot is bleached, the output energy drops to zero. But degradation is not the only loss mechanism attributed to the dye: Quenching of emission processes and insufficient quantum yield further complicate the situation. Therefore different methods have been applied to stabilize the system or to reduce the optical stress with lower thresholds [147]. Another way is to replace the organic dyes by inorganic materials like fluorescent semiconductor nanoparticles. They are more stable to high intensities of pump light and degradation can be prevented by the usage of core shell or hybrid particles. On the other hand, the introduction of inorganic guest materials into organic CLC is not as easy as for organic dyes. The defined synthesis of low molar mass and polymeric surfactants is necessary to obtain a homogeneous distribution of the inorganic guest particles. To ensure a high miscibility between the inorganic and the organic part a geometrical shape match was needed, in addition to the chemical match through surfactants. As nanoparticles are available in anisotropic shapes, nanorods were the shape of choice to fit the form of calamitic mesogens. Because NP and mesogens have shown to phase separate because of their different shape despite surface modifications [166]. In the following sections general aspects about hybrid nanorods, the synthesis of polymeric surfactants and the behavior of surface modified nanorods in cellulosic CLC will be described.

3.3.2 Fluorescent Hybrid Nanorods

Metallic nanoparticles [167] with tunable fluorescence properties are available in spherical shapes and have been used for optoelectronic devices. However spherical particles aggregate in organic liquid crystals consisting of rodlike mesogens [166]. Thus the use of nanorods and large calamitic mesogens, like modified cellulose

seems attractive to obtain a miscible system. To combine the fluorescence properties of spherical particles with an anisotropic shape, we chose hybrid nanorods consisting of a spherical cadmium selenide (CdSe) core and a cylindrical cadmium sulfide (CdS) shell [125]. Using highly sophisticated synthetic strategies, one can produce spherical cores - providing the optical properties - with rodlike shells - providing the shape-match. The particles are synthesized via a seeded mediated growth approach. The CdSe cores are synthesized first, yielding the desired fluorescence qualities. In a second reaction, they act as seeds for the CdS shell. The anisotropy of the shell is controlled by surfactants during the reaction, which preferably attach to certain crystal surfaces, while other parts of the crystal are more exposed to the solution and grow faster. Factors like synthesis temperature, concentration of reactants as well as nature and amount of surfactant enable one to tune the NP's optical and geometrical properties in various ways (see figure 3.34).
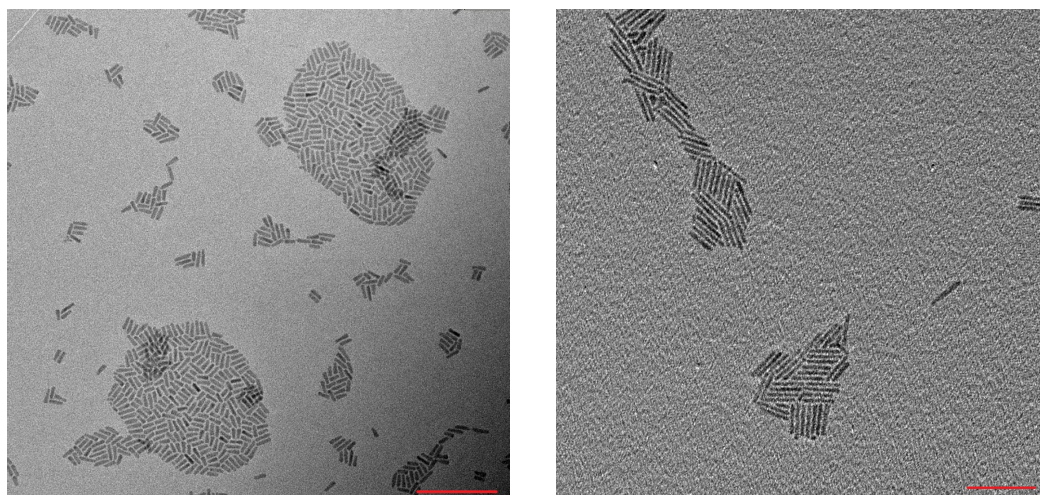
Figure 3.34: TEM images of the used CdS@CdSe nanorods.
The scale bar indicates 100 nm.

The used surfactant trioctyl phosphate makes the NP soluble in organic solvents, a basis for easy surfactant exchange with polymers. The nanorods show a very low polydispersity and their lengths are very similar to those of the CTC. However, their big diameter will play a role in the following sections, though. With certain surface modifications and at high concentrations NP are capable of forming liquid crystalline phases, similar to nematics and smectics [168, 57, 56] and have been shown to stabilize liquid crystalline phases [136].

3.3.3 Synthesis of Polymeric Surfactants

The surface modification of the CdS@CdSe nanorods was done with block copolymers, synthesized via RAFT polymerization (see section 1.5). These polymers contain an anchor block for the attachment to the particle's surface and a solubility increasing block, structurally similar to the solvents used for the CLC. As EGMEA or HA were used as solvents and are, like many acrylates, polymerizable via the RAFT technique, the latter block was made from these molecules. In addition DEGEEA was used to synthesize this block, too. After the synthesis of the first block made of one of these acrylates, a reactive ester monomer, pentafluorophenol acrylate (PFPA), was polymerized to give the diblock copolymer. The reactive ester block can easily be converted into an anchor block via a substitution reaction. Amines carrying the desired anchor group yield, in a polymer analogous reaction, the final anchor entity. Due to the high number of attachment groups per polymer, the bond to the particle's surface is much stronger than for low molecular weight surfactants, containing only one attachment group. If one group does detach from the surface, the polymer will still be bound to it, while surfactants with only one group lose contact to the particle. The anchor group of the polymer does replace low molecular weight ligands due to this chelate effect. Detaching several small molecules by replacing them with one large molecule at the same time increases entropy. The nanorods are covered with trioctyl phosphate from their synthesis. The bond of the phosphate group is strong enough to cover the surface under equilibrium conditions, but sufficiently fragile to provide growth conditions. Thinking of the polymeric surfactants, there are three reasons why thiols are the anchor group of choice: They bind very strongly to the CdS shell, displace ligands from synthesis and do not affect the NP's fluorescence properties. However, thiols are susceptible to oxidation reactions. Therefore we used an amine containing a disulfide group capped with a methyl ether (cysteamine methyl disulfide (CMD) see molecule 6 in figure 3.35). As shortly described in the caption to figure 3.35 the acrylate being utilized as solvent of the CLC, or a similar one, is polymerized with a chain transfer agent. This block increases the solubility of the polymer, and hence of the NP, in the acrylic solvent. The chain transfer agent is carefully chosen to be reactive towards this and the following monomer, which contains a reactive ester moiety. After a two step synthesis the diblock copolymer can be reacted with different anchor molecules, to prepare polymers attachable to different nanoparticles from the same polymer. The reaction with an amine substitutes the pentafluorophenol and the anchor entity becomes part of the second block.
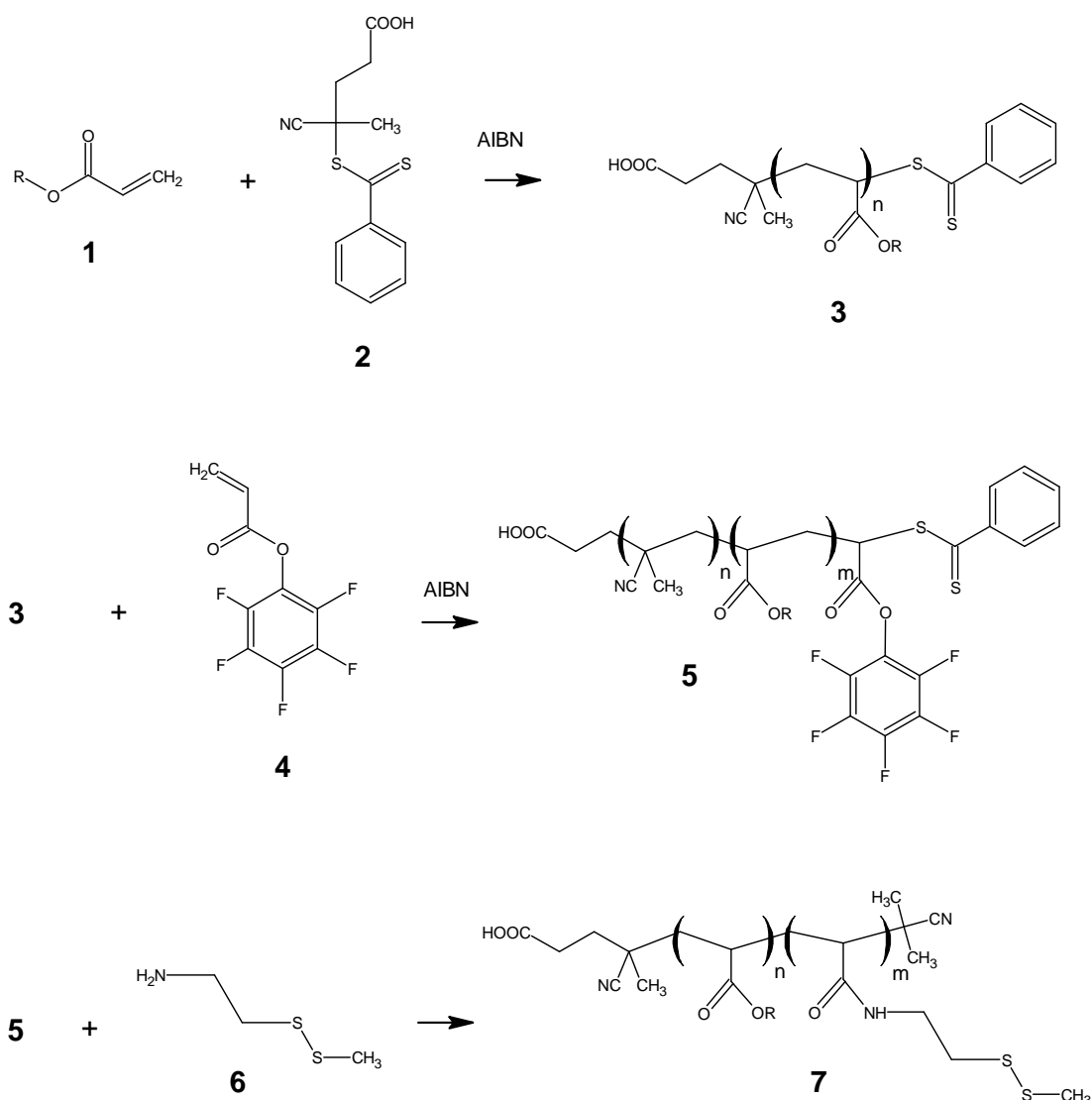
Figure 3.35: Schematic synthesis of block copolymers as surfactants. The acrylate (1) is polymerized with a CTA (2) to the first block (3) and PFPA (4) is added to obtain the diblock copolymer (5). The substitution reaction with CMD (6) finally yields the polymeric surfactant (7). For detailed information see figure 4.3.

During this reaction, or via a deactivation reaction, the CTA endgroup is cleaved from the polymer. The length of each block can be roughly calculated, since each monomer behaves differently, e.g. with CTA, solvent and temperature, exact chain lengths can be achieved empirically. The first block was synthesized in different lengths from 25 to 100 units, while the second block was set at around 20 units. For the first block 200 units are realizable, but the number of units in the PFPA block is decreasing with increasing length of the first block. A different surfactant
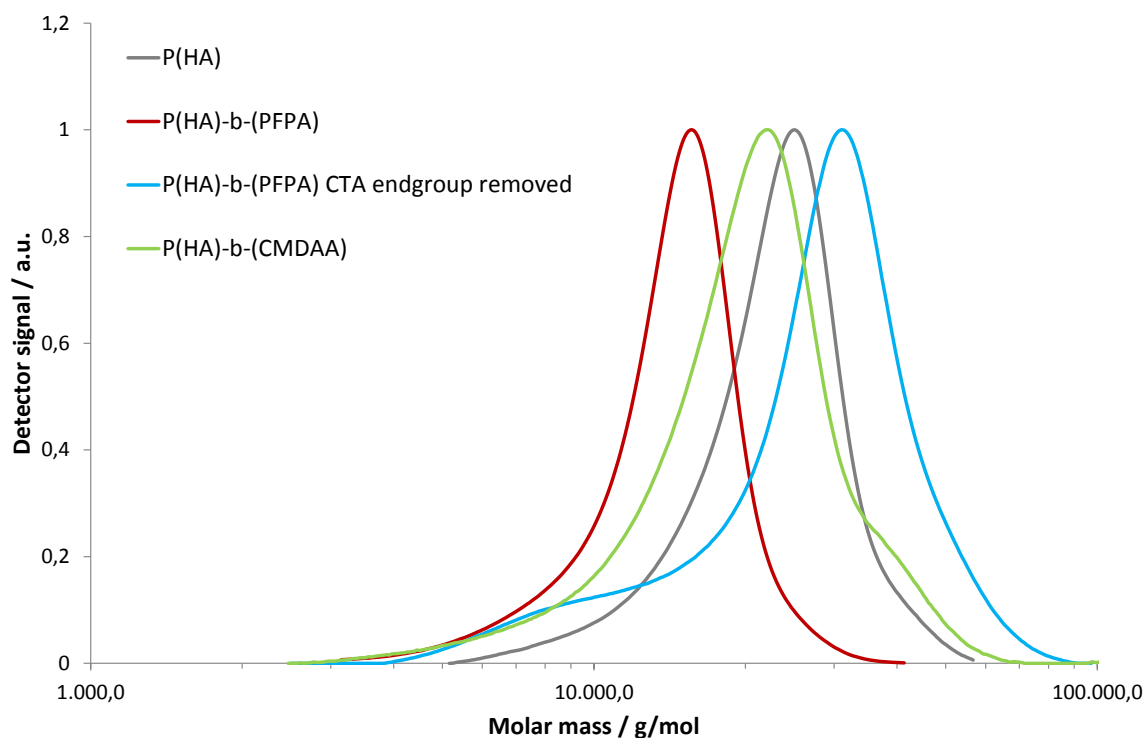
Figure 3.36: GPC curves of all steps towards $P(HA)_{100}$-b-$(CMDAA)_{20}$. Values of molar mass are in poly(styrene) equivalents. See figure 3.37 for chemical structure. The swelling behavior of the different polymers cause irregular shifts of the maxima, limiting the molar mass determination via GPC.

for nanoparticles is poly(ethylene glycol) (PEG) capped with a thiol functionality. These polymers are commercially available but sensitive towards oxidation of the thiol group. Figures 3.37 and 3.38 give an overview of the used polymeric surfactants.

3.3.4 Nanoparticles in Cellulosic CLC

Polymeric surfactants improve the nanoparticle's solubility in acrylic solvents used to dissolve high amounts of CTC. During the exchange of surfactants, low molecular weight surfactants are removed by polymeric ones. At first the nanoparticles are dissolved in chloroform or tetrahydrofurane and washed from residual materials from synthesis by repeating centrifugation. Second the polymer is added and the solution is exposed to ultrasonication for a sufficient mixing. After a certain time the NP are precipitated through the addition of a non-solvent and subsequent centrifugation. By repeating a dissolving - precipitation cycle the low molecular weight

P(HA)$_n$-b-(CMDAA)$_m$

Poly(hexyl acrylate)$_n$-block-(cysteamine methyl disulfide acrylic amide)$_m$

P(EGMEA)$_n$-b-(CMDAA)$_m$

Poly(ethylene glycol methyl ether acrylate)$_n$-block-(cysteamine methyl disulfide acrylic amide)$_m$

P(DEGEEA)$_n$-b-(CMDAA)$_m$

Poly(diethylene glycol ethyl ether acrylate)$_n$-block-(cysteamine methyl disulfide acrylic amide)$_m$
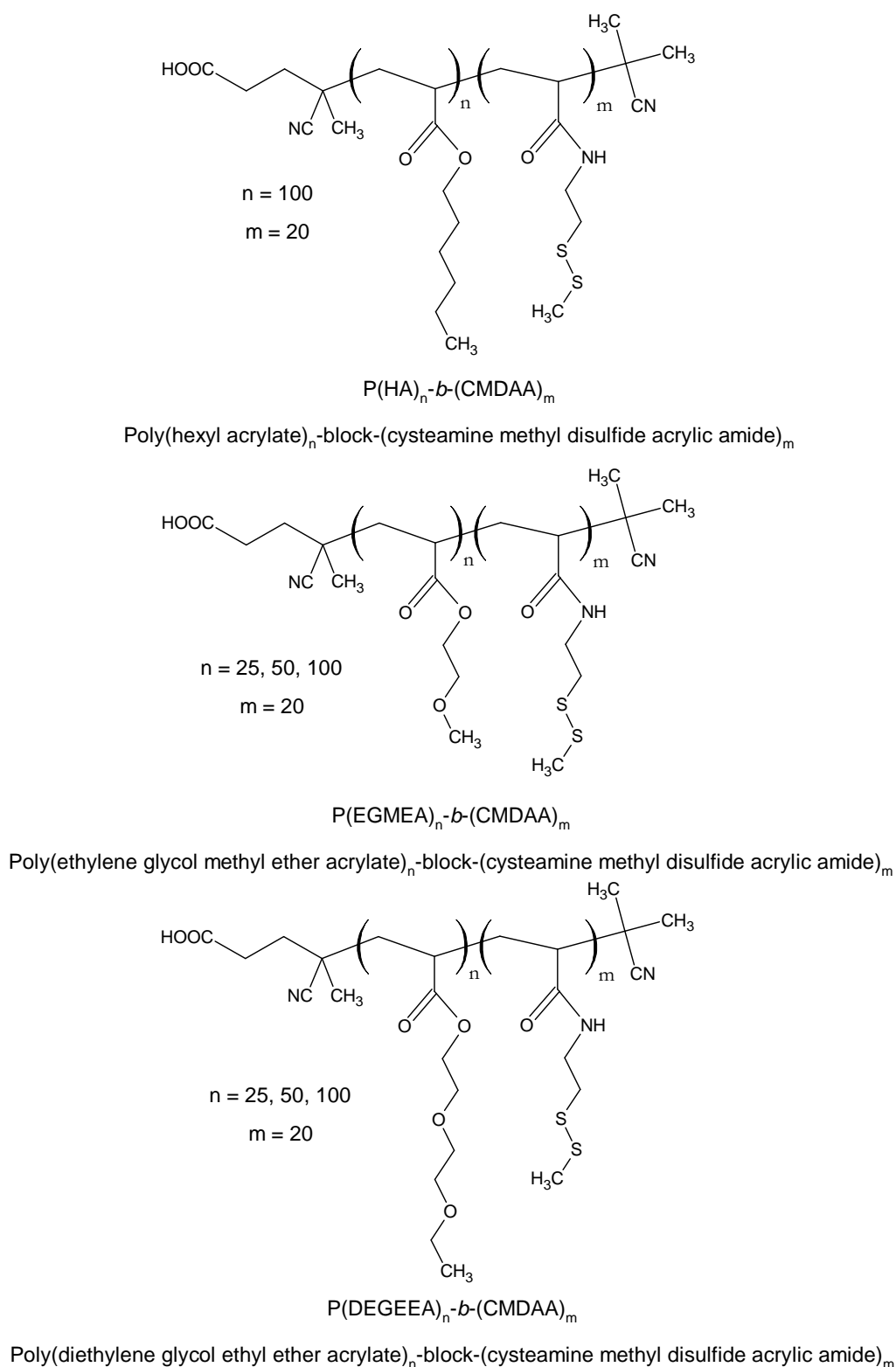
Figure 3.37: Overview of the synthesized polymer surfactants via RAFT polymerization based on acrylic monomers.

n = 16, 44, 112

P(EG)$_n$-SH
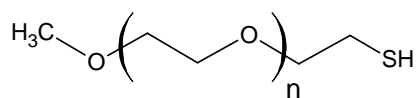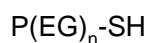
Poly(ethylene glycol)$_n$-thiol

Figure 3.38: Overview of the purchased polymeric surfactants based on PEG.

surfactants are removed from the solution. Afterwards polymer coated NP can be transferred into the solvent of the final CLC. Nevertheless, sometimes the precipitation was not possible after polymer coating, due to a highly increased solubility in organic solvents, and especially in the liquid that was meant to induce precipitation. On the other hand the polymer with EGMEA and DEGEEA as the first block did not yield well dispersed solutions of NP in acrylics. We suppose that the anchor blocks are hidden inside the polymer random coil or that during precipitation of the NP the polymer collapses in this medium, loosing its surfactants properties.

The transfer of the polymer coated NP prior to the addition of the CTC has two advantages: The liquids viscosity is much lower than in the CLC state and the particles can be distributed homogeneously in the solvent and supposedly in the CLC. Addition of NP to an already mixed CLC is rather difficult because the solution is almost saturated with CTC and highly viscous. The NP can only slowly move into the CLC because of their size and limited movability. Furthermore they are not applicable as a powder, so a small amount of liquid is needed which changes the concentrations in the CLC, affecting the optical properties. The first step is thus to transfer the polymer coated NP into the acrylic solvent to yield a homogeneous distribution. Afterwards CTC are added and the mixture is stirred mechanically. For comparison figure 3.39 shows how NP behave in solution and CLC without any additional surface modification, only covered with the material from synthesis.

In the acrylic solvent (top picture) the fluorescent microscopy image shows only aggregates of NP. This behavior is expected, since trioctyl phosphate does not provide a sufficient solubility in HA. Hence the NP try to minimize their interface with HA trough aggregation. As the NP are already aggregated, the situation does not change after the addition of 46% w/w CTC. After two hours of stirring, the mixture only shows aggregated NP. Due to the increased viscosity in the CLC this pattern remains unchanged for several hours. To achieve a homogeneous distribution in
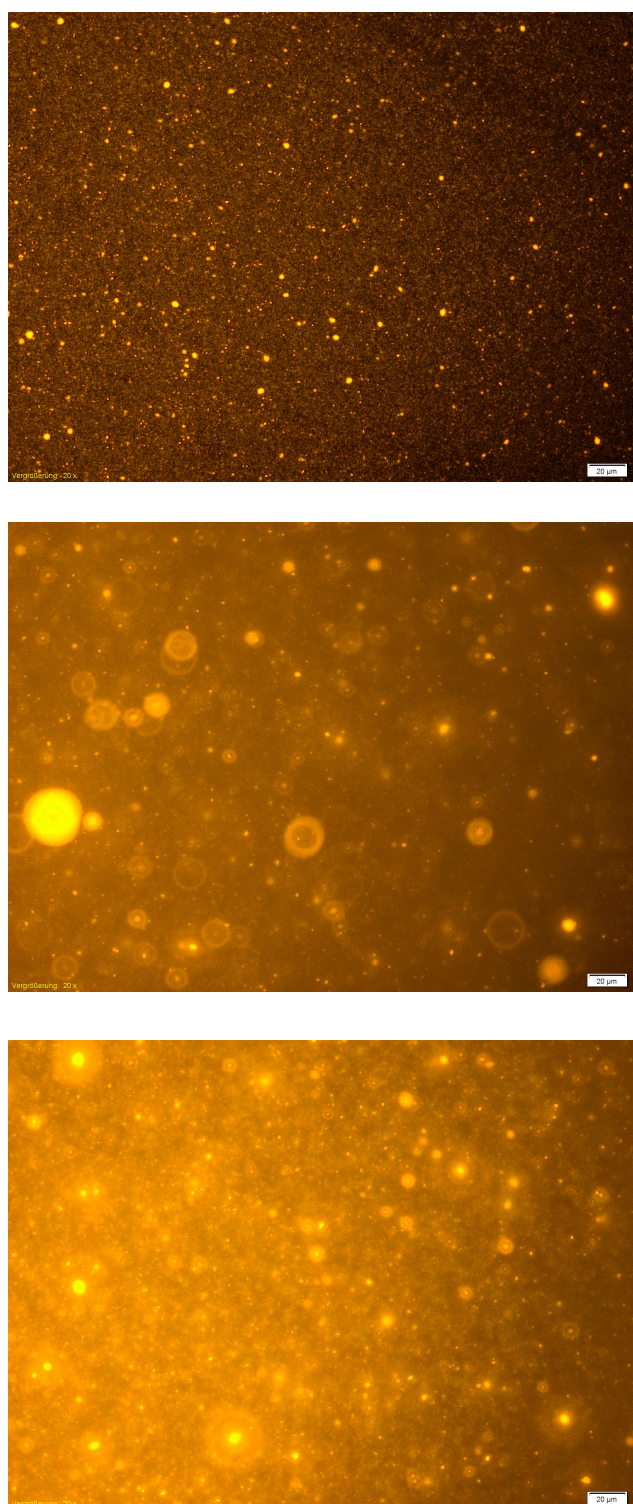
Figure 3.39: Fluorescence microscopy images of unmodified NP in HA/DEGDMA 80%/20% w/w mixture (top), with 46% w/w CTC (140 nm) directly after stirring (middle) and several hours later.
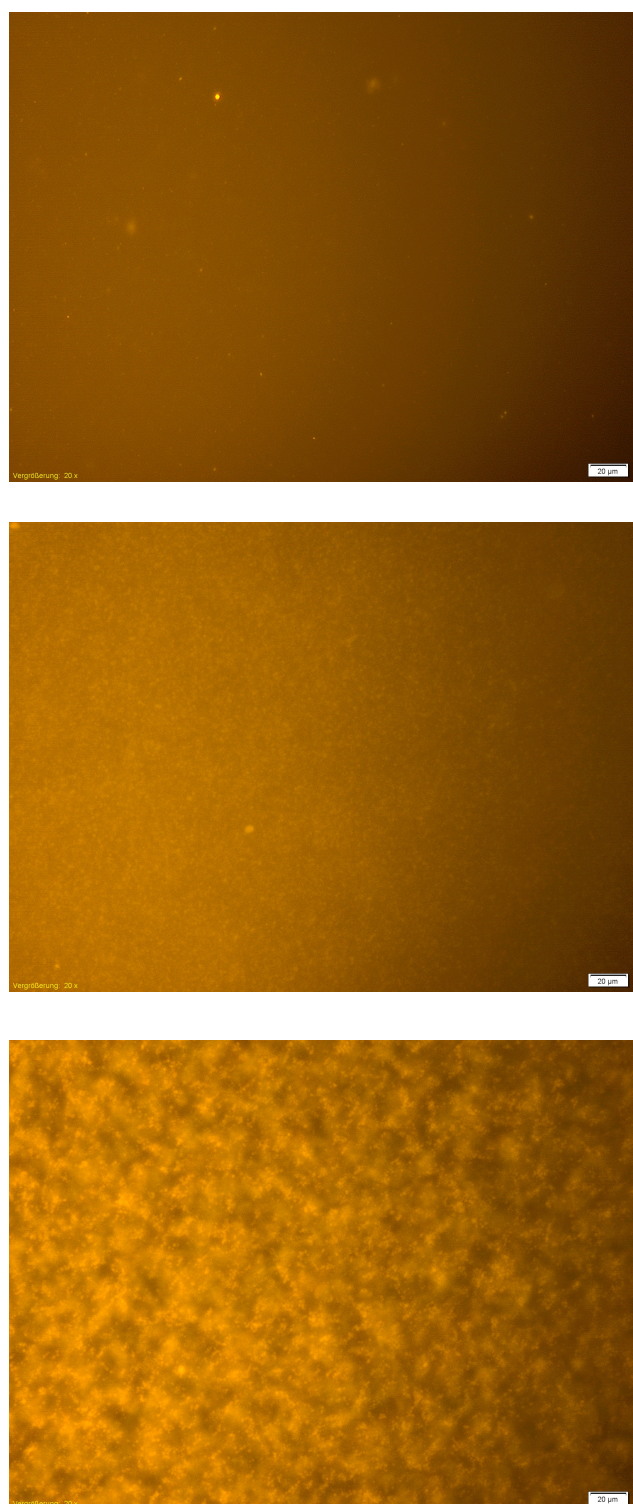
Figure 3.40: Fluorescence microscopy images of P(HA)$_{100}$-b-(CMDAA)$_{20}$ modified NP in HA/DEGDMA 80%/20% w/w mixture (top), with 46% w/w CTC (140 nm) directly after stirring (middle) and several hours later.
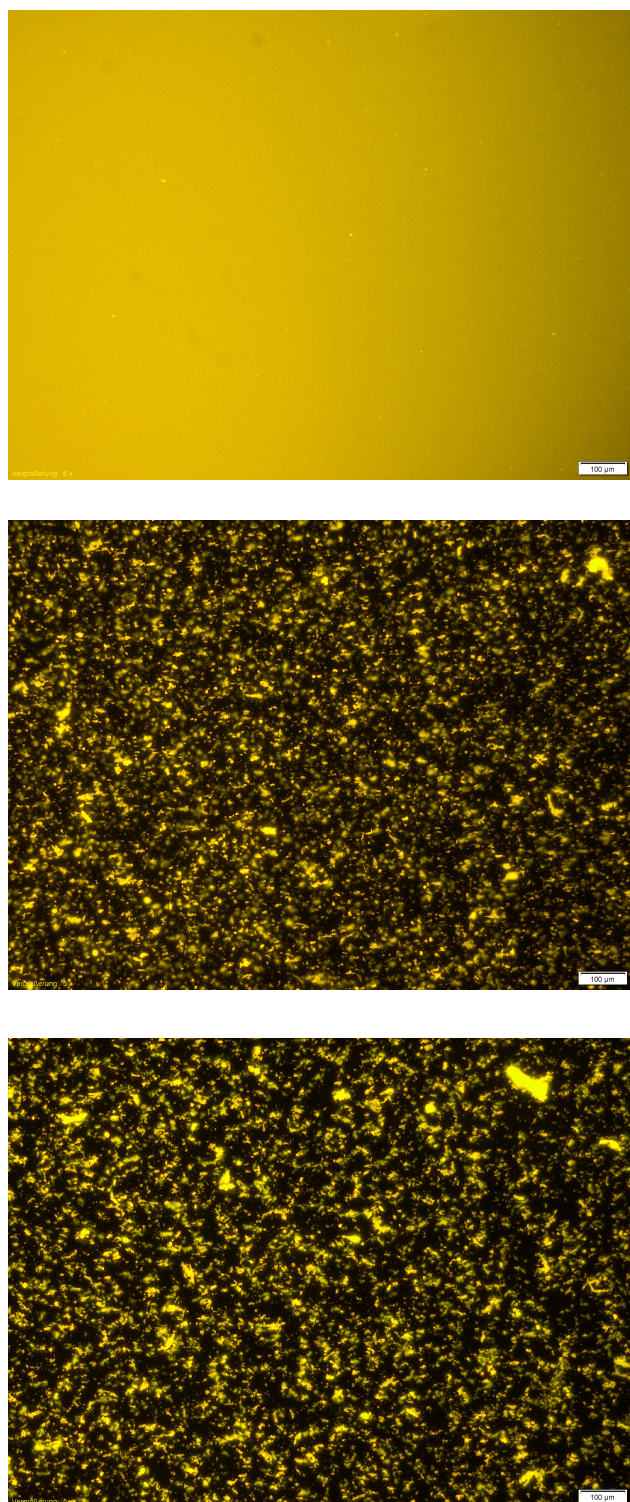
Figure 3.41: Fluorescence microscopy images of P(HA)$_{100}$-*b*-(CMDAA)$_{20}$ modified NP in EGMEA/DEGDMA 80%/20% w/w mixture (top), with 46% w/w CTC (140 nm) directly after stirring (middle) and several hours later.
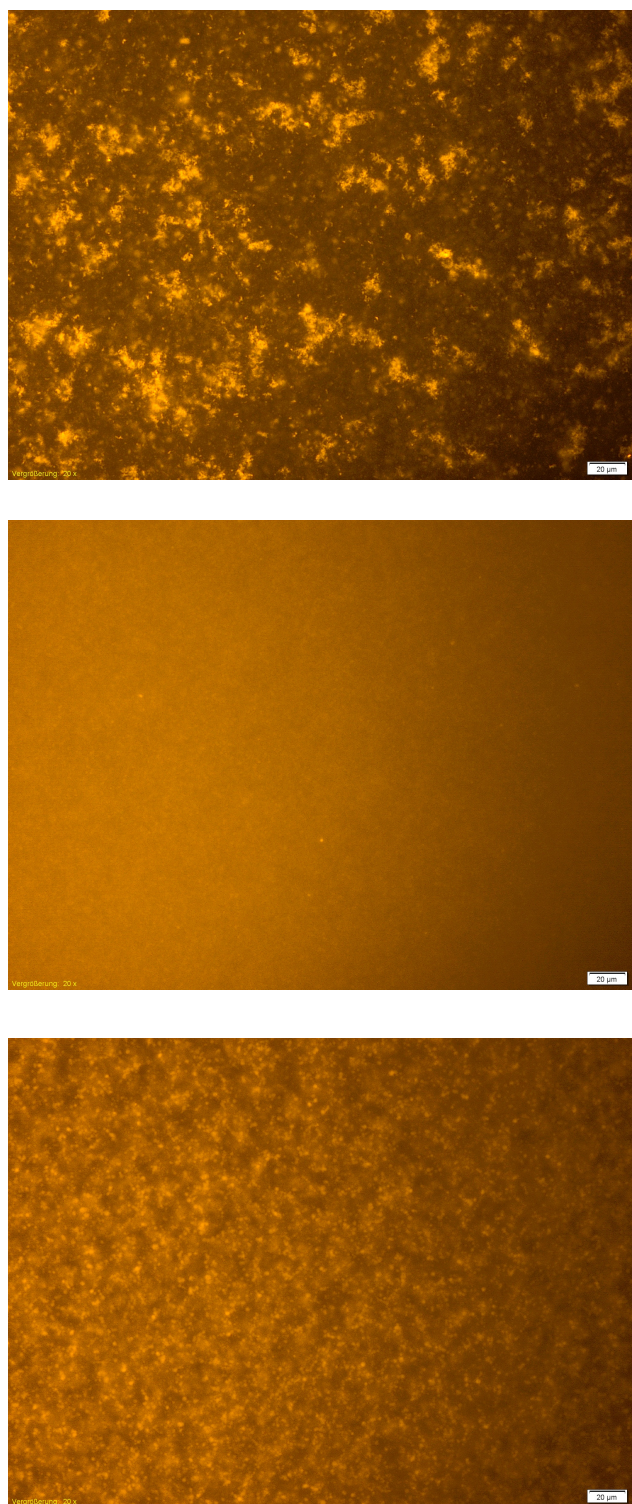
Figure 3.42: Fluorescence microscopy images of P(EG)$_{16}$-SH modified NP in HA/DEGDMA 80%/20% w/w mixture (top), with 46% w/w CTC (140 nm) directly after stirring (middle) and several hours later.

CLC a polymer modification is necessary and the solution must be homogeneous even before the CTC are added. It is important to prevent aggregation because otherwise NP lose their fluorescent properties and the threshold of the resulting lasing film increases dramatically.

The situation changes significantly when the NP are coated with the polymer surfactant $P(HA)_{100}$-b-(CMDAA). In figure 3.40 the situation shown is similar than in figure 3.39 with the difference of surface modification. Here the first block of the polymeric surfactant is made of the solvent used. Accordingly the nanoparticles form a homogeneous solution with only a few numbers of aggregates. The polymer here has two functions: It camouflages the chemical structure of the NP and due to its size it hinders NP in getting to close to form agglomerates. This solution is a good starting point to prepare homogeneous composites from. However the influence of the mesogens, which are the major ingredient in the CLC, leads to a aggregation of the nanoparticles. We believe that this is due to difference in thickness between the NP and CTC. An increase / decrease of the P(HA) block length slightly slows down/speeds up the agglomeration process. Thus only small aggregates are visible directly after stirring and they grow in size during the following hours. This fact is very important, because the liquid crystals needs several hours to align in order to provide the optical properties needed for feedback mechanism. In figure 3.41 the NP are coated with $P(HA)_{100}$-b-(CMDAA) and dissolved EGMEA/DEGDMA 80%/20% w/w. The agglomeration process after the addition of 46% w/w CTC is almost faster than in the previous case. Although NP with this polymer coating yielded homogeneous solutions in HA and EGMEA, both mixed with DEGDMA, the shape mismatch dominates the solution behavior in highly concentrated CTC solutions. In comparison to unmodified NP the miscibility could be increased but is still not sufficient enough for the aim to incorporate fluorescent NP into cholesteric, cellulose based films. The length of the NP is in the same range as the one for CTC, but the diameter of the NP is up to 50 times larger. Figure 3.43 gives an estimate about the size relations. A TEM image of 80 nm CdS@CdSe nanorods is shown in figure 3.34on the right. The nanorods shown on the left are much shorter but their diameter is very similar. Hence the results of composites with shorter nanorods were comparable to those of 80 nm long nanorods. The polymer modification also further increases the diameter. In a densely packed CLC the pitch is around 400 nm which correspond to $\approx$ 500 nematic layers of CTC. A NP with a 50 times larger diameter penetrates almost 50 layers. At this distance the twist angle between the bottom and the 50th layer is $30°$. The NP on the other hand is completely rigid and

hence disturbs the alignment of the CTC. Although it is not required for the gain material to be oriented with the mesogens to achieve lasing, it is not possible for the NP to align in any way with the cholesteric helix, without disturbing it. Even very small nanorods with a diameter below 10 nm, pass through many nematic layers. The same happens with spherical nanoparticles, since they are already in a geometrical shape mismatch.
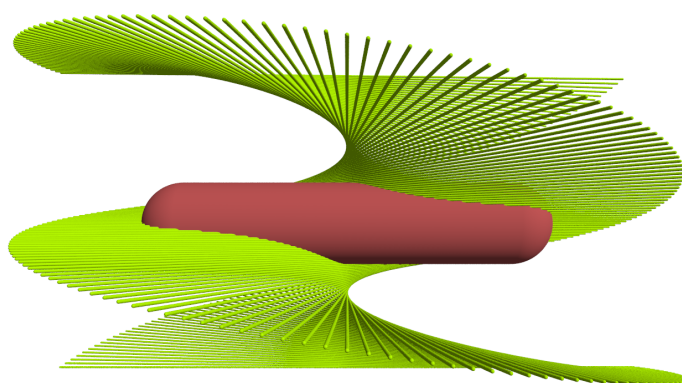
Figure 3.43: Size relation between 140 nm CTC (green, fully extended shape) and a 80 nm nanorod (red).

In the third case (figure 3.42) the NP were coated with PEG polymers containing a thiol endgroup as the surface anchor. PEG is known to be soluble in various organic solvents. It is assumed to provide a lower solubility of NP in HA as the tailored block copolymers, but a much higher solubility in the resulting CLC. In the top row picture the mixture shows NP with the smallest available PEG polymers on the surface in HA. Like in the unmodified case the NP tend to form aggregates which are getting smaller after the addition of CTC. In the final CLC, even after several hours, the NP show a more homogeneous distribution than in the pure solvent but the overall situation is similar the one with the block copolymers.

So far the focus was on the homogeneous distribution of NPs in the liquid crystalline host. Their integration reduces the optical properties of the CLC films and makes them an insufficient gain material in combination with CTC. As the CLC is very sensitive to any disturbance, the alignment is affected very easily. There is a need of sufficient feedback for lasing, so a well oriented sample is inevitable. The amount of gain material is usually between 0.1 and 1% w/w. All CLC films with NP showed a decreased intensity of reflected light and hence a weaker feedback performance.

3.3.5 Conclusion

Films of lyotropic derivatives of cellulose show remarkable optical properties after the improvements described in section 3.2. On the other hand fluorescent nanoparticles provide a very suitable replacement for organic dyes and are promising materials for the application as gain materials in mirrorless lasing devices. However, the combination of both materials include some challenges. The liquid crystal is in need of a precise tuning to show peak performance. Any factor changed and the very sensitive host material does not provide a sufficient feedback. Regarding surface chemistry and shape, the inorganic nanorods seemed to be a perfect match for a calamitic CLC, but the size difference is too big to allow full miscibility. However the aggregates formed do disturb the CLC's alignment. At this point a homogeneous mixture of inorganic nanorods and organic CTC liquid crystals with improved optical properties is not realizable.

3.4 Composites of Cellulosic CLC with Organic Dyes

3.4.1 Introduction

Since the beginning of mirrorless lasing devices, organic dyes were utilized for gain materials, but the bleaching during the optical pumping is still an issue. Therefore decreasing of lasing threshold, reduces optical stress to the gain material. A reduction can be achieved by improving dye concentration or film thickness [169], the cavity regarding its quality with anisotropically shaped dyes [170], applying different alignment to increase pump efficiency [171] or the use of defect mode devices [114]. As shown in the previous section a replacement with inorganic nanorods is not possible so far. In order to show that the feedback structures prepared from cellulose derivatives are capable to provide feedback for defined bandedge lasing, organic dyes were incorporated. There are numerous dyes commercially available and very often they are soluble in a wide range of solvents. Otherwise they can be tailored with tools of organic chemistry. At concentrations necessary, they do not have any disturbing influence to the liquid crystal because of their small size. Hence they are incorporated into the cholesteric structure very easily. The following sections provide an overview about required properties of laser dyes, the dyes chosen and different ways how to prepare composites with organic dyes.

3.4.2 Organic Laser Dyes

Organic laser dyes [172] are not only used in mirrorless laser devices but in many kinds of dye lasers. The ultimate aim for every dye laser is continuous wave operation, i.e. permanent laser output over a long time range. Therefore the threshold is essentially to be decreased to zero, to run the pump source at minimum power. This can be achieved in two ways: The quality of the cavity is perfected and any loss mechanism dedicated to it is eliminated, second the gain material is tuned to provide maximum gain at lowest excitation. Besides well known dyes like DCM or PM597, there have been lots of attempts to synthesize specialized dyes only for mirrorless lasing devices [173]. The specific characteristics a dye must posses to be valuable for lasing are: A high absorption coefficient at excitation and a low absorption at lasing wavelength, a high quantum yield, a high stability with respect to heat, degradation and light, a short fluorescence lifetime and a low probability of intersystem crossing to the triplet state. Furthermore the dyes must be of a high purity because impurities quench the laser output. The application of these materials is not just limited to lasers, they are also used in many different optoelectronic devices like organic LED. Many lasing systems base upon inorganic materials, which are very robust and produced at low cost. These devices are limited to very narrow emission bands at specific wavelengths. Organic dyes, on the other hand, usually have broad emission bands and due to the big amount of different materials, the whole spectrum of visible light can be covered. A broad emission allows a system with wavelength tunability, if the cavity mode selection can be influenced, as one finds it in the case for CLC.

Laser dyes are complex molecules with specific aromatic structures and are categorized into different classes defined by similar chemical features. Structures (auxochrome groups) attached to the aromatic system can be tailored to influence either the optical behavior or the solubility of the molecule.Going into detail of dye laser operation, one can describe it as a four level process [82]. Upon absorption of a pump photon one electron is excited from the S_0 ground state to the S_1 excited state. All levels include several vibrational and rotational sublevels which cause bandwidths for absorption and emission bands to be bigger than a single line. By inelastic collisions the excited dye molecule populates the lowest vibrational state of S_1. This crossing is nonradiative but releases heat to the system. From this level a radiative transition can occur when the electron decays into the ground state and, again after inelastic collisions, it populates the lowest vibrational state in S_0. This process is known as fluorescence. If the pump intensity is high enough, a popu-

lation inversion can be obtained, meaning that more molecules are in the excited than there are in the ground state. Since the exited state is very short-lived, emission from the dye occurs. The emitting photon crosses the exited gain material and stimulates emission of a second photon which has the same phase, wavelength and direction. As the resonator in lasing devices sends these photons through the gain material multiple times, this photon emission is highly amplified. This stimulated emission is the basis for lasing oscillation. Nevertheless, there are various loss mechanisms which are to be overcome to finally achieving laser output. The overlap of emission and absorption bands, where the dye absorbs the emitted radiation, and intersystem crossing, where the excited singlet state converts into an excited triplet state, are two of them. The latter one is most important because its lifetime is very long. After an electron spin reversion from S_1 to T_1 a second reversion is necessary for the decay to the ground state. Both happen with a low probability and therefore take a lot of time in which the dye molecule is not able to participate in the stimulated emission. After intersystem crossing, another exited state, T_2, is involved. The triplet excitation band is located at longer wavelengths than the emission band from S_1 to S_0. The T_1 to T_2 excitation has a higher probability, because there is no spin reversion necessary. This so-called triplet quenching allows many dye lasers only to operate with pulsed pumping. Losses trough triplet states involvement can be reduced with additives that relax triplet states into ground states, structural engineering of the chemical structure for a more rigid molecule or a permanent flow of the dye solution reducing the exposure of the dye to the pump source.
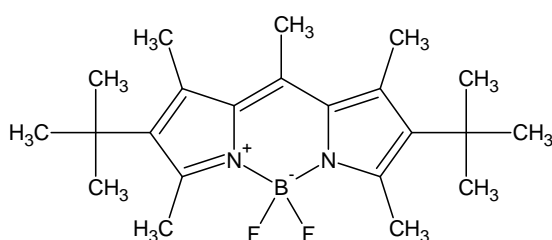
Figure 3.44: Chemical structure of PM597

While solubility is another important factor, two different dyes were chosen to be incorporated into the cellulosic CLC: PM597, a dye of the pyromethene family, whose structure is shown in figure 3.44 and YP whose structure is not published by the manufacturer. The first dye was chosen because of its very high solubility in acrylic solvents and very high quantum yield. The second one has a limited solubility in

acrylates but the soluble amount is sufficiently high and it is known for its very high photochemical stability. Three more reasons were the very cheap price, an emission wavelength around 500 nm and its low toxicity. Outside of laser research this dye is distributed by the manufacturer Dayglo for the staining of balloons. Both dyes show low overlap between their emission and absorption bands and low probability for intersystem crossing. The position of the emission wavelength is very important for this section. Additives, mandatory for well defined optical properties of the CLC host, shift the position of the PBG to the blue. Therefore the emission band should be in a similar wavelength range, to provide a sufficient overlap with the PBG. On this reason PM597, emitting at 600 nm, is not a good choice, but different techniques for tuning the CLC and the shift of emission bands in different solvents made it possible to use this dye.

Many dyes have been tested for being the gain material inside a cellulosic host material. Several coumarins for example show a good solubility in acrylates, too, but precipitate after the addition of the mesogens, or their emission band goes too far in the red. Generally CLC are tunable over a wide range of wavelengths through temperature change, but CLC made of CTC are very limited with regard to this method.

3.4.3 Preparation of Composites with Organic Dyes

Generally there are two ways to prepare composites of a guest material with the cellulosic host CLC. The first way is, as already described for the inorganic NP case (section 3.3), to mix the dye with the acrylic solvent, add the CTC and prepare the film from the homogeneous mixture. If the dye is soluble in both materials, the pure solvent and the CLC respectively, its distribution will be very homogeneous in the final film. However, as mentioned in section 3.3 the CLC host is very sensitive to any impurity that does not belong to the LC material. Furthermore a polymerization is, in depending on the dye and its concentration, impossible, since all the UV light applied for polymerization may be absorbed by the dye, which converts it into fluorescence and a lot of heat, again affecting the CLC. Only composites with very small dye concentrations (0.1% w/w and below) or with dyes that do not absorb between 320 and 380 nm (like PM597) can be prepared with this method. However the quality of the CLC's reflectance was always negatively influenced, if a dye was dissolved prior to polymerization. For these reasons an additional way was used for the preparation of composite films. The host material was prepared as a polymerized film without the dye. Afterwards the coverslips of the LC cells were

removed and the solid films were swollen in a dye solution with a low molecular weight solvent. The host can be prepared as a pure material without impurities and tuned to the desired optical properties. With this method dyes that are soluble in the acrylic solvents can migrate into the structure and the dye's fluorescence is not shifted due to any solvent influence, because the CLC film is already polymerized. In addition the dye's properties are not affected by additives used to improve the CLC's optical qualities. Nevertheless the film must remain on a glass substrate to maintain its flat shape which may result in a dye gradient along the film normal, as not all surfaces are exposed to the dye solution. Furthermore there is no control about the amount of dye which is incorporated because different dyes have different affinities to the host material. This method works very well for organic dyes, but is not applicable to inorganic NP, due to their size.
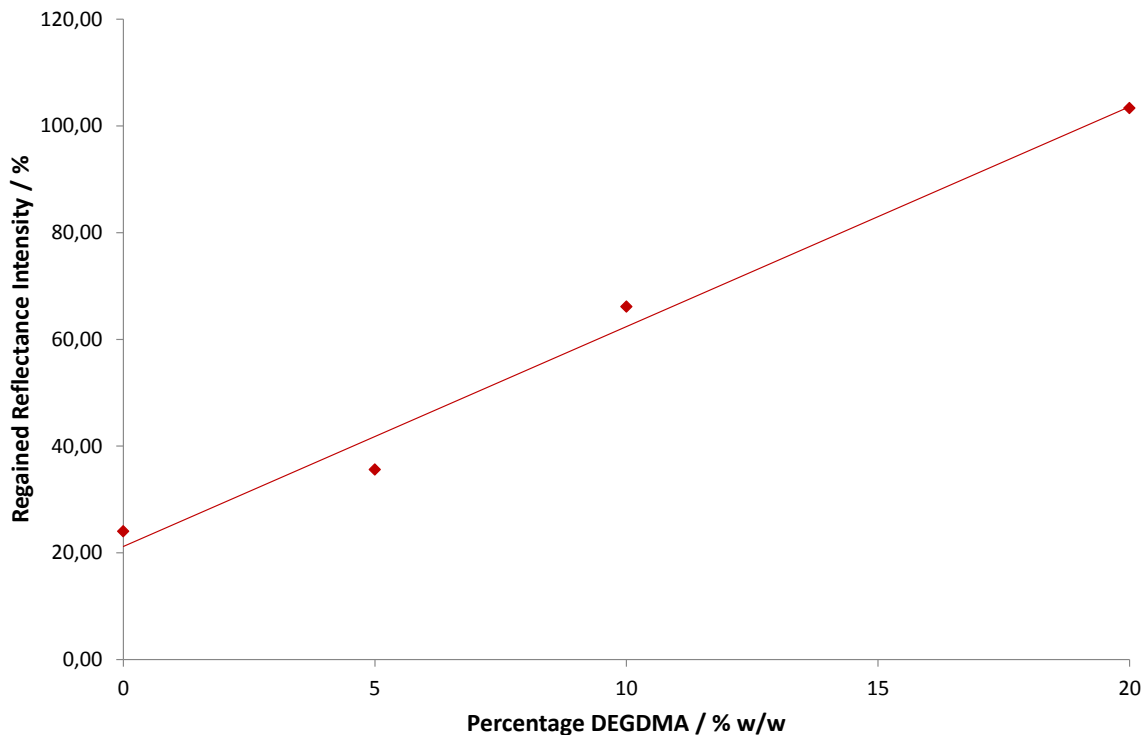
Figure 3.45: Swelling behavior of crosslinked CLC in dependence to the amount of DEGDMA as part of the solvent mixture for the CLC. The regained intensity of reflectance after a swelling cycle is shown.

For the swelling process it is necessary, that the film regains its initial optical qualities. This requires a certain amount of crosslinking DEGDMA in the acrylic solvent. During the swelling in an organic solvent, usually toluene, the whole sample expands and the pitch increases. The pores of the polymer network enlarge, allowing

solvent and dye molecules to migrate into the film. After one day the film is taken out of the dye solution, washed with pure solvent and placed in vacuum to remove the solvent from the film. Now the pores, as well as the pitch, shrink to their initial value and the dye molecules stay inside the cholesteric structure. To ensure that the cholesteric structure regains its pre-swelling state, the amount of crosslinking acrylate needs to be chosen carefully. Figure 3.45 shows the relationship of regained intensity of reflectance perpendicular to the film, depending on the amount of DEGDMA in the CLC solvent mixture. An amount of 20% w/w is needed to regain the total initial reflectance. Structures in samples with a lower amount of DEGDMA are destroyed or realigned with a worse quality. Interestingly one finds an up to 250 nm red-shift of the SR during the swelling process which is reversed during drying the sample. Until the complete removal of the swelling solvent, there are some small sidepeaks visible in UV-VIS spectra. This is because the film is always attached to one glass slide and hence the parts of the film closer to the glass do not swell as much as the parts with exposed surfaces. This creates a pitch gradient along the film normal which vanishes after a complete removal of the swelling solvent (see figure 3.46).

3.4.4 Conclusion

The preparation of composites with organic dyes is much easier than with inorganic NP, once a soluble dye is found. Very small dye concentrations or samples with PM 597 can be prepared and polymerized directly. However, the swelling method provides better possibilities for tuning the host independently and without any disturbing impurities, although the amount of dye is not well controllable and its distribution is not as homogeneous as expected. After careful preparation of the host CLC, swelling with a dye solution and removal of the swelling solvent, films with optical properties like shown in figure 3.47 are available.

The reflectance intensity is close to the theoretically predicted value, the excitation band is outside of the SR and gives the optimal pump wavelength. The bandedge of the PBG overlaps with the maximum of the emission band of the dye. Samples like these are fixed through polymerization and therefore stable towards the pump light. Additionally no coverslip is in need which reflects parts of the pump light. Besides samples with YP some with PM597 have been prepared via dissolution of the dye in the solvent and film preparation afterwards utilizing temperature treatment. Here the reflectance properties of the CLC are not sufficient for bandedge lasing but another lasing mode appears (see section 3.5.5). In comparison to YP, PM597 did
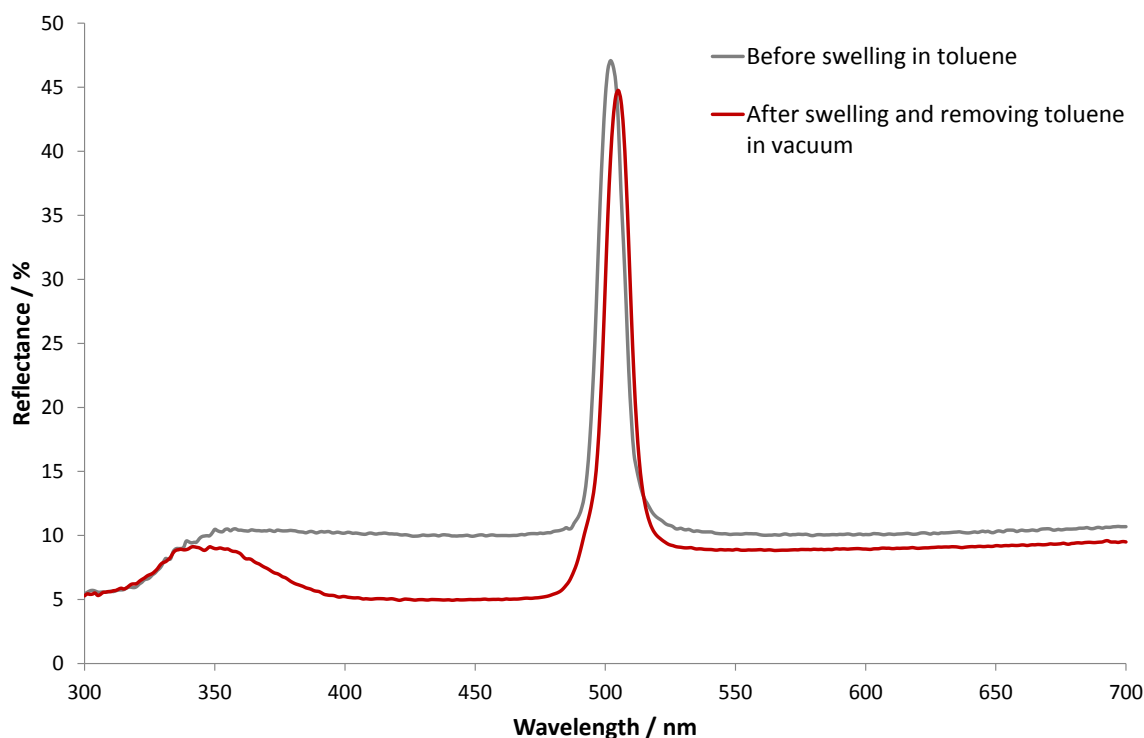
Figure 3.46: Reflectance spectra of a corsslinked CTC (in EGMEA/DEGDMA 80%/20%) film before and after swelling in a toluene/YP solution. Differences in reflectance between 350 and 480 nm are due to the absorbance of the incorporated dye (see figure 3.47 for comparison).

show a lower affinity to the host with the swelling method, only giving hardly stained films.

3.5 Lasing in Composites of Cellulosic CLC and Organic Dyes

3.5.1 Introduction

Lasing in cholesteric liquid crystals is known since its first demonstration in 1971 [99, 174]. CLC provide, through their periodic refractive index modulation, a feedback mechanism by Bragg scattering. Macroscopically the feature of this modulation appears as the selective reflection of light if the size of the periodicity is in the same range as the wavelengths of visible light. A gain material dispersed in this structure exhibits a modified fluorescence pattern due to the manipulation of optical properties of the host material. Upon sufficient optical excitation, the flu-
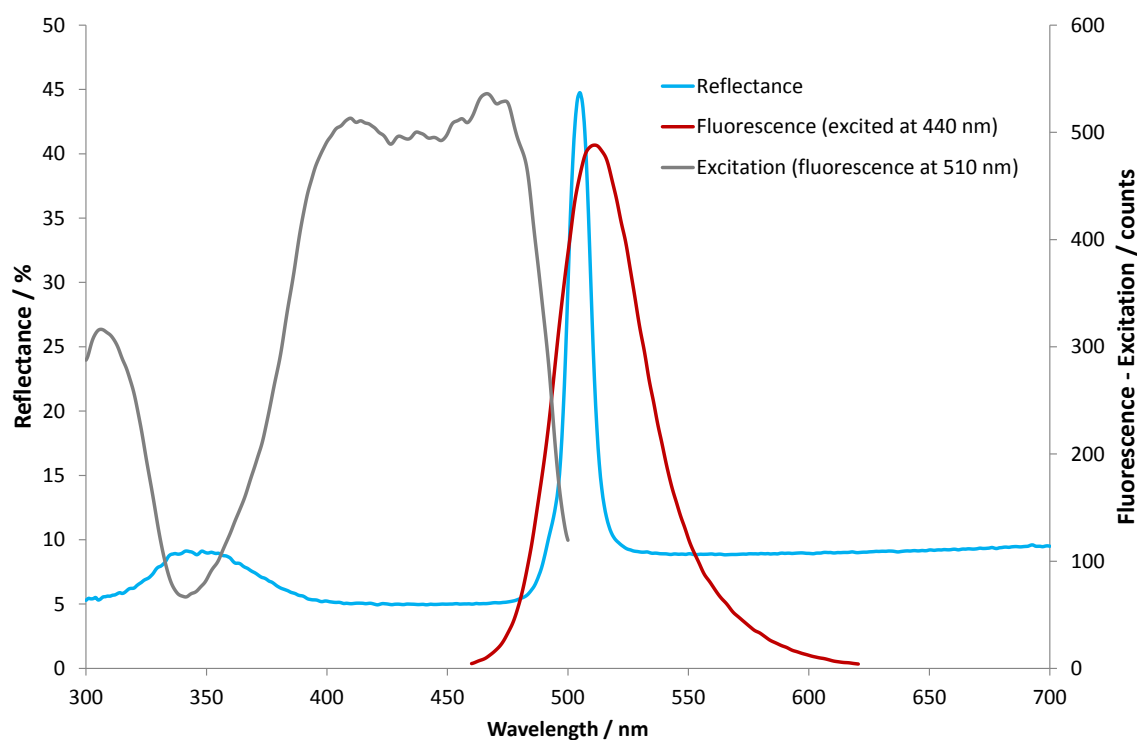
Figure 3.47: Reflectance (blue), excitation (grey) and fluorescence (red) spectra of a composite made of cellulosic CLC and YP

orescence is suppressed and very narrow laser lines are produced because of the distributed feedback and its mode selectivity. The position of the output wavelength is tunable with various external stimuli, giving these systems the possibility to cover a wide range of wavelengths. Many experiments have been performed to extend the tunability range, reduce threshold, improve cavity quality and stabilization of these systems until a continuous wave output is achieved. Apart from composites of low molecular weight liquid crystals with organic dyes, there is only a very small number of papers dealing with lyotropic polymers as host material (see section 1.3.3). All of them claim that the possible degree of mesogen alignment and refractive index anisotropy are too low, to see lasing as it is shown in low molecular weight CLC. Section 3.2 shows the way to cholesteric films made of lyotropic LCP with optimized optical properties, capable to provide a satisfactory feedback. In combination with organic dyes, these films were excited with a laser pump source. The following sections describe a comparison between low molecular weight and polymeric CLC. The behavior of the cellulosic films under optical pumping and a conclusion of these materials as a replacement for their low molecular weight counterparts. Lyotropic LCP, especially those based on cellulose, are

indeed an interesting alternative, because they are a renewable resource, available in large quantities for a low prize. In combination with non-toxic gain materials and biodegradable solvents, the samples are easily recycled after their life time.

3.5.2 Low Molar Mass versus Polymeric Feedback Materials

Since the optical emission of a gain material inside a CLC is related to the density of states, a closer look at the reflectance band of low molecular weight CLC is necessary. The DOS inside the PBG is equal to zero but has two maxima at both bandedges. Here the photon group velocity is decreased to zero and the long dwell times inside the CLC strongly support stimulated emission. However, there is a series of long lived transmission modes at each bandedge, with decreasing intensity when gaining distance to the center of the PBG [175]. These modes are visible in a properly resolved reflectance spectra of a low molecular weight CLC, shown in the top image of figure 3.48. A fine structure at both bandedges can be seen. If compared with figure 1.19 this fine structure represents the density of available optical states.

Image b in figure 3.48 shows how the fluorescence of the gain material is changing. Inside the CLC, above the clearing point, where the material is isotropic, a broad fluorescence band is obtained while in the cholesteric state the band changes significantly following one of the circular polarized twist senses. Following the other twist sense, the fluorescence is not affected [103] because it can pass through the CLC without any hindrance and influence of the periodic structure. Within the PBG the fluorescence is completely suppressed but at the bandedges several sharp lines appear. The highest line is located at the long wavelength bandedge, because this mode has the lowest threshold, due to the parallel alignment between the mesogens and the resonant mode (in-plane standing wave). The high density of electromagnetic modes and the alignment of the transition dipole moment of the dye with respect to the electric field of the standing wave, work together to enhance the fluorescence. At the other bandedge there are several lines located, too. Here the resonant mode is perpendicular to the local director representing the out-of-plane standing wave. Both modes are available for laser emission depending on the orientation of the dye's dipole transition moment with respect to the local director. In addition there are, according to the DOS, several weaker lines. If the pump intensity is now raised above the lasing threshold, the emission of the dye changes again. The whole fluorescence collapses into a very sharp single line (image c in figure 3.48). This line is located at the position where the DOS is the
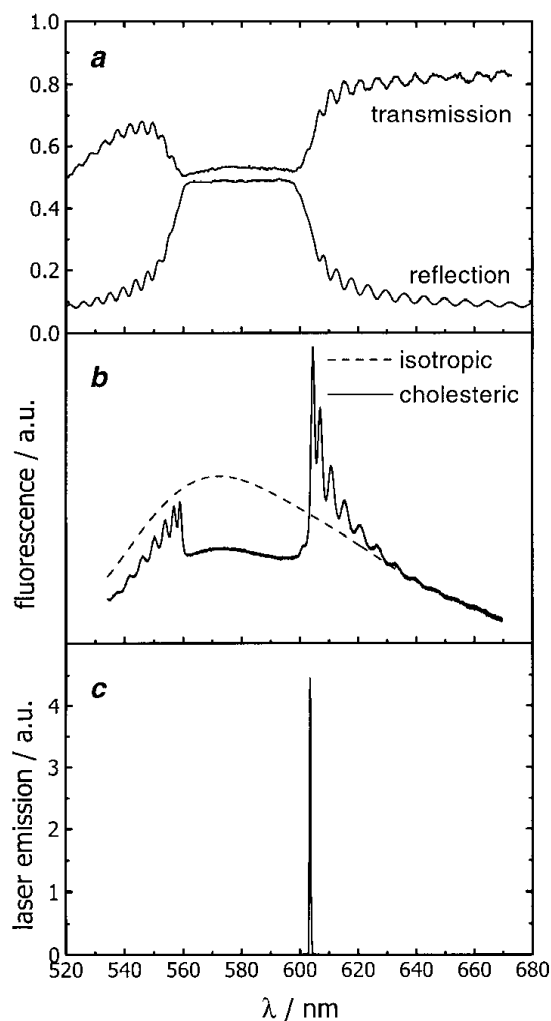
Figure 3.48: Optical spectra of a low molar mass CLC: a) transmittance and reflectance, b) fluorescence and c) laser output [176].

highest for the dye molecules to relax from the excited state. Further increasing of the pump power results in multimode lasing because then the threshold of modes with a lower DOS will be reached, too.

The requirements for the observation of these facts are a well aligned CLC in the planar state, a well dispersed gain material and the overlap of CLC reflectance and dye emission. Only perfectly aligned, monodomain or multidomain with few defects, CLC in the planar state create such spectra. However, a fine structure was not encountered so far for samples made of derivatives of cellulose (see figure 3.47). The alignment of the liquid crystal provides values of reflectance predicted by theory but far from the degree of order known for low molar mass CLC. A polydomain structure or defects cause the lack of a fine structure at the bandedges [176]. As de-

fects generate allowed transmission states inside the PBG and their thresholds are known to be among the lowest - the reflectance inside the PBG is the highest - one should expect defect mode lasing when pumping a cellulosic composite (see section 3.5.5). Another factor is the low birefringence of cellulosic polymers. The resulting SR bandwidth is very small, usually below 25 nm and hence the difference between the DOS at both bandedges is not as significant as for wide PBG materials. A wide PBG creates a gap between the thresholds for both bandedge modes and very often only one bandedge overlaps with the dye's emission. This ensures, with increasing pump intensity, that only one resonant mode will win the competition of modes and a single mode output is generated. With a very narrow bandwidth the situation is completely different. Both resonant modes have very similar thresholds and often both overlap with the emission band. At higher pump powers there will be a strong mode competition and small multimode peaks may appear. Sometimes it can be possible that modes from both bandedges merge into multimode structures. While bandedges are very sharp for low molar mass CLC, they are more soft in the cellulose CLC case. Here the highest DOS is distributed over a range of wavelengths and the laser output will have a broader bandwidth. An imperfect alignment also creates higher thresholds due to a decreased cavity quality. Higher threshold means that higher pump powers are needed to generate a laser output. These high input powers have two consequences: There will be many modes above threshold and the sample is exposed to a lot of optical stress. Here a polymerized sample is of advantage. The reduction of lasing thresholds is still the most pronounced challenge in dye laser experiments. It can be done by either enhancing the quality of the cavity, so that a lower gain and therefore a lower pump intensity, is needed to cross the threshold or by improving the gain output to overcome resonator losses. The identification of lasing [177] is an important issue to solve during excitation experiments with dye doped cellulosic CLC. Stimulated emission can happen even outside a resonator if the pump power is sufficiently high. It results in line narrowing and in an increased fluorescence output. However, it has to be clearly distinguished from true lasing action. Laser lines have a more narrow linewidth, especially dye lasers generate very narrow lines with FWHM below 0.1 nm. The output light is highly monochromatic. Second there is a strong directionality of the laser light. In the case of CLC this direction is parallel to the optical axis. The output light is circular polarized with the same twist sense than the cholesteric host. An additional factor is the threshold behavior of output intensity and linewidth. Before reaching the threshold, the output fluorescence and the input energy are linearly

dependent. Above the threshold, the gradient of this dependency changes abruptly and the linewidth collapses from a broad emission band into a narrow laser line. Last but no least the light emission will be characteristic of and influenced by the gain material and the resonator. The sharp line, emitted above threshold pump power, must be associated to the position of the CLC reflectance band. It is either located at one of the bandedges or in the center of the PBG. There is only one lasing mode, where the last condition is not completely fulfilled: Random lasing. In section 3.5.5 this kind of lasing will be shown and discussed. Another phenomenon associated with lasing from CLC are interference rings and fringes. If the sample is placed in front of a sheet of paper, the laser output generates a bright spot in the middle parallel to the film normal. This spot is surrounded by a ring pattern and sometimes fringes. The fringes are produced from multiple reflections at the sample boundaries, but the rings are the result of light scattering interference. Light is scattered at domain boundaries surrounding well aligned CLC domains. These phenomena produce ring patterns [178]. So far they only have been reported for low molecular weight CLC, where large perfectly aligned domains are achievable. It has been reported that the polymerization of a low molar mass CLC results in a lack of the ring patterns [176].
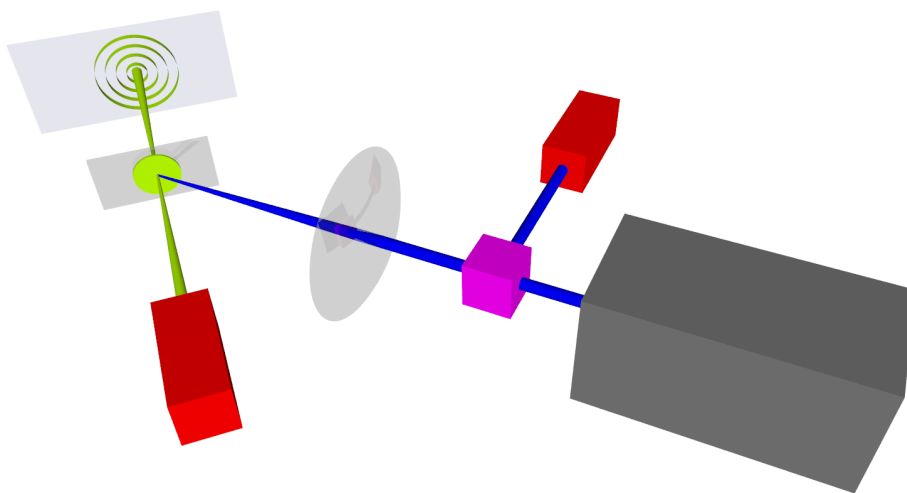
Figure 3.49: Schematic of the pump laser setup. The OPO pump laser (grey box) emits blue (to pump YP) or green (to pump PM597) light which is focused on the sample at 45 ° incidence using a lens. A beamsplitter (pink box) splits the beam towards a power meter (red box) to determine the input power. The greenish (YP) or red (PM597) emission from the sample is recorded with a spectrometer or a second power meter measured the output power (second red box). The interference pattern was imaged at a screen parallel to the sample's substrate.

The following sections describe two examples of defined bandedge lasing and the one case of random lasing in a sample where emission and PBG were misaligned. All excitation experiments were done with the same setup (figure 3.49). An optical parametric oscillator was used as the pump source, because of its variable wavelength output. The intensity of the pump light was controlled via the power of the pump source and a polarizer. The sample was hit by the pump beam at an angle of 45° to minimize reflections of the pump beam on the film surface and to ensure a deep penetration to the dye molecules inside the film. A focal lens focused the spot in the middle of the film and spectrometer or energy meter heads were placed perpendicular to the film. All experiments were done under pulsed excitation with a repetition rate of 1 or 2 Hz.

3.5.3 Bandedge Lasing with YP

Figure 3.50 (top) shows the reflectance and emission properties of a cellulosic CLC film, polymerized and swollen in a saturated YP solution in toluene. Its fluorescence and excitation bands can be seen in figure 3.47. The sample was pumped with 450 nm from an OPO laser. Below the threshold only the dye's fluorescence appears in dependence to the input energy. The fluorescence band shape was not influenced by the presence of the CLC's PBG as reported for low molar mass CLC. The PBG is to narrow to affect the broad fluorescence of the dye. Additionally it is possible that a lot of dye is not interacting with the cavity. This happens if dye molecules are very close to the boundaries of the sample, because a certain film thickness is mandatory the exhibit a measurable bandgap. The mentioned figure was taken as the pump intensity reached the threshold of the sample. As expected, due to the very close bandedges, single lasing modes appear at both bandedges. In comparison to the pump beam at 450 nm with a bandwidth of 0.5 nm the modes are very narrow, but appear broader because of time averaging during spectra collection. The red graph shows the unpolarized emission of the film, while the blue curve was taken with a filter, only transparent for right handed circular polarized light. Their total intensity is reduced due to the absorbance of the filter. The spectrum of left handed circular polarized light shows the same amount of background fluorescence but no emerging sharp peaks. This twist sense is not supported by the cavity of a right handed CLC. The background fluorescence will not be quenched inside of the bandgap because of dye molecules that do not interact with the cavity, for reasons already mentioned. It is difficult to define the exact boundaries of the bandedge, as the edges are not very sharp and hence a small range of wavelengths is
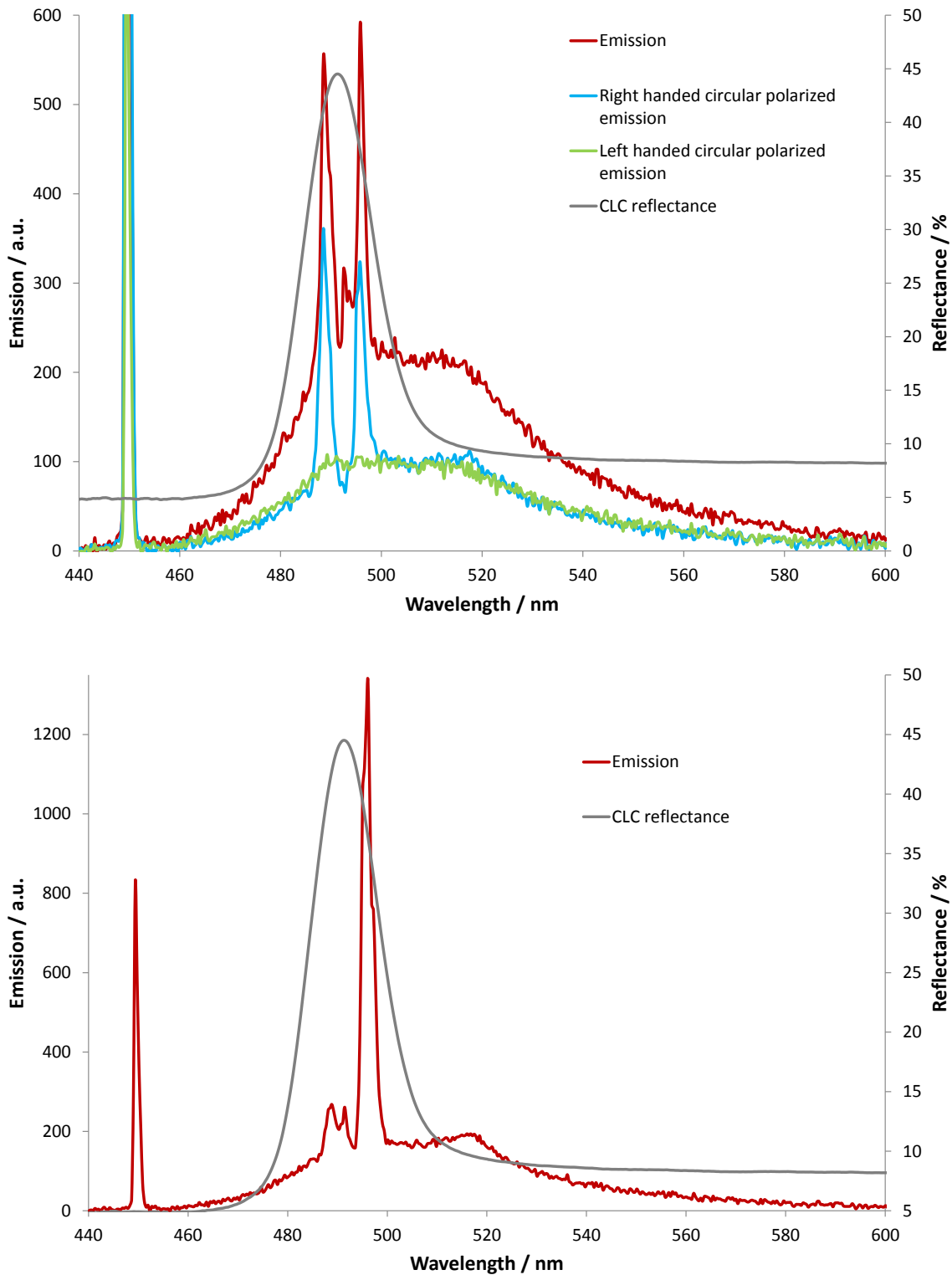
Figure 3.50: Emission of a YP doped cellulosic CLC film at (top) and above threshold (pump laser at 450 nm).
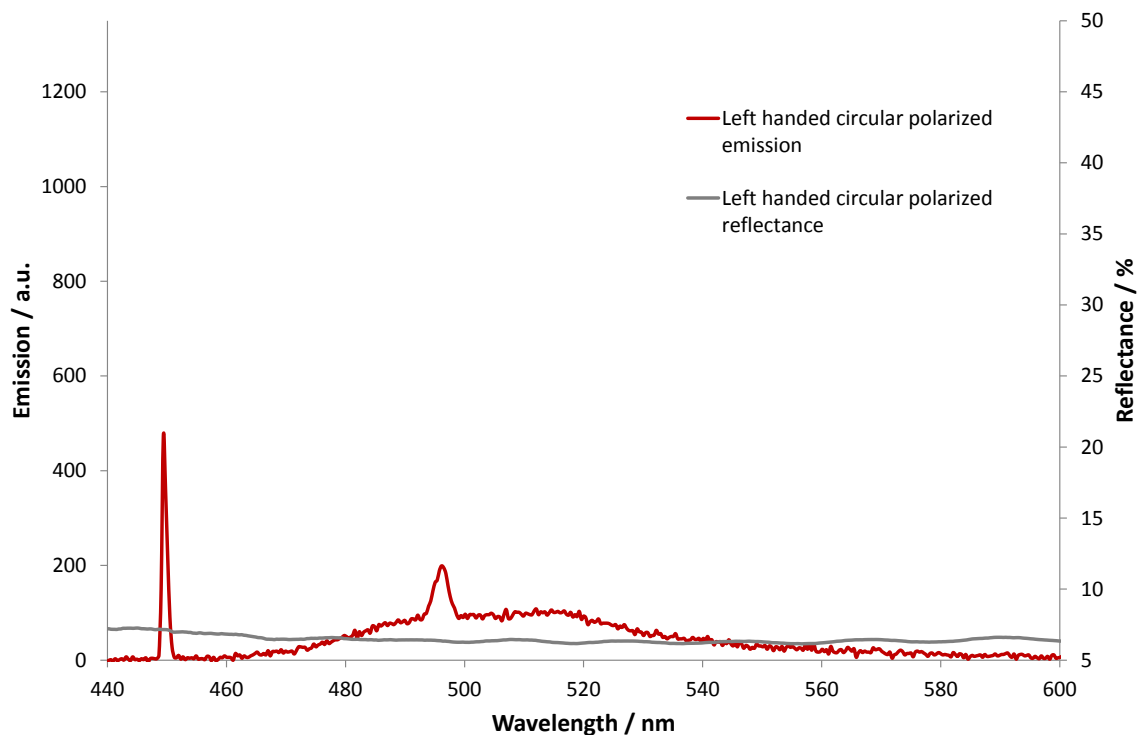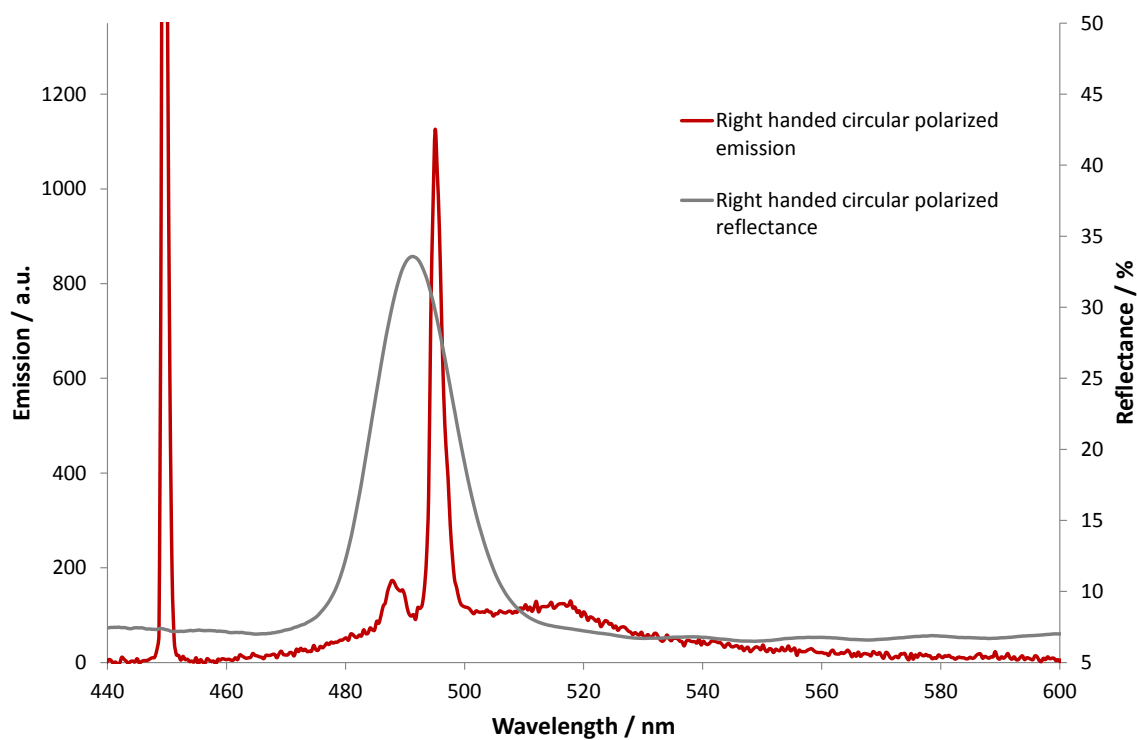
Figure 3.51: Right (top) and left handed circular polarized emission of a YP doped cellulosic CLC film above threshold(pump laser at 450 nm).

available in the bandedge region, creating peaks with shapes like a combination of very close single mode emissions, which can be seen in figure 3.50 bottom. It shows the emission of the same sample at pump intensity above the threshold without any polarization filter. Now only the mode at the long wavelength bandedge is supported by the cavity. Small lines inside the bandgap do belong to defect mode emissions, which are not sufficiently supported by the cavity.

Figure 3.52: Interference rings and fringes of a YP doped cellulosic CLC film above threshold. The sample under white light (top, left), the excitation pulse without sample (top, right), the sample under excitation (bottom, left) and the same situation using a filter to remove the pump light.

Both images in figure 3.51 show the circular polarization of the reflectance as well as of the emission. The reflectance band reflects RCPL and hence the lasing peaks have the same sense of rotation. In the case of using a RCPL filter (bottom) no

reflectance and no lasing emission appears, but the intensity of background fluorescence remains the same. The relation of the emission peaks towards the position of the PBG and its polarization proof bandedge lasing in addition to the interference patterns shown in figure 3.52. The top left image shows the sample under white light illumination in the sample holder in front of a white sheet of paper. The pump beam, and its optical structure, caused by optical elements of the setup, can be seen in the right top image. The bottom row shows the excited sample above threshold without (left) and with (right) a filter removing the pump light's wavelength. The remaining small bright spot is, despite the use of a filter, from the pump beam. The intensity pattern of the film's emission is described by a round spot in the middle with an undefined boundary surrounded by five rings. On the left hand side, some bright lines appear caused by multiple reflections at the film boundaries - the interference fringes. This is the first time, to our knowledge, that an interference pattern was observed for a cavity made of lyotropic cellulose derivatives or other polymers. However, the pattern is not as sharp and regular as known from low molar mass compounds. The appearance of this pattern explains two main characteristics: The sample is well aligned providing sufficient feedback for mirrorless lasing, but it consists of multiple well aligned domains separated by boundaries [178]. The film is not as turbid as one would expect for a multidomain structure because of the low birefringence of the cellulose derivatives. The lack of the pattern's sharpness is a result of the same reasons. These experiments were conducted under pulsed excitation with a repetition rate of 1 Hz. Due to heat dissipated into the CLC or degradation of the material, non-polymerized samples with a similar composition do survive only a few shoots until the spot needs to be changed. On the other hand, polymerization stabilizes the CLC and extends the life time of a pumped spot to about 50 - 100 shots. For a larger amount of pump shots the threshold must be further reduced.

So far it was not possible to report about threshold data because of a damage to the pump laser prior to threshold experiments. Earlier samples showed a threshold in the region between 500 μJ and 2 mJ. These values are very high compared tot hose in literature, which are as low as some nJ per pulse [114] for defect mode samples due to the maximum of reflectance inside the PBG. The threshold values are assigned to the cavity losses. Very high thresholds cause the need of high pump energies to obtain lasing emission from the sample. These high input energies leads to a quick cavity and dye degradation and hence must be lowered due to optimization of the feedback quality and the interplay between the cavity and the

dye. Although remarkable results have been achieved for lyotropic LCP, there is still room for improvement and lowering the threshold.

3.5.4 Bandedge Lasing with PM597

In the second case samples with PM597, a red emitting dye which can be pumped with the second harmonic of Nd-YAG lasers, were prepared. Samples with YP require the swelling method for dye incorporation, as YP absorbs in the UV region and therefore prevents initiation of polymerization. PM597 can be dissolved in the acrylic solvent and shows a very high solubility in EGMEA and HA. The solution stays homogeneous after the addition of 46% w/w 140 nm CTC and the films of these composites are polymerizable with UV-light. The properties of such composites is discussed using the following three figures (3.53 - 3.55) that show the optical properties and the lasing behavior of a polymerized 25 μm thick film with 0.3% w/w PM597.
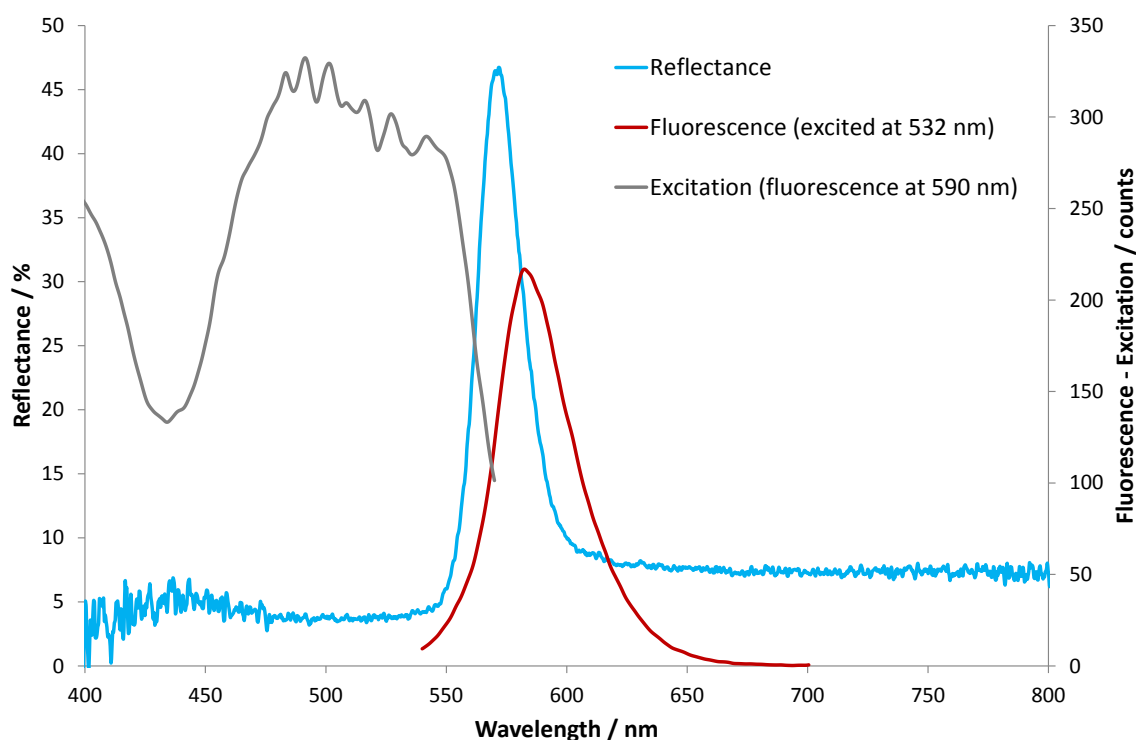
Figure 3.53: Optical properties of a 25 μm thick cellulosic CLC - PM597 composite film with a dye concentration of 0.3% w/w.

To overlap the dye's emission with the SR of the CLC host, the sample was cured at 30 °C overnight and polymerized at this temperature. The low energy bandedge
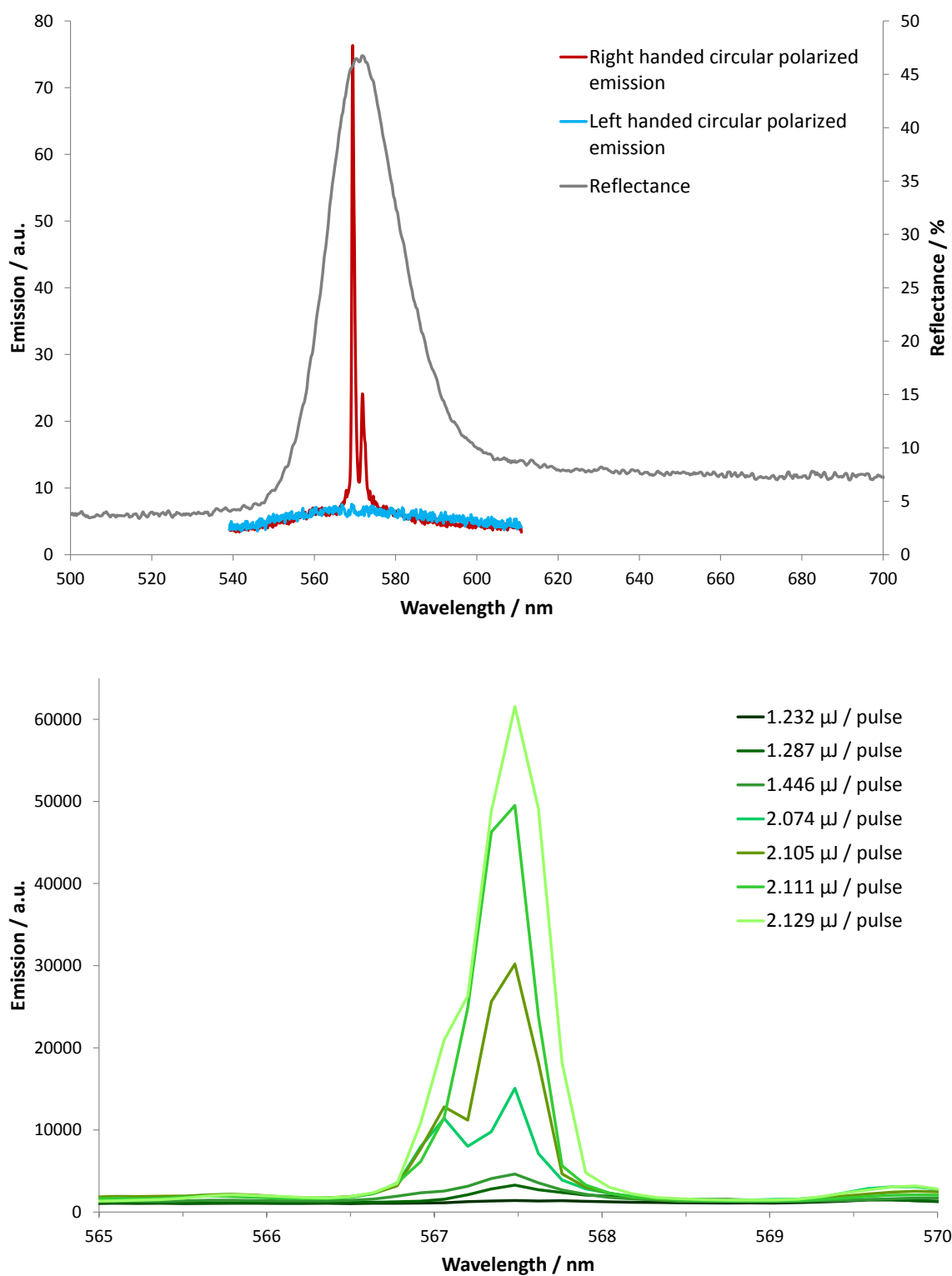
Figure 3.54: Lasing (top) and emission linewidth of the 25 μm thick PM597 doped cellulosic CLC film (shown in figure 3.53, pump laser at 532 nm).

clearly overlaps with the maximum of the fluorescence (figure 3.53) and the excitation spectrum shows possible pump wavelengths for this sample. The use of the commonly available second harmonic of a Nd-YAG laser simplifies the pump procedure, since no tunable OPO laser is necessary. Pumping the sample with ns-pulses at 532 nm the output shown in figure 3.54 (top) was recorded. The emission above the threshold is right handed circularly polarized and its position is very close to the bandedge. Due to the soft bandedges there are various wavelengths available for laser emission.
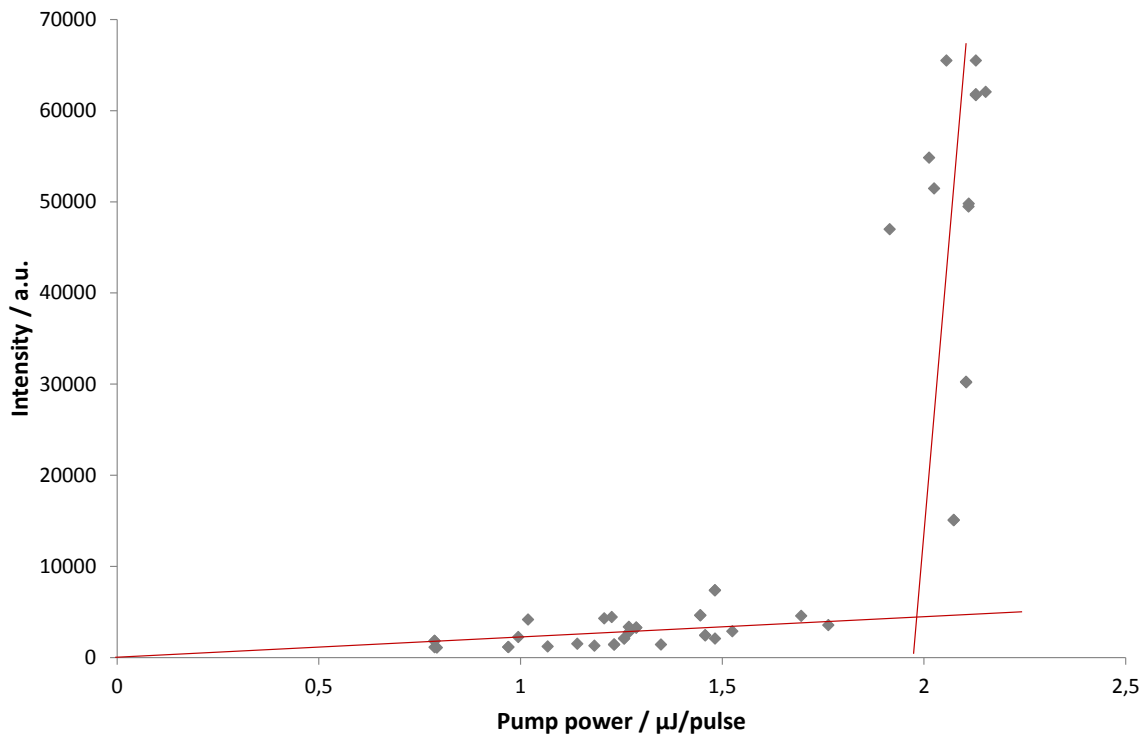
Figure 3.55: Threshold behavior of the 25 μm thick cellulosic CLC - PM597 composite film (shown in figure 3.53) with a dye concentration of 0.3% w/w.

Surprisingly the emission takes place at the high energy bandedge, which only barely overlaps with the dye's fluorescence. Emission at the other bandedge was expected due to a predicted lower threshold and a maximum optical gain at this wavelength. So far we do not have any reasonable explanation, which bandedge is chosen during optical pumping in each case. As already described we assume that the thresholds for both bandedges are very similar, in contrast to wide bandgap materials. Another possible reason could be that, since the wavelength of lasing emission is very close to the center of the PBG, we are dealing with a defect mode. They have been reported to show lower thresholds than bandedge modes. There

are several factors which might cause an increased number of domains and hence more domain boundaries. On one hand there is a heat treatment for red-shifting the SR, on the other hand the dye added before polymerization. The resulting inhomogeneity may support the defect mode emission although the optical gain at this position is not maximum. For this narrow PBG materials it is not possible to distinguish between bandedge or defect mode emission.
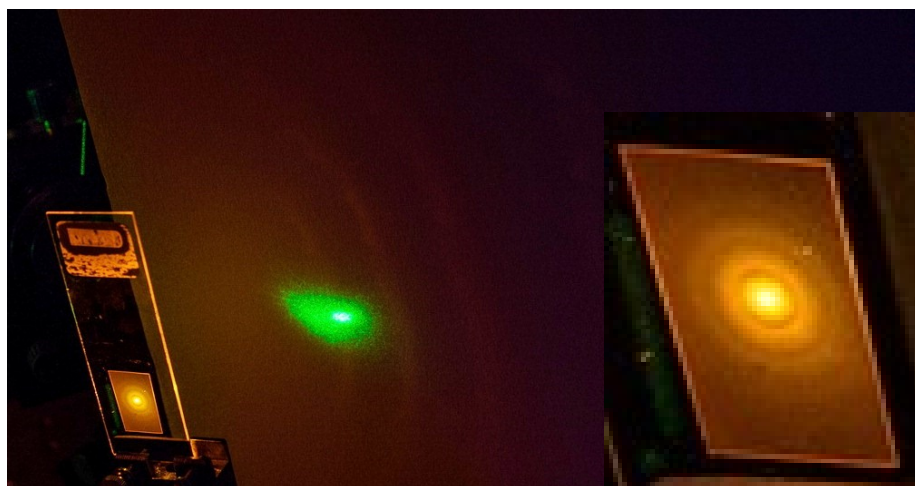
Figure 3.56: Interference ring pattern of a PM597 doped CLC film pumped with a 532 nm Nd-YAG pulse (green spot) at 2 Hz. A weak ring pattern is apparent on the screen as well as on the sample itself, where the pump beam hits the sample. A magnification of the pumped spot is shown as inset on the right.

Three additional proofs of the lasing emission are shown in figures 3.54 (bottom), 3.55 and 3.56. Extremely narrow emission is a main characteristic of dye laser. The emission here develops as a very narrow line with increasing pump power. Its FWHM is around 0.5 nm but spectra measurement includes time averaging causing a slight broadening. It can be considered to be in the range of 0.3 to 0.1 nm in width. However, the shape of the laser line suggest a combination of two very close lines. It is caused by the soft bandedges and the resulting numerous frequencies available for cavity support. Samples with a sharp bandedge do usually provide only one frequency. The second proof is the threshold behavior of the emission. Below the threshold, the fluorescence output of the film increases linearly with increasing pump power, but at 2 μJ / pulse its gradient changes rapidly. At this point the broad fluorescence collapses into a narrow lasing emission and its intensity increases rapidly with minor increasing of the pump power. A threshold value of 2 μJ / pulse is very high in comparison to some nJ / pulse reported for defect mode lasers [114] but comparable to other CLC systems based on polymerized CLC

[179] or on polymeric mesogens [120]. The quality of the CLC cavity reflects in this value, as lots of resonator losses require a higher optical gain and hence higher pump powers or higher dye concentrations. However, this value was expected to be higher than for low molecular weight CLC, as the quality of the CLC alignment and hence its feedback quality is still lower in the CTC case. Here the necessity of polymerization becomes apparent [179]. At this pump power level the dye's emission and the pump source itself create a lot of heat inside the CLC, changing its optical properties. Locally the pitch is increased and does not match the wavelengths of the dye's emission anymore. After more than 10 pulses this spot is defective, due to the fact that the CTC do not realign after cooling down. A polymerized film survives at least 50 to 100 pulses per spot without changing the pitch. Further increase of the pump intensity leads to degradation of the CTC polymers. A polymerized sample with a lowered threshold is supposed to withstand an even larger number of pump pulses. As presented earlier for YP stained samples 3.52, an interference pattern is apparent during optical excitation. Figure 3.56 shows a ring pattern on the screen placed parallel to the film's substrate. Due to the low brightness on this image the ring pattern is also visible on the sample itself, where the pump beam hits the sample (see inset for magnification). This pattern is not caused by the pump beam, because thebright green spot on the screen, which is reflected from the sample's surface does not show any similar intensity variations. It is created by the multidomain structure of the CLC host due to multiple reflections at the domain boundaries and is a clear evidence for a well aligned CLC cavity.

The quality of the CLC host could be increased if the dye is introduced to the film via the swelling method used for the preparation of composites with YP. However, the solubility of PM597 is much higher in the used acrylates than of YP. Using the swelling method for the incorporation of PM597 results in significantly reduced staining. In addition the amount of incorporated dye cannot be controlled precisely. Besides the heat treatment and the dye influences, the use of fluorinated additives shift the SR to the blue, which has to be compensated with increasing cure temperatures. These facts limit the use of PM597 although it is a very desirable dye for dye lasing samples, due to its optical properties and efficiency.

The spectra in figures 3.57 and 3.58 show a series of 50 μm thick, polymerized samples with different PM597 concentrations (0.1, 0.3 and 0.6% w/w). All samples were prepared in the same way as the previous one. All samples show similar optical properties regarding the CLC host and regarding the dye emissionrelative to its concentration.
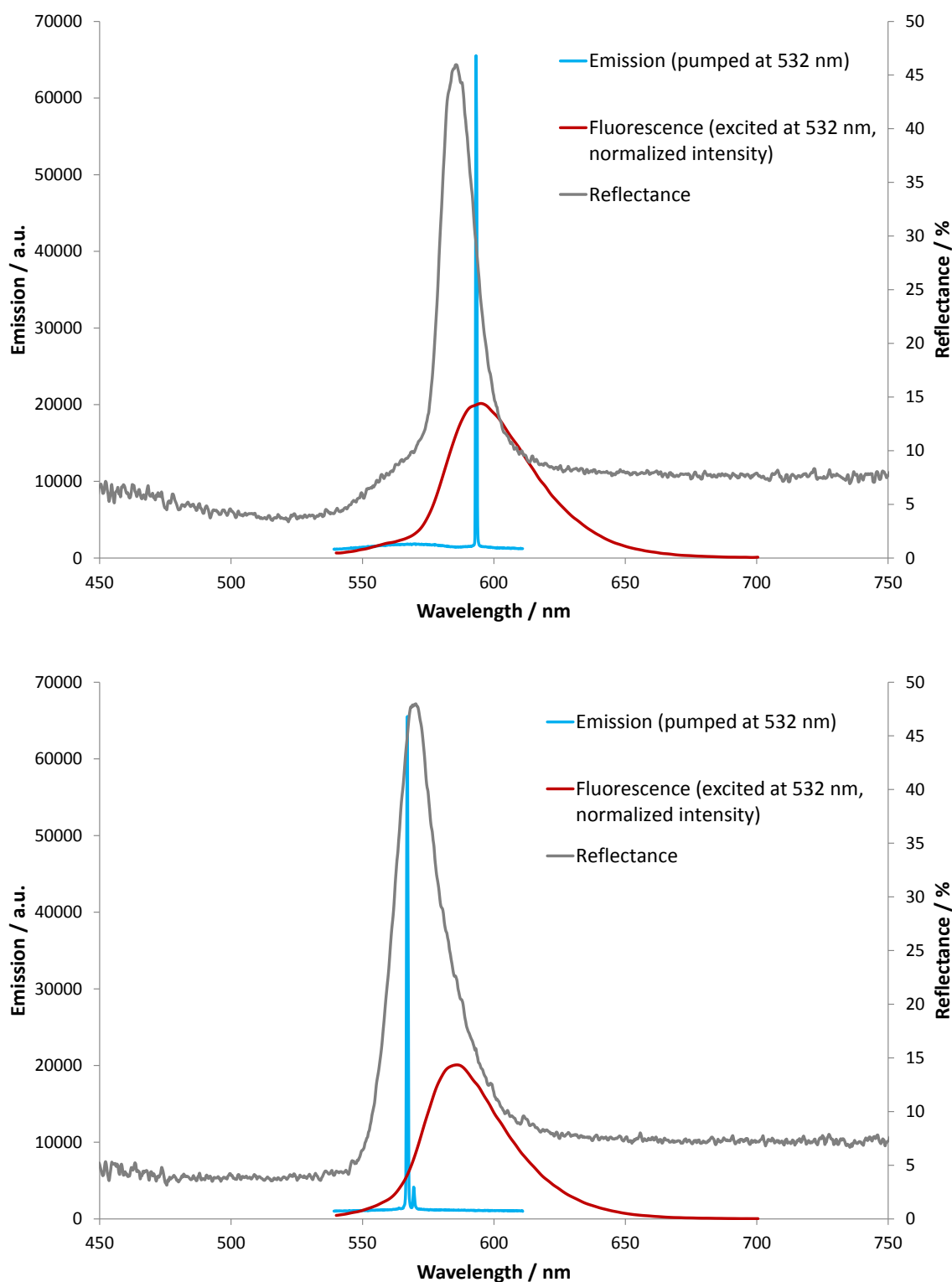
Figure 3.57: Lasing of 50 μm thick PM597 doped cellulosic CLC films with 0.1% w/w (top) and 0.3% w/w dye content (pump laser at 532 nm).
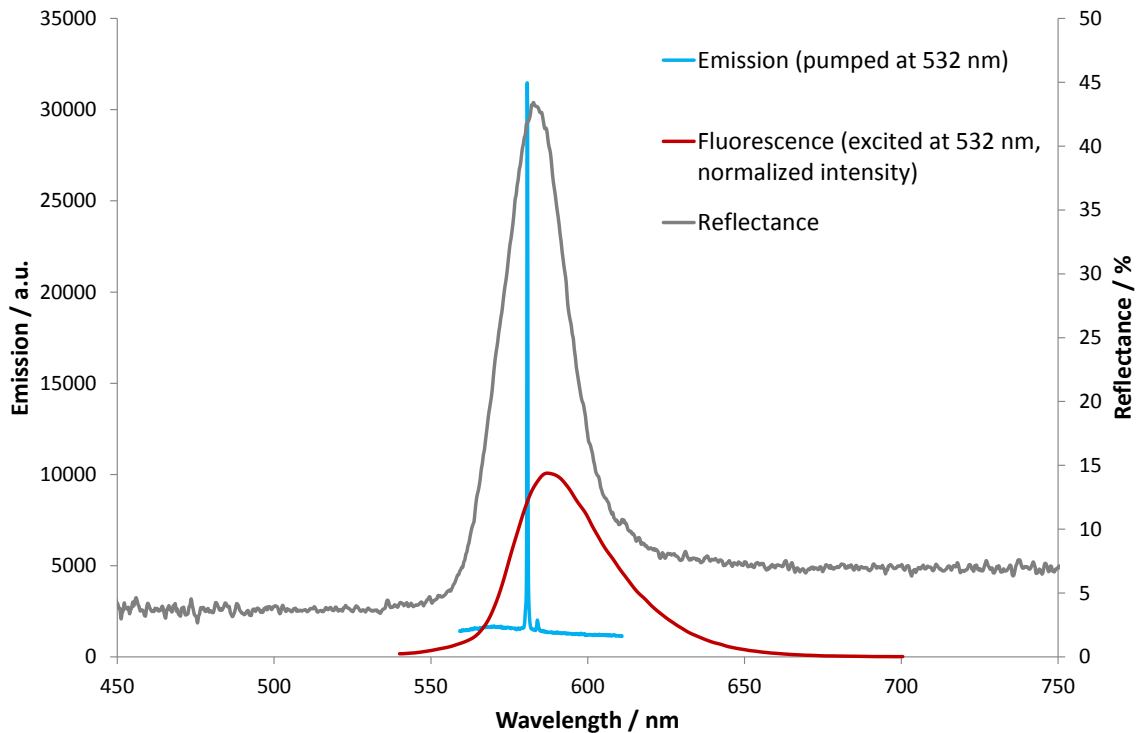
Figure 3.58: Lasing of a 50 μm thick PM597 doped cellulosic CLC film with a 0.6% w/w dye content (pump laser at 532 nm).

The first sample with the 0.1% w/w dye content (figure 3.57 top) represents the situation one would expect. The emission takes place at the maximum of optical gain and at the low energy bandedge. It is clearly located at the bandedge and shows a very narrow linewidth. On the other hand the sample with 0.3 and 0.6% w/w dye content have slightly shifted positions of the PBG, but the low energy bandedge still overlaps with the maximum of fluorescence. However the emission in both samples take place at the high energy bandedge or very close to the center of the PBG and not at maximum optical gain. These three sample are a good example that even with very similar configurations it is not predictable at which wavelength the emission will appear, du to the very narrow PBG. It becomes even more interesting if figure 3.59, showing the thresholds of these samples, is considered. The threshold for the sample with the lowest dye content is around 2 μJ / pulse, in the same region as the previous film. With increasing the dye concentration to 0.3% w/w the threshold is reduced by 50% to 1 μJ / pulse. This fact is most interesting as the emission wavelength is located at the edge of the fluorescence band. As already mentioned, the threshold can be reduced with increasing cavity quality or increasing optical gain. The larger amount of dye provides more optical gain and

hence the threshold is decreased. However, there is also the possibility of a defect mode for this sample, as center and bandedge of the PBG cannot be distinguished clearly.Furthermore the threshold value returns to a high value of 2.2 μJ / pulse with the highest dye content, although here the highest optical gain is expected. On the other hand there is a counterproductive effect. As the dye is dissolved in the CLC before aligning, it is considered as an impurity by the CLC and therefore disturbs the alignment of the host with increasing concentration. Although the reflectance values of all three samples are very similar, it looks like the quality of the cavity is reduced with increasing dye content. Furthermore the output intensity of the 0.6 % w/w sample is reduced by 50%. This fact shows the importance of an alternative method to incorporate dye into the CTC host material.
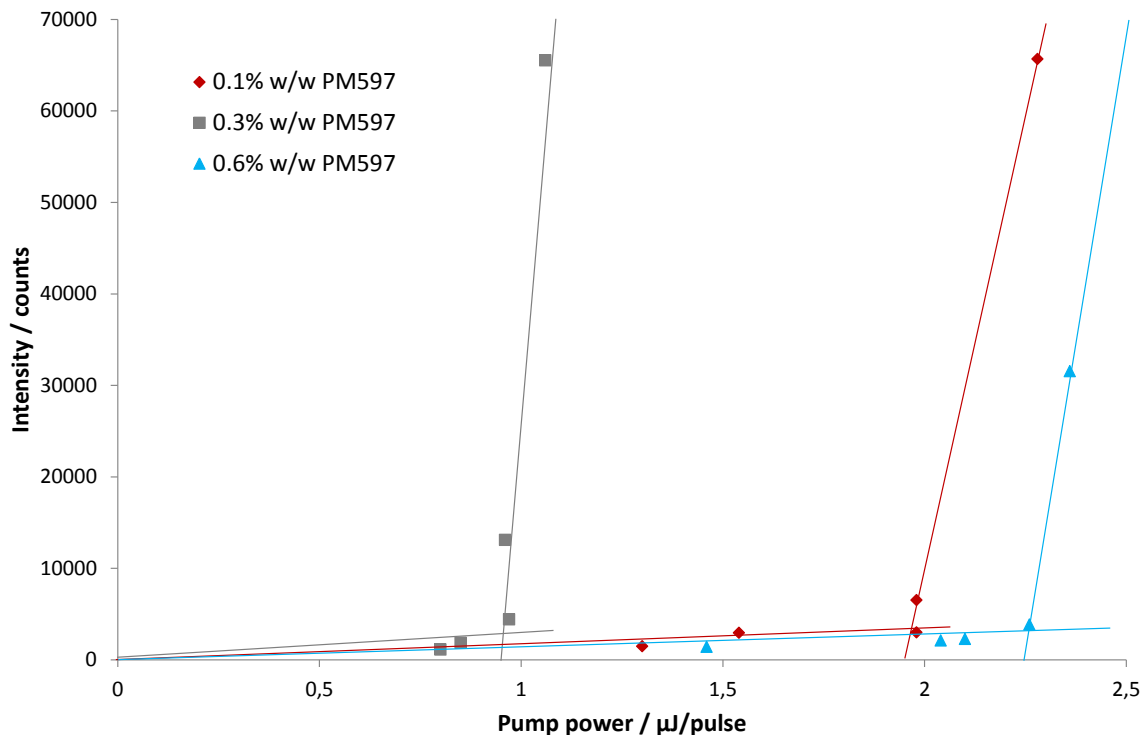
Figure 3.59: Threshold behavior of the 50 μm thick cellulosic CLC - PM597 composite films (shown in figures 3.57 and 3.58) with different dye concentrations.

3.5.5 Random Lasing with PM597

The third example of a mirrorless lasing films has been prepared with PM597, too. This film has been prepared with 0.1% w/w of dye and the dye was dissolved in the acrylic solvent prior to the addition of the mesogens. Due to the use of TFE as an additive, the film was heated before polymerization to overlap the PBG with the dye's emission band. As shown in the top image of figure 3.60 the reflectance band is of high intensity but, after the heat treatment, it does have a broader FWHM. The low energy wavelength bandedge overlaps with the maximum of the emission band. All requirements of bandedge lasing are present, but surprisingly a very intense lasing peak shows up at very low pump energies. The unexpected part is the position of the lasing peak, which is located at the high energy wavelength bandedge, that does not overlap with the dye's emission. This output is, in addition, not circular polarized and broader than the emission of the previous lasing sample. From the lack of polarization, the bandwidth and the position, we assume that this is random lasing. Such lasing modes have already been reported to appear in cellulosic films [117], though they were much thicker films. The reported films were 500 μm, while the here described ones are only 50 μm thick. An enlarged thickness was prepared to enlarge the optical path of the randomly scattered light increasing its time inside the material and reducing losses. Random lasing in cellulosic films is possible because of random scattering at domain boundaries. However, the scattering is not very effective due to the low birefringence of the cellulosic mesogens. It is therefore interesting that such a thin film in combination with a weak birefringent material is suitable to support random lasing modes. As the background fluorescence does completely collapse into the single peak it seems to be an effective "cavity". Another interesting effect of this sample is presented in figure 3.61. At certain pump spots an additional laser mode appears in the spectrum. It is very narrow and mostly of higher intensity than the random lasing signal. Its position can not be defined very well, because it is not clear to differentiate it between bandedge and center of the PBG. As this peak shows a right handed circular polarization it must be support by either a bandedge or a defect mode. From the point of a multidomain structure of the CLC with some inhomogeneities a defect mode emission is more probable. The inhomogeneity of the film is proofed by the fact that this narrow signal only appears at some of the pumped spots, when a defect cavity is in the center of the spot. In all other spots only random lasing occurs.
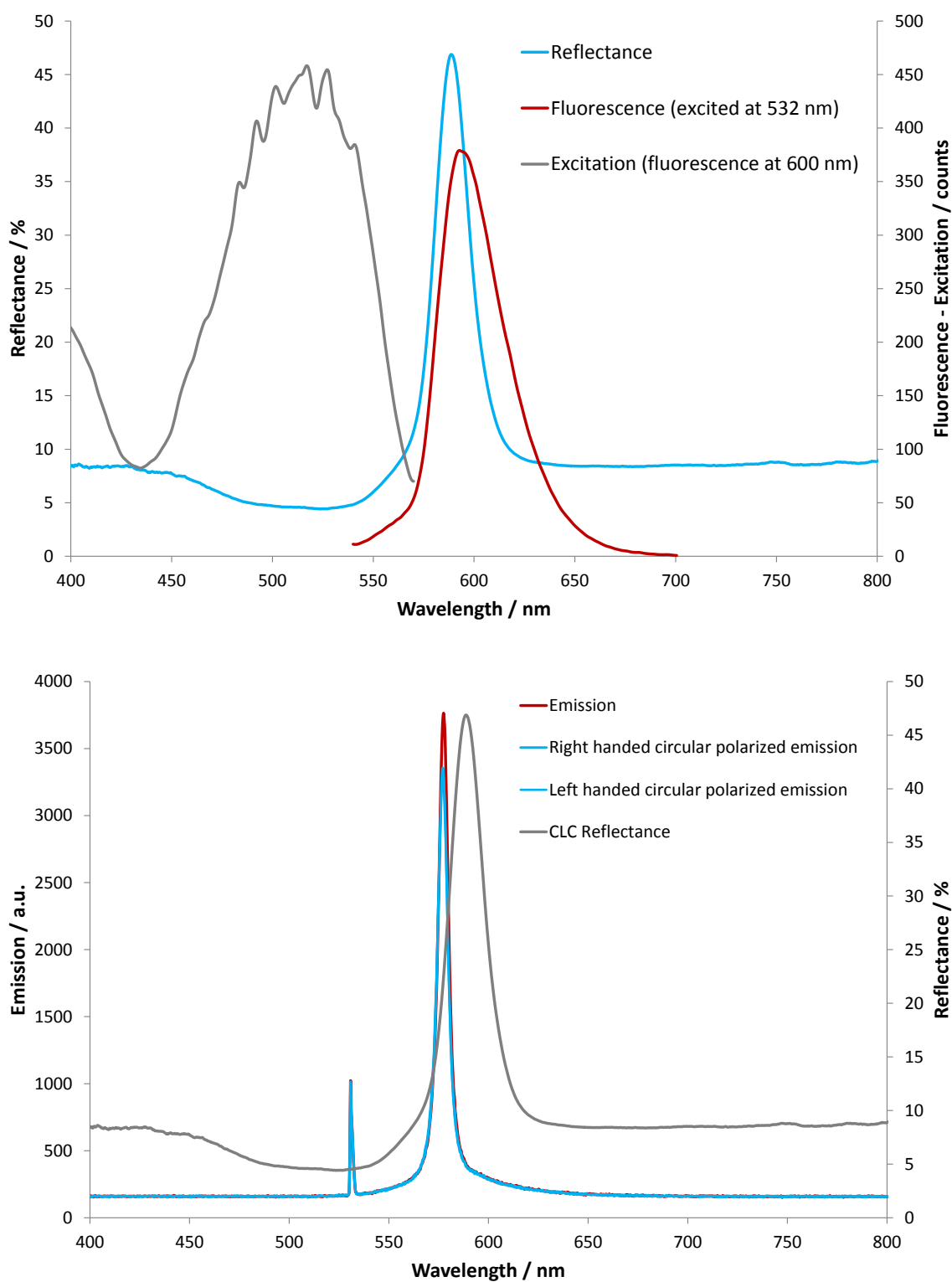
Figure 3.60: Optical properties (top) and emission of a PM597 doped cellulosic CLC film above threshold (pump laser at 532 nm).
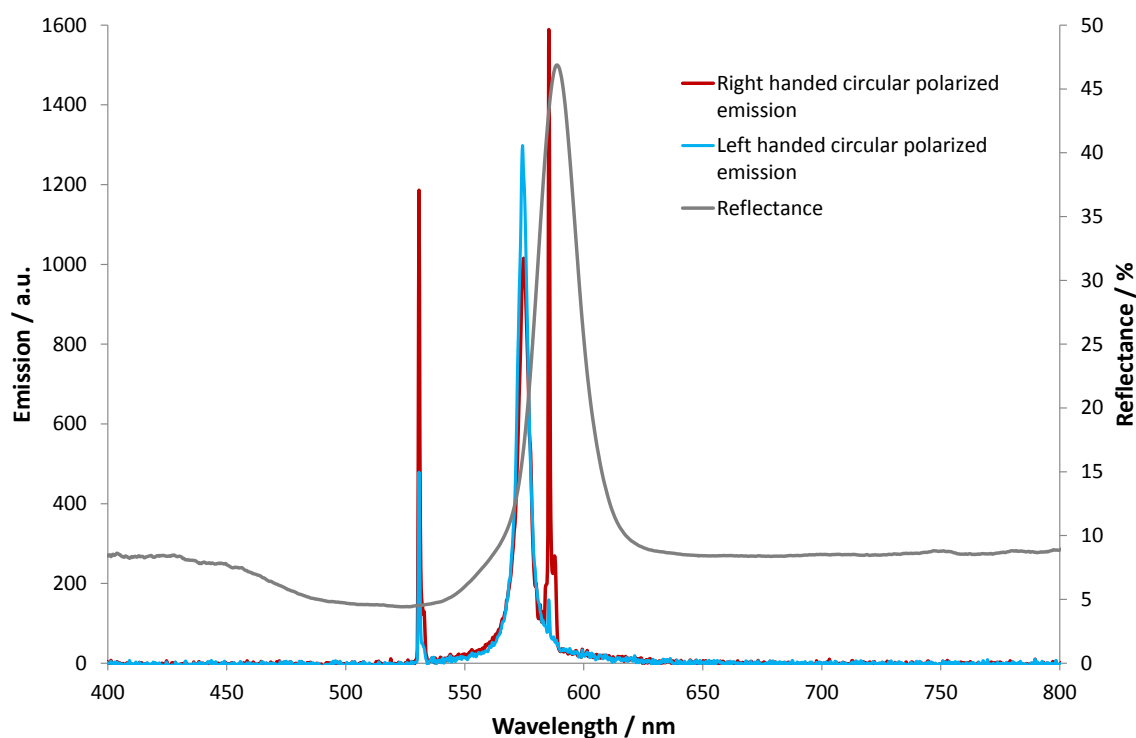
Figure 3.61: Multimode emission of a cellulosic CLC - PM597 composite film (pump laser at 532 nm).

3.5.6 Conclusion

For the first time, after significant improvement of the host material and careful preparation of the composites, defined bandedge lasing has been demonstrated with lyotropic LCP as host material - in this case derivatives of cellulose. By accident two additional lasing modes, random and defect lasing, were shown with the same host. All results proof that the optimization of the CLC's alignment was needed to achieve and provide a laser-sufficient feedback, a way of feedback which was claimed not to be realizable in this kind of host material. Nevertheless, the data shows that there is still room for improvement until a perfectly aligned CLC made of polymers is obtained. So far they are not at the same level as low molar mass compounds. A polydomain arrangement of well aligned domains causes interference patterns, only known from low molar mass CLC. This domain structure is an improvement of aligning LCP but at the same time it offers the ways to random and defect mode lasing. Considering all samples many proofs were found to verify the lasing nature of the recorded emissions. A data set of this quality was not reported so far for LCP cavities and especially not for derivatives of cellulose. The

use of a renewable and biodegradable resources, modified with simple synthesis methods, is desirable to replace expensive low molecular weight compounds. Polymerization fixes the film permanently and enhances its lifetime. In general, these materials are interesting for many optoelectronic applications like spectroscopy or communications. To achieve a wide range of different lasing wavelength, a setup with a cheap pump laser and a variety of different films replace very expensive and big conventional systems like OPO laser. At the 2012 International Liquid Crystal Conference in Mainz, the group around Coles presented the first realization of such a CLC-laser, being able to emit different wavelengths just by changing the CLC cell.

3.6 Microparticles of cellulosic CLC

Parts of this section have already been published [180].

3.6.1 Introduction

The usual method to process cholesteric samples is the preparation of thin films between two glass plates. However, there has been growing activity in the synthesis of defined micro- and nanometer-sized objects from all kinds of liquid crystalline materials [181, 182, 183, 184, 144]. They are interesting because of the interaction between the mesogens' alignment and the confined geometry. Temperature induced phase separation has been utilized to prepare dispersions of cholesteric droplets in matrix polymers [185, 186, 187]. The textures of these droplets have been characterized by polarized optical microscopy. In the case of parallel surface alignment Xu and Crooker found that the director configuration in the droplets depends strongly on the ratio between the helical pitch-length (p) and the diameter of the droplets (D) [187]. In the case of highly chiral cholesterics (p $>$D) the alignment of the mesogens follows the Frank-Pryce model [188, 189]. It predicts a concentric orientation of the mesogens around the droplets with the pitch axis aligned axially and one S = 2 disclination line along a radius. Recently we showed that microfluidics is another effective method to prepare droplets and solid particles from liquid crystalline materials with diameters in the micrometer range with a very narrow size distribution. For this, we injected a polymerizable, nematic liquid crystalline monomer through a thin needle into a co-flowing stream of an immiscible carrier fluid [144]. This resulted in the continuous formation of equally sized monomer droplets dispersed in the carrier fluid. While flowing in a microtube, these droplets

were irradiated with UV-light to initiate radical polymerization inside them, yielding solid particles. We found that the flowing motion induced a nonequilibrium alignment of the mesogens inside the droplets. By photopolymerisation we could permanently fix this orientation, yielding liquid crystalline particles with inherently interesting properties [190]. Following the results of the preparation of droplets and polymerized particles from a lyotropic cholesteric liquid crystal based on cellulose derivatives using microfluidics will be presented. At first the lyotropic liquid crystal system and the characterization of the bulk material is introduced. The description of the microfluidic assisted synthesis of micrometer-sized beads from this material is followed by the characterization of these particles by polarized optical microscopy and the discussion possible director configurations.

3.6.2 Preparation and Characterization of Cholesteric Microparticles
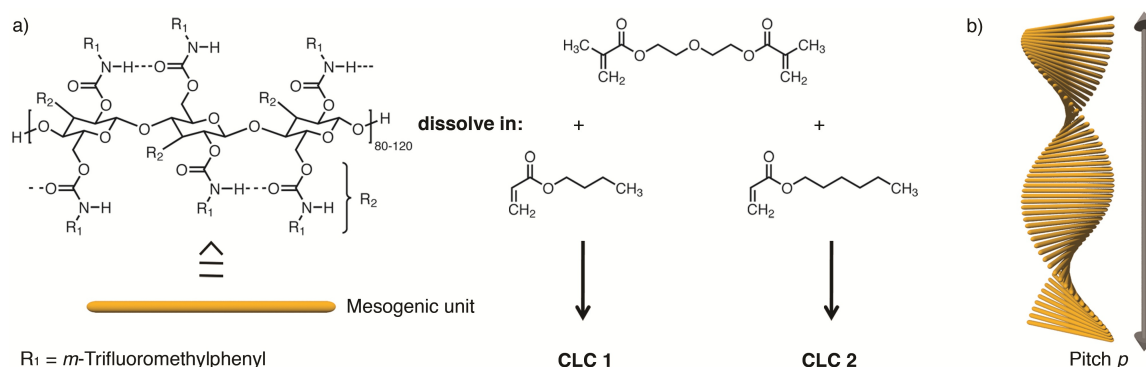
Figure 3.62: The chemical structure of the used cellulose derivative and the hydrogen bonding forcing the polymer into a rod-like shape. Furthermore the polymerizable solvents for lyotropic CLC 1 and CLC 2 are displayed. Mixtures of 20% w/w (16% mol) diethylene glycol dimethacrylate (top) and 80% w/w butyl- (bottom left) and hexyl-acrylates (bottom right) were used. (b) shows the helical arrangement of the cellulosic mesogens in the liquid crystalline phase.

The mesogenic unit consisted of rod shaped CTC with m-trifluoromethyl phenyl residues, providing a good solubility in different acrylates and methacrylates (Fig. 1). The material was synthesized according to known procedures [29, 62] in a one step synthesis from hydrolyzed native cellulose. Depending on the initial length of the cellulose, the mesogens have a typical length of several hundred nm. If shorter mesogens are desired, CTC can be degraded to any shorter length by acidic treatment (see section 3.2.3). Furthermore this allows tuning the material to certain

selective reflection wavelengths. In this study we used CTC with the above mentioned residues and a molecular weight of $M_n = 280\ 000\ \frac{g}{mol}$ corresponding to a length of about 200 nm. Various acrylates and methacrylates were tested as a solvent for the mesogens in order to optimize the lyotropic mixture concerning viscosity and processability in the microfluidic setup. The goal was to reduce viscosity and to obtain a low vapor pressure of the mixture to decrease evaporation. Additionally the selective reflection was tuned to be within the wavelength of visible light. The best results were obtained with acrylic esters containing alkyl residues. Acrylic esters with short alkyl chains had an insufficiently low boiling point. Hence quick evaporation of the solvent led to an increasing concentration of the mesogens, thus influencing the pitch.On the other hand long alkyl residues caused sticky mixtures with high viscosities or low solubility for the CTC. Butyl acrylate (CLC 1) and hexyl acrylate (CLC 2) seemed to be optimal compromises (figure 3.62).
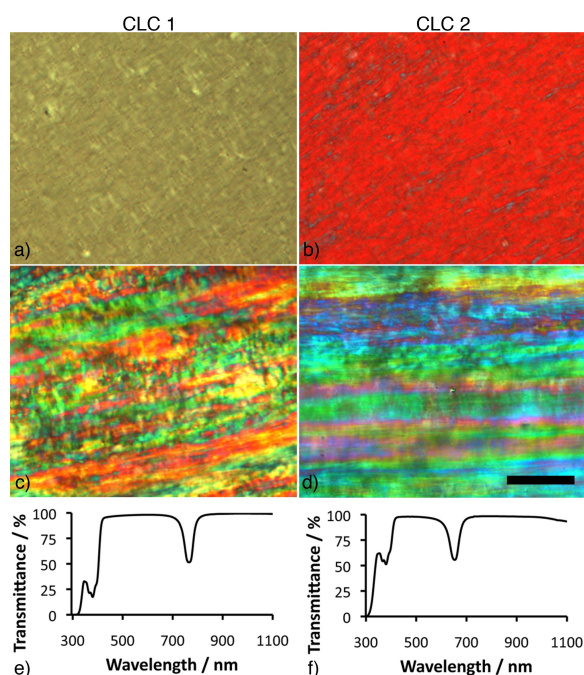
Figure 3.63: The textures of CLC 1 and 2 prepared as a film between two glass plates (a and b) and prepared in a glass capillary (c and d). (e) and (f) display transmittance spectra of the films sandwiched between glass plates. The peaks in the range of 600–800 nm represent the selective reflection, between 350 and 400 nm the absorbance of the used UV-initiator. Both samples show a selective reflection with intensity very close to the theoretical limit of 50%. The scale bar corresponds to 200 μm.

The liquid crystalline mixtures were prepared by mechanical stirring overnight. First a UV-initiator was dissolved in the monomer mixture (butyl or hexyl acry-

late with diethylene glycol methacrylate), followed by 45% w/w of CTC. After 60 min the mesogens were dissolved and stirring overnight ensured a homogeneous solution showing opalescent colors. Allowing the sample to stand for a few hours afterwards released air bubbles from the mixture. CLC films with planar orientation were prepared between two glass plates and additionally by filling glass capillaries (figure 3.63). The mesogens were oriented parallel to the glass substrates with the helical axis aligned perpendicular to it because of biaxial shearing in the first and flowing motion in the latter cases. Additional alignment layers made from polyimides may help to achieve a more homogeneous orientation. Photopolymerization of these mixtures leads to the formation of semi-interpenetrating networks of cellulose carbanilates in a polyacrylate network, in which the cholesteric structure is locked in unchanged [29, 62]. The typical textures of the cholesteric films prepared between glass slides are shown in figure 3.63 a and b. The CLCs show a Grandjeantexture without any visible color for CLC 1 (a) and colored in red for CLC 2 (b). This corresponds to the position of the maximum of the selective reflection, which is 770 nm for CLC 1 and 660 nm for CLC 2, respectively (figure 3.63 e and f). In contrast the textures of the same samples oriented with flow motion in a glass capillary show many different colors with lines parallel to the flow motion (figure 3.63 c and d). This is a result of the still very high viscosity in comparison to the low molecular weight samples. The flow disturbs the orientation of the cholesteric helices and the viscosity is too high to allow a complete reorientation before crosslinking. Differences in the orientation of the cholesteric helix axis are - most probably - the origin of the material's colorful appearance.

Figure 3.64 shows a schematic drawing of the microfluidic setup utilized to prepare particles from the cholesteric materials CLC 1 and CLC 2. A solution of polyvinyl alcohol (M_n = 88 $\frac{kg}{mol}$) in water (5% w/w) was used as a continuous phase. Water does not mix with the monomer components in CLC 1 and 2 and does not dissolve the cellulose derivative. Polyvinyl alcohol was added to adjust the viscosity of the continuous phase to the dispersed phase. Both liquids were filled in syringes that were pressurized by two syringe pumps. The liquid crystalline material was injected through a thin needle from fused silica (inner diameter 100 μm, outer diameter 165 μm) into a co-flowing stream of the polyvinyl alcohol solution. The mixing was performed in a T-junction connected to microtubes from teflon. The injection yielded an emulsion of equally sized droplets of the cholesteric material in the aqueous polyvinyl alcohol solution flowing in a microtube. This tube was put in thermal contact with a hotplate, thus controlling the temperature of the droplets.

Focused UV-light with a wavelength of 323 nm - 385 nm was directly shone onto the tube from a waveguide. This initiated the decomposition of the photoinitiator, yielding radicals that led to a polymerization of the monomers in the droplets. At the end of the assembly, solid cholesteric particles surrounded by polyvinyl alcohol solution were collected continuously. The conversion of the photopolymerization was determined by NMR experiments for a different, but chemically comparable, system [190].
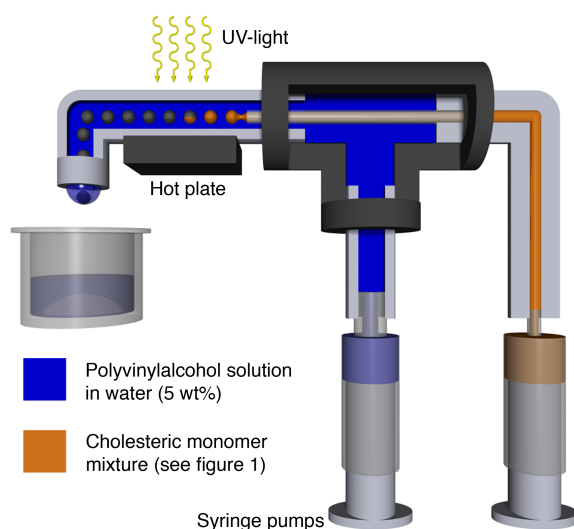
Figure 3.64: A schematic drawing of the microfluidic setup that was utilized to prepare micrometer-sized particles from the lyotropic cholesteric liquid crystal introduced in figure 3.62. The liquid crystalline material was injected through a thin needle into a co-flowing stream of an aqueous solution of polyvinyl alcohol in water. Both phases were pressurized by two syringe pumps. The resulting LC droplets were polymerized by irradiation with UV-light while flowing in a microtube.

The reaction was quantitatively under the flow conditions used in this study. Consequently we expect the particles to be crosslinked homogeneously. The dispersions were washed repeatedly with water to remove the polyvinyl alcohol. The obtained particles were stiff at ambient conditions, thus allowing an uncomplicated handling. By exposing them to a good solvent for the matrix polymer (tetrahydrofuran, THF) the particles could be swollen reversibly. Thereby their volume increased by a factor of roughly 4, characteristic for weakly crosslinked networks. Figure 3.65 a and c show photographs of several particles from CLC 1 and CLC 2. The CLC 1 particles (a) have a mean diameter of 273 μm while the ones from CLC 2 (c) have a size of 337 μm. The difference in size is due to the lower viscosity of CLC 1 compared to CLC 2. As shown for another system [190], the size of the particles can be

controlled easily by varying the flow rate ratio between the liquid crystal mixture and the aqueous phase. Both samples have a very narrow size distribution with polydispersity indices lower than 2%. Comparing figures 3.65 a and c we find that the particles from CLC 1 appear darker than the ones from CLC 2 in transmission microscopy.
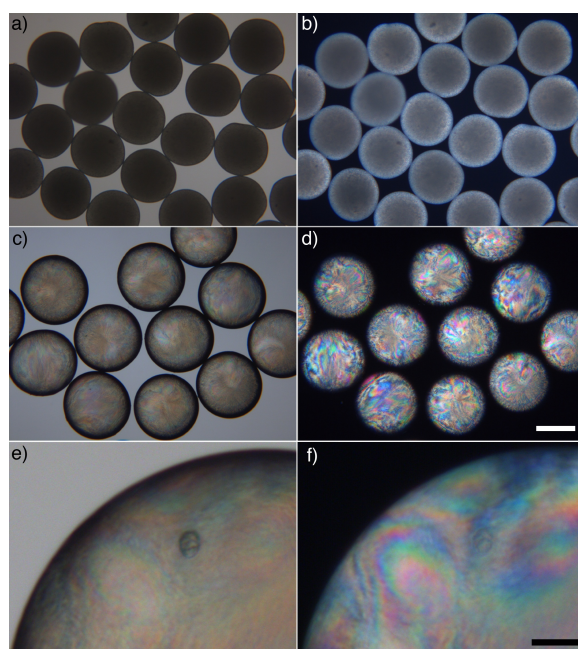
Figure 3.65: Microscopy images of polymerized microbeads made from two different cholesteric materials. The photos on the right side were taken between crossed polarizers (POM), thus revealing the liquid crystalline textures. The particles in (a) and (b) consist of CLC 1 (defined in figure 3.62) which has a pitch of 770 nm. They are highly scattering, thus appearing as dark circles (a) with no characteristic texture (b) in a polarizing optical microscope. Images (c) and (d) show particles made from CLC 2 (pitch length of 650 nm). They are slightly transparent and have an opalescent appearance, characteristic for the presence of a selective reflection. Their texture is similar to the one observed in thin films of the material. (e) and (f) show magnifications of the second sample. The upper scale bar corresponds to 200 μm, the lower one to 100 μm.

Consequently the first sample strongly scatters visible light, which is typical for a liquid crystalline system with many small domains (polydomain sample). The spheres from CLC 2 on the other hand are more transparent, thus indicating a more regularly ordered director field. Careful inspection of the particles after magnification (figure 3.65 e) reveals a slightly opalescent appearance of this sample. We argue that this is the consequence of a selective reflection at visible wavelengths of light as discussed in the introduction. The effect is observable because the CLC's selective reflection maximum in CLC 2 is 660 nm, consequently within the wavelength

of visible light. The selective reflection in CLC 1 on the other hand amounts to 770 nm, corresponding to light in the IR region, thus leading to no visible selective reflection. The photographs on the right side of figure 3.65 (b, d and f) were taken between crossed polarizers (POM). In this mode, only birefringent materials are visible as colored spots. Both samples show birefringence but their textures look very different. The scattering of the particles from CLC 1 is very high and they appear as white circles (figure 3.65 b).
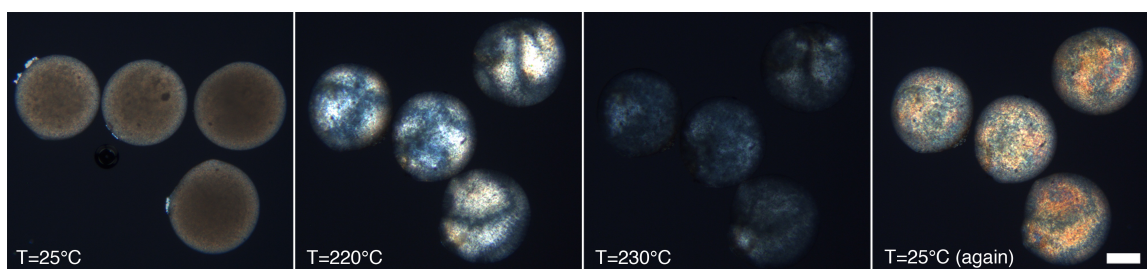
Figure 3.66: Polarized optical microscopy images of particles from CLC 1 at different temperatures. At 25 °C the material is opaque and no LC-texture can be seen. Close to the phase transition the spheres turn transparent and a Maltese-cross texture becomes visible. At 230 °C the liquid crystal becomes isotropic, indicated by a loss of birefringence. During cooling back to 25 °C the cholesteric phase reappears and remains visible. The scale bar corresponds to 100 μm.

We assume that because of the long pitch of CLC 1 there is a competition between cholesteric and nematic-like ordering during flow, which leads to a poor orientation (multidomain sample). Since the selective reflection is close to 800 nm it is not visible to the eye. The more transparent particles from CLC 2 show a colored texture (figures 3.65 d and f), which is identical with the one of the liquid crystalline bulk material (660 nm), if it was filled into a capillary by flow (figure 3.63 d). From this we conclude that a flowing motion of the cholesteric material, either as a bulk when filling the capillaries or as droplets in the microfluidic setup, induces a non-equilibrium state of the director. This alignment led to the characteristic texture visible in figure 3.63 d and 3.65 d. We performed heating experiments on the particles in order to determine if they show a phase transition. Figure 3.66 displays four particles from CLC 1 during heating in a polarizing microscope. Due to the high aspect ratios of the cellulose mesogens and the polymerized matrix the temperature of phase transitions in these materials are very high. At room temperature the sample showed the scattering and white appearance as discussed above. With increasing temperature on approaching the clearing point the material became more transparent. At 220 °C a Maltese-cross texture was visible. At 230 °C the particles

became almost completely dark, indicating that they lost all birefringence. Upon cooling, birefringence reappeared. However, the samples did not return to their initial, scattering state but remained in the Maltese-cross texture. During a second heating - cooling cycle the sample cleared reversibly and returned to the Maltese-cross texture. It has to be considered that at elevated temperatures probably two effects overlap each other: On one hand, the degree of order within the liquid crystalline phase decreased due to faster movement of the mesogens in a soft elastomer matrix (swelling ratio of nearly 4 possible). On the other hand, the hydrogen bonds responsible for the mesogen's stiffness dissociated, leading to a shortening of the mesogen's persistence length [191, 157], which further increased its mobility within the weakly crosslinked matrix polymer. In combination, both effects resulted in a phase transition to the isotropic phase. During cooling, they re-organized in an ordered phase, as indicated by re-appearance of birefringence. However, they aligned in a different - more ordered - pattern than during their synthesis under flowing conditions, which brings forth the Maltese-cross pattern.

In another set of experiments it was the aim to improve the mesogen's alignment in the resulting microparticles. Therefore the CLC mixture was diluted with acetone for two purposes: The liquid crystal has a much lower viscosity, making it processable more easily in microfluidics. Furthermore, the acetone does migrate into the water phase during the flow, leaving back the pure CLC. The resulting contraction of the particle, during the flow time until polymerization, applies some shear movement, in addition to the flow induced shear, helping the alignment of the CLC.
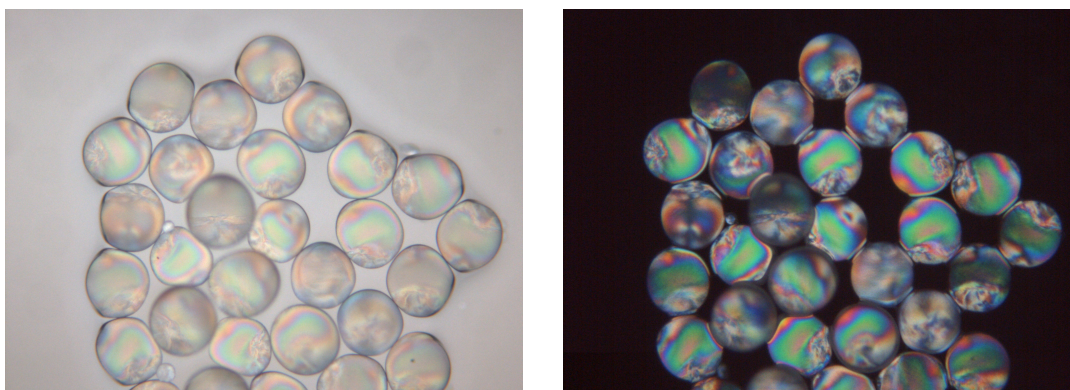

Figure 3.67: Microscopy images under white light illumination (left) and between crossed polarizers.

Figure 3.67 shows microscopy images of microparticles prepared from diluted CLC. This particles clearly show area much better aligned than the ones prepared from pure CLC. These areas show a homogeneous color between crossed polarizers, that

changes according to the incident angle dependency of the reflected wavelength and the curvature of the particle. It is also visible that the well aligned areas are like equators and the poles of the particles still show the pattern known from the previous ones. The shear due to the volume shrinkage after the removal of acetone seems to be more effective in the equatorial area, or the mesogens do have difficulties to align in the pole areas and hence create defect structures. We assume the equatorial areas to have a radial orientation of helix axes and a parallel surface anchoring of the mesogens. Usually films are tempered for several hours to reach the equilibrium state of alignment, but unpolymerized particles do not change after preparation. This may be caused by the high viscosity and additional hindrance in movability resulting from of the spherical particle boundary.

As reported for CLC films, the viscosity and the overall optical properties, based on a well alignment, can be optimized via choosing the right solvent for the mesogens and adding certain additives. The solvent of choice for CLC films is EGMEA. However, its miscibility with other organics does not allow to use it for microfluidics. The acrylic solvent of the CLC should remain inside the particle to maintain a constant concentration of mesogens in the CLC. Therefore an immiscible carrier fluid was chosen, preventing migration of acrylates into the carrier fluid. In addition the viscosity of the carrier fluid must be adapted to the CLC's viscosity, to ensure a sufficient "rip off" of particles from the needle. So far no solvent that is immiscible with EGMEA has been found. It mixes with very polar solvents like acids or water and with very non-polar ones like hexane, silicon oil or perfluorinated organics. If a CLC with EGMEA is processed in the microfluidic setup, the CTC material precipitates after the EGMEA has moved into the carrier fluid. The result is that all the optimization applied to CLC films is not applicable to the microfluidic experiments.

3.6.3 Conclusion

Comparing the properties of our cholesteric particles prepared under flowing conditions with the droplets obtained by temperature induced phase separation [187] we found similarities but also differences. In the former publications a parallel surface alignment of the mesogens within the droplets was determined. We assume that this is also the case in our particles due to the presence of polyvinyl alcohol in the surrounding medium during their preparation. The authors of the former contributions proposed an alignment of the mesogens according to the Frank-Pryce model in their cholesteric droplets. However, for droplets with a diameter much bigger than the helical pitch they found a Maltese-cross texture, similar to nematic

structures. Right after the particle's preparation, we do not find such a texture in our particles. The analysis of the texture was impossible, most likely because due to the longer helix pitch and scattering. The particles from the second sample (CLC 2) showed a intensely colored texture that was obviously a consequence of their preparation under flowing conditions. When heating the particles, shortly before the transition to the isotropic phase, this colored texture changed to a Maltese-cross, similar to the results obtained by the other authors. From this we conclude that the non-equilibrium alignment of the mesogens obtained from the flowing conditions was replaced by the thermodynamically stable Frank-Pryce structure, once the mesogens were sufficiently mobile. Upon cooling, the mesogens remained in this configuration. The spheres from CLC 1 showed no selective reflection of visible light due to their long helix pitch (figure 3.63 e). On the other hand, the ones from CLC 2 had an opalescent look, which we consider as a selective light reflection. This corresponds well to their shorter pitch of 660 nm (figure 3.63 f).

It is indeed possible to prepare particles with a better alignment but this does not apply to the whole particle, but only to some areas. The whole optimization, as described for cellulosic CLC films, can not be transferred to the microfluidic setup, due to solvent miscibility issues. Hence the particles show well aligned regions but, in the same manner as it is important for lasing in CLC films, this degree of alignment will not allow a sufficient feedback for lasing out of the particles as described by [90]. Anyway, the texture and defect formation of lyotropic cellulose derivatives in confined geometries is interesting to study and give a better understanding of how CLCs can be oriented at surfaces and with shear motion.

4 Experimentals

4.1 Characterization, Devices and Chemicals

The following listed devices were used for characterization and preparation of products and films:

Centrifuge:
Mulfifuge 1 L-R and Fresco 17 both from Heraeus equipped with a 29 cm and 14 cm rotor, respectively .

Elementary analysis:
Vario EL cube from Elementar with corresponding software.

GPC:
Jasco GPC system running on THF with PU-1580 pump, AS-1555 autosampler, DG-2080-53 degasser, UV-1575 UV detector, RI-1530 refractive index detector and a Mini Dawn three angle light scattering detector from Wyatt. A PSS data interface UDC-810 converted the data readable to the software WinGPC version 7 and Unichrome. The liquid flow rate was 1 $\frac{mL}{min}$ and toluene was used as internal standard. Calibration was done with PSS ReadyCal poly(styrene) standards and sample concentration was in the range between 1 and 3 $\frac{mg}{mL}$. The setup comprised three chromatographic columns with pore sizes from 10^2 to $10^6 \mathring{A}$ and one filter column.

Fluorescence microscopy:
Olympus BX 53 fluorescence microscope with an Olympus camera XC 30 and software Cell^D version 3.4.

Fluorescence spectroscopy:
Perkin-Elmer LS 50 B Luminescence Spectrometer with software FL Winlab version 2 and spectrofluorometer Fluorolog 3 Horiba Jovin Ybon fitted with a Hamamatsu

PMT R928P.

IR:

Jasco FT/IR 4100 spectrometer with corresponding ATR unit and software Spectra-Manager version 2.

Light scattering:

Dynamic light scattering experiments were done with an ALV-Goniometer-SP-125 with ALV5000-Onboard-Correlator and Software ALV 3.0. Static light scattering experiments were done with an ALV-Goniometer-SP-86 and software ALV-ODIL. Curves were measured at 293 K, using a He-Ne Laser-Unisys 632.8 nm in an ID 2 cm cuvette. The solvent was methanol with 50 mM lithium bromide.

NMR:

^{1}H-NMR spectra were measured with a Bruker AC300 at 300 MHz, ^{19}F-NMR spectra with a Bruker DRX400 at 400 MHz at 25 °C. The spectra were analyzed with ACDlabs 9.0 1D NMR Manager software. All chemical shifts are in ppm relative to the signal of tetramethyl silane.

ORD:

Perkin-Elmer 241MC Polarimeter with a custom made holder for film samples.

Plasma oven:

Plasma Prep 5 from Gala instruments.

POM:

Olympus BX51 equipped with a ColorView camera and a hot stage LTS 350 from Linkam.

Pump laser and power meter:

Opolette 355II with a UV tunable laser system (5ns pulse width) and Molectron power meter model 4000 with detector heads J4.

Reflectance measurements (Ulbricht sphere):

Perkin-Elmer LAMBDA 1050 with integration sphere.

Spincoater:

SCE-150 from LOT Oriel and ST 146 from Convac.

UV polymerization:

LOT Oriel LSE340 / 850 27B light source with 100-500 W output, used with a filter transparent between 320 and 380 nm.

UV-VIS:

Transmittance spectra were measured with a Jasco V-630, a Jasco ETC-717 temperature controller and software SpectraManager version 2. Reflectance spectra were measured with a Shimadzu UV 2102 PC and software Shimadzu UVPC version 3.9. Additional reflectance spectra were recorded with Ocean Optics UV-VIS spectrometer U 2000 and software Spectra Suite.

Viscosity measurements:

UDS 200 manufactured by Anton Paar with a Z4 cylinder and AR1000 from TA Instruments with a cone shaped disc of 2 cm diameter and 1° angle. The software used was Rheoplus 32 version 3.4 for UDS and Rheology Advantage Instrument Control AR version 3 for TA.

All chemicals were, if not stated otherwise, used as received from commercial suppliers, like Sigma Aldrich, Acros and TCI. All solvents were of p.a. degree of purity and dioxane was distilled prior use with standard methods. The CTA for RAFT polymerization was kindly provided by Dr. Katja Nilles. The initiator AIBN (Azobisisobutyronitrile) was recrystallized from diethyl ether. The low molecular weight CLC, used to dope cellulosic LC, was provided by Merck (MDA-00-3907).

4.2 Synthesis of Cellulose Derivatives

All cellulose tricarbanilates were synthesized according to the following procedure [62, 29]: Avicell PH101 (10 g, $\approx$ 0.25 mmol) was dried over night at 80 °C in vacuum prior to usage. It was placed in a round bottom flask and under a nitrogen atmosphere 200 mL pyridine (water content below 50 ppm) was added. The mixture was heated to 85 °C and the cellulose was swollen for 3 hours. The isocyanate (0.15 mol) was added via a syringe to the dispersion. After two hours the cellulose was completely dissolved in the solvent, but it was allowed to react over

night to give a yellowish clear solution. The warm solution was poured into a five fold amount of 70/30 v/v methanol/water. The precipitate was filtered and dried at 80 °C in vacuum. Dissolution in 300 mL acetone yielded a yellowish solution and any solid residues were removed by centrifugation. Again, precipitation was done with a five fold amount of the previously used mixture. The dried solid was redissolved in 150 mL acetone and precipitated a third time under the same conditions. After drying it was pestled to give a colorless powder (yield 90 - 100%). *m*-trifluoro-methyl phenyl derivatives, which were used for film preparation in this thesis, were reacted three times with the same reaction conditions to obtain the highest possible DS. In cycle two and three, the equivalents of isocyanate were reduced to half of the amount of the first reaction cycle.
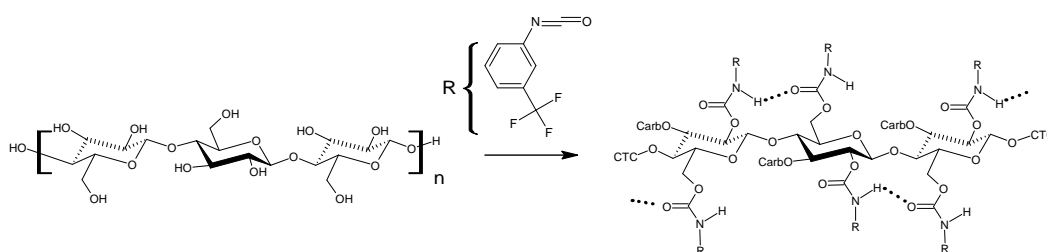
Figure 4.1: Scheme of the CTC synthesis starting with cellulose.

4.2.1 Acidic Degradation

The synthesis of shorter mesogens was done by acidic degradation of CTC obtained from Avicell PH101. The initial CTC (1 g) was dissolved in 15 mL ethylene glycol monomethyl ether at 100 °C under a nitrogen atmosphere. After one hour at this temperature 400 mg (2.1 mmol) *p*-toluene sulfonic acid was injected. The product solution was poured into the five fold volume of water for precipitation. The product was filtered and washed with water. Drying over night at 80 °C in vacuum and pestling yielded a colorless powder (85 - 95% yield).

4.3 Film Preparation

The solvent mixture for the CLC was placed in a 5 - 10 mL vial. Additives, initiator (Lucirin TPO, 1% w/w regarding to the amount of acrylic solvent), dye or low molecular weight LC were dissolved in the liquid. The CTC were added as a powder on top of the liquid (figure 4.2 left). A bend syringe needle was utilized as a stirrer

and punched through the cap of the vial to prevent solvent evaporation. Depending on the used solvent the stirring time was between 3 and 5 hours at a rotation speed of 60 rpm. The resulting CLC showed iridescent colors, if the pitch was in the wavelength range of visible light (figure 4.2 right). Air bubbles were removed with centrifugation. If Lucirin TPO was used, the stirring as well as the whole film preparation was carried out under UV light protection.
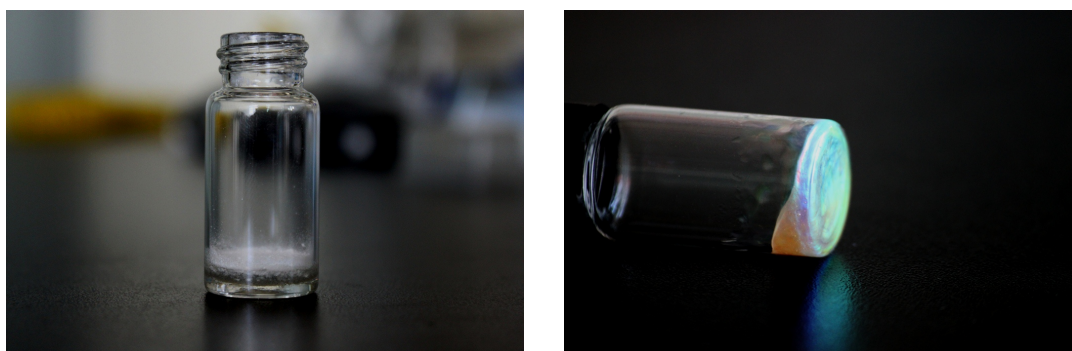
Figure 4.2: Photographs of the CLC mixture before (left) and after stirring.

Standard microscope glass slides and cover slips were cleaned with a 2% v/v solution of Hellmanex III in purified water and additional ultrasonication for 15 minutes. The cleaning agent was washed away three times with purified water and ultrasonication for 15 minutes each. The water was removed by rinsing the slides with *iso*-propanol and drying with compressed air. Before the film preparation the slides were treated with oxygen plasma for 10 minutes and were unidirectionally rubbed with Kimwipe cellulose sheets 10 times. Dust from the rubbing was removed with compressed gaseous nitrogen. A drop of the CLC was placed on one slide with a spatula and covered with the coverslip in an antiparallel manner, regarding to the rubbing direction. Spacers of polyester foil were put in between the two glass slides to control the sample thickness. The samples were left at RTP or slightly elevated temperatures to equilibrate for 24 hours. Afterwards polymerization was done with a mercury lamp at 500 watt and a filter transparent between 320 and 380 nm for one minute. To obtain free standing films the coverslip was removed with a scalpel and the film was pealed of the glass slide. For doping the films with organic dyes only the coverslip was removed and the film remained on the glass slide to ensure a flat surface after the swelling procedure. The sample was put into the dye solution in a sealed vessel over night. Residual dye solution was washed away with pure solvent and the films were dried at RTP in vacuum.

4.4 Synthesis of Polymeric Surfactants

All purchased monomers were distilled prior use to remove impurities , e.g. large amounts of DEGMEA in commercially available EGMEA and inhibitors. The desired DP can not be synthesized only by adjusting the equivalents of CTA and the monomer. Test polymerizations have been conducted to determine the values of CTA needed for a specified block length. The following table provides information about the reaction time and the equivalent of the initiator relative to the amount of CTA to obtain a high yield of defined polymers. A DP of 100 was desired, while impurities cause an increase of DP.

Reaction time hours	Initiator eq.	Yield %	DP	PDI
24	0.125	60	131	1.2
24	0.25	80	126	1.4
48	0.125	75	135	1.22
48	0.25	90	123	1.4

The best compromise between high yield and control is given with 0.125 eq of initiator relative to the amount of the used CTA and a reaction time of 48 hours. Polymeric surfactants that increasing the solubility of CdS@CdSe NP in CLC with HA or EGMEA as solvents were synthesized according to the following procedure: At first a block of HA, EGMEA or DEGEEA was polymerized using 4-cyano-4-((thiobenzoyl)sulfanyl)pentanoic acid as CTA and AIBN as initiator. Second, a block of PFPA was polymerized onto the first block. Afterwards the CTA endgroup was cleaved and the reactive ester moieties were converted in a polymer analogous reaction to yield the anchor functionality for the NP's surface.
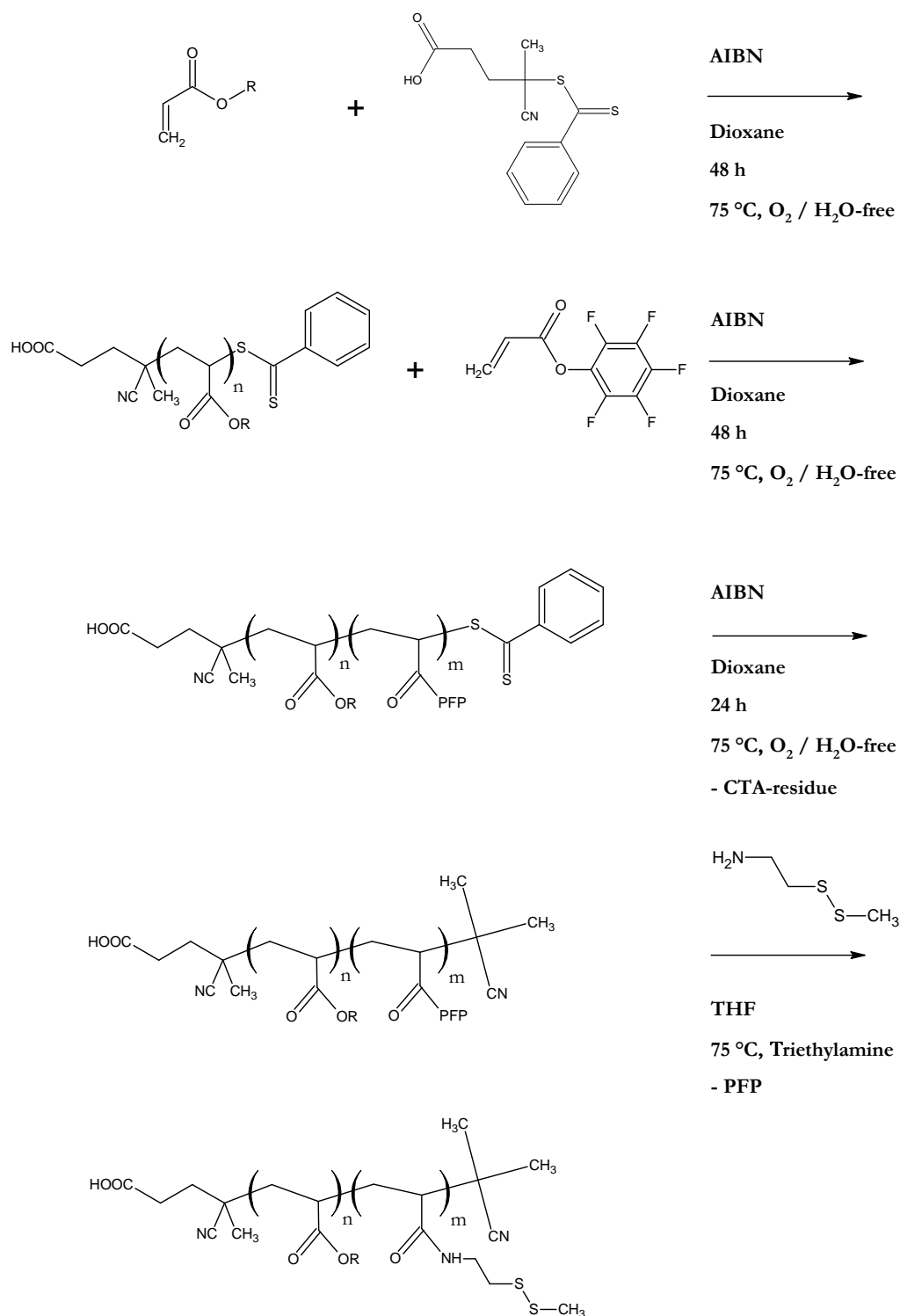
Figure 4.3: Detailed synthesis of polymeric surfactants

4.4.1 P(HA)$_{100}$-*b*-(CMDAA)$_{20}$

To obtain a DP of $\approx$ 100, HA (2 g, 15.77 mmol) was put into a Schlenk tube with 46 mg (0.157 mmol) CTA, 3.3 mg (0.02 mmol) AIBN and 6 mL dry dioxane. The solution was degassed using freeze pumping for four times and refilling with nitrogen or argon gas. The tube was placed in a 75 °C oil bath for 48 hours. The reaction was quenched by freezing the solution in liquid nitrogen. After melting at RTP the product was precipitated in a five fold volume of ice cold methanol. It was separated from the liquid via centrifugation, dissolved in THF and precipitated in ice cold methanol twice to yield a red, highly viscous oil (75% yield). GPC measurement indicated a PDI of 1.2 and a DP of 97.
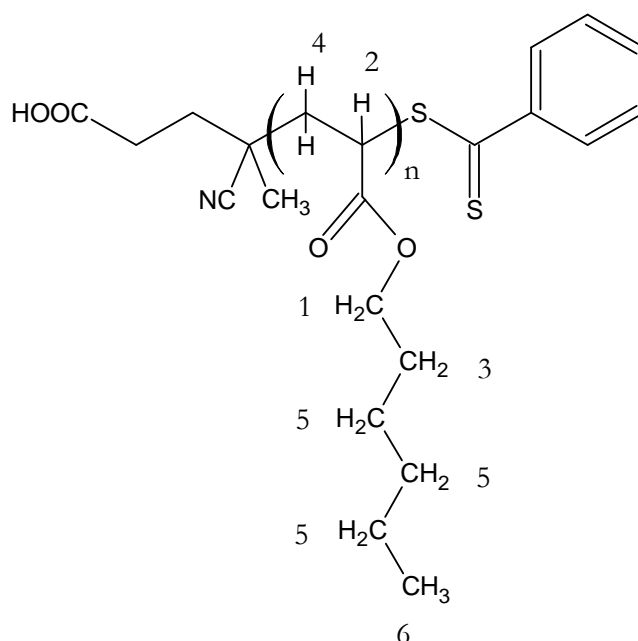
Figure 4.4: Chemical structure of P(HA).

^{1}H-NMR (300 MHz, CDCl$_3$): δ (ppm) =

3.99	(2 H, br m, H$_1$)
2.25	(1 H, br m, H$_2$)
1.84	(2 H, br m, H$_3$)
1.6	(2 H, br m, H$_4$)
1.31	(6 H, br m, H$_5$)
0.9	(3 H, br m, H$_6$)

Signals of the CTA endgroups were barely visible. Broad peaks in NMR spectra indicated the presence of a polymeric product. The signals of hydrogen atoms connected to the polymer backbone are sometimes split depending on tacticity and the orientation of the monomer in the polymer backbone: Face to face or face to tail.

In the second step P(HA) (1.3 g, 0.1 mmol) was dissolved in 6 mL dry dioxane with 952 mg (4 mmol) PFPA and 2.05 mg (0.0125 mmol) AIBN and degassed as previously described to obtain a block of $\approx$ 20 PFPA units. After 48 hours in a 75 °C oil bath the reaction was stopped with liquid nitrogen and the product was precipitated in a ten fold volume of ice cold methanol. The crude product was dissolved in 5 mL THF and again precipitated in ice cold methanol. Additional precipitations in ethanol and hexane removed homoblock P(HA) and P(PFPA) to yield a red, highly viscous P(HA)-*b*-(PFPA) diblock copolymer (65% yield).

Figure 4.5: Chemical structure of P(HA)-*b*-(PFPA).

^{1}H-NMR (300 MHz, CDCl$_3$): δ (ppm) =

In addition to peaks from P(HA)

3.1	(1 H, br m, H$_1$)
2.52 and 2.14	(2 H, br m, H$_2$)

^{19}F-NMR (380 MHz, CDCl$_3$): δ (ppm) =

-153.7	(2 F, d, F$_1$)
-158.3	(1 F, s, F$_2$)
-163.5	(2 F, s, F$_3$)

Broad peaks in NMR spectra indicated the presence of a polymeric product. The signals of hydrogen atoms connected to the polymer backbone are split depending

on the orientation of the monomer in the polymer backbone: Face to face or face to tail. A block length characterization using GPC measurements was not reliable anymore, because the swelling behavior of the diblock copolymer was completely different from the monoblock polymer. However the PDI was measured as 1.25. Therefore the determination of the PFPA blocklength was done via ^{1}H-NMR resulting in a DP of 18.

The dithiobenzene endgroup from the CTA is susceptible to oxidation and substitution reactions. As the conversion of the reactive ester group is a substitution reaction and oxidation of the dithiobenzene group may lead to a connection of two polymer chains, it is advisable to cleave this moiety from the polymer [192]. For this purpose 400 mg (0.031 mmol) of P(HA)-b-(PFPA) and 152 mg (0.93 mmol) AIBN were dissolved in 4 mL dry dioxane and placed in a 80 °C hot oil bath for three hours. After quenching the reaction with liquid nitrogen the product was precipitated in ice cold methanol. The product was purified by dissolution in THF and precipitation in methanol two more times yielding a colorless, highly viscous oil (60% yield). NMR and GPC measurements proofed only a slight degradation of the polymer during the cleavage reaction. The PDI increased from 1.25 to 1.3.

During the last step the reactive ester moiety is converted to the anchor functionality in a polymer analogous reaction. The P(HA)-b-(PFPA) diblock copolymer (200 mg, 0.015 mmol) was dissolved in 5 mL THF. The amine CMD (110 mg, 0.9 mmol) and triethylamine (90 mg, 0.9 mmol) were added and the solution was stirred at 45 °C for 24 hours. The product was precipitated in a ten fold volume of cold methanol, redissolved in THF and successively precipitated twice. The progress of the substitution reaction was monitored with ^{19}F-NMR spectra as the signals vanished after the removing the PFP after precipitation of the polymer. The final polymeric surfactant was obtained as a colorless, highly viscous oil (50% yield). In the ^{1}H-NMR spectrum only the signals from the polymer backbone were clearly identified. The CMD group may be inside the polymer random coil and invisible to the spectrometer. The PDI was measured with GPC to be 1.35.
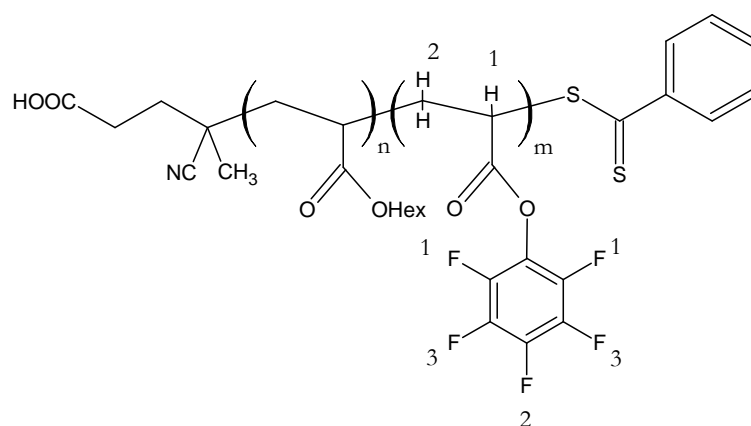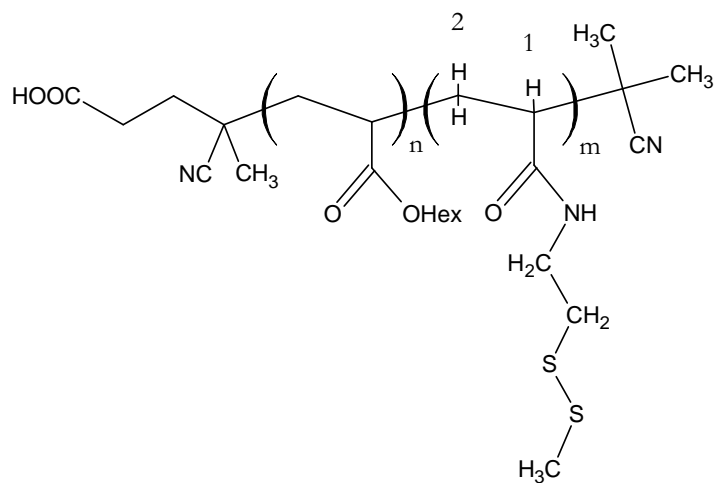
Figure 4.6: Chemical structure of P(HA)-*b*-(CMDAA).

^{1}H-NMR (300 MHz, CDCl$_3$): δ (ppm) =

In addition to peaks from P(HA)

2.88   (1 H, br m, H$_1$)

2.45   (2 H, br m, H$_2$)

4.4.2 P(EGMEA, DEGEEA)$_{25, 50, 100}$-*b*-(CMDAA)$_{20}$

To obtain a DP of ≈ 50, EGMEA (1 g, 7.70 mmol) was put into a Schlenk tube with 45.2 mg (0.154 mmol) CTA, 3.1 mg (0.02 mmol) AIBN and 6 mL dry dioxane. For a DP of 25 and 100 the amounts of the CTA and AIBN were divided by 0.5 and 2, respectively. The solution was degassed using freeze pumping for four times and refilling with nitrogen or argon gas. The tube was placed in a 75 °C oil bath for 48 hours. The reaction was quenched by freezing the solution in liquid nitrogen. After melting at RTP the product was precipitated in a five fold volume of ice cold hexane/diethyl ether 1/1. It was separated from the liquid via centrifugation, dissolved in THF and precipitated in ice cold hexane/diethyl ether 1/1 twice to yield a red, highly viscous oil (80-85% yield). P(DEGEEA)$_{25, 50, 100}$ was synthesized with the same procedure. GPC measurement indicated the following PDI:

Polymer	PDI	DP
P(EGMEA)$_{25}$	1.27	42
P(EGMEA)$_{50}$	1.28	68
P(EGMEA)$_{100}$	1.36	92
P(DEGEEA)$_{25}$	1.08	52
P(DEGEEA)$_{50}$	1.09	79
P(DEGEEA)$_{100}$	1.15	124
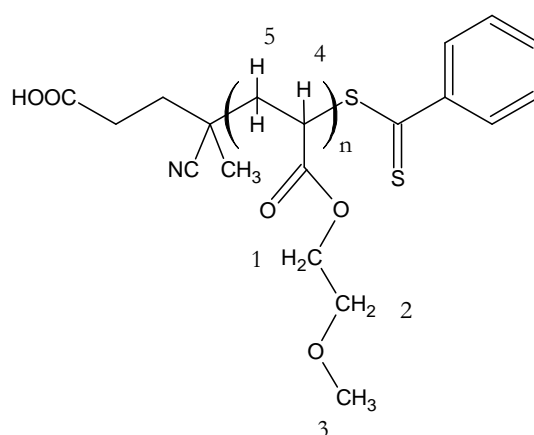
Figure 4.7: Chemical structure of P(EGMEA).

^{1}H-NMR (300 MHz, CDCl$_3$): δ (ppm) =

4.18	(2 H, br m, H$_1$)
3.55	(2 H, br m, H$_2$)
3.34	(3 H, br m, H$_3$)
2.37	(1 H, br m, H$_4$)
1.9, 1.6 and 1.50	(2 H, br m, H$_5$)

Signals of the CTA endgroups were barely visible. Broad peaks in NMR spectra indicated the presence of a polymeric product. The signals of hydrogen atoms connected to the polymer backbone are sometimes split depending on tacticity and the orientation of the monomer in the polymer backbone: Face to face or face to tail.
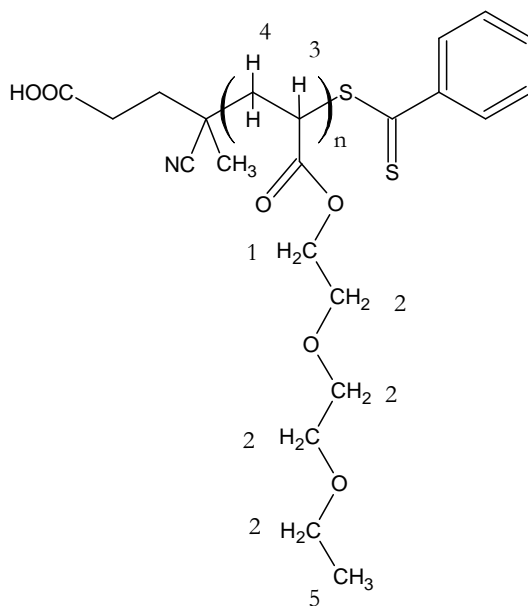
Figure 4.8: Chemical structure of P(DEGEEA).

^{1}H-NMR (300 MHz, CDCl$_3$): δ (ppm) =

4.16	(2 H, br m, H$_1$)
3.45 - 3.64	(8 H, br m, H$_2$)
2.3	(1 H, br m, H$_3$)
1.88, 1.62 and 1.48	(2 H, br m, H$_4$)
1.17	(3 H, br m, H$_5$)

Signals of the CTA endgroups were barely visible. Broad peaks in NMR spectra indicated the presence of a polymeric product. The signals of hydrogen atoms connected to the polymer backbone are sometimes split depending on tacticity and the orientation of the monomer in the polymer backbone: Face to face or face to tail.

In the second step P(EGMEA)$_{25, 50, 100}$ or P(DEGEEA)$_{25, 50, 100}$ (n mmol) was dissolved in $\frac{6mL}{1 g polymer}$ dry dioxane with 40 - 50n mmol PFPA and 0.125n mmol AIBN and degassed as previously described to obtain a block of $\approx$ 20 PFPA units. After 48 hours in a 75 °C oil bath the reaction was stopped with liquid nitrogen and the product was precipitated in a ten fold volume of ice cold hexane/diethyl ether 1/1. The crude product was dissolved in 5 mL THF and precipitated repeatedly in ice cold hexane/diethyl ether 1/1 to yield a red, highly viscous P(EGMEA)$_{25, 50, 100}$-*b*-(PFPA)$_{20}$ or P(DEGEEA$_{25, 50, 100}$)-*b*-(PFPA)$_{20}$ diblock copolymers (60-70% yield). A block length characterization using GPC measurements was not reliable anymore,

because the swelling behavior of the diblock copolymer was completely different from the monoblock polymer. However the following PDI values were measured:

Polymer	PDI	DP
P(EGMEA)$_{25}$-b-P(PFPA)$_{20}$	1.33	42 - 23
P(EGMEA)$_{50}$-b-P(PFPA)$_{20}$	1.31	68 - 18
P(EGMEA)$_{100}$-b-P(PFPA)$_{20}$	1.46	92 - 25
P(DEGEEA)$_{25}$-b-P(PFPA)$_{20}$	1.17	52 - 14
P(DEGEEA)$_{50}$-b-P(PFPA)$_{20}$	1.22	79 - 9
P(DEGEEA)$_{100}$-b-P(PFPA)$_{20}$	1.41	124 - 9
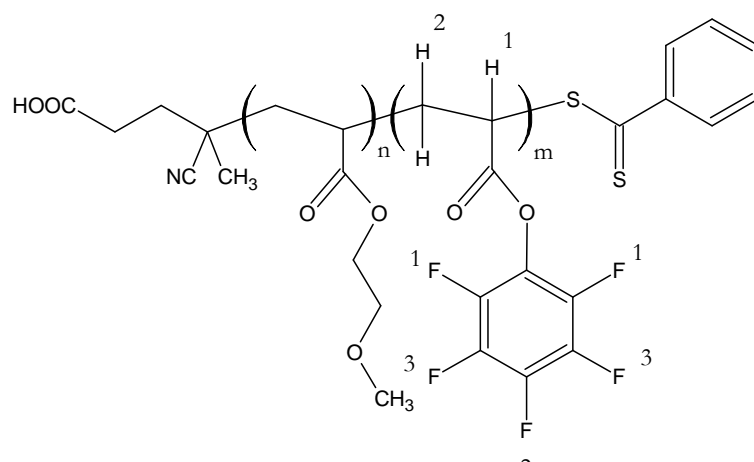
Figure 4.9: Chemical structure of P(EGMEA)-b-(PFPA).

^{1}H-NMR (300 MHz, CDCl$_3$): δ (ppm) =

In addition to peaks from P(EGMEA)

3.1   (1 H, br m, H$_1$)

2.14   (2 H, br m, H$_2$)

^{19}F-NMR (380 MHz, CDCl$_3$): δ (ppm) =

-153.7   (2 F, d, F$_1$)

-157.1   (1 F, s, F$_2$)

-162.5   (2 F, s, F$_3$)

Figure 4.10: Chemical structure of P(DEGEEA)-*b*-(PFPA).

^{1}H-NMR (300 MHz, CDCl$_3$): δ (ppm) =

In addition to peaks from P(DEGEEA)
3.05   (1 H, br m, H$_1$)
2.08   (2 H, br m, H$_2$)

^{19}F-NMR (380 MHz, CDCl$_3$): δ (ppm) =

-153.5   (2 F, d, F$_1$)
-157.1   (1 F, s, F$_2$)
-162.5   (2 F, s, F$_3$)

The dithiobenzene endgroup from the CTA was cleaved and the reactive ester moiety was converted with CMD as described in the previous section. The polymers were precipitated in cold diethyl ether/hexane 30%/70% v/v after the cleavage reaction and in cold diethyl ether after the polymer analogous conversion. NMR and GPC measurements proofed only a slight degradation of the polymer during the cleavage reaction. The progress of the substitution reaction was monitored with ^{19}F-NMR spectra as the signals vanished after removing the PFP via precipitation of the polymer. The final polymeric surfactants were obtained as a colorless, highly viscous oils (30 - 60% yield). In the ^{1}H-NMR spectrum only the signals from the polymer backbone were clearly identified. The CMD group may be inside the polymer random coil and invisible to the spectrometer. The PDI were measured with GPC:

Polymer	PDI
P(EGMEA)$_{25}$-*b*-P(CMDAA)$_{20}$	1.42
P(EGMEA)$_{50}$-*b*-P(CMDAA)$_{20}$	1.7
P(EGMEA)$_{100}$-*b*-P(CMDAA)$_{20}$	1.55
P(DEGEEA)$_{25}$-*b*-P(CMDAA)$_{20}$	1.27
P(DEGEEA)$_{50}$-*b*-P(CMDAA)$_{20}$	1.3
P(DEGEEA)$_{100}$-*b*-P(CMDAA)$_{20}$	1.48

Figure 4.11: Chemical structure of P(EGMEA)-*b*-(CMDAA).

^{1}H-NMR (300 MHz, CDCl$_3$): δ (ppm) =

In addition to peaks from P(EGMEA)
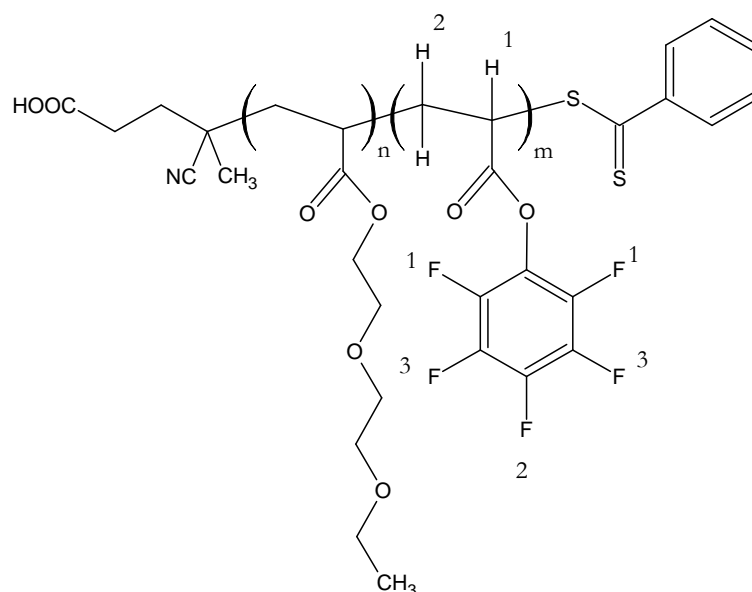2.88   (1 H, br m, H$_1$)
2.45   (2 H, br m, H$_2$)
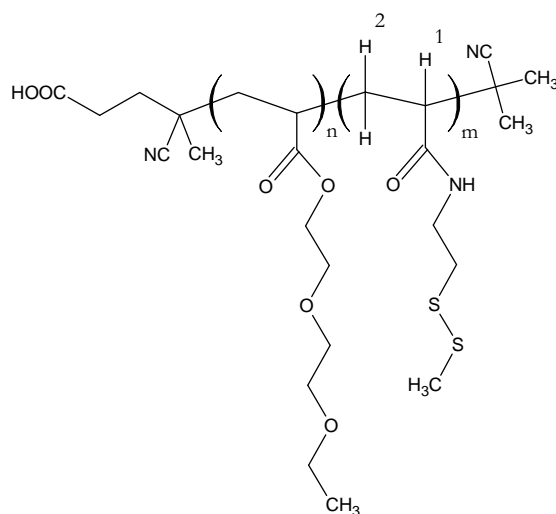
Figure 4.12: Chemical structure of P(DEGEEA)-*b*-(CMDAA).

^{1}H-NMR (300 MHz, CDCl$_3$): δ (ppm) =

In addition to peaks from P(DEGEEA)

2.79 (1 H, br m, H$_1$)

2.36 (2 H, br m, H$_2$)

4.4.3 Synthesis of PFPA

PFPA was synthesized according to [193]: Pentafluorophenol (35 g, 0.19 mol) and triethylamine (27.7 mL, 0.20 mol) were dissolved in 550 mL diethylether and cooled to 0 °C. Acryloyl chloride (18 mL, 0.21 mol) was added dropwise keeping the solution below 5 °C and stirred mechanically at RTP over night. The precipitated triethylamino hydrochloride was filtered from the solution and the solvent was removed using a rotary evaporator. The crude product was purified by column chromatography (R$_f$ of PFPA = 0.68) on silica gel with petroleum ether (boiling point 40 - 60 °C) to yield a yellowish liquid (75% yield).
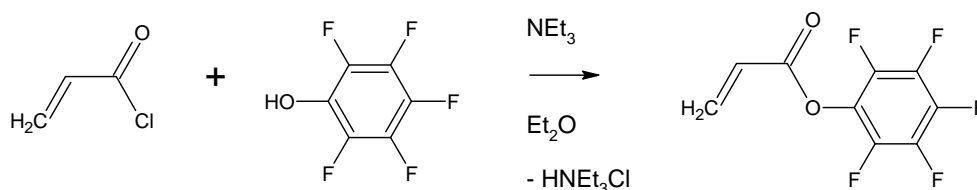
Figure 4.13: Synthesis of PFPA.
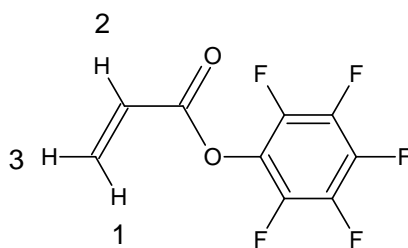
Figure 4.14: Chemical structure of PFPA.

^{1}H-NMR (300 MHz, CDCl$_3$): δ (ppm) =

6.71 (1 H, dd, $^3J_{HH}$ = 27 Hz, $^2J_{HH}$ = 1.05 Hz, H$_1$)

6.39   (1 H, dd, $^3J_{HH}$ = 18 Hz, $^3J_{HH}$ = 12 Hz, H$_2$)

6.19 (1 H, dd, $^3J_{HH}$ = 10.8 Hz, $^2J_{HH}$ = 1.2 Hz, H$_3$)

4.4.4 Synthesis of CMD

Cysteamine methyl disulfide was synthesized according to [194]: Methyl methane thiosulfonate (1.5 mL, 15.8 mmol) was dissolved in 60 mL methanol and combined with a solution of cysteamine hydrochloride (1.52 g, 13.4 mmol) in 60 mL methanol at 0 °C under nitrogen atmosphere. The solution was stirred at RTP for 12 hours and concentrated under vacuum. The concentrate was dissolved in 180 mL dichloromethane, washed twice with 20% w/w sodium hydroxide in water and once with pure water. After drying over sodium sulfate and the dichloromethane was removed with a rotatory evaporator. The crude product was purified via column chromatography (R_f of CMD = 0.125 - 0.425) on silica gel and chloroform/methanol 10/1 to yield a yellowish liquid (90% yield).
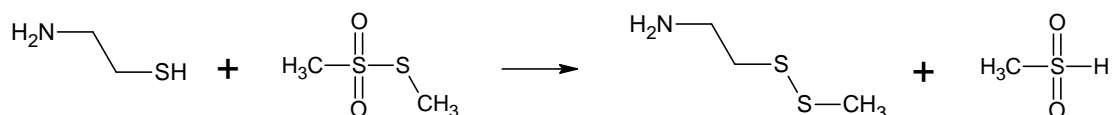
Figure 4.15: Synthesis of CMD.
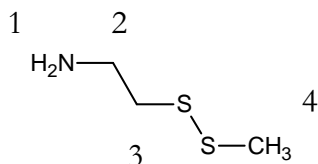
Figure 4.16: Chemical structure of CMD.

^{1}H-NMR (300 MHz, CDCl$_3$): δ (ppm) =

4.91 (2 H, s, H$_1$)
2.98 (2 H, t, H$_2$)
2.83 (2 H, t, H$_3$))
2.45 (3 H, s, H$_4$)

4.5 Surface Modification of Nanoparticles

For the coating of nanoparticles with polymers the same procedure was used for commercially purchased as well as synthesized polymeric surfactants: A chloroform solution of CdS@CdSe nanorods (0.5 mL) was put into a small vial with 0.3 mL of methanol. Centrifugation at 13,300 rpm yielded a small pellet, which was redispersed in 0.5 mL THF utilizing ultasonication. The polymeric surfactant was added as a solution in a small volume of THF and the mixture was treated with ultrasonication for 15 minutes. The low molar mass surfactant from the NP's synthesis was washed from the solution via repeated precipitation with methanol and redispersion in THF. Finally the pellet of functionalized NP was dissolved in the acrylic solvent of the resulting CLC via ultrasonication for 15 minutes.

4.6 Preparation of CLC Microparticles

Micrometer sized droplets were prepared with the microfluidic setup shown in figure 3.64. The liquid crystalline mixture was prepared as described previously (section 4.3) with HA/DEGDMA 80/20 w/w. The CLC was filled into a syringe either as a pure material or diluted 30%/70% w/w acetone/CLC . A 6% w/w solution of poly vinylalcohol (M$_w$ = 195,000 $\frac{g}{mol}$) in water with a flow rate of 10 $\frac{mL}{h}$ was used as the stationary phase. The liquid crystalline mixture was pumped through a capillary with an inner diameter of 100 μm and a flow rate of 0.04 $\frac{mL}{h}$. The setup was equipped with a transparent polymerization tube with an inner diameter of 750 μm and a length of approximately 50 cm. Depending on the flow rate, the time the particles were exposed to UV illumination was 10 - 20 seconds. All experiments were conducted at RTP.

5 Summary

In this thesis, cholesteric films of liquid crystalline cellulose derivatives with improved optical properties were prepared. The combination of different tuning strategies yielded optical qualities similar to theoretically predicted values and known from low molar mass compounds. Composites of the cholesteric material with inorganic as well as organic chromophores were fabricated. The incorporation of inorganic materials involved the synthesis of tailored polymeric surfactants, mediating guest-host interactions. The optical properties of the organic chromophores were matched with those of the cholesteric films and their behavior under optical excitation was studied with regard to mirrorless lasing devices. The cholesteric liquid crystal was, besides film preparation, fabricated in confined spherical geometries, as micrometer sized particles. The tool utilized for the preparation was microfluidics and the particles were examined via optical methods.

Based on known CLC mixtures made of cellulose derivatives in acrylates, every ingredient has been varied systematically to affect the optical properties in an improving way. It was shown that the viscosity of the liquid crystalline mixture and a specific control over hydrogen bonds has a significant impact on the quality of the mesogen's alignment. Intramolecular hydrogen bonds were necessary to maintain the stretched polymer conformation, but intermolecular ones needed to be interrupted, preventing polymer agglomeration. The careful choice of the acrylic solvent mixture, hydrogen bond influencing additives, the synthetic realization of highly substituted CTC and mechanical stirring of solutions at the upper concentration limit of the liquid crystalline regime were the basis for an increased movability of the used CTC mesogens. In combination with a tuned substrate treatment and film preparation method, cholesteric films with optical qualities, known only from low molar mass CLC were prepared. Subsequent polymerization allowed permanent fixing of the alignment and the fabrication of free standing and insensitive films.

The incorporation of inorganic NP into the cholesteric host was mediated via block copolymers, obtained via controlled radical polymerization methods. Besides the shape match between the rod-shaped mesogens and the nanorods, an increased

miscibility of both components was achieved. The polymeric surfactants consisted of a solubility increasing block, made from the same acrylate that was used as a solvent for CTC, and an anchor block attaching to the NP's surface. However, in a densely packed system the difference in dimension between the mesogens and the nanorods induced phase separation. Additional differences in polarity between the pure acrylic solvent and the resulting CLC and long equilibration times further causes slow agglomeration of the NP. Furthermore, the cholesteric order was disturbed by the NP. Nanorods are, in principle, valuable substitutes for organics, but their utilization in cellulosic CLC was not to be combined with a high quality alignment of the cholesteric structure.

On the other hand, organic dyes were introduced into the host material very easily. A swelling process of polymerized films in a dye solution or dissolving dyes in non-polymerized CLC was used for incorporation of the organic chromophores. With the first method the CLC could be aligned and polymerized without any disturbance due to dye molecules. The optical properties of dye and CLC were matched, with regard to mirrorless lasing devices. The dye was optically excited and laser emission supported by the cholesteric cavity was obtained. The polarization and wavelength of the emitted radiation as well as its bandwidth, the obtained interference pattern and threshold behavior of the emission proofed the feedback mechanism that was not believed to be realizable in liquid crystalline polymers. On the other hand random lasing samples were obtained by accident because of misaligned optical features due to the multidomain structure of the CLC films.

Utilization of a microfluidic co-flow injection device enabled us to transfer the properties of cellulosic CLC from the planar film shape to spherical micrometer sized particles. The improvement of the CLC towards low viscosity and an increased movability of the mesogens provided a clear advantage for this technique. The pure material yielded particles with distorted mesogen alignment similar to films prepared by capillary flow. Dilution of the CLC with a solvent that migrated into the carrier phase during particle preparation provided the basis for particles with well ordered areas. On the contrary, most of the improvements, applied to CLC films, were not applicable, due to solvent incompatibility between the mobile and the stationary phase.

Although cellulose derivatives were known for their liquid crystalline behavior for decades and synthesized in mass production, their application as feedback material was affected by bad optical properties. In comparison to low molar mass compounds, the low degree of order in the CLC phase was the cause. With the

improved material, defined lasing emission was shown and characterized. Derivatives of cellulose are desirable materials, because, as a renewable resource, they are available in large amounts for a low price and need only simple derivatization reactions. The fabrication of CLC films with tunable lasing emission, for which this thesis can provide a starting point, is in good agreement with today's requirements of modern technology and its miniaturization.

6 Zusammenfassung

Im Rahmen dieser Arbeit wurden cholesterische Filme aus flüssigkristallinen Cellulosederivaten mit verbesserten optischen Eigenschaften hergestellt. Die Kombination aus verschiedenen Methoden führte zu einer optischen Qualität, wie sie aus theoretischen Vorhersagen und von niedermolekularen Cholesteren bekannt war. Komposite aus dem cholesterischen Flüssigkristall mit anorganischen als auch organischen Farbstoffen wurden hergestellt. Anorganische Nanopartikel benötigten eine maßgeschneiderte Oberflächenfunktionalisierung mittels Tensiden, bestehend aus Blockcopolymeren. Die optischen Eigenschaften von cholesterischer Matrix und organischem Dotanden wurden, mit Hinblick auf spiegelloses Lasen, aufeinander abgestimmt und das Verhalten unter optischer Anregung untersucht. Neben der Präparation von dünnen Filmen wurde der Flüssigkristall in einem mikrofluidischen Reaktor zu Mikropartikeln verarbeitet und diese auf ihre optischen Eigenschaften und Mesogenanordnung hin charakterisiert.

Ausgehend von bereits bekannten Flüssigkristallen basierend auf Mischungen von Cellulosderivaten in Acrylaten wurden alle Bestandteile systematisch variiert um die optischen Eigenschaften positiv zu beeinflussen. Es stellte sich heraus, dass die Viskosität der flüssigkristallinen Mischung und ein gezieltes Beeinflussen von Wasserstoffbrückenbindungen einen signifikanten Einfluss auf die Qualität der Mesogenorientierung haben. Intramolekulare Wasserstoffbrücken sind notwendig um die gestreckte Konformation des Polymerrückgrates aufrecht zu erhalten, wohingegen intermolekuare Wasserstoffbrücken unterdrückt werden müssen um Polymeraggregation zu verhindern. Die richtige Wahl der Acrylatmischungen, die Wirkung von Wasserstoffbrücken beeinflussenden Additiven, die synthetische Realisation eines möglichst hohen Substitutionsgrades am Cellulosepolymer und der Einsatz mechanischen Rührens von Lösungen am oberen Konzentrationslimit der flüssigkristallinen Phase waren die Grundlage für eine verbesserte Orinetierung der verwendeten Cellulosetricarbanilate. Im Zusammenspiel mit einer speziellen Substratbehandlung und Art der Filmpräparation wurden cholesterische Filme mit optischen Eigenschaften erhalten, die bisher nur von niedermolekularen Cholesteren bekannt waren. Anschließende Polymerisation gestattete eine per-

manente Fixierung der Orientierung und die Herstellung von freistehenden und äußeren Einflüssen unabhängigen Filmen.

Die Einbettung anorganischer Nanostäbchen in die cholesterische Matrix erfolgte mittels Blockcopolymeren, die über kontrollierte radikalische Polymerisation zugänglich sind. Neben der ähnlichen Gestalt der Nanopartikel bezüglich der stäbchenförmigen Mesogene, konnte so eine deutliche Steigerung der Misch-barkeit beider Komponenten erzielt werden. Die polymeren Tenside bestanden aus einem löslichkeitsvermittelndem Block, polymerisiert aus dem gleichen Acrylat welches als Lösungsmittel für Mesogene dient und einem Ankerblock für eine feste Bindung an die Partikeloberfläche. Jedoch führte die Größe der Nanopartikel in den dicht gepackten flüssigkristallinen Phasen als auch dessen lange Equilibrationsdauer zur langsamen Phasenseparation. Für weitere Experimente wurde daher auf organische Farbstoffe zurückgegriffen. Grundsätzlich eignen sich anorganische Nanopartikel als Ersatz für organische Farbstoffe, jedoch ist deren Verwendung in cellulosebasierten Flüssigkristallen nicht unter Erhaltung des hohen Niveaus der cholesterischen Ordnung zu verwirklichen.

Organische Farbstoffe hingegen lassen sich ohne weitere Probleme in den Flüssigkristall einbringen. Die Einführung eines organischen Farbstoffes ist durch Quellen eines polymerisierten Films oder durch direktes Lösen im Flüssigkristall vor der Polymerisation leicht durchzuführen. Mit der ersten Methode kann die Matrix ohne Beeinflussung durch den Farbstoff orientiert und polymerisiert werden. Die optischen Eigenschaften der flüssigkristallinen Matrix wurden mit denen des eingeführten Farbstoffes überlappt, dass die Bedingungen für spiegelloses Lasen erfüllt waren. Optische Anregung des Farbstoffes durch einen Pumplaser führte zur Laseremission, unterstützt durch den cholesterischen Resonator. Die Polarisation und Wellenlänge der emittierten Strahlung, die Linienbreite und die erhaltenen Interferenzmuster zeigen einen Feedbackmechanismus, der in dieser Qualität für hochmolekulare lytrope Flüssigkristalle als nicht realisierbar galt. Unter Ausnutzung von nicht optimalen optischen Eigenschaften konnte mit einer anderen Probe auch "Random Lasing" erzeugt werden.

Der Aufbau eines mikrofluidischen Flussreaktors wurde genutzt um die Eigenschaften der cellulosebasierten Cholesteren von flachen Filmen auf sphärische Mikropartikel zu übertragen. Die Optimierung bezüglich einer niedrigen Viskosität und einer erweiterten Beweglichkeit der Mesogene ist auch bei dieser Methode von Nutzen. Die Verarbeitung des reinen Flüssigkristalls führte zu Mikropartikeln mit gestörter Mesogenanordnung. Eine Verdünnung des Flüssigkristalls mit einem

Lösungsmittel, welches im Reaktor die Partikel verlässt, erzeugte eine deutliche Verbesserung der cholesterischen Ordnung in den kugelförmigen Partikeln. Jedoch konnten die meisten Verbesserungsmethoden, welche bei Filmen zu sehr guten Ergebnisse führten, aufgrund von Lösungsmittelinkompatibilität nicht angewendet werden.

Obwohl Derivate der Cellulose seit einigen Jahrzehnten für ihre flüssigkristallinen Eigenschaften bekannt sind und heutzutage großindustriell für verschiedenste Anwendungen produziert werden, war deren Anwendung als Resonatoren für Laser bisher durch schlechte optische Eigenschaften limitiert. Verglichen mit den Ergebnissen von niedermolekularen Cholesteren, war die Orientierung der polymeren Mesogene der Hauptgrund. Mit dem deutlich verbesserten Material konnte definiertes Lasing erreicht und nachgewiesen werden. Derivate der Cellulose sind hier besonders interessant, da sie, basierend auf nachwachsenden Rohstoffen, nach einfachen Reaktionen in großen Mengen und zu günstigen Preisen zur Verfügung stehen und bioabbaubar sind. Die in dieser Arbeit entwickelte Herstellung von Polymerfilmen und die dadurch entstehende Möglichkeit, Laserwellenlängen frei wählen zu können, trägt den gewachsenen Anforderungen heutiger Technologien und deren Miniaturisierung Rechnung.

7 List of Publications

WENZLIK, D.; OHM, C.; SERRA, C.; ZENTEL, R.: Preparation of cholesteric particles from cellulose derivatives in a microfluidic setup. *Soft Matter* 7 (2011), pp. 2340-2344.

WENZLIK, D.; ZENTEL, R.: *Macromolecular Chemistry and Physics* (2013), submitted.

WENZLIK, D.; VARANYTSIA, A.; MUKHERJEE, S.; MUNOZ, A.; PALFFY-MUHORAY, P.; ZENTEL, R.: in preparation.

8 Abbreviations

5CB	4-pentyl-4'-cyanobiphenyl
ATRP	Atom transfer radical polymerization
CD	Circular dichroism
CdS	Cadmium sulfide
CdSe	Cadmium selenide
CLC	Cholesteric liquid crystal
CMD(AA)	Cysteamine methyl disulfide (acrylic amide)
CTA	Chain transfer agent
CTC	Cellulose tricarbamtes
δ	Chemical shift (ppm)
DBR	Distributed bragg reflection
DCM	4-(Dicyanomethyl)-2-methyl-6-(4-dimethyl-amino-styryl)-4-H-pyran (organic dye)
DEGDMA	Diethylene glycol dimethacrylate
DEGEEA	Diethylene glycol ethyl ether acrylate
DEGMEA	Diethylene glycol methyl ether acrylate
DFB	Distributed feedback
DOS	Density of states
DP	Degree of polymerization
DS	Degree of substitution
EGMEA	Ethylene glycol methyl ether acrylate
EQ	Equivalents
FWHM	Full width at half maximum
GPC	Gel permeation chromatography
HA	Hexyl acrylate
HFIP	Hexafluoro isopropanol
IR	Infrared
LC	Liquid crystal
LCE	Liquid crystal elastomer

LCL	Liquid crystal laser
LCP	Liquid crystalline polymer
LED	Light emitting diode
LCPL	Left handed circular polarized light
LPL	Linear polarized light
M_w	Weight average molar mass
Nd-YAG	neodymium-doped yttrium aluminum garnet
NLC	Nematic liquid crystal
NMP	Nitroxide mediated polymerization
NP	Nanoparticle
ORD	Optical rotation dispersion
PBA	Poly (p-benzamide)
PBLG	Poly (γ-benyl-L-glutamate)
PBG	Photonic bandgap
PC	Photonic crystal
PFPA	Pentafluorophenol acrylate
PM597	Pyromethene 597 (organic dye)
PTFE	Poly (tetrafluoro ethylene)
RAFT	Reversible addition fragmentation chain transfer
RCPL	Right handed circular polarized light
RTP	Room temperature (22-25°C)
rpm	Rounds per minute
SmA	Smectic A
SmC	Smectic C
SmC*	chiral Smectic C
SR	Selective reflection
TEM	Transmission electron microscopy
TFAA	Trifluoroacetic acid
TFE	Trifluoro ethanol
THF	Tetrahydro furane
UV-VIS	Ultraviolett-Visible light
V(E)CSEL	Vertical (external) cavity surface emitting laser
WGR/M	Wispering gallery resonator/mode
YP	Yellow Potomac (organic dye)

9 Bibliography

[1] COLLINGS, P. J.: *Liquid Crystals: Nature's delicate phase of matter*. Princeton University Press, Princeton, 2002

[2] PALFFY-MUHORAY, P.: Orientationally Ordered Soft Matter: The Diverse World of Liquid Crystals. *Electronic-Liquid Crystal Communications* (2007)

[3] REINITZER, F.: Beiträge zur Kenntniss des Cholesterins. *Monatshefte für Chemie / Chemical Monthly* 9 (1888), No. 1, pp. 421–441

[4] REINITZER, F.: Contributions to the Knowledge of Cholesterol. *Liquid Crystals* 5 (1989), No. 1, pp. 7–18

[5] LEHMANN, O.: Zur Geschichte der flüssigen Kristalle. *Annalen der Physik* 330 (1908), No. 5, pp. 852–860

[6] TAMMANN, G.: Ueber die sogenannten flüssigen Krystalle. *Annalen der Physik* 309 (1901), No. 3, pp. 524–530

[7] LUDESCHER, M. ; WOHINZ, J. W.: *Vom Erzherzog zur scientific community*. http://www.austria-lexikon.at/af/Wissenssammlungen-/Bibliothek/TUGraz_200_Jahre/Die_Technik_in_Graz/Vom_Erzherzog_zur-_-scientific_community. January 2013

[8] VORLÄNDER, D.: *Chemische Kristallographie der Flüssigkeiten*. Akademische Verlagsgesellschaft, Leipzig, 1924

[9] FRIEDEL, G.: The mesomorphic states of matter. *Annales de Physique* 18 (1922), pp. 273–474

[10] ONSAGER, L.: The effect of shape on the interaction of colloidal paticles. *Annals of the New York Academy of Sciences* 51 (1949), No. 4, pp. 627–659

[11] MAIER, W. ; SAUPE, A.: Klärpunkt und Anisotropie der molekularen Polarisierbarkeit kristallinflüssiger Substanzen. *Zeitschrift für Naturforschung Part*

a - Astrophysik Physik und Physikalische Chemie 12 (1957), No. 8, pp. 668–669

[12] MAIER, W. ; SAUPE, A.: Eine einfache molekulare Theorie des nematischen kristallinflüssigen Zustandes. *Zeitschrift für Naturforschung Part a - Astrophysik Physik und Physikalische Chemie* 13 (1958), No. 7, pp. 564–566

[13] FLORY, P. J. ; GORDON, M. (Ed.) ; PLATE, N. A. (Ed.): *Advances in Polymer Science: Liquid Crystal Polymers I*. Springer-Verlag, Berlin, 1984

[14] DE GENNES, P. G.: *The Physics of Liquid Crystals*. Oxford University Press, Oxford, 1974

[15] LESLIE, F. M.: Continuum theory for nematic liquid crystals. *Continuum Mechanics and Thermodynamics* 4 (1992), No. 3, pp. 167–175

[16] BROWN, G. H. ; SHAW, W. G.: The Mesomorphic State - Liquid Crystals. *Chemical Reviews* 57 (1957), No. 6, pp. 1049–1157

[17] KENT STATE UNIVERSITY: *Liquid Crystal Institute*. http://www.lcinet.kent.edu/. November 2012

[18] HEILMEIER, G. H. ; ZANONI, L. A.: Guest-host interactions in nematic liquid crstals. A new electro-optic effect. *Applied Physics Letters* 13 (1968), No. 3, pp. 91–92

[19] SAUPE, A. ; JAKLI, A.: *One- and Two-dimensional Fluids*. CRC Press, Boca Raton, 2006

[20] DEMUS, D. ; STEGEMEYER, H. (Ed.): *Topics in Physical Chemistry: Liquid Crystals*. Steinkopff Verlag, Darmstadt, 1994

[21] CHANDRASEKHAR, S. ; SADASHIVA, B. K. ; SURESH, K. A.: Liquid crystals of disc-like molecules. *Pramana* 9 (1977), No. 5, pp. 471–480

[22] PELZL, G. ; DIELE, S. ; WEISSFLOG, W.: Banana-Shaped Compounds - A New Field of Liquid Crystals. *Advanced Materials* 11 (1999), No. 9, pp. 707–724

[23] ZIMMERMANN, H. ; POUPKO, R. ; LUZ, Z. ; BILLARD, J.: Pyramidic mesohases. *Zeitschrift für Naturforschung Section a - Journal of Physical Sciences* 40 (1985), No. 2, pp. 149–160

[24] MATSUO, Y.: C60 Derivatives Having Self-Assembly Capabilities. *Fullerenes, Nanotubes and Carbon Nanostructures* 18 (2010), No. 4-6, pp. 338–352

[25] KOSA, T. ; SUKHOMLINOVA, L. ; SU, L. ; TAHERI, B. ; WHITE, T. J. ; BUNNING, T. J.: Light-induced liquid crystallinity. *Nature* 485 (2012), No. 7398, pp. 347–349

[26] MAGNUS, M.: *Michel-Levy Farbtafel.* http://www.zeiss.co.in/C1256CFB00-332E16/0/798D0009B37D12E8C1257830004ABF0F-/$file/70_2_0110_d_-michel_levy.pdf. January 2013

[27] KITZEROW, H.-S. ; BAHR, C. ; KUBALL, H.-G. ; HOEFER, T. ; KITZEROW, H.-S. (Ed.) ; BAHR, C. (Ed.): *Chirality in Liqud Crystals.* Springer-Verlag, New York, 2001

[28] SHIBAEV, P. V. ; CHIAPPETTA, D. ; SANFORD, R. L. ; PALFFY-MUHORAY, P. ; MOREIRA, M. ; CAO, W. ; GREEN, M. M.: Color Changing Cholesteric Polymer Films Sensitive to Amino Acids. *Macromolecules* 39 (2006), No. 12, pp. 3986–3992

[29] MÜLLER, M. ; ZENTEL, R.: Cholesteric phases and films from cellulose derivatives. *Macromolecular Chemistry and Physics* 201 (2000), No. 15, pp. 2055–2063

[30] CHOI, S. S. ; MORRIS, S. M. ; HUCK, W. T. S. ; COLES, H. J.: The switching properties of chiral nematic liquid crystals using electrically commanded surfaces. *Soft Matter* 5 (2009), No. 2, pp. 354–362

[31] DIERKING, I.: *Textures of Liquid Crystals.* Wiley VCH, Weinheim, 2003

[32] WU, H. M. ; TANG, J. H. ; LUO, Q. ; SUN, Z. M. ; ZHU, Y. M. ; LU, Z. H. ; WEI, Y.: Liquid-crystal alignment of rubbed polyimide films: A microscopic investigation. *Applied Physics B: Lasers and Optics* 62 (1996), No. 6, pp. 613–618

[33] CUMINAL, M.-P. ; TOUHARI, F. ; BRUNET, M. ; COHEN-SOLAL, G.: Topography of Thin Teflon Layers and Induced Orientation of Nematic Liquid Crystals. *Molecular Crystals and Liquid Crystals* 333 (1999), 2012/05/28, pp. 181–191

[34] Ozaki, R. ; Shinpo, T. ; Moritake, H.: Improvement of orientation of planar cholesteric liquid crystal by rapid thermal processing. *Applied Physics Letters* 92 (2008), No. 16, pp. 163304–3

[35] Tien, C. J. ; Huang, C. Y.: Improvement in Planar Orientation of the Polymer-Stabilized Cholesteric Liquid Crystal Cells. *Japanese Journal of Applied Physics* 47 (2008), No. 11, pp. 8515–8517

[36] Dong, Y. ; Yuan, Q. ; Huang, Y.: Textures and disclinations in the cholesteric liquid-crystalline phase of a cyanoethyl chitosan solution. *Journal of Polymer Science Part B: Polymer Physics* 38 (2000), No. 7, pp. 980–986

[37] Nawa, N.: Mondomain of the focal conic texture in cholesteric liquid crystals. *Japanese Journal of Applied Physics Part 1-Regular Papers Short Notes & Review Papers* 29 (1990), No. 8, pp. 1521–1522

[38] Zhu, Y.-M. ; Yang, D.-K.: Observation of Pattern Evolution during Homeotropic-Focal Conic Transition in Cholesteric Liquid Crystals. *Phys. Rev. Lett.* 82 (1999), pp. 4855–4858

[39] Meister, R. ; Halle, M. A. ; Dumoulin, H. ; Pieranski, P.: Structure of the cholesteric focal conic domains at the free surface. *Physical Review E* 54 (1996), No. 4, pp. 3771–3782

[40] Chilaya, G.: Always Cholesterics but Sometimes Chiral Smectic C, TGB and Blue Phases. *Molecular Crystals and Liquid Crystals* 561 (2012), No. 1, pp. 8–35

[41] Rosenblatt, C. S. ; Pindak, R. ; Clark, N. A. ; Meyer, R. B.: The parabolic focal conic: a new smectic a defect. *J. Phys. France* 38 (1977), pp. 1105–1115

[42] Gvozdovskyy, I. ; Yaroshchuk, O. ; Serbina, M. ; Yamaguchi, R.: Photoinduced helical inversion in cholesteric liquid crystal cells with homeotropic anchoring. *Opt. Express* 20 (2012), No. 4, pp. 3499–3508

[43] Kent State University: *Liquid Crystal Institute*. http://dept.kent.edu/spie/liquidcrystals/textures2.html. January 2013

[44] Kikuchi, H. ; Yokota, M. ; Hisakado, Y. ; Yang, H. ; Kajiyama, T.: Polymer-stabilized liquid crystal blue phases. *Nat Mater* 1 (2002), No. 1, pp. 64–68

[45] CASTLES, F. ; DAY, F. V. ; MORRIS, S. M. ; KO, D. H. ; GARDINER, D. J. ; QASIM, M. M. ; NOSHEEN, S. ; HANDS, P. J. W. ; CHOI, S. S. ; FRIEND, R. H. ; COLES, H. J.: Blue-phase templated fabrication of three-dimensional nanostructures for photonic applications. *Nat Mater* 11 (2012), No. 7, pp. 599–603

[46] CHUNG, K. ; YU, S. ; HEO, C.-J. ; SHIM, J. W. ; YANG, S.-M. ; HAN, M. G. ; LEE, H.-S. ; JIN, Y. ; LEE, S. Y. ; PARK, N. ; SHIN, J. H.: Flexible, Angle-Independent, Structural Color Reflectors Inspired by Morpho Butterfly Wings. *Advanced Materials* 24 (2012), No. 18, pp. 2375–2379

[47] DONALD, A. M. ; WINDLE, A. H. ; HANNA, S.: *Liquid Crystalline Polymers 2nd Edition*. Cambridge University Press, Cambridge, 2006

[48] BRUCE, D. W. ; HEYNS, K. ; VILL, V.: Vorlander's wheel. *Liquid Crystals* 23 (1997), No. 6, pp. 813–819

[49] ELLIOTT, A. ; AMBROSE, E. J.: Evidence of chain folding in polypeptides and proteins. *Discussions of the Faraday Society* 9 (1950), No. 0, pp. 246–251

[50] ZENTEL, R.: *Handbook of Liquid Crystals, Vol. 3, High molecular weight liquid crystals*. Wiley VCH, Weinheim, 1998

[51] GRAY, D. G.: Chiral nematic ordering of polysaccharides. *Carbohydrate Polymers* 25 (1994), No. 4, pp. 277–284

[52] TERBOJEVICH, M. ; COSANI, A. ; CONIO, G. ; MARSANO, E. ; BIANCHI, E.: Chitosan: chain rigidity and mesophase formation. *Carbohydrate Research* 209 (1991), pp. 251–260

[53] STRZELECKA, T. E. ; DAVIDSON, M. W. ; RILL, R. L.: Multiple Liquid Crystal Phases of DNA at High Concentrations. *Nature* 331 (1988), No. 6155, pp. 457–460

[54] PAPKOV, S. P. ; GORDON, M. (Ed.) ; PLATE, N. A. (Ed.): *Advances in Polymer Science: Liquid Crystal Polymers I*. Springer-Verlag, Berlin, 1984

[55] OHM, C. ; BREHMER, M. ; ZENTEL, R.: Liquid Crystalline Elastomers as Actuators and Sensors. *Advanced Materials* 22 (2010), pp. 3366–3387

[56] ZORN, M. ; MEUER, S. ; TAHIR, M. N. ; KHALAVKA, Y. ; SÖNNICHSEN, C. ; TREMEL, W. ; ZENTEL, R.: Liquid crystalline phases from polymer functionalised semiconducting nanorods. *Journal of Materials Chemistry* 18 (2008), No. 25, pp. 3050–3058

[57] MEUER, S. ; OBERLE, P. ; THEATO, P. ; TREMEL, W. ; ZENTEL, R.: Liquid Crystalline Phases from Polymer-Functionalized TiO$_2$ Nanorods. *Advanced Materials* 19 (2007), No. 16, pp. 2073–2078

[58] BERG, J. M. ; TYMOCZKO, J. L. ; STRYER, L.: *Biochemie 5. Auflage*. Spektrum Akademischer Verlag, Heidelberg, 2003

[59] BARTHEL, S. ; HEINZE, T.: Acylation and carbanilation of cellulose in ionic liquids. *Green Chemistry* 8 (2006), No. 3, pp. 301–306

[60] MORMANN, W. ; MICHEL, U.: Hydrocelluloses with low degree of polymerisation from liquid ammonia treated cellulose. *Carbohydrate Polymers* 50 (2002), No. 4, pp. 349–353

[61] MORMANN, W. ; MICHEL, U.: Improved synthesis of cellulose carbamates without by-products. *Carbohydrate Polymers* 50 (2002), No. 2, pp. 201–208

[62] ZENTEL, R. ; MÜLLER, M. ; KELLER, H.: Solid opalescent films originating from urethanes of cellulose. *Advanced Materials* 9 (1997), No. 2, pp. 159–162

[63] GOISSEDET, P. E. C.: *French Patent No. 1,357,450: Manufacture of new products derived from cellulose*. 1920

[64] GEORGIA COLLEGE: *Cellulose*. http://chemistry.gcsu.edu/ metzker/Common-/Structures/Carbohydrates/cellulose.png. January 2013

[65] SIEKMEYER, M. ; ZUGENMAIER, P.: Solvent dependence of lyotropic liquid-crystalline phases of cellulose tricarbanilate. *Die Makromolekulare Chemie* 191 (1990), No. 5, pp. 1177–1196

[66] AHARONI, S. M.: Rigid Backbone Polymers, XIII: Effects of the Nature of the Solvent on the Lyotropic Mesomorphicity of Cellulose Acetate. *Molecular Crystals and Liquid Crystals* 56 (1980), 2012/12/12, pp. 237–241

[67] SATO, T. ; TERAMOTO, A.: *Advances in Polymer Science: Biopolymers, Liquid Crystalline Polymers and Phase Emulsion*. Springer Berlin, Heidelberg, 1996

[68] ZUGENMAIER, P.: *Handbook of Liquid Crystals, Vol 3, High molecular weight liquid crystals*. Wiley VCH, Weinheim, 1998

[69] UEMATSU, I. ; UEMATSU, Y. ; GORDON, M. (Ed.) ; PLATE, N. A. (Ed.): *Advances in Polymer Science: Liquid Crystal Polymers I*. Springer-Verlag, Berlin, 1984

[70] MEETEN, G. H. ; NAVARD, P.: The cholesteric nature of cellulose triacetate solutions. *Polymer* 23 (1982), No. 12, pp. 1727–1731

[71] WENZLIK, D. ; ZENTEL, R.: in preparation. (2013)

[72] SIXOU, P. ; GILLI, J. M. ; TENBOSCH, A. ; FRIED, F. ; MAISSA, P. ; VARICHON, L. ; GODINHO, M. H.: Cholesteric mesophases. *Physica Scripta* T35 (1991), pp. 47–52

[73] HOU, H. ; REUNING, A. ; WENDORFF, J. H. ; GREINER, A.: Tuning of the pitch height of thermotropic cellulose esters. *Macromolecular Chemistry and Physics* 201 (2000), pp. 2050–2054

[74] MAJOINEN, J. ; KONTTURI, E. ; IKKALA, O. ; GRAY, D.: SEM imaging of chiral nematic films cast from cellulose nanocrystal suspensions. *Cellulose* 19 (2012), No. 5, pp. 1599–1605

[75] TIPLER, P. A. ; MOSCA, G.: *Physik 2.Auflage*. Elsevier Spektrum Akademischer Verlag, München, 2004

[76] JOANNOPOULOS, J. D. ; VILLENEUVE, P. R. ; FAN, S. H.: Photonic crystals: Putting a new twist on light. *Nature* 386 (1997), No. 6621, pp. 143–149

[77] YABLONOVITCH, E.: Inhibited Spontaneous Emission in Solid-State Physics and Electronics. *Physical Review Letters* 58 (1987), No. 20, pp. 2059

[78] JOHN, S.: Strong localization of photons in certain disordered dielectric superlattices. *Physical Review Letters* 58 (1987), No. 23, pp. 2486

[79] FLEISCHHAKER, F. ; ZENTEL, R.: Opale: Photonische Kristalle. *Chemie in unserer Zeit* 41 (2007), No. 1, pp. 38–44

[80] VRIES, H. de: Rotary power and other optical properties of certain liquid crystals. *Acta Crystallographica* 4 (1951), No. 3, pp. 219–226

[81] MITOV, M.: Cholesteric Liquid Crystals with a Broad Light Reflection Band. *Advanced Materials* 24 (2012), No. 47, pp. 6260–6276

[82] KNEUBÜHL, F. K. ; SIGRIST, M. W.: *Laser*. Teubner Studienbücher, Stuttgart, 1999

[83] SCHINDEWOLF, U.: Der Laser und seine Anwendung in der Chemie. *Chemie in unserer Zeit* 6 (1972), No. 1, pp. 17–26

[84] Zhao, K. ; Zhang, Q. ; Chini, M. ; Wu, Y. ; Wang, X. ; Chang, Z.: Tailoring a 67 attosecond pulse through advantageous phase-mismatch. *Optics Letters* 37 (2012), No. 18, pp. 3891–3893

[85] Einstein, A.: Strahlungsemission und -absorption nach der Quantentheorie. *Deutsche Physikalische Gesellschaft, Verhandlungen* 18 (1916), pp. 318–323

[86] Ladenburg, R.: Untersuchungen über die anomale Dispersion angeregter Gase II Anomale Dispersion in angeregtem Neon Einfluss von Strom und Druck, Bildung und Vernichtung angeregter Atome. *Zeitschrift für Physik* 48 (1928), pp. 26–50

[87] Gordon, J. P. ; Zeiger, H. J. ; Townes, C. H.: Molecular Microwave Oscillator and New Hyperfine Structure in the Microwave Spectrum of NH_3. *Physical Reviews* 95 (1954), Jul, pp. 282–284

[88] Maiman, T. H.: Stimulated Optical Radiation in Ruby. *Nature* 187 (1960), No. 4736, pp. 493–494

[89] Dodabalapur, A. ; Chandross, E. A. ; Berggren, M. ; Slusher, R. E.: APPLIED PHYSICS: Organic Solid-State Lasers: Past and Future. *Science* 277 (1997), No. 5333, pp. 1787–1788

[90] Humar, M. ; Musevic, I.: 3D microlasers from self-assembled cholesteric liquid-crystal microdroplets. *Opt. Express* 18 (2010), No. 26, pp. 26995–27003

[91] Matsko, A. ; Ilchenko, V.: Optical resonators with whispering-gallery modes-part I: basics. *Selected Topics in Quantum Electronics, IEEE Journal of* 12 (2006), No. 1, pp. 3 – 14

[92] Ilchenko, V. ; Matsko, A.: Optical resonators with whispering-gallery modes-part II: applications. *Selected Topics in Quantum Electronics, IEEE Journal of* 12 (2006), No. 1, pp. 15 – 32

[93] Kuwata-Gonokami, M. ; Jordan, R. H. ; Dodabalapur, A. ; Katz, H. E. ; Schilling, M. L. ; Slusher, R. E. ; Ozawa, S.: Polymer microdisk and microring lasers. *Opt. Lett.* 20 (1995), No. 20, pp. 2093–2095

[94] Reiss, S. M.: *Biophotonics development*. http://www.bioopticsworld.com-/articles/print/volume-5/issue-2/features/driving-biophotonics-innovation-nih-new-innovator-award-part-1.html. January 2013

[95] BLINOV, L. M. ; BARTOLINO, R. ; BLINOV, L. M. (Ed.) ; BARTOLINO, R. (Ed.): *Liquid Crystal Microlasers*. Transworld Research Network, Kerala, India, 2010

[96] COLES, H. ; MORRIS, S.: Liquid crystal lasers. *Nat Photon* 4 (2010), No. 10, pp. 676–685

[97] COLES, H. ; MORRIS, S. ; FORD, A. D. ; HANDS, P. J. W. ; WILKINSON, T. D. ; BLINOV, L. M. (Ed.) ; BARTOLINO, R. (Ed.): *Liquid Crystal Microlasers*. Transworld Research Network, Kerala, India, 2010

[98] MUNOZ, A. ; MCCONNEY, M. E. ; KOSA, T. ; LUCHETTE, P. ; SUKHOMLINOVA, L. ; WHITE, T. J. ; BUNNING, T. J. ; TAHERI, B.: Continuous wave mirrorless lasing in cholesteric liquid crystals with a pitch gradient across the cell gap. *Opt. Lett.* 37 (2012), No. 14, pp. 2904–2906

[99] KOGELNIK, H. ; SHANK, C. V.: Stimulated emission in a periodic structure. *Applied Physics Letters* 18 (1971), No. 4, pp. 152–154

[100] GOLDBERG, J. M.: *Tunable Internal-Feedback Liquid Crystal-Dye Laser, US patent No. 3,771,065*. 1973

[101] ILCHISHIN, I. P. ; TIKHONOV, E. A. ; TISHCHENKO, V. G. ; SHPAK, M. T.: Generation of a tunable radiation by impurity cholesteric liquid crystals. *JETP Letters* 32 (1980), No. 1, pp. 24–27

[102] ILCHISHIN, I. P. ; TIKHONOV, E. A. ; TOLMACHEV, A. V. ; FEDORYAKO, A. P. ; SHPAK, M. T.: Harmonic distortion of the nematic liquid crystal structure with induced gyrotropy which manifests in the distributed feedback laser. *Ukrainskii Fizicheskii Zhurnal* 33 (1988), No. 10, pp. 1492–1494

[103] SCHMIDTKE, J. ; STILLE, W.: Fluorescence of a dye-doped cholesteric liquid crystal film in the region of the stop band: theory and experiment. *The European Physical Journal B - Condensed Matter and Complex Systems* 31 (2003), No. 2, pp. 179–194

[104] MOREIRA, M. ; RELAIX, S. ; CAO, W. ; TAHERI, B. ; PALFFY-MUHORAY, P. ; BLINOV, L. M. (Ed.) ; BARTOLINO, R. (Ed.): *Liquid Crystal Microlasers*. Transworld Research Network, Kerala, India, 2010

[105] ROGALSKI, M. ; PALMER, S.: *Quantum physics*. CRC Press, Amsterdam, Netherlands, 1999

[106] OZAKI, M. ; MATSUHISA, Y. ; YOSHIDA, H. ; OZAKI, R. ; FUJII, A.: Photonic crystals based on chiral liquid crystal. *Physica Status Solidi a-Applications and Materials Science* 204 (2007), pp. 3777–3789

[107] MUNOZ F, A. ; PALFFY-MUHORAY, P. ; TAHERI, B.: Ultraviolet lasing in cholesteric liquid crystals. *Opt. Lett.* 26 (2001), No. 11, pp. 804–806

[108] CAO, W. ; MUNOZ, A. ; PALFFY-MUHORAY, P. ; TAHERI, B.: Lasing in a three-dimensional photonic crystal of the liquid crystal blue phase II. *Nat Mater* 1 (2002), No. 2, pp. 111–113

[109] YANG, Y.-C. ; KEE, C.-S. ; KIM, J.-E. ; PARK, H. Y. ; LEE, J.-C. ; JEON, Y.-J.: Photonic defect modes of cholesteric liquid crystals. *Physical Review E* 60 (1999), No. 6, pp. 6852

[110] KOPP, V. I. ; GENACK, A. Z.: Twist Defect in Chiral Photonic Structures. *Physical Review Letters* 89 (2002), No. 3, pp. 033901

[111] ZAPOTOCKY, M. ; RAMOS, L. ; POULIN, P. ; LUBENSKY, T. C. ; WEITZ, D. A.: Particle-Stabilized Defect Gel in Cholesteric Liquid Crystals. *Science* 283 (1999), No. 5399, pp. 209–212

[112] MATSUI, T. ; OZAKI, M. ; YOSHINO, K.: Tunable photonic defect modes in a cholesteric liquid crystal induced by optical deformation of helix. *Physical Review E* 69 (2004), No. 6, pp. 061715

[113] YOSHIDA, H. ; LEE, C. H. ; FUJII, A. ; OZAKI, M.: Tunable Chiral Photonic Defect Modes in Locally Polymerized Cholesteric Liquid Crystals. *Molecular Crystals and Liquid Crystals* 477 (2007), No. 1, pp. 255/[749]–262/[756]

[114] OZAKI, M. ; OZAKI, R. ; MATSUI, T. ; YOSHINO, K.: Twist-defect-mode lasing in photopolymerized cholesteric liquid crystal. *Japanese Journal of Applied Physics Part 2-Letters* 42 (2003), No. 5A, pp. L472–L475

[115] HANDS, P. J. W. ; GARDINER, D. J. ; MORRIS, S. M. ; MOWATT, C. ; WILKINSON, T. D. ; COLES, H. J.: Band-edge and random lasing in paintable liquid crystal emulsions. *Applied Physics Letters* 98 (2011), No. 14

[116] WIERSMA, D. S. ; CAVALIERI, S.: Light emission: A temperature-tunable random laser. *Nature* 414 (2001), No. 6865, pp. 708–709

[117] HE, B. ; LIAO, Q. ; HUANG, Y.: Random lasing in a dye doped cholesteric liquid crystal polymer solution. *Optical Materials* 31 (2008), No. 2, pp. 375–379

[118] FINKELMANN, H. ; KIM, S. T. ; MUÑOZ, A. ; PALFFY-MUHORAY, P. ; TAHERI, B.: Tunable Mirrorless Lasing in Cholesteric Liquid Crystalline Elastomers. *Advanced Materials* 13 (2001), No. 14, pp. 1069–1072

[119] SHIBAEV, P. V. ; KOPP, V. ; GENACK, A. ; HANELT, E.: Lasing from chiral photonic band gap materials based on cholesteric glasses. *Liquid Crystals* 30 (2003), No. 12, pp. 1391–1400

[120] SHIBAEV, P. V. ; TANG, K. ; GENACK, A. Z. ; KOPP, V. ; GREEN, M. M.: Lasing from a Stiff Chain Polymeric Lyotropic Cholesteric Liquid Crystal. *Macromolecules* 35 (2002), No. 8, pp. 3022–3025

[121] OHTA, T. ; SONG, M. H. ; TSUNODA, Y. ; NAGATA, T. ; SHIN, K. C. ; ARAOKA, F. ; TAKANISHI, Y. ; ISHKAWA, K. ; WATANABE, J. ; NISHIMURA, S. ; TOYOOKA, T. ; TAKEZOE, H.: Monodomain film formation and lasing in dye-doped polymer cholesteric liquid crystals. *Japanese Journal of Applied Physics Part 1-Regular Papers Short Notes & Review Papers* 43 (2004), No. 9A, pp. 6142–6144

[122] SHIBAEV, P. V. ; CROOKER, B. ; MANEVICH, M. ; HANELT, E.: Mechanically tunable microlasers based on highly viscous chiral liquid crystals. *Applied Physics Letters* 99 (2011), No. 23, pp. 233302–3

[123] SERGEEV, G. B.: Nanochemistry of metals. *Uspekhi Khimii* 70 (2001), No. 10, pp. 915–933

[124] CHEN, H. ; KOU, X. ; YANG, Z. ; NI, W. ; WANG, J.: Shape- and Size-Dependent Refractive Index Sensitivity of Gold Nanoparticles. *Langmuir* 24 (2008), No. 10, pp. 5233–5237

[125] CARBONE, L. ; NOBILE, C. ; DE GIORGI, M. ; SALA, F. D. ; MORELLO, G. ; POMPA, P. ; HYTCH, M. ; SNOECK, E. ; FIORE, A. ; FRANCHINI, I. R. ; NADASAN, M. ; SILVESTRE, A. F. ; CHIODO, L. ; KUDERA, S. ; CINGOLANI, R. ; KRAHNE, R. ; MANNA, L.: Synthesis and Micrometer-Scale Assembly of Colloidal CdSe/CdS Nanorods Prepared by a Seeded Growth Approach. *Nano Letters* 7 (2007), No. 10, pp. 2942–2950

[126] GAPONIK, N. ; HICKEY, S. G. ; DORFS, D. ; ROGACH, A. L. ; EYCHMÜLLER, A.: Progress in the Light Emission of Colloidal Semiconductor Nanocrystals. *Small* 6 (2010), No. 13, pp. 1364–1378

[127] RÖSSLER, A. ; SKILLAS, G. ; PRATSINIS, S. E.: Nanopartikel - Materialien der Zukunft: Maßgeschneiderte Werkstoffe. *Chemie in unserer Zeit* 35 (2001), No. 1, pp. 32–41

[128] KLIMOV, V. I.: Nanocrystal Quantum Dots From fundamental photophysics to multicolor lasing. *Los Alamos Science* 28 (2003), pp. 214–221

[129] SUN, C.-J. ; WU, Y. ; XU, Z. ; HU, B. ; BAI, J. ; WANG, J.-P. ; SHEN, J.: Enhancement of quantum efficiency of organic light emitting devices by doping magnetic nanoparticles. *Applied Physics Letters* 90 (2007), No. 23, pp. 232110–3

[130] QI, H. ; HEGMANN, T.: Impact of nanoscale particles and carbon nanotubes on current and future generations of liquid crystal displays. *Journal of Materials Chemistry* 18 (2008), No. 28, pp. 3288–3294

[131] BEEK, W. J. E. ; WIENK, M. M. ; JANSSEN, R. J.: Efficient Hybrid Solar Cells from Zinc Oxide Nanoparticles and a Conjugated Polymer. *Advanced Materials* 16 (2004), No. 12, pp. 1009–1013

[132] KICKELBICK, G.: Nanokomposite: anorganisch + organisch: Homogen und doch so heterogen. *Chemie in unserer Zeit* 39 (2005), No. 1, pp. 46–53

[133] WEGNER, G.: Nanocomposites of Hairy-Rod Macromolecules: Concepts, Constructs, and Materials. *Macromolecular Chemistry and Physics* 204 (2003), No. 2, pp. 347–357

[134] HEGMANN, T. ; QI, H. ; MARX, V.: Nanoparticles in Liquid Crystals: Synthesis, Self-Assembly, Defect Formation and Potential Applications. *Journal of Inorganic and Organometallic Polymers and Materials* 17 (2007), No. 3, pp. 483–508

[135] COURSAULT, D. ; GRAND, J. ; ZAPPONE, B. ; AYEB, H. ; LÉVI, G. ; FÉLIDJ, N. ; LACAZE, E.: Linear Self-Assembly of Nanoparticles Within Liquid Crystal Defect Arrays. *Advanced Materials* 24 (2012), No. 11, pp. 1461–1465

[136] YOSHIDA, H. ; TANAKA, Y. ; KAWAMOTO, K. ; KUBO, H. ; TSUDA, T. ; FUJII, A. ; KUWABATA, S. ; KIKUCHI, H. ; OZAKI, M.: Nanoparticle-Stabilized Cholesteric Blue Phases. *Applied Physics Express* 2 (2009), No. 12

[137] BITAR, R. ; AGEZ, G. ; MITOV, M.: Cholesteric liquid crystal self-organization of gold nanoparticles. *Soft Matter* 7 (2011), No. 18, pp. 8198–8206

[138] MOAD, G. ; RIZZARDO, E. ; THANG, S. H.: Radical addition-fragmentation chemistry in polymer synthesis. *Polymer* 49 (2008), No. 5, pp. 1079–1131

[139] ROTH, P. J. ; WISS, K. T. ; ZENTEL, R. ; THEATO, P.: Synthesis of Reactive Telechelic Polymers Based on Pentafluorophenyl Esters. *Macromolecules* 41 (2008), No. 22, pp. 8513–8519

[140] SERRA, C. A. ; CHANG, Z.: Microfluidic-Assisted Synthesis of Polymer Particles. *Chemical Engineering & Technology* 31 (2008), No. 8, pp. 1099–1115

[141] OHM, C.: *Preparation of defined micro- and nanometre sized structures from liquid crystalline elastomers*, Johannes Gutenberg-University, Mainz, Germany, Dissertation, 2010

[142] SUGIURA, S. ; NAKAJIMA, M. ; ITOU, H. ; SEKI, M.: Synthesis of Polymeric Microspheres with Narrow Size Distributions Employing Microchannel Emulsification. *Macromolecular Rapid Communications* 22 (2001), No. 10, pp. 773–778

[143] DENDUKURI, D. ; TSOI, K. ; HATTON, T. A. ; DOYLE, P. S.: Controlled Synthesis of Nonspherical Microparticles Using Microfluidics. *Langmuir* 21 (2005), No. 6, pp. 2113–2116

[144] OHM, C. ; SERRA, C. ; ZENTEL, R.: A Continuous Flow Synthesis of Micrometer-Sized Actuators from Liquid Crystalline Elastomers. *Advanced Materials* 21 (2009), No. 47, pp. 4859–4862

[145] OHM, C. ; MORYS, M. ; FORST, F. R. ; BRAUN, L. ; EREMIN, A. ; SERRA, C. ; STANNARIUS, R. ; ZENTEL, R.: Preparation of actuating fibres of oriented main-chain liquid crystalline elastomers by a wetspinning process. *Soft Matter* 7 (2011), No. 8, pp. 3730–3734

[146] CIPPARRONE, G. ; MAZZULLA, A. ; PANE, A. ; HERNANDEZ, R. J. ; BARTOLINO, R.: Chiral Self-Assembled Solid Microspheres: A Novel Multifunctional Microphotonic Device. *Advanced Materials* 23 (2011), No. 48, pp. 5773–5778

[147] HUANG, Y. ; CHEN, L.-P. ; DOYLE, C. ; ZHOU, Y. ; WU, S.-T.: Spatially tunable laser emission in dye-doped cholesteric polymer films. *Applied Physics Letters* 89 (2006), No. 11, pp. 111106–3

[148] SNATZKE, G.: Optische Rotationsdispersion und Circulardichroismus: Methodik und Anwendung auf die Konformationsanalyse. *Fresenius' Journal of Analytical Chemistry* 235 (1968), No. 1, pp. 1–10

[149] REUNING, A.: *Optische Eigenschaften von cholesterischen Guest-Host-Systemen: Fluoreszenzfarbstoffe in Celluloseestern und zyklischen Siloxanen*, Philipps-University, Marburg, Germany, Dissertation, 2002

[150] ZHOU, X. ; HUANG, Y.: Cellulose derivative-based cholesteric networks. *Journal of Applied Polymer Science* 96 (2005), No. 5, pp. 1648–1653

[151] CHIBA, R. ; NISHIO, Y. ; SATO, Y. ; OHTAKI, M. ; MIYASHITA, Y.: Preparation of Cholesteric (Hydroxypropyl)cellulose/Polymer Networks and Ion-Mediated Control of Their Optical Properties. *Biomacromolecules* 7 (2006), No. 11, pp. 3076–3082

[152] HANLEY, S. J. ; GIASSON, J. ; REVOL, J.-F. ; GRAY, D. G.: Atomic force microscopy of cellulose microfibrils: comparison with transmission electron microscopy. *Polymer* 33 (1992), No. 21, pp. 4639 – 4642. – ISSN 0032-3861

[153] KASAI, W. ; KUGA, S. ; MAGOSHI, J. ; KONDO, T.: Compression Behavior of Langmuir-Blodgett Monolayers of Regioselectively Substituted Cellulose Ethers with Long Alkyl Side Chains. *Langmuir* 21 (2005), No. 6, pp. 2323–2329

[154] FISCHER, M.: *Polymeranaloge Carbanilierung von Cellulose*, Technische Universität Dresden, Dissertation, 2004

[155] WENZLIK, D.: *Helikale Überstrukturen aus fluoreszierenden Nanokristallen: Anorganische Nanostäbchen in cholesterischer Flüsigkristallmatrix*, Johannes Gutenberg-Uniersity, Mainz, Germany, Diplomarbeit, 2009

[156] KIM, S. I. ; PYO, S. M. ; REE, M. ; PARK, M. ; KIM, Y.: Alignment of Liquid-Crystals on Rubbed Polyimide Films Prepared from Various Precursor Polymers. *Molecular Crystals and Liquid Crystals Science and Technology. Section A. Molecular Crystals and Liquid Crystals* 316 (1998), pp. 209 – 214

[157] GUPTA, A. K. ; MARCHAL, E. ; BURCHARD, W.: Effect of Temperature on the Flexibility of Cellulose Tricarbanilate in Dioxane and Ethyl Acetate by Dielectric Measurements. *Macromolecules* 8 (1975), No. 6, pp. 843–849

[158] LEMATRE, J. ; DAYAN, S. ; SIXOU, P.: Anisotropic Solutions of Cellulose Acetate in Trifluoroacetic Acid. Proof of Cholesteric Order by Circular Dichroism. *Molecular Crystals and Liquid Crystals* 84 (1982), 2012/11/21, pp. 267–273

[159] KHANCHICH, O. ; KUZNETSOVA, S.: Temperature-concentration conditions of liquid-crystalline-phase formation in cellulose ethers and esters in trifluoroacetic acid. *Polymer Science Series A* 53 (2011), No. 4, pp. 311–316

[160] SHIPOVSKAYA, A. B. ; MIKUL'SKII, G. F. ; TIMOFEEVA, G. N.: Structurization and Optical Activity in Cellulose Triacetate Modified with Trifluoroacetic Acid Vapor. *Russian Journal of Applied Chemistry* 77 (2004), No. 1, pp. 148–153

[161] RITCEY, A. M. ; GRAY, D. G.: Circular reflectivity from the cholesteric liquid crystalline phase of (2-ethoxypropyl)cellulose. *Macromolecules* 21 (1988), No. 5, pp. 1251–1255

[162] WEI, S. K. H. ; CHEN, S. H. ; DOLGALEVA, K. ; LUKISHOVA, S. G. ; BOYD, R. W.: Robust organic lasers comprising glassy-cholesteric pentafluorene doped with a red-emitting oligofluorene. *Applied Physics Letters* 94 (2009), No. 4

[163] WANG, L. ; HUANG, Y.: Structural Characteristics and Defects in Ethyl-Cyanoethyl Cellulose/Acrylic Acid Cholesteric Liquid Crystalline System. *Macromolecules* 37 (2003), No. 2, pp. 303–309

[164] OZAKI, R. ; SHINPO, T. ; OZAK, M. ; MORITAKE, H.: Reorientation of cholesteric liquid crystal molecules using acoustic streaming. *Japanese Journal of Applied Physics Part 2-Letters & Express Letters* 46 (2007), No. 20-24, pp. L489–L491

[165] OZAKI, R. ; SHINPO, T. ; OZAKI, M. ; MORITAKE, H.: Lasing in cholesteric liquid crystal oriented by acoustic streaming. *Japanese Journal of Applied Physics* 47 (2008), No. 2, pp. 1363–1366

[166] POULIN, P. ; FRANCES, N. ; MONDAIN-MONVAL, O.: Suspension of spherical particles in nematic solutions of disks and rods. *Physical Review E* 59 (1999), No. 4, pp. 4384–4387

[167] BIJU, V. ; ITOH, T. ; ANAS, A. ; SUJITH, A. ; ISHIKAWA, M.: Semiconductor quantum dots and metal nanoparticles: syntheses, optical properties, and biological applications. *Analytical and Bioanalytical Chemistry* 391 (2008), No. 7, pp. 2469–2495

[168] TALAPIN, D. V. ; SHEVCHENKO, E. V. ; MURRAY, C. B. ; KORNOWSKI, A. ; FORSTER, S. ; WELLER, H.: CdSe and CdSe/CdS Nanorod Solids. *Journal of the American Chemical Society* 126 (2004), No. 40, pp. 12984–12988

[169] CAO, W. ; MARINO, A. ; ABBATE, G. ; PALFFY-MUHORAY, P. ; TAHERI, B.: Lasing Tresholds of Cholesteric Liquid Crystals Lasers. *Electronic-Liquid Crystal Communications* (2004)

[170] ARAOKA, F. ; SHIN, K.-C. ; TAKANISHI, Y. ; ISHIKAWA, K. ; TAKEZOE, H. ; ZHU, Z. ; SWAGER, T. M.: How doping a cholesteric liquid crystal with polymeric dye improves an order parameter and makes possible low threshold lasing. *Journal of Applied Physics* 94 (2003), No. 1, pp. 279–283

[171] INOUE, Y. ; YOSHIDA, H. ; INOUE, K. ; FUJII, A. ; OZAKI, M.: Improved Lasing Threshold of Cholesteric Liquid Crystal Lasers with In-Plane Helix Alignment. *Applied Physics Express* 3 (2010), No. 10

[172] SHANKARLING, G. ; JARAG, K.: Laser Dyes. *Resonance* 15 (2010), pp. 804–818

[173] UCHIMURA, M. ; WATANABE, Y. ; ARAOKA, F. ; WATANABE, J. ; TAKEZOE, H. ; KONISHI, G. i.: Development of Laser Dyes to Realize Low Threshold in Dye-Doped Cholesteric Liquid Crystal Lasers. *Advanced Materials* 22 (2010), No. 40, pp. 4473–4478

[174] SHANK, C. V. ; BJORKHOL.JE ; KOGELNIK, H.: Tunable distributed-feedback dye laser. *Applied Physics Letters* 18 (1971), No. 9, pp. 395–&

[175] KOPP, V. I. ; ZHANG, Z.-Q. ; GENACK, A. Z.: Lasing in chiral photonic structures. *Progress in Quantum Electronics* 27 (2003), No. 6, pp. 369–416

[176] SCHMIDTKE, J. ; STILLE, W. ; FINKELMANN, H. ; KIM, S.: Laser Emission in a Dye Doped Cholesteric Polymer Network. *Advanced Materials* 14 (2002), No. 10, pp. 746–749

[177] SAMUEL, I. D. W. ; NAMDAS, E. B. ; TURNBULL, G. A.: How to recognize lasing. *Nat Photon* 3 (2009), No. 10, pp. 546–549

[178] HUANG, C. Y. ; HU, C. Y.: Interference ring patterns from cholesteric liquid crystal cells. *Japanese Journal of Applied Physics Part 1-Regular Papers Brief Communications & Review Papers* 44 (2005), No. 7A, pp. 5076–5081

[179] MATSUI, T. ; OZAKI, R. ; FUNAMOTO, K. ; OZAKI, M. ; YOSHINO, K.: Flexible lasers made from cholesteric liquid crystal polymers. *Molecular Crystals and Liquid Crystals* 413 (2004), No. 1, pp. 507–514

[180] WENZLIK, D. ; OHM, C. ; SERRA, C. ; ZENTEL, R.: Preparation of cholesteric particles from cellulose derivatives in a microfluidic setup. *Soft Matter* 7 (2011), No. 6, pp. 2340–2344

[181] OHM, C. ; HABERKORN, N. ; THEATO, P. ; ZENTEL, R.: Template-Based Fabrication of Nanometer-Scaled Actuators from Liquid-Crystalline Elastomers. *Small* 7 (2011), No. 2, pp. 194–198

[182] HASELOH, S. ; OHM, C. ; SMALLWOOD, F. ; ZENTEL, R.: Nanosized Shape-Changing Colloids from Liquid Crystalline Elastomers. *Macromolecular Rapid Communications* 32 (2011), No. 1, pp. 88–93

[183] OOSTEN, C. L. van ; BASTIAANSEN, C. W. M. ; BROER, D. J.: Printed artificial cilia from liquid-crystal network actuators modularly driven by light. *Nature Materials* 8 (2009), No. 8, pp. 677–682

[184] YANG, H. ; BUGUIN, A. ; TAULEMESSE, J.-M. ; KANEKO, K. ; MERY, S. ; BERGERET, A. ; KELLER, P.: Micron-Sized Main-Chain Liquid Crystalline Elastomer Actuators with Ultralarge Amplitude Contractions. *Journal of the American Chemical Society* 131 (2009), No. 41, pp. 15000–15004

[185] KITZEROW, H. S. ; CROOKER, P. P.: Behaviour of polymer dispersed cholesteric droplets with negative dielectric anisotropy in electric fields. *Liquid Crystals* 11 (1992), No. 4, pp. 561 – 568

[186] KITZEROW, H. S. ; CROOKER, P. P.:   Electric field effects on the droplet structure in polymer dispersed cholesteric liquid crystals. *Liquid Crystals* 13 (1993), No. 1, pp. 31 – 43

[187] XU, F. ; CROOKER, P. P.:   Chiral nematic droplets with parallel surface anchoring. *Physical Review E* 56 (1997), No. 6, pp. 6853–6860

[188] ROBINSON, C.:   Cholesteric phase in polypeptide solutions and biological structures. *Molecular Crystals* 1 (1966), No. 4, pp. 467–494

[189] ROBINSON, C. ; WARD, J. C. ; BEEVERS, R. B.:   Liquid Crystalline Structure in Polypeptide solution. *Discussions of the Faraday Society* (1958), No. 25, pp. 29–42

[190] OHM, C. ; FLEISCHMANN, E.-K. ; KRAUS, I. ; SERRA, C. ; ZENTEL, R.:   Control of the Properties of Micrometer-Sized Actuators from Liquid Crystalline Elastomers Prepared in a Microfluidic Setup. *Advanced Functional Materials* 20 (2010), No. 24, pp. 4314–4322

[191] YANAI, H. ; SATO, T.: Local Conformation of the Cellulosic Chain in Solution. *Polym. J* 38 (2006), No. 3, pp. 226–233

[192] JOCHUM, F. D. ; BORG, L. zur ; ROTH, P. J. ; THEATO, P.: Thermo- and Light-Responsive Polymers Containing Photoswitchable Azobenzene End Groups. *Macromolecules* 42 (2009), No. 20, pp. 7854–7862

[193] JOCHUM, F. D. ; THEATO, P.:   Temperature- and Light-Responsive Polyacrylamides Prepared by a Double Polymer Analogous Reaction of Activated Ester Polymers. *Macromolecules* 42 (2009), No. 16, pp. 5941–5945

[194] THEATO, P.:   *Synthese und Untersuchung von neuen α,ω-funktionalisierten Lipopolymeren zum Aufbau von polymerunterstützten Lipiddoppelschichten*, Johannes Gutenberg-Universität, Mainz, Dissertation, 2001

10 Acknowledgement

TEM/SEM pictures and   for light scattering experiments.

- The graduate school "Material Science in Mainz", the graduate school "IRTG 1404" and the DFG through the SFB 625 for financial support.

Besides the support concerning scientific issues I would like to acknowledge some people helping me outside of the university. First of all I would like to thank my parents, my grandmother, my sister and all family members for their patience and support through almost nine years of studies. It is good to know that there is always someone you can rely on. Second I would like to acknowledge all the help by my parents in law and   when I was at my second home and most important I am very grateful to my girlfriend   for supporting me to all intents and purposes.